Introduction to Aircraft Stability and Control
Course Notes for M&AE 5070

David A. Caughey

Sibley School of Mechanical & Aerospace Engineering
Cornell University
Ithaca, New York 14853-7501

2011

Contents

1 Introduction to Flight Dynamics **1**

1.1 Introduction 1

1.2 Nomenclature 3

1.2.1 Implications of Vehicle Symmetry 4

1.2.2 Aerodynamic Controls 5

1.2.3 Force and Moment Coefficients 5

1.2.4 Atmospheric Properties 6

2 Aerodynamic Background **11**

2.1 Introduction 11

2.2 Lifting surface geometry and nomenclature 12

2.2.1 Geometric properties of trapezoidal wings 13

2.3 Aerodynamic properties of airfoils 14

2.4 Aerodynamic properties of finite wings 17

2.5 Fuselage contribution to pitch stiffness 19

2.6 Wing-tail interference 20

2.7 Control Surfaces 20

3 Static Longitudinal Stability and Control **25**

3.1 Control Fixed Stability 25

3.2 Static Longitudinal Control 28
3.2.1 Longitudinal Maneuvers – the Pull-up 29
3.3 Control Surface Hinge Moments 33
3.3.1 Control Surface Hinge Moments 33
3.3.2 Control free Neutral Point 35
3.3.3 Trim Tabs 36
3.3.4 Control Force for Trim 37
3.3.5 Control-force for Maneuver 39
3.4 Forward and Aft Limits of C.G. Position 41

4 Dynamical Equations for Flight Vehicles 45

4.1 Basic Equations of Motion 45
4.1.1 Force Equations 46
4.1.2 Moment Equations 49
4.2 Linearized Equations of Motion 50
4.3 Representation of Aerodynamic Forces and Moments 52
4.3.1 Longitudinal Stability Derivatives 54
4.3.2 Lateral/Directional Stability Derivatives 59
4.4 Control Derivatives 69
4.5 Properties of Elliptical Span Loadings 70
4.5.1 Useful Integrals 71
4.6 Exercises 71

5 Dynamic Stability 75

5.1 Mathematical Background 75
5.1.1 An Introductory Example 75
5.1.2 Systems of First-order Equations 79

5.2 Longitudinal Motions 81
5.2.1 Modes of Typical Aircraft 82
5.2.2 Approximation to Short Period Mode 86
5.2.3 Approximation to Phugoid Mode 88
5.2.4 Summary of Longitudinal Modes 89
5.3 Lateral/Directional Motions 89
5.3.1 Modes of Typical Aircraft 92
5.3.2 Approximation to Rolling Mode 95
5.3.3 Approximation to Spiral Mode 96
5.3.4 Approximation to Dutch Roll Mode 97
5.3.5 Summary of Lateral/Directional Modes 99
5.4 Stability Characteristics of the Boeing 747 101
5.4.1 Longitudinal Stability Characteristics 101
5.4.2 Lateral/Directional Stability Characteristics 102

6 Control of Aircraft Motions **105**

6.1 Control Response 105
6.1.1 Laplace Transforms and State Transition 105
6.1.2 The Matrix Exponential 106
6.2 System Time Response 109
6.2.1 Impulse Response 109
6.2.2 Doublet Response 109
6.2.3 Step Response 110
6.2.4 Example of Response to Control Input 111
6.3 System Frequency Response 113
6.4 Controllability and Observability 113

6.4.1 Controllability 114
6.4.2 Observability 118
6.4.3 Controllability, Observability, and MATLAB 118
6.5 State Feedback Design 119
6.5.1 Single Input State Variable Control 121
6.5.2 Multiple Input-Output Systems 130
6.6 Optimal Control 130
6.6.1 Formulation of Linear, Quadratic, Optimal Control 130
6.6.2 Example of Linear, Quadratic, Optimal Control 135
6.6.3 Linear, Quadratic, Optimal Control as a Stability Augmentation System . . . 138
6.7 Review of Laplace Transforms 143
6.7.1 Laplace Transforms of Selected Functions 144

Chapter 1

Introduction to Flight Dynamics

Flight dynamics deals principally with the response of aerospace vehicles to perturbations in their flight environments and to control inputs. In order to understand this response, it is necessary to characterize the aerodynamic and propulsive forces and moments acting on the vehicle, and the dependence of these forces and moments on the flight variables, including airspeed and vehicle orientation. These notes provide an introduction to the engineering science of flight dynamics, focusing primarily of aspects of stability and control. The notes contain a simplified summary of important results from aerodynamics that can be used to characterize the forcing functions, a description of static stability for the longitudinal problem, and an introduction to the dynamics and control of both, longitudinal and lateral/directional problems, including some aspects of feedback control.

1.1 Introduction

Flight dynamics characterizes the motion of a flight vehicle in the atmosphere. As such, it can be considered a branch of systems dynamics in which the system studies is a flight vehicle. The response of the vehicle to aerodynamic, propulsive, and gravitational forces, and to control inputs from the pilot determine the attitude of the vehicle and its resulting flight path. The field of flight dynamics can be further subdivided into aspects concerned with

- **Performance**: in which the short time scales of response are ignored, and the forces are assumed to be in quasi-static equilibrium. Here the issues are maximum and minimum flight speeds, rate of climb, maximum range, and time aloft (endurance).
- **Stability and Control**: in which the short- and intermediate-time response of the attitude and velocity of the vehicle is considered. Stability considers the response of the vehicle to perturbations in flight conditions from some dynamic equilibrium, while control considers the response of the vehicle to control inputs.
- **Navigation and Guidance**: in which the control inputs required to achieve a particular trajectory are considered.

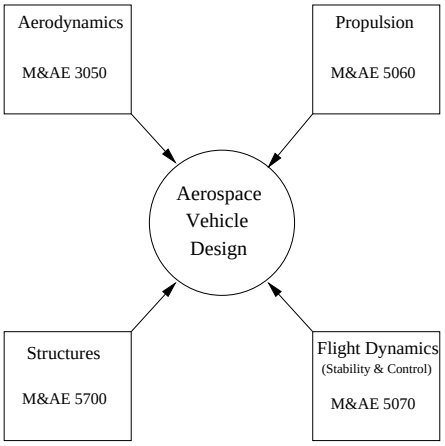

Figure 1.1: The four engineering sciences required to design a flight vehicle.

In these notes we will focus on the issues of stability and control. These two aspects of the dynamics can be treated somewhat independently, at least in the case when the equations of motion are linearized, so the two types of responses can be added using the principle of superposition, and the two types of responses are related, respectively, to the *stability* of the vehicle and to the ability of the pilot to *control* its motion.

Flight dynamics forms one of the four basic engineering sciences needed to understand the design of flight vehicles, as illustrated in Fig. 1.1 (with Cornell M&AE course numbers associated with introductory courses in these areas). A typical aerospace engineering curriculum with have courses in all four of these areas.

The aspects of stability can be further subdivided into (a) static stability and (b) dynamic stability. Static stability refers to whether the initial tendency of the vehicle response to a perturbation is toward a restoration of equilibrium. For example, if the response to an infinitesimal increase in angle of attack of the vehicle generates a pitching moment that reduces the angle of attack, the configuration is said to be statically stable to such perturbations. Dynamic stability refers to whether the vehicle ultimately returns to the initial equilibrium state after some infinitesimal perturbation. Consideration of dynamic stability makes sense only for vehicles that are statically stable. But a vehicle can be statically stable and dynamically unstable (for example, if the initial tendency to return toward equilibrium leads to an overshoot, it is possible to have an oscillatory divergence of continuously increasing amplitude).

Control deals with the issue of whether the aerodynamic and propulsive controls are adequate to trim the vehicle (i.e., produce an equilibrium state) for all required states in the flight envelope. In addition, the issue of "flying qualities" is intimately connected to control issues; i.e., the controls must be such that the maintenance of desired equilibrium states does not overly tire the pilot or require excessive attention to control inputs.

Several classical texts that deal with aspects of aerodynamic performance [1, 5] and stability and control [2, 3, 4] are listed at the end of this chapter.

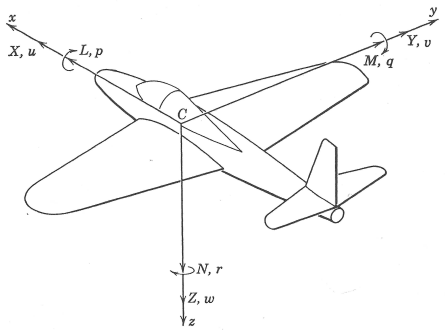

Figure 1.2: Standard notation for aerodynamic forces and moments, and linear and rotational velocities in body-axis system; origin of coordinates is at center of mass of the vehicle.

1.2 Nomenclature

The standard notation for describing the motion of, and the aerodynamic forces and moments acting upon, a flight vehicle are indicated in Fig. 1.2.

Virtually all the notation consists of consecutive alphabetic triads:

- The variables x, y, z represent coordinates, with origin at the center of mass of the vehicle. The x-axis lies in the symmetry plane of the vehicle[1] and points toward the nose of the vehicle. (The precise direction will be discussed later.) The z-axis also is taken to lie in the plane of symmetry, perpendicular to the x-axis, and pointing approximately down. The y axis completes a right-handed orthogonal system, pointing approximately out the right wing.
- The variables u, v, w represent the instantaneous components of linear velocity in the directions of the x, y, and z axes, respectively.
- The variables X, Y, Z represent the components of aerodynamic force in the directions of the x, y, and z axes, respectively.
- The variables p, q, r represent the instantaneous components of rotational velocity about the x, y, and z axes, respectively.
- The variables L, M, N represent the components of aerodynamic moments about the x, y, and z axes, respectively.
- Although not indicated in the figure, the variables ϕ, θ, ψ represent the angular rotations, relative to the equilibrium state, about the x, y, and z axes, respectively. Thus, $p = \dot{\phi}$, $q = \dot{\theta}$, and $r = \dot{\psi}$, where the dots represent time derivatives.

The velocity components of the vehicle often are represented as angles, as indicated in Fig. 1.3. The velocity component w can be interpreted as the angle of attack

$$\alpha \equiv \tan^{-1} \frac{w}{u} \tag{1.1}$$

[1] Virtually all flight vehicles have bi-lateral symmetry, and this fact is used to simplify the analysis of motions.

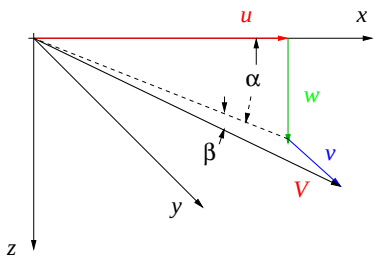

Figure 1.3: Standard notation for aerodynamic forces and moments, and linear and rotational velocities in body-axis system; origin of coordinates is at center of mass of the vehicle.

while the velocity component v can be interpreted as the sideslip angle

$$\beta \equiv \sin^{-1} \frac{v}{V} \tag{1.2}$$

1.2.1 Implications of Vehicle Symmetry

The analysis of flight motions is simplified, at least for small perturbations from certain equilibrium states, by the bi-lateral symmetry of most flight vehicles. This symmetry allows us to decompose motions into those involving *longitudinal* perturbations and those involving *lateral/directional* perturbations. Longitudinal motions are described by the velocities u and v and rotations about the y-axis, described by q (or θ). Lateral/directional motions are described by the velocity v and rotations about the x and/or z axes, described by p and/or r (or ϕ and/or ψ). A longitudinal equilibrium state is one in which the lateral/directional variables v, p, r are all zero. As a result, the side force Y and the rolling moment p and yawing moment r also are identically zero. A longitudinal equilibrium state can exist only when the gravity vector lies in the x-z plane, so such states correspond to wings-level flight (which may be climbing, descending, or level).

The important results of vehicle symmetry are the following. If a vehicle in a longitudinal equilibrium state is subjected to a perturbation in one of the longitudinal variables, the resulting motion will continue to be a longitudinal one – i.e., the velocity vector will remain in the x-z plane and the resulting motion can induce changes only in u, w, and q (or θ). This result follows from the symmetry of the vehicle because changes in flight speed ($V = \sqrt{u^2 + v^2}$ in this case), angle of attack ($\alpha = \tan^{-1} w/u$), or pitch angle θ cannot induce a side force Y, a rolling moment L, or a yawing moment N. Also, if a vehicle in a longitudinal equilibrium state is subjected to a perturbation in one of the lateral/directional variables, the resulting motion will *to first order* result in changes only to the lateral/directional variables. For example, a positive yaw rate will result in increased lift on the left wing, and decreased lift on the right wing; but these will approximately cancel, leaving the lift unchanged. These results allow us to gain insight into the nature of the response of the vehicle to perturbations by considering longitudinal motions completely uncoupled from lateral/directional ones, and vice versa.

1.2.2 Aerodynamic Controls

An aircraft typically has three aerodynamic controls, each capable of producing moments about one of the three basic axes. The *elevator* consists of a trailing-edge flap on the horizontal tail (or the ability to change the incidence of the entire tail). Elevator deflection is characterized by the deflection angle δ_e. Elevator deflection is defined as positive when the trailing edge rotates downward, so, for a configuration in which the tail is aft of the vehicle center of mass, the control derivative

$$\frac{\partial M_{cg}}{\partial \delta_e} < 0$$

The *rudder* consists of a trailing-edge flap on the vertical tail. Rudder deflection is characterized by the deflection angle δ_r. Rudder deflection is defined as positive when the trailing edge rotates to the left, so the control derivative

$$\frac{\partial N_{cg}}{\partial \delta_r} < 0$$

The *ailerons* consist of a pair of trailing-edge flaps, one on each wing, designed to deflect differentially; i.e., when the left aileron is rotated up, the right aileron will be rotated down, and vice versa. Aileron deflection is characterized by the deflection angle δ_a. Aileron deflection is defined as positive when the trailing edge of the aileron on the right wing rotates up (and, correspondingly, the trailing edge of the aileron on the left wing rotates down), so the control derivative

$$\frac{\partial L_{cg}}{\partial \delta_a} > 0$$

By vehicle symmetry, the elevator produces only pitching moments, but there invariably is some cross-coupling of the rudder and aileron controls; i.e., rudder deflection usually produces some rolling moment and aileron deflection usually produces some yawing moment.

1.2.3 Force and Moment Coefficients

Modern computer-based flight dynamics simulation is usually done in dimensional form, but the basic aerodynamic inputs are best defined in terms of the classical non-dimensional aerodynamic forms. These are defined using the dynamic pressure

$$Q = \frac{1}{2}\rho V^2 = \frac{1}{2}\rho_{\mathrm{SL}} V_{\mathrm{eq}}^2$$

where ρ is the ambient density at the flight altitude and V_{eq} is the *equivalent airspeed*, which is defined by the above equation in which ρ_{SL} is the standard sea-level value of the density. In addition, the vehicle reference area S, usually the wing planform area, wing mean aerodynamic chord $\bar{c}$, and wing span b are used to non-dimensionalize forces and moments. The force coefficients are defined as

$$\begin{aligned} \mathbf{C}_X &= \frac{X}{QS} \\ \mathbf{C}_Y &= \frac{Y}{QS} \\ \mathbf{C}_Z &= \frac{Z}{QS} \end{aligned} \tag{1.3}$$

while the aerodynamic moment coefficients are defined as

$$\begin{aligned} \mathbf{C}_l &= \frac{L}{QSb} \\ \mathbf{C}_m &= \frac{M}{QS\bar{c}} \\ \mathbf{C}_n &= \frac{N}{QSb} \end{aligned} \tag{1.4}$$

Note that the wing *span* is used as the reference moment arm for the rolling and yawing moments, while the mean aerodynamic chord is used for the pitching moment.

Finally, we often express the longitudinal forces in terms of the lift L and drag D, and define the corresponding lift and drag coefficients as

$$\begin{aligned} \mathbf{C}_L &\equiv \frac{L}{QS} = -\mathbf{C}_Z \cos\alpha + \mathbf{C}_X \sin\alpha \\ \mathbf{C}_D &\equiv \frac{D}{QS} = -\mathbf{C}_Z \sin\alpha - \mathbf{C}_X \cos\alpha \end{aligned} \tag{1.5}$$

Note that in this set of equations, L represents the *lift force*, not the rolling moment. It generally will be clear from the context here, and in later sections, whether the variable L refers to the lift force or the rolling moment.

1.2.4 Atmospheric Properties

Aerodynamic forces and moments are strongly dependent upon the ambient density of the air at the altitude of flight. In order to standardize performance calculations, standard values of atmospheric properties have been developed, under the assumptions that the atmosphere is static (i.e., no winds), that atmospheric properties are a function only of altitude h, that the temperature is given by a specified piecewise linear function of altitude, and that the acceleration of gravity is constant (technically requiring that properties be defined as functions of *geopotential* altitude. Tables for the properties of the Standard Atmosphere, in both SI and British Gravitational units, are given on the following pages.

h (m)	T (K)	p (N/m^2)	ρ (kg/m^3)	a (m/s)
0	288.15	101325.00	1.225000	340.29
500	284.90	95460.78	1.167268	338.37
1000	281.65	89874.46	1.111641	336.43
1500	278.40	84555.84	1.058065	334.49
2000	275.15	79495.01	1.006488	332.53
2500	271.90	74682.29	0.956856	330.56
3000	268.65	70108.27	0.909119	328.58
3500	265.40	65763.78	0.863225	326.58
4000	262.15	61639.91	0.819125	324.58
4500	258.90	57727.98	0.776770	322.56
5000	255.65	54019.55	0.736111	320.53
5500	252.40	50506.43	0.697100	318.48
6000	249.15	47180.64	0.659692	316.43
6500	245.90	44034.45	0.623839	314.36
7000	242.65	41060.35	0.589495	312.27
7500	239.40	38251.03	0.556618	310.17
8000	236.15	35599.41	0.525162	308.06
8500	232.90	33098.64	0.495084	305.93
9000	229.65	30742.07	0.466342	303.79
9500	226.40	28523.23	0.438895	301.63
10000	223.15	26435.89	0.412701	299.46
10500	219.90	24474.00	0.387720	297.27
11000	216.65	22631.70	0.363912	295.07
11500	216.65	20915.84	0.336322	295.07
12000	216.65	19330.06	0.310823	295.07
12500	216.65	17864.52	0.287257	295.07
13000	216.65	16510.09	0.265478	295.07
13500	216.65	15258.34	0.245350	295.07
14000	216.65	14101.50	0.226749	295.07
14500	216.65	13032.37	0.209557	295.07
15000	216.65	12044.30	0.193669	295.07
15500	216.65	11131.14	0.178986	295.07
16000	216.65	10287.21	0.165416	295.07
16500	216.65	9507.26	0.152874	295.07
17000	216.65	8786.45	0.141284	295.07
17500	216.65	8120.29	0.130572	295.07
18000	216.65	7504.64	0.120673	295.07
18500	216.65	6935.66	0.111524	295.07
19000	216.65	6409.82	0.103068	295.07
19500	216.65	5923.85	0.095254	295.07
20000	216.65	5474.72	0.088032	295.07

Table 1.1: Properties of the International Standard Atmosphere; SI units.

h (ft)	T (°R)	p (lbf/ft^2)	ρ (slug/ft^3)	a (ft/s)
0	518.67	2116.20	0.002377	1116.44
1000	515.10	2040.84	0.002308	1112.60
2000	511.54	1967.66	0.002241	1108.74
3000	507.97	1896.62	0.002175	1104.87
4000	504.41	1827.68	0.002111	1100.99
5000	500.84	1760.78	0.002048	1097.09
6000	497.27	1695.87	0.001987	1093.17
7000	493.71	1632.92	0.001927	1089.25
8000	490.14	1571.87	0.001868	1085.31
9000	486.57	1512.68	0.001811	1081.35
10000	483.01	1455.31	0.001755	1077.38
11000	479.44	1399.72	0.001701	1073.40
12000	475.88	1345.86	0.001648	1069.40
13000	472.31	1293.69	0.001596	1065.38
14000	468.74	1243.17	0.001545	1061.35
15000	465.18	1194.25	0.001496	1057.31
16000	461.61	1146.91	0.001447	1053.25
17000	458.05	1101.10	0.001400	1049.17
18000	454.48	1056.78	0.001355	1045.08
19000	450.91	1013.92	0.001310	1040.97
20000	447.35	972.48	0.001266	1036.84
21000	443.78	932.42	0.001224	1032.70
22000	440.21	893.70	0.001183	1028.55
23000	436.65	856.30	0.001143	1024.37
24000	433.08	820.18	0.001103	1020.18
25000	429.52	785.30	0.001065	1015.97
26000	425.95	751.63	0.001028	1011.74
27000	422.38	719.14	0.000992	1007.50
28000	418.82	687.79	0.000957	1003.24
29000	415.25	657.56	0.000923	998.96
30000	411.69	628.42	0.000889	994.66
31000	408.12	600.33	0.000857	990.34
32000	404.55	573.27	0.000826	986.01
33000	400.99	547.20	0.000795	981.65
34000	397.42	522.10	0.000765	977.27
35000	393.85	497.95	0.000737	972.88
36000	390.29	474.70	0.000709	968.47
37000	389.97	452.42	0.000676	968.07
38000	389.97	431.19	0.000644	968.07
39000	389.97	410.96	0.000614	968.07
40000	389.97	391.67	0.000585	968.07
41000	389.97	373.29	0.000558	968.07
42000	389.97	355.78	0.000532	968.07
43000	389.97	339.08	0.000507	968.07
44000	389.97	323.17	0.000483	968.07
45000	389.97	308.00	0.000460	968.07

Table 1.2: Properties of the International Standard Atmosphere; British Gravitational units.

Bibliography

[1] John Anderson, **Introduction to Flight**, McGraw-Hill, New York, Fourth Edition, 2000.

[2] Bernard Etkin & Lloyd D. Reid, **Dynamics of Flight; Stability and Control**, John Wiley & Sons, New York, Third Edition, 1998.

[3] Robert C. Nelson, **Flight Stability and Automatic Control**, McGraw-Hill, New York, Second Edition, 1998.

[4] Edward Seckel, **Stability and Control of Airplanes and Helicopters**, Academic Press, New York, 1964.

[5] Richard Shevell, **Fundamentals of Flight**, Prentice Hall, Englewood Cliffs, New Jersey, Second Edition, 1989.

Chapter 2

Aerodynamic Background

Flight dynamics deals principally with the response of aerospace vehicles to perturbations in their flight environments and to control inputs. In order to understand this response, it is necessary to characterize the aerodynamic and propulsive forces and moments acting on the vehicle, and the dependence of these forces and moments on the flight variables, including airspeed and vehicle orientation. These notes provide a simplified summary of important results from aerodynamics that can be used to characterize these dependencies.

2.1 Introduction

Flight dynamics deals with the response of aerospace vehicles to perturbations in their flight environments and to control inputs. Since it is changes in orientation (or *attitude*) that are most important, these responses are dominated by the generated aerodynamic and propulsive moments. For most aerospace vehicles, these moments are due largely to changes in the lifting forces on the vehicle (as opposed to the drag forces that are important in determining performance). Thus, in some ways, the prediction of flight stability and control is easier than the prediction of performance, since these lifting forces can often be predicted to within sufficient accuracy using inviscid, linear theories.

In these notes, I attempt to provide a uniform background in the aerodynamic theories that can be used to analyze the stability and control of flight vehicles. This background is equivalent to that usually covered in an introductory aeronautics course, such as one that might use the text by Shevell [6]. This material is often reviewed in flight dynamics texts; the material presented here is derived, in part, from the material in Chapter 1 of the text by Seckel [5], supplemented with some of the material from Appendix B of the text by Etkin & Reid [3]. The theoretical basis for these linear theories can be found in the book by Ashley & Landahl [2].

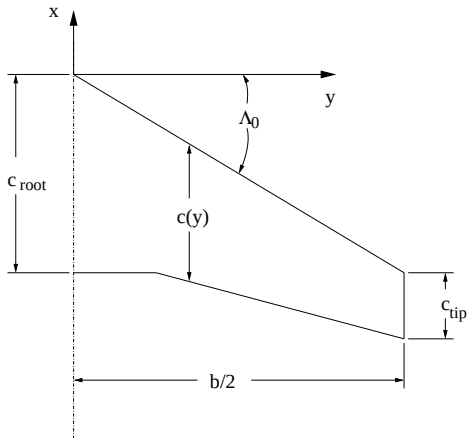

Figure 2.1: Planform geometry of a typical lifting surface (wing).

2.2 Lifting surface geometry and nomenclature

We begin by considering the geometrical parameters describing a lifting surface, such as a wing or horizontal tail plane. The projection of the wing geometry onto the x-y plane is called the wing *planform*. A typical wing planform is sketched in Fig. 2.1. As shown in the sketch, the maximum lateral extent of the planform is called the wing span b, and the area of the planform S is called the wing area.

The wing area can be computed if the spanwise distribution of local section chord $c(y)$ is known using

$$S = \int_{-b/2}^{b/2} c(y)\,\mathrm{d}y = 2\int_{0}^{b/2} c(y)\,\mathrm{d}y, \tag{2.1}$$

where the latter form assumes bi-lateral symmetry for the wing (the usual case). While the span characterizes the lateral extent of the aerodynamic forces acting on the wing, the *mean aerodynamic chord* $\bar{c}$ characterizes the axial extent of these forces. The mean aerodynamic chord is usually approximated (to good accuracy) by the *mean geometric chord*

$$\bar{c} = \frac{2}{S}\int_{0}^{b/2} c^2\,\mathrm{d}y \tag{2.2}$$

The dimensionless ratio of the span to the mean chord is also an important parameter, but instead of using the ratio $b/\bar{c}$ the *aspect ratio* of the planform is defined as

$$\mathbf{AR} \equiv \frac{b^2}{S} \tag{2.3}$$

Note that this definition reduces to the ratio b/c for the simple case of a wing of rectangular planform (having constant chord c).

The lift, drag, and pitching moment coefficients of the wing are defined as

$$\begin{aligned} \mathbf{C}_L &= \frac{L}{QS} \\ \mathbf{C}_D &= \frac{D}{QS} \\ \mathbf{C}_m &= \frac{M}{QS\bar{c}} \end{aligned} \tag{2.4}$$

where

$$Q = \frac{\rho V^2}{2}$$

is the dynamic pressure, and L, D, M are the lift force, drag force, and pitching moment, respectively, due to the aerodynamic forces acting on the wing.

Conceptually, and often analytically, it is useful to build up the aerodynamic properties of lifting surfaces as integrals of sectional properties. A wing section, or *airfoil*, is simply a cut through the lifting surface in a plane of constant y. The lift, drag, and pitching moment coefficients of the airfoil section are defined as

$$\begin{aligned} \mathbf{c}_\ell &= \frac{\ell}{Q\bar{c}} \\ \mathbf{C}_d &= \frac{d}{Q\bar{c}} \\ \mathbf{C}_{m\text{sect}} &= \frac{m}{Q\bar{c}^2} \end{aligned} \tag{2.5}$$

where ℓ, d, and m are the lift force, drag force, and pitching moment, per unit span, respectively, due to the aerodynamics forces acting on the airfoil section. Note that if we calculate the wing lift coefficient as the chord-weighted average integral of the section lift coefficients

$$\mathbf{C}_L = \frac{2}{S}\int_0^{b/s} \mathbf{c}_\ell c \,\mathrm{d}y \tag{2.6}$$

for a wing with *constant* section lift coefficient, then Eq. (2.6) gives

$$\mathbf{C}_L = \mathbf{c}_\ell$$

2.2.1 Geometric properties of trapezoidal wings

The planform shape of many wings can be approximated as trapezoidal. In this case, the root chord c_{root}, tip chord c_{tip}, span b, and the sweep angle of any constant-chord fraction Λ_n completely specify the planform. Usually, the geometry is specified in terms of the wing taper ratio $\lambda = c_{\text{tip}}/c_{\text{root}}$; then using the geometric properties of a trapezoid, we have

$$S = \frac{c_{\text{root}}(1+\lambda)}{2} b \tag{2.7}$$

and

$$\mathbf{AR} = \frac{2b}{c_{\text{root}}(1+\lambda)} \tag{2.8}$$

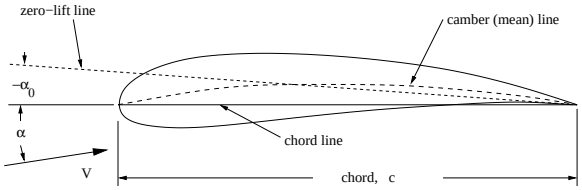

Figure 2.2: Geometry of a typical airfoil section.

The local chord is then given as a function of the span variable by

$$c = c_{\text{root}} \left[1 - (1 - \lambda) \frac{2y}{b} \right] \tag{2.9}$$

and substitution of this into Eq. (2.2) and carrying out the integration gives

$$\bar{c} = \frac{2(1 + \lambda + \lambda^2)}{3(1 + \lambda)} c_{\text{root}} \tag{2.10}$$

The sweep angle of any constant-chord fraction line can be related to that of the leading-edge sweep angle by

$$\mathbf{AR} \tan \Lambda_n = \mathbf{AR} \tan \Lambda_0 - 4n \frac{1 - \lambda}{1 + \lambda} \tag{2.11}$$

where $0 \leq n \leq 1$ is the chord fraction (e.g., 0 for the leading edge, 1/4 for the quarter-chord line, etc.). Finally, the location of any chord-fraction point on the mean aerodynamic chord, relative to the wing apex, can be determined as

$$\begin{aligned} \bar{x}_n = \frac{2}{S} \int_0^{b/2} x_n c \, \mathrm{d}y &= \frac{2}{S} \int_0^{b/2} (n c_{\text{root}} + y \tan \Lambda_n) \, \mathrm{d}y \\ &= \frac{3(1 + \lambda)\bar{c}}{2(1 + \lambda + \lambda^2)} \left\{ n + \left(\frac{1 + 2\lambda}{12} \right) \mathbf{AR} \tan \Lambda_n \right\} \end{aligned} \tag{2.12}$$

Alternatively, we can use Eq. (2.11) to express this result in terms of the leading-edge sweep as

$$\frac{\bar{x}_n}{\bar{c}} = n + \frac{(1 + \lambda)(1 + 2\lambda)}{8(1 + \lambda + \lambda^2)} \mathbf{AR} \tan \Lambda_0 \tag{2.13}$$

Substitution of $n = 0$ (or $n = 1/4$) into either Eq. (2.12) or Eq. (2.13) gives the axial location of the leading edge (or quarter-chord point) of the mean aerodynamic chord relative to the wing apex.

2.3 Aerodynamic properties of airfoils

The basic features of a typical airfoil section are sketched in Fig. 2.2. The longest straight line from the trailing edge to a point on the leading edge of the contour defines the *chord line*. The length of this line is called simply the *chord c*. The locus of points midway between the upper and lower surfaces is called the mean line, or *camber line*. For a symmetric airfoil, the camber and chord lines coincide.

For low speeds (i.e., Mach numbers $\mathbf{M} << 1$), and at high Reynolds numbers $\mathbf{Re} = Vc/\nu >> 1$, the results of thin-airfoil theory predict the lifting properties of airfoils quite accurately for angles of attack not too near the stall. Thin-airfoil theory predicts a linear relationship between the section lift coefficient and the angle of attack α of the form

$$\mathbf{c}_\ell = a_0 \left(\alpha - \alpha_0\right) \tag{2.14}$$

as shown in Fig. 2.3. The theory also predicts the value of the lift-curve slope

$$a_0 = \frac{\partial \mathbf{c}_\ell}{\partial \alpha} = 2\pi \tag{2.15}$$

Thickness effects (not accounted for in thin-airfoil theory) tend to increase the value of a_0, while viscous effects (also neglected in the theory) tend to decrease the value of a_0. The value of a_0 for realistic conditions is, as a result of these counter-balancing effects, remarkably close to 2π for most practical airfoil shapes at the high Reynolds numbers of practical flight.

The angle α_0 is called the *angle for zero lift*, and is a function only of the shape of the camber line. Increasing (conventional, sub-sonic) camber makes the angle for zero lift α_0 increasingly negative. For camber lines of a given family (i.e., shape), the angle for zero lift is very nearly proportional to the magnitude of camber – i.e., to the maximum deviation of the camber line from the chord line.

A second important result from thin-airfoil theory concerns the location of the *aerodynamic center*. The aerodynamic center of an airfoil is the point about which the pitching moment, due to the distribution of aerodynamic forces acting on the airfoil surface, is independent of the angle of attack. Thin-airfoil theory tells us that the aerodynamic center is located on the chord line, one quarter of the way from the leading to the trailing edge – the so-called *quarter-chord* point. The value of the pitching moment about the aerodynamic center can also be determined from thin-airfoil theory, but requires a detailed calculation for each specific shape of camber line. Here, we simply note that, for a given shape of camber line the pitching moment about the aerodynamic center is proportional to the amplitude of the camber, and generally is negative for conventional subsonic (concave down) camber shapes.

It is worth emphasizing that thin-airfoil theory neglects the effects of viscosity and, therefore, cannot predict the behavior of airfoil stall, which is due to boundary layer separation at high angles of attack. Nevertheless, for the angles of attack usually encountered in controlled flight, it provides a very useful approximation for the lift.

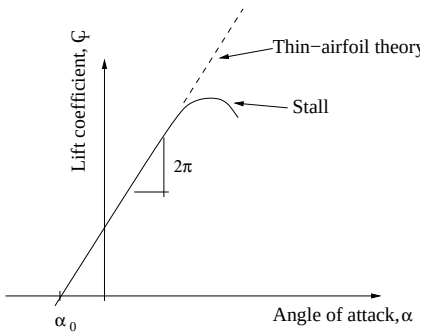

Figure 2.3: Airfoil section lift coefficient as a function of angle of attack.

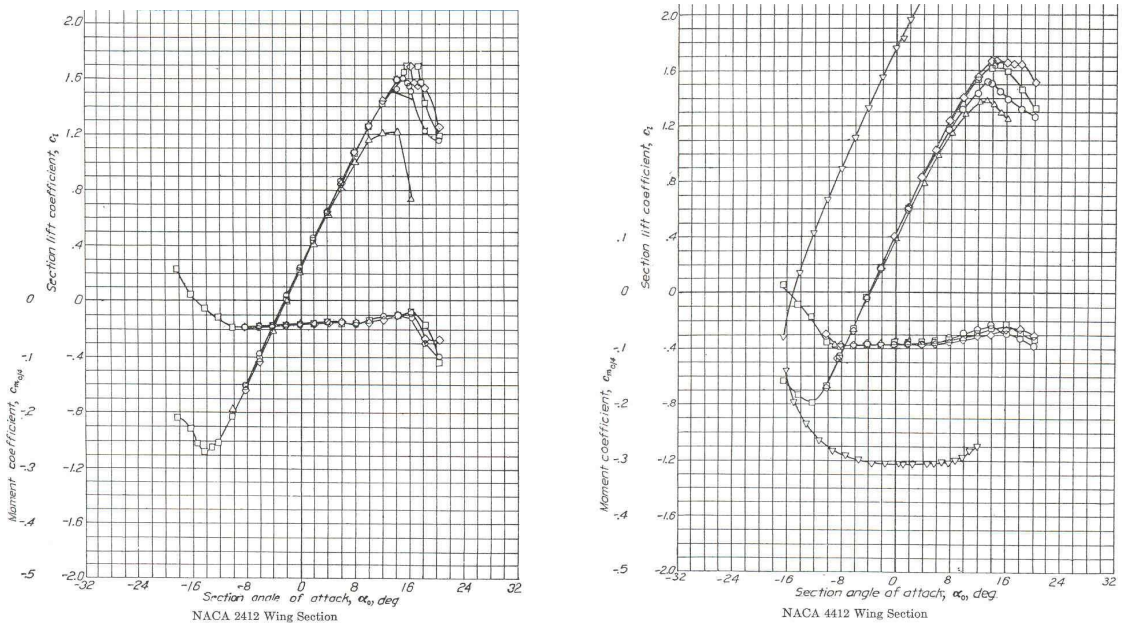

Figure 2.4: Airfoil lift and moment coefficients as a function of angle of attack; wind tunnel data for two cambered airfoil sections. Data from Abbott & von Doenhoff [1].

Finally, wind tunnel data for two cambered airfoil sections are presented in Fig. 2.4. Both airfoils have the same thickness distributions and camber line shapes, but the airfoil on the right has twice as much camber as the one on the left (corresponding to 4 per cent chord, versus 2 per cent for the airfoil on the left). The several curves correspond to Reynolds numbers ranging from $\mathbf{Re} = 3 \times 10^6$ to $\mathbf{Re} = 9 \times 10^6$, with the curves having larger values of $\mathbf{c}_{\ell_{\max}}$ corresponding to the higher Reynolds numbers. The outlying curves in the plot on the right correspond to data taken with a 20 per cent chord split flap deflected (and are not of interest here).

Note that these data are generally consistent with the results of thin-airfoil theory. In particular:

1. The lift-curve slopes are within about 95 per cent of the value of $a_0 = 2\pi$ over a significant range of angles of attack. Note that the angles of attack in Fig. 2.4 are in degrees, whereas the $a_0 = 2\pi$ is *per radian*;

2. The angle for zero lift of the section having the larger camber is approximately twice that of the section having the smaller camber; and

3. The moment coefficients measured about the quarter-chord point are very nearly independent of angle of attack, and are roughly twice as large for the airfoil having the larger camber.

2.4 Aerodynamic properties of finite wings

The vortex structures trailing downstream of a finite wing produce an induced downwash field near the wing which can be characterized by an *induced angle of attack*

$$\alpha_i = \frac{\mathbf{C}_L}{\pi e \mathbf{AR}} \tag{2.16}$$

For a straight (un-swept) wing with an elliptical spanwise loading, lifting-line theory predicts that the induced angle of attack α_i is constant across the span of the wing, and the *efficiency factor* $e = 1.0$. For non-elliptical span loadings, $e < 1.0$, but for most practical wings α_i is still nearly constant across the span. Thus, for a finite wing lifting-line theory predicts that

$$\mathbf{C}_L = a_0 \left(\alpha - \alpha_0 - \alpha_i\right) \tag{2.17}$$

where a_0 is the wing section lift-curve slope and α_0 is the angle for zero lift of the section. Substituting Eq. (2.16) and solving for the lift coefficient gives

$$\mathbf{C}_L = \frac{a_0}{1 + \frac{a_0}{\pi e \mathbf{AR}}}(\alpha - \alpha_0) = a(\alpha - \alpha_0) \tag{2.18}$$

whence the *wing* lift-curve slope is given by

$$a = \frac{\partial \mathbf{C}_L}{\partial \alpha} = \frac{a_0}{1 + \frac{a_0}{\pi e \mathbf{AR}}} \tag{2.19}$$

Lifting-line theory is asymptotically correct in the limit of large aspect ratio, so, in principle, Eq. (2.18) is valid only in the limit as $\mathbf{AR} \to \infty$. At the same time, slender-body theory is valid in the limit of vanishingly small aspect ratio, and it predicts, independently of planform shape, that the lift-curve slope is

$$a = \frac{\pi \mathbf{AR}}{2} \tag{2.20}$$

Note that this is one-half the value predicted by the limit of the lifting-line result, Eq. (2.19), as the aspect ratio goes to zero. We can construct a single empirical formula that contains the correct limits for both large and small aspect ratio of the form

$$a = \frac{\pi \mathbf{AR}}{1 + \sqrt{1 + \left(\frac{\pi \mathbf{AR}}{a_0}\right)^2}} \tag{2.21}$$

A plot of this equation, and of the lifting-line and slender-body theory results, is shown in Fig. 2.5.

Equation (2.21) can also be modified to account for wing sweep and the effects of compressibility. If the sweep of the quarter-chord line of the planform is $\Lambda_{c/4}$, the effective section incidence is increased by the factor $1/\cos\Lambda_{c/4}$, relative to that of the wing,[1] while the dynamic pressure of the flow normal to the quarter-chord line is reduced by the factor $\cos^2\Lambda_{c/4}$. The section lift-curve slope is thus reduced by the factor $\cos\Lambda_{c/4}$, and a version of Eq. (2.21) that accounts for sweep can be written

$$a = \frac{\pi \mathbf{AR}}{1 + \sqrt{1 + \left(\frac{\pi \mathbf{AR}}{a_0 \cos\Lambda_{c/4}}\right)^2}} \tag{2.22}$$

[1] This factor can best be understood by interpreting a change in angle of attack as a change in vertical velocity $\Delta w = V_\infty \, \Delta\alpha$.

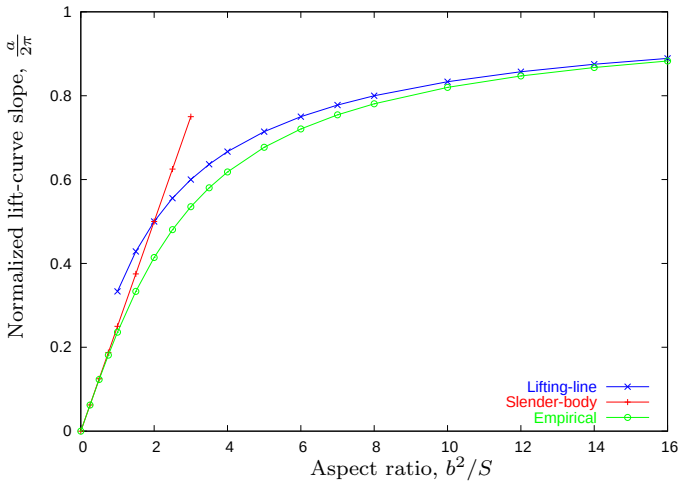

Figure 2.5: Empirical formula for lift-curve slope of a finite wing compared with lifting-line and slender-body limits. Plot is constructed assuming $a_0 = 2\pi$.

Finally, for subcritical ($\mathbf{M}_\infty < \mathbf{M}_{\text{crit}}$) flows, the Prandtl-Glauert similarity law for airfoil sections gives

$$a_{2\text{d}} = \frac{a_0}{\sqrt{1 - \mathbf{M}_\infty^2}} \tag{2.23}$$

where $\mathbf{M}_\infty$ is the flight Mach number. The Goethert similarity rule for three-dimensional wings modifies Eq. (2.22) to the form

$$a = \frac{\pi \mathbf{AR}}{1 + \sqrt{1 + \left(\frac{\pi \mathbf{AR}}{a_0 \cos \Lambda_{c/4}}\right)^2 \left(1 - \mathbf{M}_\infty^2 \cos^2 \Lambda_{c/4}\right)}} \tag{2.24}$$

In Eqs. (2.22), (2.23) and (2.24), a_0 is, as earlier, the incompressible, two-dimensional value of the lift-curve slope (often approximated as $a_0 = 2\pi$). Note that, according to Eq. (2.24) the lift-curve slope increases with increasing Mach number, but not as fast as the two-dimensional Prandtl-Glauert rule suggests. Also, unlike the Prandtl-Glauert result, the transonic limit ($\mathbf{M}_\infty \cos \Lambda_{c/4} \to 1.0$) is finite and corresponds (correctly) to the slender-body limit.

So far we have described only the lift-curve slope $a = \partial \mathbf{C}_L / \partial \alpha$ for the finite wing, which is its most important parameter as far as stability is concerned. To determine trim, however, it is also important to know the value of the pitching moment at zero lift (which is, of course, also equal to the pitching moment about the aerodynamic center). We first determine the angle of attack for wing zero lift. From the sketch in Fig. 2.6, we see that the angle of attack measured at the wing root corresponding to zero lift at a given section can be written

$$-(\alpha_0)_{\text{root}} = \epsilon - \alpha_0 \tag{2.25}$$

where ϵ is the geometric twist at the section, relative to the root. The wing lift coefficient can then be expressed as

$$\mathbf{C}_L = \frac{2}{S} \int_0^{b/2} a \left[\alpha_r - (\alpha_0)_{\text{root}}\right] c \, \mathrm{d}y = \frac{2a}{S} \left[\frac{S}{2} \alpha_r + \int_0^{b/2} (\epsilon - \alpha_0) \, c \, \mathrm{d}y\right] \tag{2.26}$$

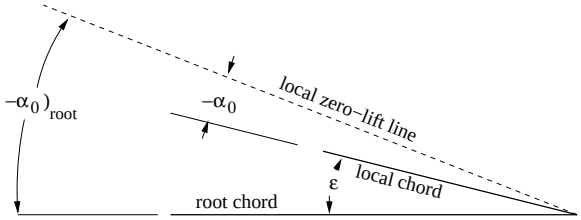

Figure 2.6: Root angle of attack corresponding to zero lift at a given section.

Setting the lift coefficient to zero and solving for the root angle of attack then yields

$$(\alpha_r)_{L=0} = \frac{2}{S}\int_0^{b/2} (\alpha_0 - \epsilon)\, c \,\mathrm{d}y \tag{2.27}$$

Now, the wing pitching moment about its aerodynamic center can be determined as the sum of contributions from the section values plus the contribution due to the *basic* lift distribution – i.e., the distribution of lifting forces at wing zero lift.[2]These contributions can be expressed as

$$\mathbf{C}_{mac} = \frac{2}{S\bar{c}}\left\{\int_0^{b/2} c^2 \left(\mathbf{C}_{mac}\right)_{\text{sect}} \,\mathrm{d}y + \int_0^{b/2} a\left[(\alpha_r)_{L=0} + \epsilon - \alpha_0\right] c x_1 \,\mathrm{d}y\right\} \tag{2.28}$$

where $x_1 = x_{ac} - x_{MAC}$ is the axial distance between the section aerodynamic center and the wing aerodynamic center. Consistent with these approximations, the wing aerodynamic center is located at the chord-weighted quarter-chord location for the wing; i.e.,

$$x_{MAC} = \frac{2}{S}\int_0^{b/2} x_{c/4} c \,\mathrm{d}y \tag{2.29}$$

Explicit expressions for this variable can be determined from Eqs. (2.12,2.13) for wings of trapezoidal planform.

2.5 Fuselage contribution to pitch stiffness

The contribution of the fuselage to the pitching moment is affected by interference effects with the wing flow field. These can be estimated using a simple strip theory (as described, for example, in Example 2.2 of the text by Nelson [4]), but here we will introduce a simple estimate for the destabilizing effect of the fuselage in the absence of interference effects.

Slender-body theory predicts a distribution of lifting force given by

$$\frac{\mathrm{d}L}{\mathrm{d}x} = 2Q\alpha\frac{\mathrm{d}S_f}{\mathrm{d}x} \tag{2.30}$$

where $S_f = \pi w^2/4$ is the equivalent cross-sectional area of the fuselage based on its width w as a function of the streamwise variable x. For a finite-length fuselage, Eq. (2.30) predicts positive lift on

[2]The basic lift distribution, of course, sums to zero lift, but is still capable of producing non-zero pitching moments when the wing is swept.

the forward part of the fuselage (where S_f is generally increasing), and negative lift on the rearward part (where S_f is generally decreasing), but the total lift is identically zero (since $S_f(0) = S_f(\ell_f) = 0$, where ℓ_f is the fuselage length).

Since the total lift acting on the fuselage is zero, the resulting force system is a pure couple, and the pitching moment will be the same, regardless of the reference point about which it is taken. Thus, e.g., taking the moment about the fuselage nose ($x = 0$), we have

$$M_f = -\int_0^{\ell_f} x \, \mathrm{d}L = -2Q\alpha \int_0^{\ell_f} x \, \mathrm{d}S_f = 2Q\alpha \int_0^{\ell_f} S_f \, \mathrm{d}x = 2Q\alpha\mathcal{V} \tag{2.31}$$

where $\mathcal{V}$ is the volume of the "equivalent" fuselage (i.e., the body having the same planform as the actual fuselage, but with circular cross-sections). The fuselage contribution to the vehicle pitching moment coefficient is then

$$\mathbf{C}_m = \frac{M_f}{QS\bar{c}} = \frac{2\mathcal{V}}{S\bar{c}}\alpha \tag{2.32}$$

and the corresponding pitch stiffness is

$$\mathbf{C}_{m\alpha} = \left(\frac{\partial \mathbf{C}_m}{\partial \alpha}\right)_{\text{fuse}} = \frac{2\mathcal{V}}{S\bar{c}} \tag{2.33}$$

Note that this is always positive – i.e., destabilizing.

2.6 Wing-tail interference

The one interference effect we will account for is that between the wing and the horizontal tail. Because the tail operates in the downwash field of the wing (for conventional, aft-tail configurations), the effective angle of attack of the tail is reduced. The reduction in angle of attack can be estimated to be

$$\varepsilon = \kappa \frac{\mathbf{C}_L}{\pi e \mathbf{AR}} \tag{2.34}$$

where $1 < \kappa < 2$. Note that $\kappa = 1$ corresponds to $\varepsilon = \alpha_i$, the induced angle of attack of the wing, while $\kappa = 2$ corresponds to the limit when the tail is far downstream of the wing. For stability considerations, it is the rate of change of tail downwash with angle of attack that is most important, and this can be estimated as

$$\frac{\mathrm{d}\varepsilon}{\mathrm{d}\alpha} = \frac{\kappa}{\pi e \mathbf{AR}} \left(\mathbf{C}_{L\alpha}\right)_{\text{wing}} \tag{2.35}$$

2.7 Control Surfaces

Aerodynamic control surfaces are usually trailing-edge flaps on lifting surfaces that can be deflected by control input from the pilot (or autopilot). Changes in camber line slope near the trailing edge of a lifting surface are very effective at generating lift. The lifting pressure difference due to trailing-edge flap deflection on a two-dimensional airfoil, calculated according to thin-airfoil theory, is plotted in Fig. 2.7 (a) for flap chord lengths of 10, 20, and 30 percent of the airfoil chord. The values plotted

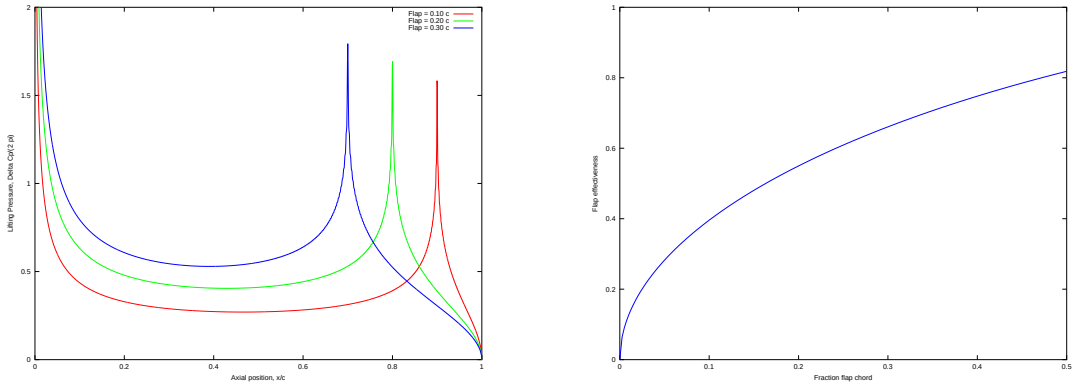

(a) Lifting pressure coefficient (b) Control effectiveness

Figure 2.7: Lifting pressure distribution due to flap deflection and resulting control effectiveness.

are per unit angular deflection, and normalized by 2π, so their integrals can be compared with the changes due to increments in angle of attack. Figure 2.7 (b) shows the *control effectiveness*

$$\frac{\partial \mathbf{C}_\ell}{\partial \delta} \tag{2.36}$$

also normalized by 2π. It is seen from this latter figure that deflection of a flap that consists of only 25 percent chord is capable of generating about 60 percent of the lift of the entire airfoil pitched through an angle of attack equal to that of the flap deflection. Actual flap effectiveness is, of course, reduced somewhat from these ideal values by the presence of viscous effects near the airfoil trailing edge, but the flap effectiveness is still nearly 50 percent of the lift-curve slope for a 25 percent chord flap for most actual flap designs.

The control forces required to change the flap angle are related to the aerodynamic moments about the hinge-line of the flap. The aerodynamic moment about the hinge line is usually expressed in terms of the dimensionless hinge moment coefficient, e.g., for the elevator hinge moment H_e, defined as

$$\mathbf{C}_{h_e} \equiv \frac{H_e}{\frac{1}{2}\rho V^2 S_e c_e} \tag{2.37}$$

where S_e and c_e are the elevator planform area and chord length, respectively; these are based on the area of the control surface aft of the hinge line.

The most important characteristics related to the hinge moments are the restoring tendency and the floating tendency. The *restoring tendency* is the derivative of the hinge moment coefficient with respect to control deflection; e.g., for the elevator,

$$\mathbf{C}_{h_{\delta_e}} = \frac{\partial \mathbf{C}_{h_e}}{\partial \delta_e} \tag{2.38}$$

The *floating tendency* is the derivative of the hinge moment coefficient with respect to angle of attack; e.g., for the elevator,

$$\mathbf{C}_{h_{e_{\alpha_t}}} = \frac{\partial \mathbf{C}_{h_e}}{\partial \alpha_t} \tag{2.39}$$

where α_t is the angle of attack of the tail.

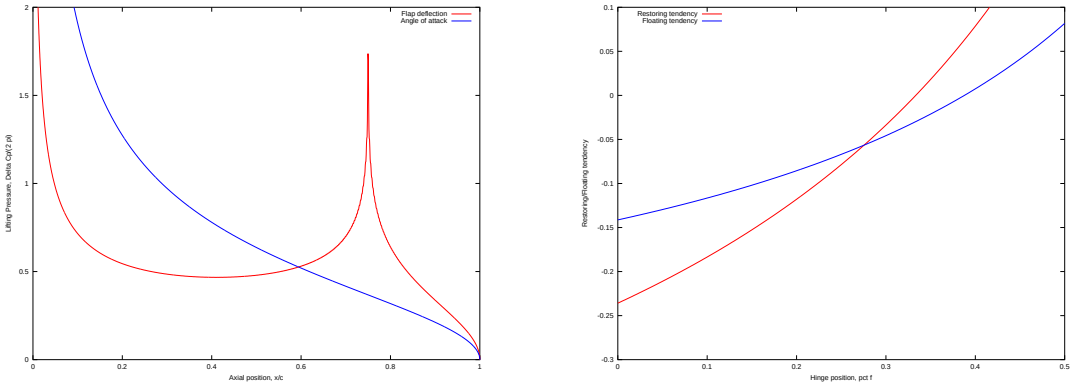

(a) Lifting pressure coefficient

(b) Hinge moment derivatives

Figure 2.8: Lifting pressure distributions (normalized by 2π) due to flap deflection and to change in angle of attack, and resulting restoring and floating tendencies of control flap. Results of thin-airfoil theory for 25 percent chord trailing-edge flap.

The restoring and floating tendencies are due primarily to the moments produced about the control flap hinge line by the lifting pressures induced by changes in either control position or angle of attack. The thin-airfoil approximations to these lifting pressure distributions are illustrated in Fig. 2.8 (a) for a 25 percent chord trailing edge flap. The plotted values of $\mathbf{\Delta C}_p$ are normalized by 2π, so the average value of the $\mathbf{\Delta C}_p$ due to angle of attack change is unity (corresponding to a lift curve slope of 2π). Figure 2.8 (b) illustrates the corresponding floating and restoring tendencies as functions of the hinge line location, measured in fraction of flap chord. It is seen that both tendencies are negative for hinge lines located ahead of approximately the 33 percent flap chord station. While these results, based on inviscid, thin-airfoil theory are qualitatively correct, actual hinge moment coefficients are affected by viscous effects and leakage of flow between the flap and the main lifting surface, so the results presented here should be used only as a guide to intuition.

Bibliography

[1] Ira H. Abbott & Albert E. von Doenhoff, **Theory of Wing Sections; Including a Summary of Data**, Dover, New York, 1958.

[2] Holt Ashley & Marten Landahl, **Aerodynamics of Wings and Bodies**, Addison-Wesley, Reading, Massachusetts, 1965.

[3] Bernard Etkin & Lloyd D. Reid, **Dynamics of Flight; Stability and Control**, John Wiley & Sons, New York, Third Edition, 1998.

[4] Robert C. Nelson, **Flight Stability and Automatic Control**, McGraw-Hill, New York, Second Edition, 1998.

[5] Edward Seckel, **Stability and Control of Airplanes and Helicopters**, Academic Press, New York, 1964.

[6] Richard Shevell, **Fundamentals of Flight**, Prentice Hall, Englewood Cliffs, New Jersey, Second Edition, 1989.

Chapter 3

Static Longitudinal Stability and Control

The most critical aspects of static longitudinal stability relate to control forces required for changing trim or performing maneuvers. Our textbook [1] treats primarily the situation when the controls are fixed. This is, of course, and idealization, even for the case of powered, irreversible controls, as the position of the control surfaces can he held fixed only to the extent of the maximum available control forces. The opposite limit – that of free control surfaces – also is an idealization, limited by the assumptions of zero friction in the control positioning mechanisms. But, just as the control fixed limit is useful in determining control *position* gradients, the control free limit is useful in determining control *force* gradients. And these latter are among the most important vehicle properties in determining handling qualities.

3.1 Control Fixed Stability

Even for the controls-fixed case, our text is a bit careless with nomenclature and equations, so we review the most important results for this case here. We have seen that for the analysis of longitudinal stability, terms involving products of the drag coefficient and either vertical displacements of the vehicle center-of-gravity or sines of the angle of attack can be neglected. Then, with the axial locations as specified in Fig. 3.1 the pitching moment about the vehicle c.g. can be written

$$\mathbf{C}_{mcg} = \mathbf{C}_{m0_w} + \mathbf{C}_{Lw}\left(\frac{x_{\rm cg}}{\bar{c}} - \frac{x_{\rm ac}}{\bar{c}}\right) - \eta\frac{S_t}{S}\mathbf{C}_{Lt}\left[\frac{\ell_t}{\bar{c}} - \left(\frac{x_{\rm cg}}{\bar{c}} - \frac{x_{\rm ac}}{\bar{c}}\right)\right] + \mathbf{C}_{mf} \tag{3.1}$$

where we assume that $\mathbf{C}_{m0_t} = 0$, since the tail is usually symmetrical. Note that, as is the usual convention when analyzing *static* longitudinal stability and control, the positive direction of the x-axis is taken to be *aft*;[1]thus, e.g., the second term on the right-hand side of Eq. (3.1) contributes to a positive (nose-up) pitching moment for positive lift when the c.g. is aft of the wing aerodynamic center.

[1]Also, the origin of the x-axis is taken, by convention, to be at the leading edge of the mean aerodynamic chord of the wing, and distances are normalized by the length of the wing mean aerodynamic chord. Thus, for example, we might specify the location of the vehicle center-of-gravity as being at *30 per cent m.a.c.*

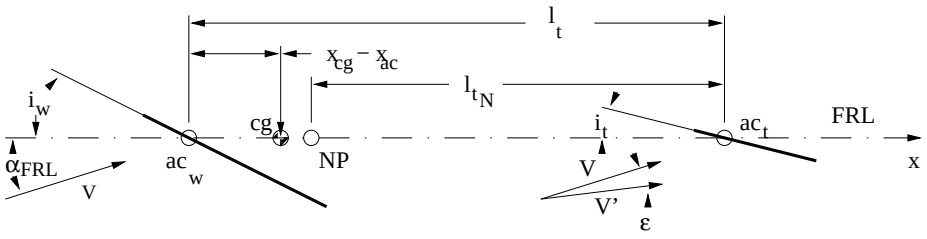

Figure 3.1: Geometry of wing and tail with respect to vehicle c.g., basic neutral point, and wing aerodynamic center. Note that positive direction of the x-axis is aft.

Grouping the terms involving the c.g. location, this equation can be written

$$\mathbf{C}_{m_{\mathrm{cg}}} = \mathbf{C}_{m0_w} + \left(\frac{x_{\mathrm{cg}}}{\bar{c}} - \frac{x_{\mathrm{ac}}}{\bar{c}}\right)\left[\mathbf{C}_{Lw} + \eta\frac{S_t}{S}\mathbf{C}_{Lt}\right] - \eta V_H \mathbf{C}_{Lt} + \mathbf{C}_{mf} \tag{3.2}$$

where $V_H = \frac{\ell_t S_t}{\bar{c}S}$ is the *tail volume parameter*. Note that this definition is based on the distance between the aerodynamic centers of the wing and tail, and is therefore independent of the vehicle c.g. location. Note that the total *vehicle* lift coefficient is

$$\mathbf{C}_L = \frac{L_w + L_t}{QS} = \mathbf{C}_{Lw} + \eta\frac{S_t}{S}\mathbf{C}_{Lt} \tag{3.3}$$

where $\eta = Q_t/Q$ is the tail efficiency factor, and this total vehicle lift coefficient is exactly the quantity appearing in the square brackets in Eq. (3.2). Now, we can introduce the dependence of the lift coefficients on angle of attack as

$$\begin{aligned}\mathbf{C}_{Lw} &= \mathbf{C}_{L\alpha_w}\left(\alpha_{FRL} + i_w - \alpha_{0_w}\right)\\ \mathbf{C}_{Lt} &= \mathbf{C}_{L\alpha_t}\left(\alpha_{FRL} + i_t - \left[\varepsilon_0 + \frac{\mathrm{d}\varepsilon}{\mathrm{d}\alpha}\alpha_{FRL}\right]\right)\end{aligned} \tag{3.4}$$

Note that, consistent with the usual use of symmetric sections for the horizontal tail, we have assumed $\alpha_{0_t} = 0$. Introducing these expressions into Eq. (3.3), the latter can be expressed as

$$\mathbf{C}_L = \mathbf{C}_{L\alpha_w}\left(i_w - \alpha_{0_w}\right) + \eta\frac{S_t}{S}\mathbf{C}_{L\alpha_t}\left(i_t - \varepsilon_0\right) + \left(\mathbf{C}_{L\alpha_w} + \eta\frac{S_t}{S}\left[1 - \frac{\mathrm{d}\varepsilon}{\mathrm{d}\alpha}\right]\mathbf{C}_{L\alpha_t}\right)\alpha_{FRL} \tag{3.5}$$

This equation has the form

$$\mathbf{C}_L = \mathbf{C}_{L0} + \mathbf{C}_{L\alpha}\alpha_{FRL} \tag{3.6}$$

where the *vehicle* lift curve slope is

$$\mathbf{C}_{L\alpha} = \mathbf{C}_{L\alpha_w} + \eta\frac{S_t}{S}\left(1 - \frac{\mathrm{d}\varepsilon}{\mathrm{d}\alpha}\right)\mathbf{C}_{L\alpha_t} \tag{3.7}$$

and

$$\mathbf{C}_{L0} = \mathbf{C}_{L\alpha_w}\left(i_w - \alpha_{0_w}\right) + \eta\frac{S_t}{S}\mathbf{C}_{L\alpha_t}\left(i_t - \varepsilon_0\right) \tag{3.8}$$

is the vehicle lift coefficient at zero (fuselage reference line) angle of attack. Finally, if we define the vehicle angle of attack relative to the angle of attack for zero *vehicle* lift, i.e.,

$$\alpha \equiv \alpha_{FRL} - \alpha_0 \tag{3.9}$$

where

$$\alpha_0 = -\frac{\mathbf{C}_{L0}}{\mathbf{C}_{L\alpha}} \tag{3.10}$$

then

$$\mathbf{C}_L = \mathbf{C}_{L\alpha}\alpha \tag{3.11}$$

where $\mathbf{C}_{L\alpha}$ is the vehicle lift curve slope, given by Eq. (3.7).

Introducing the angle of attack into Eq. (3.2), the expression for the vehicle pitching moment coefficient becomes

$$\begin{aligned}\mathbf{C}_{m\mathrm{cg}} =& \mathbf{C}_{m0_w} + \left(\frac{x_{\mathrm{cg}}}{\bar{c}} - \frac{x_{\mathrm{ac}}}{\bar{c}}\right)\left[\mathbf{C}_{L\alpha_w}\left(i_w - \alpha_{0_w}\right) + \eta\frac{S_t}{S}\mathbf{C}_{L\alpha_t}\left(i_t - \varepsilon_0\right)\right] - \eta V_H \mathbf{C}_{L\alpha_t}\left(i_t - \varepsilon_0\right) + \\ & \left\{\left(\frac{x_{\mathrm{cg}}}{\bar{c}} - \frac{x_{\mathrm{ac}}}{\bar{c}}\right)\left[\mathbf{C}_{L\alpha_w} + \eta\frac{S_t}{S}\left(1 - \frac{\mathrm{d}\varepsilon}{\mathrm{d}\alpha}\right)\mathbf{C}_{L\alpha_t}\right] - \eta V_H\left(1 - \frac{\mathrm{d}\varepsilon}{\mathrm{d}\alpha}\right)\mathbf{C}_{L\alpha_t} + \mathbf{C}_{m\alpha_f}\right\}\alpha_{FRL}\end{aligned} \tag{3.12}$$

This can be expressed in terms of the angle of attack from zero vehicle lift as

$$\begin{aligned}\mathbf{C}_{m\mathrm{cg}} = \mathbf{C}_{m0_w} &+ \left(\frac{x_{\mathrm{cg}}}{\bar{c}} - \frac{x_{\mathrm{ac}}}{\bar{c}}\right)\left[\mathbf{C}_{L\alpha_w}\left(i_w - \alpha_{0_w}\right) + \eta\frac{S_t}{S}\mathbf{C}_{L\alpha_t}\left(i_t - \varepsilon_0\right)\right] - \eta V_H \mathbf{C}_{L\alpha_t}\left(i_t - \varepsilon_0\right) \\ &+ \mathbf{C}_{m\alpha}\alpha_0 + \left\{\left(\frac{x_{\mathrm{cg}}}{\bar{c}} - \frac{x_{\mathrm{ac}}}{\bar{c}}\right)\mathbf{C}_{L\alpha} - \eta V_H \mathbf{C}_{L\alpha_t}\left(1 - \frac{\mathrm{d}\varepsilon}{\mathrm{d}\alpha}\right) + \mathbf{C}_{m\alpha_f}\right\}\alpha\end{aligned} \tag{3.13}$$

This equation has the form

$$\mathbf{C}_m = \mathbf{C}_{m0} + \mathbf{C}_{m\alpha}\alpha \tag{3.14}$$

with the *vehicle* pitching moment coefficient at zero lift

$$\mathbf{C}_{m0} = \mathbf{C}_{m0_w} + \left(\frac{x_{\mathrm{cg}}}{\bar{c}} - \frac{x_{\mathrm{ac}}}{\bar{c}}\right)\left[\mathbf{C}_{L\alpha_w}\left(i_w - \alpha_{0_w}\right) + \eta\frac{S_t}{S}\mathbf{C}_{L\alpha_t}\left(i_t - \varepsilon_0\right)\right] - \eta V_H \mathbf{C}_{L\alpha_t}\left(i_t - \varepsilon_0\right) + \mathbf{C}_{m\alpha}\alpha_0 \tag{3.15}$$

and the vehicle pitch stiffness

$$\mathbf{C}_{m\alpha} = \left(\frac{x_{\mathrm{cg}}}{\bar{c}} - \frac{x_{\mathrm{ac}}}{\bar{c}}\right)\mathbf{C}_{L\alpha} - \eta V_H \mathbf{C}_{L\alpha_t}\left(1 - \frac{\mathrm{d}\varepsilon}{\mathrm{d}\alpha}\right) + \mathbf{C}_{m\alpha_f} \tag{3.16}$$

Note that Eq. (3.15) can be simplified (using Eq. (3.16)) to

$$\mathbf{C}_{m0} = \mathbf{C}_{m0_w} - \eta V_H \mathbf{C}_{L\alpha_t}\left[i_t - \varepsilon_0 + \left(1 - \frac{\mathrm{d}\varepsilon}{\mathrm{d}\alpha}\right)\alpha_0\right] + \mathbf{C}_{m\alpha_f}\alpha_0 \tag{3.17}$$

Note that Eq. (3.17) correctly shows that the pitching moment at zero net vehicle lift is independent of the c.g. location, as it must be (since at zero lift the resultant aerodynamic force must sum to a pure couple).

The basic (or control-fixed) *neutral point* is defined as the c.g. location for which the vehicle is neutrally stable in pitch – i.e., the c.g. location for which the pitch stiffness goes to zero. From Eq. (3.16) the neutral point is seen to be located at

$$\frac{x_{NP}}{\bar{c}} = \frac{x_{\mathrm{ac}}}{\bar{c}} + \eta V_H \frac{\mathbf{C}_{L\alpha_t}}{\mathbf{C}_{L\alpha}}\left(1 - \frac{\mathrm{d}\varepsilon}{\mathrm{d}\alpha}\right) - \frac{\mathbf{C}_{m\alpha_f}}{\mathbf{C}_{L\alpha}} \tag{3.18}$$

Note that Eq. (3.16) for the pitch stiffness can be expressed as

$$\mathbf{C}_{m\alpha} = \left\{ \frac{x_{\rm cg}}{\bar{c}} - \left[\frac{x_{\rm ac}}{\bar{c}} + \eta V_H \frac{\mathbf{C}_{L\alpha_t}}{\mathbf{C}_{L\alpha}} \left(1 - \frac{{\rm d}\varepsilon}{{\rm d}\alpha} \right) - \frac{\mathbf{C}_{m\alpha_f}}{\mathbf{C}_{L\alpha}} \right] \right\} \mathbf{C}_{L\alpha} \tag{3.19}$$

where the quantity in square brackets is exactly the location of the basic neutral point, as shown in Eq. (3.18). Thus, we can write

$$\mathbf{C}_{m\alpha} = \left\{ \frac{x_{\rm cg}}{\bar{c}} - \frac{x_{NP}}{\bar{c}} \right\} \mathbf{C}_{L\alpha} \tag{3.20}$$

or, alternatively,

$$\frac{\partial \mathbf{C}_m}{\partial \mathbf{C}_L} = -\left(\frac{x_{NP}}{\bar{c}} - \frac{x_{\rm cg}}{\bar{c}} \right) \tag{3.21}$$

Thus, the pitch stiffness, measured with respect to changes in vehicle lift coefficient, is proportional to the distance between the c.g. and the basic neutral point. The quantity in parentheses on the right-hand side of Eq. (3.21), i.e., the distance between the vehicle c.g. and the basic neutral point, expressed as a percentage of the wing mean aerodynamic chord, is called the vehicle *static margin*.[2]

3.2 Static Longitudinal Control

The elevator is the aerodynamic control for pitch angle of the vehicle, and its effect is described in terms of the *elevator effectiveness*

$$a_e = \frac{\partial \mathbf{C}_{Lt}}{\partial \delta_e} \tag{3.22}$$

where $\mathbf{C}_{Lt}$ is the lift coefficient of the horizontal tail and δ_e is the elevator deflection, considered positive trailing edge down. The horizontal tail lift coefficient is then given by

$$\mathbf{C}_{Lt} = \frac{\partial \mathbf{C}_{Lt}}{\partial \alpha_t} \left(\alpha + i_t - \varepsilon \right) + a_e \delta_e \tag{3.23}$$

and the change in *vehicle* lift coefficient due to elevator deflection is

$$\mathbf{C}_{L\delta_e} = \eta \frac{S_t}{S} a_e \tag{3.24}$$

while the change in vehicle pitching moment due to elevator deflection is

$$\begin{aligned} \mathbf{C}_{m\delta_e} &= -\eta \frac{S_t}{S} a_e \left[\frac{\ell_t}{\bar{c}} + \frac{x_{\rm ac} - x_{\rm cg}}{\bar{c}} \right] \\ &= -\mathbf{C}_{L\delta_e} \left[\frac{\ell_t}{\bar{c}} + \frac{x_{\rm ac} - x_{\rm cg}}{\bar{c}} \right] \end{aligned} \tag{3.25}$$

The geometry of the moment arm of the tail lift relative to the vehicle c.g. (which justifies the second term in Eq. (3.25)) is shown in Fig. 3.1.

The vehicle is in equilibrium (i.e., is trimmed) at a given lift coefficient $\mathbf{C}_{L\rm trim}$ when

$$\begin{aligned} \mathbf{C}_{L\alpha}\alpha + \mathbf{C}_{L\delta_e}\delta_e &= \mathbf{C}_{L\rm trim} \\ \mathbf{C}_{m\alpha}\alpha + \mathbf{C}_{m\delta_e}\delta_e &= -\mathbf{C}_{m0} \end{aligned} \tag{3.26}$$

[2] Again, it is worth emphasizing that the location of the basic neutral point, and other special c.g. locations to be introduced later, are usually described as fractional distances along the wing mean aerodynamic chord; e.g. we might say that the basic neutral point is located at 40 per cent m.a.c.

These two equations can be solved for the unknown angle of attack and elevator deflection to give

$$\begin{aligned} \alpha_{\text{trim}} &= \frac{-\mathbf{C}_{L\delta_e}\mathbf{C}_{m0} - \mathbf{C}_{m\delta_e}\mathbf{C}_{L\text{trim}}}{\Delta} \\ \delta_{\text{trim}} &= \frac{\mathbf{C}_{L\alpha}\mathbf{C}_{m0} + \mathbf{C}_{m\alpha}\mathbf{C}_{L\text{trim}}}{\Delta} \end{aligned} \tag{3.27}$$

where

$$\Delta = -\mathbf{C}_{L\alpha}\mathbf{C}_{m\delta_e} + \mathbf{C}_{m\alpha}\mathbf{C}_{L\delta_e} \tag{3.28}$$

Note that the parameter

$$\begin{aligned} \Delta &= -\mathbf{C}_{L\alpha}\mathbf{C}_{m\delta_e} + \mathbf{C}_{m\alpha}\mathbf{C}_{L\delta_e} \\ &= -\mathbf{C}_{L\alpha}\left[-\mathbf{C}_{L\delta_e}\left(\frac{\ell_t}{\bar{c}} + \frac{x_{\text{ac}} - x_{\text{cg}}}{\bar{c}}\right)\right] + \mathbf{C}_{L\alpha}\left(\frac{x_{\text{cg}} - x_{NP}}{\bar{c}}\right)\mathbf{C}_{L\delta_e} \\ &= \mathbf{C}_{L\alpha}\mathbf{C}_{L\delta_e}\left(\frac{\ell_t}{\bar{c}} + \frac{x_{\text{ac}} - x_{NP}}{\bar{c}}\right) = \mathbf{C}_{L\alpha}\mathbf{C}_{L\delta_e}\frac{\ell_{t_N}}{\bar{c}} \end{aligned} \tag{3.29}$$

where

$$\ell_{t_N} = \ell_t + x_{\text{ac}} - x_{NP} \tag{3.30}$$

is the distance from the basic neutral point to the tail aerodynamic center. Thus, the parameter Δ is independent of the vehicle c.g. location, and is seen to be positive for conventional (aft tail) configurations, and negative for canard (forward tail) configurations.

An important derivative related to handling qualities is the control position gradient for trim, which can be seen from the second of Eqs. (3.27) to be given by

$$\left.\frac{\mathrm{d}\delta_e}{\mathrm{d}\mathbf{C}_L}\right)_{\text{trim}} = \frac{\mathbf{C}_{m\alpha}}{\Delta} \tag{3.31}$$

It is seen from Eq. (3.31) that the control position gradient, which measures the sensitivity of trimmed lift coefficient to control position, is negative for stable, aft tail configurations, and is proportional to the static margin (since Δ is independent of c.g. location and $\mathbf{C}_{m\alpha}$ is directly proportional to the static margin). In fact, using Eq. 3.29, we can see that

$$\left.\frac{\mathrm{d}\delta_e}{\mathrm{d}\mathbf{C}_L}\right)_{\text{trim}} = \frac{-1}{\mathbf{C}_{L\delta_e}}\frac{x_{NP} - x_{\text{c.g.}}}{\ell_{t_N}} \tag{3.32}$$

Thus, the control position gradient is seen to be determined by the static margin, normalized by ℓ_{t_N}, scaled by the effectiveness of the control deflection at generating lift $\mathbf{C}_{L\delta_e}$.

These results can be used in flight tests to determine the location of the basic neutral point. For each of several different c.g. positions the value of lift coefficient $\mathbf{C}_L$ is determined as a function of control position (as indicated by the data points in Fig. 3.2 (a).) For each c.g. location the value of the control position gradient is estimated by the best straight-line fit through these data, and is then plotted as a function of c.g. location. A best-fit straight line to these data, illustrated in Fig. 3.2 (b), is then extrapolated to zero control position gradient, which corresponds to the basic neutral point.

3.2.1 Longitudinal Maneuvers – the Pull-up

Another important criterion for vehicle handling qualities is the sensitivity of vehicle normal acceleration to control input. This can be analyzed by considering the vehicle in a steady pull-up. This

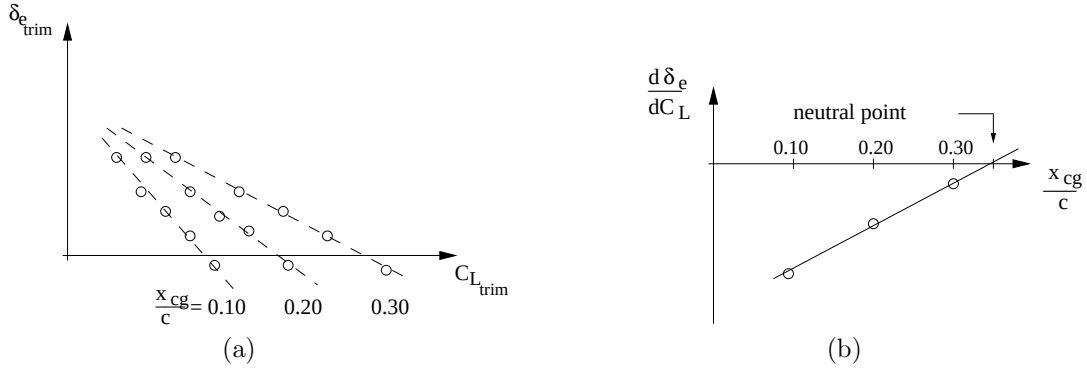

Figure 3.2: Schematic of procedure to estimate the location of the basic neutral point using control position gradient, measured in flight-test.

is a longitudinal maneuver in which the vehicle follows a curved flight path of constant radius R at constant angle of attack, as sketched in Fig. 3.3. For this maneuver, the pitch rate q is constant, and is given by

$$q = \frac{V}{R} \tag{3.33}$$

We define the dimensionless pitch rate

$$\hat{q} = \frac{q}{\frac{2V}{\bar{c}}} = \frac{\bar{c}q}{2V} \tag{3.34}$$

and will need to estimate the additional stability derivatives

$$\mathbf{C}_{Lq} \equiv \frac{\partial \mathbf{C}_L}{\partial \hat{q}} \tag{3.35}$$

and

$$\mathbf{C}_{mq} \equiv \frac{\partial \mathbf{C}_m}{\partial \hat{q}} \tag{3.36}$$

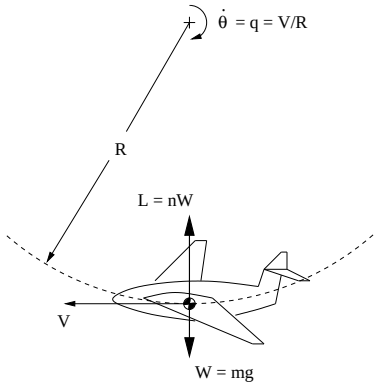

Figure 3.3: Schematic of flight path and forces acting on vehicle in a steady pull-up.

These derivatives characterize the sensitivity of vehicle lift and pitching moment to pitch rate. For vehicles with tails (either aft or canard), the largest contribution to these derivatives comes from the increment in tail lift due to the change in angle of attack of the tail arising from the rotation rate. This change in angle of attack is approximately[3]

$$\Delta\alpha_t = \frac{\ell_t}{V} q = \frac{2\ell_t}{\bar{c}} \hat{q} \tag{3.37}$$

and the resulting change in vehicle lift coefficient is

$$\Delta \mathbf{C}_L = \eta \frac{S_t}{S} \frac{\partial \mathbf{C}_{Lt}}{\partial \alpha_t} \Delta\alpha_t = 2\eta V_H \frac{\partial \mathbf{C}_{Lt}}{\partial \alpha_t} \hat{q} \tag{3.38}$$

so

$$\mathbf{C}_{Lq} = 2\eta V_H \frac{\partial \mathbf{C}_{Lt}}{\partial \alpha_t} \tag{3.39}$$

This increment in tail lift acts through the moment arm ℓ_t, so the corresponding estimate for the tail contribution to pitch damping is

$$\mathbf{C}_{mq} = -\frac{\ell_t}{\bar{c}} \mathbf{C}_{Lq} = -2\eta \frac{\ell_t}{\bar{c}} V_H \frac{\partial \mathbf{C}_{Lt}}{\partial \alpha_t} \tag{3.40}$$

The fuselage and wing (especially if the wing is swept) also contribute to the vehicle pitch damping, but it is difficult to develop simple formulas of general applicability, so these contributions will be neglected here. It should be noted that the tail contribution to pitch damping is sometimes multiplied by the factor 1.1 to account, at least approximately, for the contributions of other components. Finally, note that the derivative $\mathbf{C}_{Lq}$ will be positive for aft tail configurations (and negative for canard configurations), but the pitch damping $\mathbf{C}_{mq}$ will be always be negative, regardless of whether the tail is ahead or behind the vehicle center of gravity.

We analyze the motion at the point on the trajectory when the velocity vector is horizontal, so the balance of forces acting at the vehicle c.g. is

$$L - W = m\frac{V^2}{R} = mVq = \frac{2mV^2}{\bar{c}} \hat{q} \tag{3.41}$$

This equation can be written as

$$QS\left\{\mathbf{C}_{L\alpha}(\alpha + \Delta\alpha) + \mathbf{C}_{L\delta_e}(\delta_e + \Delta\delta_e) + \mathbf{C}_{Lq}\hat{q}\right\} - W = \frac{2mV^2}{\bar{c}} \hat{q} \tag{3.42}$$

where α and δ_e are the angle of attack and elevator deflection for trim in the unaccelerated case, and $\Delta\alpha$ and $\Delta\delta_e$ correspond to the increments in these angles due to the maneuver. If we introduce the *weight coefficient*

$$\mathbf{C}_W \equiv \frac{W/S}{Q} \tag{3.43}$$

the dimensionless form of this equation can be written

$$\left\{\mathbf{C}_{L\alpha}(\alpha + \Delta\alpha) + \mathbf{C}_{L\delta_e}(\delta_e + \Delta\delta_e) + \mathbf{C}_{Lq}\hat{q}\right\} - \mathbf{C}_W = 2\mu\hat{q} \tag{3.44}$$

where

$$\mu \equiv \frac{2m}{\rho S \bar{c}} \tag{3.45}$$

[3]Here, and in the equations through Eq. (3.40), the distance ℓ_t should represent the distance from the vehicle center-of-gravity to the aerodynamic center of the tail. The distance ℓ_t is a good approximation so long as the c.g. is near the wing aerodynamic center, which is usually the case.

is the vehicle *relative mass parameter*, which depends on ρ, the local fluid (air) density. As a result of this dependence on air density, the relative mass parameter is a function of flight altitude.

Subtracting the equilibrium values for the unaccelerated case

$$\mathbf{C}_{L\alpha}\alpha + \mathbf{C}_{L\delta_e}\delta_e - \mathbf{C}_W = 0 \tag{3.46}$$

from Eq. (3.44) gives

$$\mathbf{C}_{L\alpha}\Delta\alpha + \mathbf{C}_{L\delta_e}\Delta\delta_e = \left(2\mu - \mathbf{C}_{Lq}\right)\hat{q} \tag{3.47}$$

Finally, if we introduce the *normal acceleration parameter* n such that $L = nW$, then the force balance of Eq. (3.41) can be written in the dimensionless form

$$(n-1)\mathbf{C}_W = 2\mu\hat{q} \tag{3.48}$$

which provides a direct relation between the normal acceleration and the pitch rate, so that the lift equilibrium equation can be written

$$\mathbf{C}_{L\alpha}\Delta\alpha + \mathbf{C}_{L\delta_e}\Delta\delta_e = (n-1)\mathbf{C}_W\left(1 - \frac{\mathbf{C}_{Lq}}{2\mu}\right) \tag{3.49}$$

The pitching moment must also remain zero for equilibrium (since $\dot{q} = 0$), so

$$\mathbf{C}_{m\alpha}\Delta\alpha + \mathbf{C}_{m\delta_e}\Delta\delta_e + \mathbf{C}_{mq}\hat{q} = 0 \tag{3.50}$$

or

$$\mathbf{C}_{m\alpha}\Delta\alpha + \mathbf{C}_{m\delta_e}\Delta\delta_e = -\mathbf{C}_{mq}\frac{(n-1)\mathbf{C}_W}{2\mu} \tag{3.51}$$

Equations (3.49) and (3.51) provide two equations that can be solved for the unknowns $\Delta\alpha$ and $\Delta\delta_e$ to give

$$\begin{aligned}
\Delta\alpha &= \frac{-(n-1)\mathbf{C}_W}{\Delta}\left[\left(1 - \frac{\mathbf{C}_{Lq}}{2\mu}\right)\mathbf{C}_{m\delta_e} + \frac{\mathbf{C}_{mq}}{2\mu}\mathbf{C}_{L\delta_e}\right] \\
\Delta\delta_e &= \frac{(n-1)\mathbf{C}_W}{\Delta}\left[\left(1 - \frac{\mathbf{C}_{Lq}}{2\mu}\right)\mathbf{C}_{m\alpha} + \frac{\mathbf{C}_{mq}}{2\mu}\mathbf{C}_{L\alpha}\right]
\end{aligned} \tag{3.52}$$

where

$$\Delta = -\mathbf{C}_{L\alpha}\mathbf{C}_{m\delta_e} + \mathbf{C}_{m\alpha}\mathbf{C}_{L\delta_e} \tag{3.53}$$

is the same parameter as earlier (in Eq. (3.28)).

The control position derivative for normal acceleration is therefore given by

$$\frac{\mathrm{d}\delta_e}{\mathrm{d}n} = \frac{\mathbf{C}_W}{\Delta}\left[\left(1 - \frac{\mathbf{C}_{Lq}}{2\mu}\right)\mathbf{C}_{m\alpha} + \frac{\mathbf{C}_{mq}}{2\mu}\mathbf{C}_{L\alpha}\right] \tag{3.54}$$

Using Eq. (3.20) to express the pitch stiffness in terms of the c.g. location, we have

$$\frac{\mathrm{d}\delta_e}{\mathrm{d}n} = \frac{\mathbf{C}_W}{\Delta}\left[\left(1 - \frac{\mathbf{C}_{Lq}}{2\mu}\right)\left(\frac{x_{\mathrm{cg}}}{\bar{c}} - \frac{x_{NP}}{\bar{c}}\right) + \frac{\mathbf{C}_{mq}}{2\mu}\right]\mathbf{C}_{L\alpha} \tag{3.55}$$

The c.g. location for which this derivative vanishes is called the *basic maneuver point*, and its location, relative to the basic neutral point, is seen to be given by

$$\frac{x_{NP}}{\bar{c}} - \frac{x_{MP}}{\bar{c}} = \frac{\frac{\mathbf{C}_{mq}}{2\mu}}{1 - \frac{\mathbf{C}_{Lq}}{2\mu}} \approx \frac{\mathbf{C}_{mq}}{2\mu} \tag{3.56}$$

Since for all configurations the pitch damping $\mathbf{C}_{mq} < 0$, the maneuver point is aft of the neutral point. Also, since the vehicle relative mass parameter μ increases with altitude, the maneuver point approaches the neutral point with increasing altitude. If Eq. (3.56) is used to eliminate the variable x_{NP} from Eq. (3.55), we have

$$\frac{\mathrm{d}\delta_e}{\mathrm{d}n} = -\frac{\mathbf{C}_W \mathbf{C}_{L\alpha}}{\Delta}\left(1 - \frac{\mathbf{C}_{Lq}}{2\mu}\right)\left(\frac{x_{MP}}{\bar{c}} - \frac{x_{\mathrm{cg}}}{\bar{c}}\right) \tag{3.57}$$

where

$$\left(\frac{x_{MP}}{\bar{c}} - \frac{x_{\mathrm{cg}}}{\bar{c}}\right) \tag{3.58}$$

is called the *maneuver margin*.

3.3 Control Surface Hinge Moments

Just as the control *position* gradient is related to the pitch stiffness of the vehicle when the controls are fixed, the control *force* gradients are related to the pitch stiffness of the vehicle when the controls are allowed to float free.

3.3.1 Control Surface Hinge Moments

Since elevator deflection corresponds to rotation about a hinge line, the forces required to cause a specific control deflection are related to the aerodynamic moments about the hinge line. A free control will float, in the static case, to the position at which the elevator hinge moment is zero:

$$H_e = 0.$$

The elevator hinge moment is usually expressed in terms of the *hinge moment coefficient*

$$\mathbf{C}_{he} = \frac{H_e}{QS_e\bar{c}_e} \tag{3.59}$$

where the reference area S_e and moment arm $\bar{c}_e$ correspond to the planform area and mean chord of the control surface aft of the hinge line. Note that the elevator hinge moment coefficient is defined relative to Q, not Q_t. While it would seem to make more sense to use Q_t, hinge moments are sufficiently difficult to predict that they are almost always determined from experiments in which the tail efficiency factor is effectively included in the definition of $\mathbf{C}_{he}$ (rather than explicitly isolated in a separate factor).

Assuming that the hinge moment is a linear function of angle of attack, control deflection, etc., we write

$$\mathbf{C}_{he} = \mathbf{C}_{he_0} + \mathbf{C}_{h\alpha}\alpha + \mathbf{C}_{h\delta_e}\delta_e + \mathbf{C}_{h\delta_t}\delta_t \tag{3.60}$$

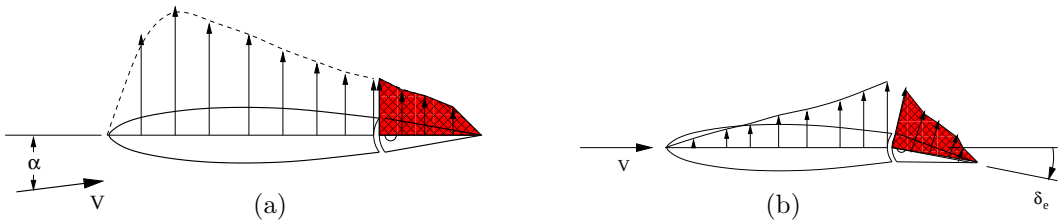

Figure 3.4: Schematic illustration of aerodynamic forces responsible for (a) floating and (b) restoring tendencies of trailing edge control surfaces. Floating (or restoring) tendency represents moment about hinge line of (shaded) lift distribution acting on control surface per unit angle of attack (or control deflection).

In this equation, α is the angle of attack (from angle for zero vehicle lift), δ_e is the elevator deflection, and δ_t is the deflection of the *control tab* (to be described in greater detail later).

The derivative $\mathbf{C}_{h_\alpha}$ characterizes the hinge moment created by changes in angle of attack; it is called the *floating tendency*, as the hinge moment generated by an increase in angle of attack generally causes the control surface to float upward. The derivative $\mathbf{C}_{h_{\delta_e}}$ characterizes the hinge moment created by a deflection of the control (considered positive trailing edge down); it is called the *restoring tendency*, as the nose-down hinge moment generated by a positive control deflection tends to restore the control to its original position. The floating tendency in Eq. (3.60) is referred to the vehicle angle of attack, and so it is related to the derivative based on tail angle of attack α_t by

$$\mathbf{C}_{h_\alpha} = \left(1 - \frac{\mathrm{d}\epsilon}{\mathrm{d}\alpha}\right) \mathbf{C}_{h_{\alpha_t}} \tag{3.61}$$

which accounts for the effects of wing induced downwash at the tail. The aerodynamic forces responsible for generating the hinge moments reflected in the floating and restoring tendencies are sketched in Fig. 3.4. Only the shaded portion of the lift distribution in these figures acts on the control surface and contributes to the hinge moment.

The angle at which the free elevator floats is determined by the fact that the hinge moment (and, therefore, the hinge moment coefficient) must be zero

$$\mathbf{C}_{he} = 0 = \mathbf{C}_{he_0} + \mathbf{C}_{h\alpha}\alpha + \mathbf{C}_{h\delta_e}\delta_{e\text{free}} + \mathbf{C}_{h\delta_t}\delta_t$$

or

$$\delta_{e\text{free}} = -\frac{1}{\mathbf{C}_{h\delta_e}} \left(\mathbf{C}_{he_0} + \mathbf{C}_{h\alpha}\alpha + \mathbf{C}_{h\delta_t}\delta_t\right) \tag{3.62}$$

The corresponding lift and moment coefficients are

$$\begin{aligned} \mathbf{C}_{L\text{free}} &= \mathbf{C}_{L\alpha}\alpha + \mathbf{C}_{L\delta_e}\delta_{e\text{free}} \\ \mathbf{C}_{m\text{free}} &= \mathbf{C}_{m0} + \mathbf{C}_{m\alpha}\alpha + \mathbf{C}_{m\delta_e}\delta_{e\text{free}} \end{aligned} \tag{3.63}$$

which, upon substituting from Eq. (3.62), can be written

$$\begin{aligned} \mathbf{C}_{L\text{free}} &= \mathbf{C}_{L\alpha}\left(1 - \frac{\mathbf{C}_{L\delta_e}\mathbf{C}_{h\alpha}}{\mathbf{C}_{L\alpha}\mathbf{C}_{h\delta_e}}\right)\alpha - \frac{\mathbf{C}_{L\delta_e}}{\mathbf{C}_{h\delta_e}}\left(\mathbf{C}_{he_0} + \mathbf{C}_{h\delta_t}\delta_t\right) \\ \mathbf{C}_{m\text{free}} &= \mathbf{C}_{m\alpha}\left(1 - \frac{\mathbf{C}_{m\delta_e}\mathbf{C}_{h\alpha}}{\mathbf{C}_{m\alpha}\mathbf{C}_{h\delta_e}}\right)\alpha + \mathbf{C}_{m0} - \frac{\mathbf{C}_{m\delta_e}}{\mathbf{C}_{h\delta_e}}\left(\mathbf{C}_{he_0} + \mathbf{C}_{h\delta_t}\delta_t\right) \end{aligned} \tag{3.64}$$

Thus, if we denote the control free lift curve slope and pitch stiffness using primes, we see from the above equations that

$$\begin{aligned} \mathbf{C}_{L_\alpha}{}' &= \mathbf{C}_{L\alpha}\left(1 - \frac{\mathbf{C}_{L\delta_e}\mathbf{C}_{h\alpha}}{\mathbf{C}_{L\alpha}\mathbf{C}_{h\delta_e}}\right) \\ \mathbf{C}_{m_\alpha}{}' &= \mathbf{C}_{m\alpha}\left(1 - \frac{\mathbf{C}_{m\delta_e}\mathbf{C}_{h\alpha}}{\mathbf{C}_{m\alpha}\mathbf{C}_{h\delta_e}}\right) \end{aligned} \tag{3.65}$$

Inspection of these equations shows that the lift curve slope is always reduced by freeing the controls, and the pitch stiffness of a stable configuration is reduced in magnitude by freeing the controls for an aft tail configuration, and increased in magnitude for a forward tail (canard) configuration (in all cases assuming that the floating and restoring tendencies both are negative).

3.3.2 Control free Neutral Point

The c.g. location at which the control free pitch stiffness vanishes is called the *control free neutral point*. The location of the control free neutral point x'_{NP} can be determined by expressing the pitch stiffness in the second of Eqs. (3.65)

$$\mathbf{C}_{m_\alpha}{}' = \mathbf{C}_{m\alpha} - \frac{\mathbf{C}_{m\delta_e}\mathbf{C}_{h\alpha}}{\mathbf{C}_{h\delta_e}}$$

as

$$\begin{aligned} \mathbf{C}_{m_\alpha}{}' &= \left(\frac{x_{\rm cg}}{\bar{c}} - \frac{x_{NP}}{\bar{c}}\right)\mathbf{C}_{L\alpha} + \frac{\mathbf{C}_{h\alpha}\mathbf{C}_{L\delta_e}}{\mathbf{C}_{h\delta_e}}\left(\frac{\ell_t}{\bar{c}} + \frac{x_{\rm ac}}{\bar{c}} - \frac{x_{\rm cg}}{\bar{c}}\right) \\ &= \left(\frac{x_{\rm cg}}{\bar{c}} - \frac{x_{NP}}{\bar{c}}\right)\mathbf{C}_{L\alpha} + \frac{\mathbf{C}_{h\alpha}}{\mathbf{C}_{h\delta_e}}\eta\frac{S_t}{S}a_e\left(\frac{\ell_t + x_{\rm ac} - x_{NP}}{\bar{c}} + \frac{x_{NP} - x_{\rm cg}}{\bar{c}}\right) \\ &= \left(\frac{x_{\rm cg}}{\bar{c}} - \frac{x_{NP}}{\bar{c}}\right)\left[\mathbf{C}_{L\alpha} - \frac{\mathbf{C}_{L\delta_e}\mathbf{C}_{h\alpha}}{\mathbf{C}_{h\delta_e}}\right] + \eta V_{H_N}\frac{\mathbf{C}_{h\alpha}a_e}{\mathbf{C}_{h\delta_e}} \end{aligned} \tag{3.66}$$

where $a_e = \partial\mathbf{C}_{Lt}/\partial\delta_e$ is the elevator effectiveness and

$$V_{H_N} = \left(\frac{\ell_t}{\bar{c}} + \frac{x_{\rm ac}}{\bar{c}} - \frac{x_{NP}}{\bar{c}}\right)\frac{S_t}{S} \tag{3.67}$$

is the tail volume ratio based on ℓ_{t_N}, the distance between the tail aerodynamic center and the basic neutral point, as defined in Eq. (3.30). The quantity in square brackets in the final version of Eq. (3.66) is seen to be simply the control free vehicle lift curve slope $\mathbf{C}_{L_\alpha}{}'$, so we have

$$\mathbf{C}_{m_\alpha}{}' = \left(\frac{x_{\rm cg}}{\bar{c}} - \frac{x_{NP}}{\bar{c}}\right)\mathbf{C}_{L_\alpha}{}' + \eta V_{H_N}\frac{\mathbf{C}_{h\alpha}a_e}{\mathbf{C}_{h\delta_e}} \tag{3.68}$$

Setting the control free pitch stiffness $\mathbf{C}_{m_\alpha}{}'$ to zero gives the distance between the control free and basic neutral points as

$$\frac{x_{NP}}{\bar{c}} - \frac{x'_{NP}}{\bar{c}} = \eta V_{H_N}\frac{a_e}{\mathbf{C}_{L_\alpha}{}'}\frac{\mathbf{C}_{h\alpha}}{\mathbf{C}_{h\delta_e}} \tag{3.69}$$

Finally, if Eq. (3.69) is substituted back into Eq. (3.68) to eliminate the variable x_{NP}, we have

$$\mathbf{C}_{m_\alpha}{}' = -\left(\frac{x'_{NP}}{\bar{c}} - \frac{x_{\rm cg}}{\bar{c}}\right)\mathbf{C}_{L_\alpha}{}' \tag{3.70}$$

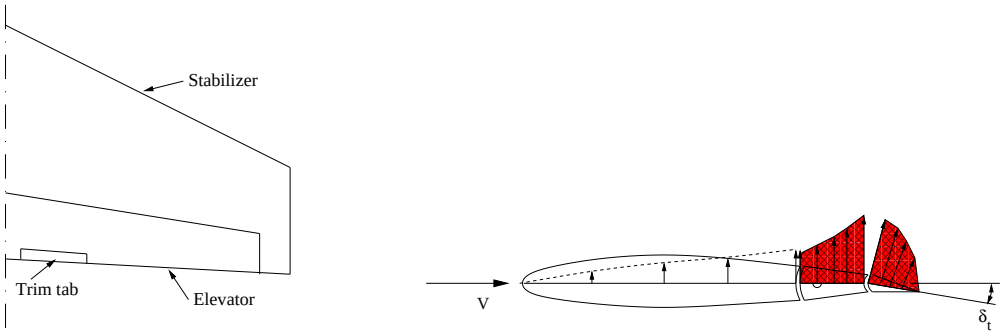

(a) (b)

Figure 3.5: (a) Typical location of trim tab on horizontal control (elevator), and (b) schematic illustration of aerodynamic forces responsible for hinge moment due to trim tab deflection.

showing that the control free pitch stiffness is directly proportional to the *control free static margin*

$$\left(\frac{x'_{NP}}{\bar{c}} - \frac{x_{\text{cg}}}{\bar{c}}\right)$$

3.3.3 Trim Tabs

Trim tabs can be used by the pilot to trim the vehicle at zero control force for any desired speed. Trim tabs are small control surfaces mounted at the trailing edges of primary control surfaces. A linkage is provided that allows the pilot to set the angle of the trim tab, relative to the primary control surface, in a way that is independent of the deflection of the primary control surface. Deflection of the trim tab creates a hinge moment that causes the elevator to float at the angle desired for trim. The geometry of a typical trim tab arrangement is shown in Fig. 3.5.

Zero control force corresponds to zero hinge moment, or

$$\mathbf{C}_{he} = 0 = \mathbf{C}_{he_0} + \mathbf{C}_{h\alpha}\alpha + \mathbf{C}_{h\delta_e}\delta_e + \mathbf{C}_{h\delta_t}\delta_t$$

and the trim tab deflection that achieves this for arbitrary angle of attack and control deflection is

$$\delta_t = -\frac{1}{\mathbf{C}_{h\delta_t}}\left(\mathbf{C}_{he_0} + \mathbf{C}_{h\alpha}\alpha + \mathbf{C}_{h\delta_e}\delta_e\right) \tag{3.71}$$

so the tab setting required for zero control force at trim is

$$\delta_{t_{\text{trim}}} = -\frac{1}{\mathbf{C}_{h\delta_t}}\left(\mathbf{C}_{he_0} + \mathbf{C}_{h\alpha}\alpha_{\text{trim}} + \mathbf{C}_{h\delta_e}\delta_{e\text{trim}}\right) \tag{3.72}$$

The values of α_{trim} and $\delta_{e\text{trim}}$ are given by Eqs. (3.27)

$$\begin{aligned} \alpha_{\text{trim}} &= \frac{-\mathbf{C}_{L\delta_e}\mathbf{C}_{m0} - \mathbf{C}_{m\delta_e}\mathbf{C}_{L\text{trim}}}{\Delta} \\ \delta_{e\text{trim}} &= \frac{\mathbf{C}_{L\alpha}\mathbf{C}_{m0} + \mathbf{C}_{m\alpha}\mathbf{C}_{L\text{trim}}}{\Delta} \end{aligned} \tag{3.73}$$

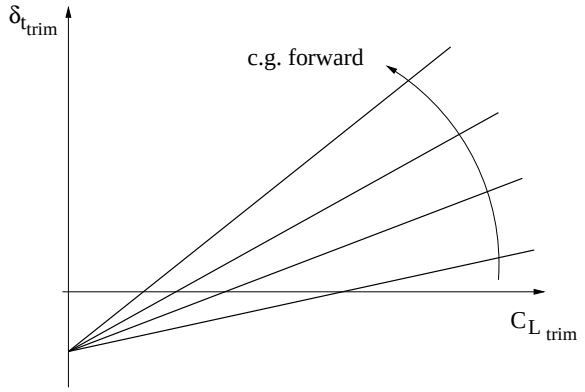

Figure 3.6: Variation in trim tab setting as function of velocity for stable, aft tail vehicle.

Substituting these values into Eq. (3.72) gives the required trim tab setting as

$$\delta_{t_{\text{trim}}} = -\frac{1}{\mathbf{C}_{h\delta_t}}\left(\mathbf{C}_{he_0} + \frac{\mathbf{C}_{m0}}{\Delta}\left(-\mathbf{C}_{h\alpha}\mathbf{C}_{L\delta_e} + \mathbf{C}_{h\delta_e}\mathbf{C}_{L\alpha}\right) + \frac{1}{\Delta}\left(-\mathbf{C}_{h\alpha}\mathbf{C}_{m\delta_e} + \mathbf{C}_{h\delta_e}\mathbf{C}_{m\alpha}\right)\mathbf{C}_{L\text{trim}}\right) \tag{3.74}$$

Note that the coefficient of $\mathbf{C}_{L\text{trim}}$ in this equation – which gives the sensitivity of the trim tab setting to the trim lift coefficient – can be written as

$$\frac{\mathrm{d}\delta_t}{\mathrm{d}\mathbf{C}_L} = -\frac{\mathbf{C}_{h\delta_e}}{\mathbf{C}_{h\delta_t}\Delta}\left(\mathbf{C}_{m\alpha} - \frac{\mathbf{C}_{h\alpha}\mathbf{C}_{m\delta_e}}{\mathbf{C}_{h\delta_e}}\right) = -\frac{\mathbf{C}_{h\delta_e}}{\mathbf{C}_{h\delta_t}\Delta}\mathbf{C}_{m_\alpha}{}' = -\frac{\mathbf{C}_{h\delta_e}}{\mathbf{C}_{h\delta_t}\Delta}\left(\frac{x'_{NP}}{\bar{c}} - \frac{x_{\text{cg}}}{\bar{c}}\right)\mathbf{C}_{L_\alpha}{}' \tag{3.75}$$

and Eq. (3.74) can be written

$$\delta_{t_{\text{trim}}} = -\frac{1}{\mathbf{C}_{h\delta_t}}\left[\mathbf{C}_{he_0} + \frac{\mathbf{C}_{m0}}{\Delta}\left(-\mathbf{C}_{h\alpha}\mathbf{C}_{L\delta_e} + \mathbf{C}_{h\delta_e}\mathbf{C}_{L\alpha}\right) + \frac{\mathbf{C}_{h\delta_e}}{\Delta}\mathbf{C}_{L_\alpha}{}'\left(\frac{x'_{NP}}{\bar{c}} - \frac{x_{\text{cg}}}{\bar{c}}\right)\mathbf{C}_{L\text{trim}}\right] \tag{3.76}$$

Thus, the tab setting for trim is a linear function of trimmed lift coefficient whose slope is proportional to the control free static margin. This variation is shown schematically for a conventional (aft tail) configuration in Fig. 3.6.

3.3.4 Control Force for Trim

As mentioned earlier, the most important aspects of stability relating to handling qualities of the vehicle are related to control *forces*. For longitudinal control, the control force F is related to the elevator hinge moment H_e through a gearing constant G, so that

$$F = GH_e \tag{3.77}$$

This equation defines a positive control force as a *pull*, corresponding to the force required to balance a positive (nose up) elevator hinge moment.[4] The units of the gearing constant G are inverse length, which can be interpreted as a mechanical advantage corresponding to radians of control deflection per unit distance (foot) of control yoke displacement.

[4]It is important to be careful when reading other books; positive control force is sometimes defined as a *push*, in which case there is a minus sign inserted on the right hand side of Eq. (3.77) and subsequently throughout the analysis.

Expressing the hinge moment in terms of the corresponding dimensionless coefficient, we have

$$F = GS_e\bar{c}_eQ\mathbf{C}_{he} = GS_e\bar{c}_eQ\left(\mathbf{C}_{he_0} + \mathbf{C}_{h\alpha}\alpha + \mathbf{C}_{h\delta_e}\delta_e + \mathbf{C}_{h\delta_t}\delta_t\right) \tag{3.78}$$

Since this equation is linear in tab deflection, the control force required for a tab setting other than the trim value is

$$F = GS_e\bar{c}_eQ\mathbf{C}_{h\delta_t}\left(\delta_t - \delta_{t_{\text{trim}}}\right) \tag{3.79}$$

and, substituting the tab setting required for trim from Eq. (3.76), we have

$$F = GS_e\bar{c}_eQ\left[\mathbf{C}_{h\delta_t}\delta_t + \mathbf{C}_{he_0} + \frac{\mathbf{C}_{m0}}{\Delta}\left(-\mathbf{C}_{h\alpha}\mathbf{C}_{L\delta_e} + \mathbf{C}_{h\delta_e}\mathbf{C}_{L\alpha}\right) + \frac{\mathbf{C}_{h\delta_e}}{\Delta}\mathbf{C}_{L\alpha}'\left(\frac{x_{\text{cg}} - x'_{NP}}{\bar{c}}\right)\mathbf{C}_{L\text{trim}}\right] \tag{3.80}$$

Finally, substituting

$$\mathbf{C}_{L\text{trim}} = \frac{W/S}{Q} \tag{3.81}$$

for level flight with $L = W$, we have

$$\begin{aligned} F =& GS_e\bar{c}_e(W/S)\frac{\mathbf{C}_{h\delta_e}\mathbf{C}_{L\alpha}'}{\Delta}\left(\frac{x_{\text{cg}} - x'_{NP}}{\bar{c}}\right) + \\ & GS_e\bar{c}_e\left[\mathbf{C}_{h\delta_t}\delta_t + \mathbf{C}_{he_0} + \frac{\mathbf{C}_{m0}}{\Delta}\left(-\mathbf{C}_{h\alpha}\mathbf{C}_{L\delta_e} + \mathbf{C}_{h\delta_e}\mathbf{C}_{L\alpha}\right)\right]\frac{1}{2}\rho V^2 \end{aligned} \tag{3.82}$$

The dependence of control force on velocity described by this equation is sketched in Fig. 3.7. Note from the equation that:

1. The control force $F \propto S_e\bar{c}_e$, i.e, is proportional to the *cube* of the size of the vehicle; control forces grow rapidly with aircraft size, and large aircraft require powered (or power-assisted) control systems.
2. The location of the c.g. (i.e., the control free static margin) affects only the constant term in the equation.
3. The vehicle weight enters only in the ratio W/S.
4. The effect of trim tab deflection δ_t is to change the coefficient of the V^2 term, and hence controls the intercept of the curve with the velocity axis.

If we denote the velocity at which the control force is zero as V_{trim}, then Eq. (3.82) gives

$$\begin{aligned} & GS_e\bar{c}_e\left(\mathbf{C}_{h\delta_t}\delta_t + \mathbf{C}_{he_0} + \frac{\mathbf{C}_{m0}}{\Delta}\left(-\mathbf{C}_{h\alpha}\mathbf{C}_{L\delta_e} + \mathbf{C}_{h\delta_e}\mathbf{C}_{L\alpha}\right)\right)\frac{1}{2}\rho V_{\text{trim}}^2 = \\ & -GS_e\bar{c}_e(W/S)\frac{\mathbf{C}_{h\delta_e}\mathbf{C}_{L\alpha}'}{\Delta}\left(\frac{x_{\text{cg}} - x'_{NP}}{\bar{c}}\right) \end{aligned} \tag{3.83}$$

so

$$F = GS_e\bar{c}_e(W/S)\frac{\mathbf{C}_{h\delta_e}\mathbf{C}_{L\alpha}'}{\Delta}\left(\frac{x_{\text{cg}} - x'_{NP}}{\bar{c}}\right)\left[1 - (V/V_{\text{trim}})^2\right] \tag{3.84}$$

and

$$\left.\frac{\mathrm{d}F}{\mathrm{d}V}\right)_{V_{\text{trim}}} = -\frac{2}{V_{\text{trim}}}GS_e\bar{c}_e(W/S)\frac{\mathbf{C}_{h\delta_e}\mathbf{C}_{L\alpha}'}{\Delta}\left(\frac{x_{\text{cg}} - x'_{NP}}{\bar{c}}\right) \tag{3.85}$$

These last two equations, which also can be interpreted in terms of Fig. 3.7, show that:

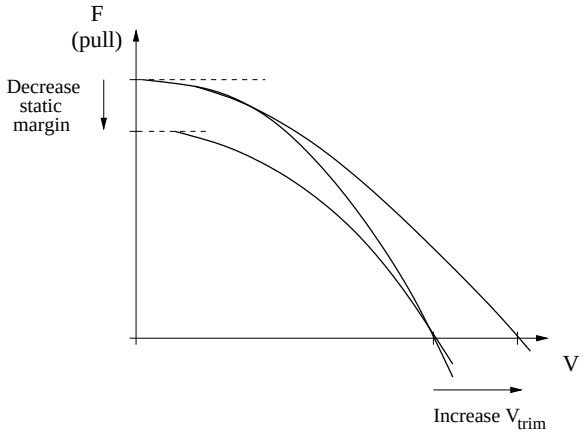

Figure 3.7: Typical variation in control force as function of vehicle velocity for stable configuration.

1. For a given control free static margin (or c.g. position) the control force gradient decreases with increasing flight velocity; and
2. At a given trim velocity, the control force gradient decreases as the c.g. is moved aft toward the control free neutral point (i.e., as the static margin is reduced).

3.3.5 Control-force for Maneuver

Perhaps the single most important stability property of an aircraft, in terms of handling properties, describes the control force required to perform a maneuver. This force must not be too small to avoid over-stressing the airframe, nor too large to avoid making the pilot work too hard.

We will again consider the steady pull-up. The change in control force required to effect the maneuver is

$$\Delta F = GS_e\bar{c}_e Q\Delta\mathbf{C}_{he} \tag{3.86}$$

where

$$\Delta\mathbf{C}_{he} = \mathbf{C}_{h\alpha}\Delta\alpha + \mathbf{C}_{h\delta_e}\Delta\delta_e + \mathbf{C}_{hq}\hat{q} \tag{3.87}$$

where $\hat{q}$ is the dimensionless pitch rate, as defined in Section 3.2.1. It was also seen in that section that the dimensionless pitch rate for a pull-up could be related directly to the excess load factor $(n-1)$, so, using Eq. (3.48), we have

$$\Delta\mathbf{C}_{he} = \mathbf{C}_{h\alpha}\Delta\alpha + \mathbf{C}_{h\delta_e}\Delta\delta_e + \frac{(n-1)\mathbf{C}_W}{2\mu}\mathbf{C}_{hq} \tag{3.88}$$

The derivative $\mathbf{C}_{hq}$ arises from the change in hinge moment due to the change in tail angle of attack arising from the pitch rate. Thus

$$\Delta\mathbf{C}_{he} = \mathbf{C}_{h\alpha_t}\Delta\alpha_t = \mathbf{C}_{h\alpha_t}\frac{2\ell_t}{\bar{c}}\hat{q} \tag{3.89}$$

and

$$\mathbf{C}_{hq} \equiv \frac{\partial\mathbf{C}_{he}}{\partial\hat{q}} = 2\frac{\ell_t}{\bar{c}}\mathbf{C}_{h\alpha_t} \tag{3.90}$$

Now, we can use the solution for $\Delta\delta_e$ from Eq. (3.52)

$$\Delta\delta_e = \frac{(n-1)\mathbf{C}_W}{\Delta}\left[\left(1-\frac{\mathbf{C}_{Lq}}{2\mu}\right)\mathbf{C}_{m\alpha}+\frac{\mathbf{C}_{mq}}{2\mu}\mathbf{C}_{L\alpha}\right] \tag{3.91}$$

along with the lift coefficient equation, Eq. (3.49), which can be written

$$\Delta\alpha = \frac{1}{\mathbf{C}_{L\alpha}}\left[(n-1)\mathbf{C}_W\left(1-\frac{\mathbf{C}_{Lq}}{2\mu}\right)-\mathbf{C}_{L\delta_e}\Delta\delta_e\right] \tag{3.92}$$

in the hinge moment equation to give

$$\Delta\mathbf{C}_{he} = \mathbf{C}_{h\alpha}\frac{n-1}{\mathbf{C}_{L\alpha}}\left[\left(1-\frac{\mathbf{C}_{Lq}}{2\mu}\right)\mathbf{C}_W-\mathbf{C}_{L\delta_e}\frac{\Delta\delta_e}{n-1}\right]+\mathbf{C}_{h\delta_e}\Delta\delta_e+\frac{(n-1)\mathbf{C}_W}{2\mu}\mathbf{C}_{hq} \tag{3.93}$$

which can be rearranged into the form

$$\frac{\Delta\mathbf{C}_{he}}{n-1} = \frac{\mathbf{C}_W}{\mathbf{C}_{L\alpha}}\left[\left(1-\frac{\mathbf{C}_{Lq}}{2\mu}\right)\mathbf{C}_{h\alpha}+\frac{\mathbf{C}_{hq}}{2\mu}\mathbf{C}_{L\alpha}\right]+\frac{\Delta\delta_e}{n-1}\mathbf{C}_{h\delta_e}\frac{\mathbf{C}_{L\alpha}{}'}{\mathbf{C}_{L\alpha}} \tag{3.94}$$

Finally, using Eq. (3.57) for $\Delta\delta_e/(n-1)$, the equation for the hinge moment increment can be written

$$\frac{\Delta\mathbf{C}_{he}}{n-1} = \frac{\mathbf{C}_W\mathbf{C}_{L\alpha}{}'\mathbf{C}_{h\delta_e}}{\Delta}\left(1-\frac{\mathbf{C}_{Lq}}{2\mu}\right)\left[\frac{x_{\rm cg}-x_{MP}}{\bar{c}}+\frac{\Delta}{\mathbf{C}_{L\alpha}{}'\mathbf{C}_{h\delta_e}}\left(\frac{\mathbf{C}_{h\alpha}}{\mathbf{C}_{L\alpha}}+\frac{\mathbf{C}_{hq}}{2\mu-\mathbf{C}_{Lq}}\right)\right] \tag{3.95}$$

The *control free maneuver point* is defined as the c.g. location for which the control force gradient (per g) (or, equivalently, the hinge moment coefficient gradient) vanishes. This is seen from Eq. (3.95) to give

$$\frac{x_{MP}-x'_{MP}}{\bar{c}} = \frac{\Delta}{\mathbf{C}_{L\alpha}{}'\mathbf{C}_{h\delta_e}}\left(\frac{\mathbf{C}_{h\alpha}}{\mathbf{C}_{L\alpha}}+\frac{\mathbf{C}_{hq}}{2\mu-\mathbf{C}_{Lq}}\right) \tag{3.96}$$

Note that this quantity is positive for aft tail configurations, and negative for forward tail (canard) configurations. Substitution of this expression back into Eq. (3.95) then gives

$$\frac{\Delta\mathbf{C}_{he}}{n-1} = \frac{\mathbf{C}_W\mathbf{C}_{L\alpha}{}'\mathbf{C}_{h\delta_e}}{\Delta}\left(1-\frac{\mathbf{C}_{Lq}}{2\mu}\right)\left(\frac{x_{\rm cg}-x'_{MP}}{\bar{c}}\right) \tag{3.97}$$

Finally, the control force gradient (per g) is

$$\begin{aligned}\frac{\partial F}{\partial n} &= \frac{\Delta F}{n-1} = GS_e\bar{c}_eQ\frac{\Delta\mathbf{C}_{he}}{n-1}\\ &= GS_e\bar{c}_eQ\frac{\mathbf{C}_W\mathbf{C}_{L\alpha}{}'\mathbf{C}_{h\delta_e}}{\Delta}\left(1-\frac{\mathbf{C}_{Lq}}{2\mu}\right)\left(\frac{x_{\rm cg}-x'_{MP}}{\bar{c}}\right)\end{aligned} \tag{3.98}$$

or, since $Q\mathbf{C}_W = W/S$,

$$\frac{\partial F}{\partial n} = GS_e\bar{c}_e(W/S)\frac{\mathbf{C}_{L\alpha}{}'\mathbf{C}_{h\delta_e}}{\Delta}\left(1-\frac{\mathbf{C}_{Lq}}{2\mu}\right)\left(\frac{x_{\rm cg}-x'_{MP}}{\bar{c}}\right) \tag{3.99}$$

The distance $\frac{x'_{MP}-x_{\rm cg}}{\bar{c}}$, seen from the above equation to be directly related to the sensitivity of normal acceleration of the vehicle to control force, is called the *control free maneuver margin*.

Note that the control force gradient (per g) is

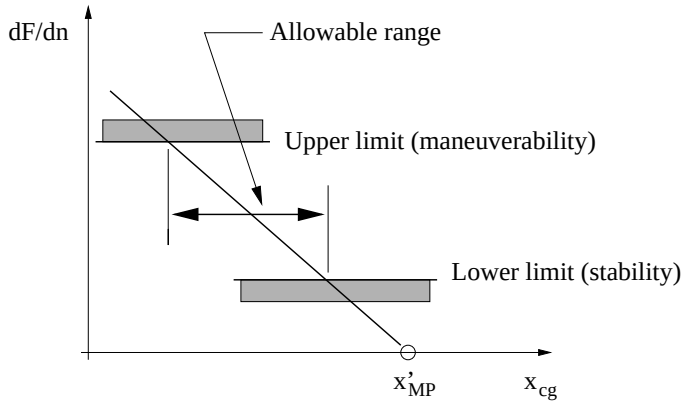

Figure 3.8: Allowable c.g. travel as imposed by limits on control force gradient (per g).

1. Directly proportional to the vehicle wing loading W/S;
2. Directly proportional to the *cube* of the linear size of the vehicle;
3. Directly proportional to the (control free) maneuver margin $(x'_{MP} - x_{\rm cg})/\bar{c}$; and
4. Independent of airspeed.

The control force gradient should be neither too small nor too large. If the gradient is too small, the vehicle will be overly sensitive to small control inputs and it will be too easy for the pilot to over stress the airframe. At the same time, the control forces required for normal maneuvers must not be larger than the pilot can supply (or so large that the pilot becomes unduly tired performing normal maneuvers). The lower and upper limits on control force gradient (per g) determine allowable rearward and forward limits on c.g. travel, as sketched in Fig. 3.8. The values of these limits will depend on the vehicle mission; in general the limits will be higher for transport aircraft, and lower for vehicles which require greater maneuverability (such as military fighters or aerobatic aircraft).

3.4 Forward and Aft Limits of C.G. Position

The various control position and force gradients impose limits on the acceptable range of travel of the vehicle center of gravity. These include (for most vehicles):

- **Rearward limits:**
  1. The vehicle must be statically stable; i.e., the c.g. must be ahead of the basic and control free neutral points.
  2. The sensitivity of vehicle velocity to control position must not be too small; i.e., the c.g. must be sufficiently far ahead of the basic neutral point.
  3. The sensitivity of vehicle normal acceleration to control force must not be too small; i.e., the c.g. must be sufficiently far ahead of the control free neutral point.
- **Forward limits:**

1. The vehicle must be trimmable at $\mathbf{C}_{L_{\max}}$; i.e., the c.g. must not be so far forward that there is insufficient elevator power to trim the vehicle at maximum lift coefficient.
2. The sensitivity of vehicle normal acceleration to control force must not be too high; i.e., the c.g. must not be so far forward that excessive control force is required to perform maneuvers for which the vehicle is intended.

Bibliography

[1] Robert C. Nelson, **Aircraft Stability and Automatic Control**, McGraw-Hill, Second edition, 1998.

Chapter 4

Dynamical Equations for Flight Vehicles

These notes provide a systematic background of the derivation of the equations of motion for a flight vehicle, and their linearization. The relationship between dimensional stability derivatives and dimensionless aerodynamic coefficients is presented, and the principal contributions to all important stability derivatives for flight vehicles having left/right symmetry are explained.

4.1 Basic Equations of Motion

The equations of motion for a flight vehicle usually are written in a body-fixed coordinate system. It is convenient to choose the vehicle center of mass as the origin for this system, and the orientation of the (right-handed) system of coordinate axes is chosen by convention so that, as illustrated in Fig. 4.1:

- the x-axis lies in the symmetry plane of the vehicle[1]and points forward;
- the z-axis lies in the symmetry plane of the vehicle, is perpendicular to the x-axis, and points down;
- the y-axis is perpendicular to the symmetry plane of the vehicle and points out the right wing.

The precise orientation of the x-axis depends on the application; the two most common choices are:

- to choose the orientation of the x-axis so that the product of inertia

$$I_{xz} = \int_{\mathrm{m}} xz \, \mathrm{d}m = 0$$

[1]Almost all flight vehicles have bi-lateral (or, left/right) symmetry, and most flight dynamics analyses take advantage of this symmetry.

The other products of inertia, I_{xy} and I_{yz}, are automatically zero by vehicle symmetry. When all products of inertia are equal to zero, the axes are said to be *principal axes*.

- to choose the orientation of the x-axis so that it is parallel to the velocity vector for an initial equilibrium state. Such axes are called *stability axes*.

The choice of principal axes simplifies the moment equations, and requires determination of only one set of moments of inertia for the vehicle – at the cost of complicating the X- and Z-force equations because the axes will not, in general, be aligned with the lift and drag forces in the equilibrium state. The choice of stability axes ensures that the lift and drag forces in the equilibrium state are aligned with the z and x axes, at the cost of additional complexity in the moment equations and the need to re-evaluate the inertial properties of the vehicle (I_x, I_z, and I_{xz}) for each new equilibrium state.

4.1.1 Force Equations

The equations of motion for the vehicle can be developed by writing Newton's second law for each differential element of mass in the vehicle,

$$\mathrm{d}\vec{F} = \vec{a}\,\mathrm{d}m \tag{4.1}$$

then integrating over the entire vehicle. When working out the acceleration of each mass element, we must take into account the contributions to its velocity from both linear velocities (u, v, w) in each of the coordinate directions as well as the $\vec{\Omega} \times \vec{r}$ contributions due to the rotation rates (p, q, r) about the axes. Thus, the time rates of change of the coordinates in an inertial frame instantaneously coincident with the body axes are

$$\begin{aligned} \dot{x} &= u + qz - ry \\ \dot{y} &= v + rx - pz \\ \dot{z} &= w + py - qx \end{aligned} \tag{4.2}$$

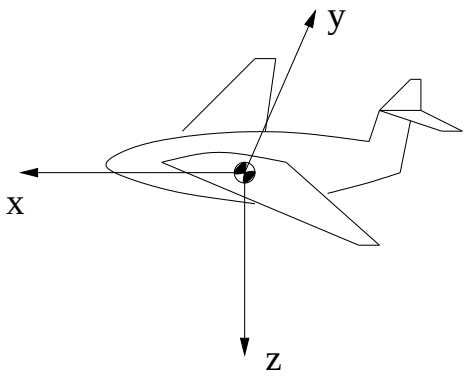

Figure 4.1: Body axis system with origin at center of gravity of a flight vehicle. The x-z plane lies in vehicle symmetry plane, and y-axis points out right wing.

and the corresponding accelerations are given by

$$\begin{aligned} \ddot{x} &= \frac{\mathrm{d}}{\mathrm{d}t}\left(u + qz - ry\right) \\ \ddot{y} &= \frac{\mathrm{d}}{\mathrm{d}t}\left(v + rx - pz\right) \\ \ddot{z} &= \frac{\mathrm{d}}{\mathrm{d}t}\left(w + py - qx\right) \end{aligned} \tag{4.3}$$

or

$$\begin{aligned} \ddot{x} &= \dot{u} + \dot{q}z + q(w + py - qx) - \dot{r}y - r(v + rx - pz) \\ \ddot{y} &= \dot{v} + \dot{r}x + r(u + qz - ry) - \dot{p}z - p(w + py - qx) \\ \ddot{z} &= \dot{w} + \dot{p}y + p(v + rx - pz) - \dot{q}x - q(u + qz - ry) \end{aligned} \tag{4.4}$$

Thus, the net product of mass times acceleration for the entire vehicle is

$$\begin{aligned} m\vec{a} = \int_{\mathrm{m}} \{&[\dot{u} + \dot{q}z + q(w + py - qx) - \dot{r}y - r(v + rx - pz)]\,\hat{\imath} + \\ &[\dot{v} + \dot{r}x + r(u + qz - ry) - \dot{p}z - p(w + py - qx)]\,\hat{\jmath} + \\ &[\dot{w} + \dot{p}y + p(v + rx - pz) - \dot{q}x - q(u + qz - ry)]\,\hat{k}\Big\}\,\mathrm{d}m \end{aligned} \tag{4.5}$$

Now, the velocities and accelerations, both linear and angular, are constant during the integration over the vehicle coordinates, so the individual terms in Eq. (4.5) consist of integrals of the form

$$\int_{\mathrm{m}} \mathrm{d}m = m$$

which integrates to the vehicle mass m, and

$$\int_{\mathrm{m}} x\,\mathrm{d}m = \int_{\mathrm{m}} y\,\mathrm{d}m = \int_{\mathrm{m}} z\,\mathrm{d}m = 0, \tag{4.6}$$

which are all identically zero since the origin of the coordinate system is at the vehicle center of mass. Thus, Eq. (4.5) simplifies to

$$m\vec{a} = m\left[(\dot{u} + qw - rv)\,\hat{\imath} + (\dot{v} + ru - pw)\,\hat{\jmath} + (\dot{w} + pv - qu)\,\hat{k}\right] \tag{4.7}$$

To write the equation corresponding to Newton's Second Law, we simply need to set Eq. (4.7) equal to the net external force acting on the vehicle. This force is the sum of the aerodynamic (including propulsive) forces and those due to gravity.

In order to express the gravitational force acting on the vehicle in the body axis system, we need to characterize the orientation of the body axis system with respect to the gravity vector. This orientation can be specified using the *Euler angles* of the body axis system with respect to an inertial system (x_f, y_f, z_f), where the inertial system is oriented such that

- the z_f axis points down (i.e., is parallel to the gravity vector $\vec{g}$);
- the x_f axis points North; and
- the y_f axis completes the right-handed system and, therefore, points East.

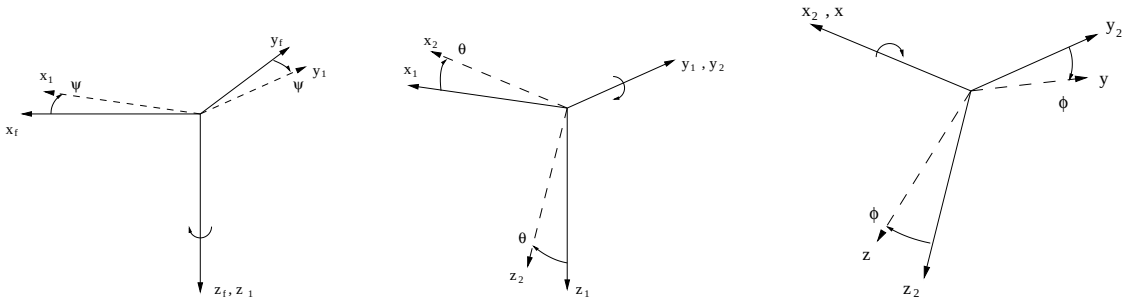

Figure 4.2: The Euler angles Ψ, Θ, and Φ determine the orientation of the body axes of a flight vehicle. (a) Yaw rotation about z-axis, nose right; (b) Pitch rotation about y-axis, nose up; (c) Roll rotation about x-axis, right wing down.

The orientation of the body axis system is specified by starting with the inertial system, then, *in the following order* performing:

1. a positive rotation about the z_f axis through the heading angle Ψ to produce the (x_1, y_1, z_1) system; then

2. a positive rotation about the y_1 axis through the pitch angle Θ to produce the (x_2, y_2, z_2) system; and, finally

3. a positive rotation about the x_2 axis through the bank angle Φ to produce the (x, y, z) system.

Thus, if we imagine the vehicle oriented initially with its z-axis pointing down and heading North, its final orientation is achieved by rotating through the heading angle Ψ, then pitching up through angle Θ, then rolling through angle Φ. This sequence of rotations in sketched in Fig. 4.2.

Since we are interested only in the orientation of the gravity vector in the body axis system, we can ignore the first rotation.[2]Thus, we need consider only the second rotation, in which the components of any vector transform as

$$\begin{pmatrix} x_2 \\ y_2 \\ z_2 \end{pmatrix} = \begin{pmatrix} \cos\Theta & 0 & -\sin\Theta \\ 0 & 1 & 0 \\ \sin\Theta & 0 & \cos\Theta \end{pmatrix} \begin{pmatrix} x_f \\ y_f \\ z_f \end{pmatrix} \tag{4.8}$$

and the third rotation, in which the components transform as

$$\begin{pmatrix} x \\ y \\ z \end{pmatrix} = \begin{pmatrix} 1 & 0 & 0 \\ 0 & \cos\Phi & \sin\Phi \\ 0 & -\sin\Phi & \cos\Phi \end{pmatrix} \begin{pmatrix} x_2 \\ y_2 \\ z_2 \end{pmatrix} \tag{4.9}$$

[2]If we are interested in determining where the vehicle is going – say, we are planning a flight path to get us from New York to London, we certainly are interested in the heading, but this is not really an issue as far as analysis of the stability and controllability of the vehicle are concerned.

Thus, the rotation matrix from the inertial frame to the body fixed system is seen to be

$$\begin{aligned}\begin{pmatrix} x \\ y \\ z \end{pmatrix} &= \begin{pmatrix} 1 & 0 & 0 \\ 0 & \cos\Phi & \sin\Phi \\ 0 & -\sin\Phi & \cos\Phi \end{pmatrix} \begin{pmatrix} \cos\Theta & 0 & -\sin\Theta \\ 0 & 1 & 0 \\ \sin\Theta & 0 & \cos\Theta \end{pmatrix} \begin{pmatrix} x_f \\ y_f \\ z_f \end{pmatrix} \\ &= \begin{pmatrix} \cos\Theta & 0 & -\sin\Theta \\ \sin\Theta\sin\Phi & \cos\Phi & \cos\Theta\sin\Phi \\ \sin\Theta\cos\Phi & -\sin\Phi & \cos\Theta\cos\Phi \end{pmatrix} \begin{pmatrix} x_f \\ y_f \\ z_f \end{pmatrix}\end{aligned} \tag{4.10}$$

The components of the gravitational acceleration in the body-fixed system are, therefore,

$$\begin{pmatrix} g_x \\ g_y \\ g_z \end{pmatrix} = \begin{pmatrix} \cos\Theta & 0 & -\sin\Theta \\ \sin\Theta\sin\Phi & \cos\Phi & \cos\Theta\sin\Phi \\ \sin\Theta\cos\Phi & -\sin\Phi & \cos\Theta\cos\Phi \end{pmatrix} \begin{pmatrix} 0 \\ 0 \\ g_0 \end{pmatrix} = g_0 \begin{pmatrix} -\sin\Theta \\ \cos\Theta\sin\Phi \\ \cos\Theta\cos\Phi \end{pmatrix} \tag{4.11}$$

The force equations can thus be written as

$$\begin{pmatrix} X \\ Y \\ Z \end{pmatrix} + mg_0 \begin{pmatrix} -\sin\Theta \\ \cos\Theta\sin\Phi \\ \cos\Theta\cos\Phi \end{pmatrix} = m \begin{pmatrix} \dot{u} + qw - rv \\ \dot{v} + ru - pw \\ \dot{w} + pv - qu \end{pmatrix} \tag{4.12}$$

where (X, Y, Z) are the components of the net aerodynamic and propulsive forces acting on the vehicle, which will be characterized in subsequent sections.

4.1.2 Moment Equations

The vector form of the equation relating the net torque to the rate of change of angular momentum is

$$\vec{G} = \begin{pmatrix} L \\ M \\ N \end{pmatrix} = \int_m (\vec{r} \times \vec{a})\, \mathrm{d}m \tag{4.13}$$

where (L, M, N) are the components about the (x, y, z) body axes, respectively, of the net aerodynamic and propulsive moments acting on the vehicle. Note that there is no net moment due to the gravitational forces, since the origin of the body-axis system has been chosen at the center of mass of the vehicle. The components of Eq.(4.13) can be written as

$$\begin{aligned} L &= \int_m (y\ddot{z} - z\ddot{y})\ \mathrm{d}m \\ M &= \int_m (z\ddot{x} - x\ddot{z})\ \mathrm{d}m \\ N &= \int_m (x\ddot{y} - y\ddot{x})\ \mathrm{d}m \end{aligned} \tag{4.14}$$

where $\ddot{x}$, $\ddot{y}$, and $\ddot{z}$ are the net accelerations in an inertial system instantaneously coincident with the body axis system, as given in Eqs. (4.4).

When Eqs. (4.4) are substituted into Eqs. (4.14), the terms in the resulting integrals are either linear or quadratic in the coordinates. Since the origin of the body-axis system is at the vehicle c.g.,

Eqs. (4.6) apply and the linear terms integrate to zero. The quadratic terms can be expressed in terms of the *moments of inertia*

$$\begin{aligned} I_x &= \int_m \left(y^2 + z^2\right) \mathrm{d}m \\ I_y &= \int_m \left(z^2 + x^2\right) \mathrm{d}m \\ I_z &= \int_m \left(x^2 + y^2\right) \mathrm{d}m \end{aligned} \tag{4.15}$$

and the *product of inertia*

$$I_{xz} = \int_m xz \, \mathrm{d}m \tag{4.16}$$

Note that the products of inertia $I_{xy} = I_{yz} = 0$, since the y-axis is perpendicular to the assumed plane of symmetry of the vehicle.

Equations (4.14) can then be written as

$$\begin{aligned} L &= I_x \dot{p} + \left(I_z - I_y\right) qr - I_{xz} \left(pq + \dot{r}\right) \\ M &= I_y \dot{q} + \left(I_x - I_z\right) rp - I_{xz} \left(p^2 - r^2\right) \\ N &= I_z \dot{r} + \left(I_y - I_x\right) pq - I_{xz} \left(qr - \dot{p}\right) \end{aligned} \tag{4.17}$$

Note that if principal axes are used, so that $I_{xz} \equiv 0$, Eqs. (4.17) simplify to

$$\begin{aligned} L &= I_x \dot{p} + \left(I_z - I_y\right) qr \\ M &= I_y \dot{q} + \left(I_x - I_z\right) rp \\ N &= I_z \dot{r} + \left(I_y - I_x\right) pq \end{aligned} \tag{4.18}$$

4.2 Linearized Equations of Motion

The equations developed in the preceding section completely describe the motion of a flight vehicle, subject to the prescribed aerodynamic (and propulsive) forces and moments. These equations are *nonlinear* and *coupled*, however, and generally can be solved only numerically, yielding relatively little insight into the dependence of the stability and controllability of the vehicle on basic aerodynamic parameters of the vehicle.

A great deal, however, can be learned by studying *linear* approximations to these equations. In this approach, we analyze the solutions to the equations describing *small perturbations* about an equilibrium flight condition. The greatest simplification of the equations arises when the equilibrium condition is chosen to correspond to a *longitudinal* equilibrium, in which the velocity and gravity vectors lie in the plane of symmetry of the vehicle; the most common choice corresponds to unaccelerated flight – i.e., to level, unaccelerated flight, or to steady climbing (or descending) flight. Such a linear analysis has been remarkably successful in flight dynamics applications,[3]primarily because:

[3]This statement should be interpreted in the context of the difficulty of applying similar linear analyses to other situations – e.g., to road vehicle dynamics, in which the stability derivatives associated with tire forces are notoriously nonlinear.

1. Over a fairly broad range of flight conditions of practical importance, the aerodynamic forces and moments are well-approximated as linear functions of the state variables; and
2. Normal flight situations correspond to relatively small variations in the state variables; in fact, relatively small disturbances in the state variables can lead to significant accelerations, i.e., to flight of considerable violence, which we normally want to avoid.

Finally, we should emphasize the caveat that these linear analyses are not good approximations in some cases – particularly for spinning or post-stall flight situations.

Thus, we will consider

1. Perturbations from a longitudinal trim condition;
2. Using stability axes;

so we can describe the state variables as

$$\begin{aligned} u &= u_0 + u(t), & p &= p(t) \\ v &= v(t), & q &= q(t) \\ w &= w(t), & r &= r(t) \\ \theta &= \Theta_0 + \theta(t), & \Phi &= \phi(t) \end{aligned} \tag{4.19}$$

Variables with the subscript $_0$ correspond to the original equilibrium (trim) state. Note that only the axial velocity u and pitch angle θ have non-zero equilibrium values. The trim values of all lateral/directional variables (v, p, r, and Φ) are zero because the initial trim condition corresponds to longitudinal equilibrium; the equilibrium value of w is zero because we are using stability axes; and the equilibrium pitch rate q is assumed zero as we are restricting the equilibrium state to have no normal acceleration.

The equations for the unperturbed initial equilibrium state then reduce to

$$\begin{aligned} X_0 - mg_0 \sin\Theta_0 &= 0 \\ Z_0 + mg_0 \cos\Theta_0 &= 0 \\ M_0 = L_0 = Y_0 = N_0 &= 0 \end{aligned} \tag{4.20}$$

and we want to solve linear approximations to the equations

$$\begin{aligned} X_0 + \Delta X - mg_0 \sin(\Theta_0 + \theta) &= m(\dot{u} + qw - rv) \\ Y_0 + \Delta Y + mg_0 \cos(\Theta_0 + \theta)\sin\phi &= m(\dot{v} + r(u_0 + u) - pw) \\ Z_0 + \Delta Z + mg_0 \cos(\Theta_0 + \theta)\cos\phi &= m(\dot{w} + pv - q(u_0 + u)) \end{aligned} \tag{4.21}$$

and

$$\begin{aligned} \Delta L &= I_x\dot{p} + (I_z - I_y)qr - I_{xz}(pq + \dot{r}) \\ \Delta M &= I_y\dot{q} + (I_x - I_z)rp + I_{xz}\left(p^2 - r^2\right) \\ \Delta N &= I_z\dot{r} + (I_y - I_x)pq + I_{xz}(qr - \dot{p}) \end{aligned} \tag{4.22}$$

Since we assume that all perturbation quantities are small, we can approximate

$$\begin{aligned} \sin(\Theta_0 + \theta) &\approx \sin\Theta_0 + \theta\cos\Theta_0 \\ \cos(\Theta_0 + \theta) &\approx \cos\Theta_0 - \theta\sin\Theta_0 \end{aligned} \tag{4.23}$$

and

$$\begin{aligned} \sin\Phi &= \sin\phi \approx \phi \\ \cos\Phi &= \cos\phi \approx 1 \end{aligned} \tag{4.24}$$

Thus, after making these approximations, subtracting the equilibrium equations, and neglecting terms that are quadratic in the small perturbations, the force equations can be written

$$\begin{aligned} \Delta X - mg_0 \cos\Theta_0 \theta &= m\dot{u} \\ \Delta Y + mg_0 \cos\Theta_0 \phi &= m\left(\dot{v} + u_0 r\right) \\ \Delta Z - mg_0 \sin\Theta_0 \theta &= m\left(\dot{w} - u_0 q\right) \end{aligned} \tag{4.25}$$

and the moment equations can be written

$$\begin{aligned} \Delta L &= I_x \dot{p} - I_{xz}\dot{r} \\ \Delta M &= I_y \dot{q} \\ \Delta N &= I_z \dot{r} - I_{xz}\dot{p} \end{aligned} \tag{4.26}$$

4.3 Representation of Aerodynamic Forces and Moments

The perturbations in aerodynamic forces and moments are functions of both, the perturbations in state variables and control inputs. The most important dependencies can be represented as follows. The dependencies in the equations describing the longitudinal state variables can be written

$$\begin{aligned} \Delta X &= \frac{\partial X}{\partial u}u + \frac{\partial X}{\partial w}w + \frac{\partial X}{\partial \delta_e}\delta_e + \frac{\partial X}{\partial \delta_T}\delta_T \\ \Delta Z &= \frac{\partial Z}{\partial u}u + \frac{\partial Z}{\partial w}w + \frac{\partial Z}{\partial \dot{w}}\dot{w} + \frac{\partial Z}{\partial q}q + \frac{\partial Z}{\partial \delta_e}\delta_e + \frac{\partial Z}{\partial \delta_T}\delta_T \\ \Delta M &= \frac{\partial M}{\partial u}u + \frac{\partial M}{\partial w}w + \frac{\partial M}{\partial \dot{w}}\dot{w} + \frac{\partial M}{\partial q}q + \frac{\partial M}{\partial \delta_e}\delta_e + \frac{\partial M}{\partial \delta_T}\delta_T \end{aligned} \tag{4.27}$$

In these equations, the control variables δ_e and δ_T correspond to perturbations from trim in the elevator and thrust (throttle) settings. Note that the Z force and pitching moment M are assumed to depend on both the rate of change of angle of attack $\dot{w}$ and the pitch rate q, but the dependence of the X force on these variables is neglected.

Also, the dependencies in the equations describing the lateral/directional state variables can be written

$$\begin{aligned} \Delta Y &= \frac{\partial Y}{\partial v}v + \frac{\partial Y}{\partial p}p + \frac{\partial Y}{\partial r}r + \frac{\partial Y}{\partial \delta_r}\delta_r \\ \Delta L &= \frac{\partial L}{\partial v}v + \frac{\partial L}{\partial p}p + \frac{\partial L}{\partial r}r + \frac{\partial L}{\partial \delta_r}\delta_r + \frac{\partial L}{\partial \delta_a}\delta_a \\ \Delta N &= \frac{\partial N}{\partial v}v + \frac{\partial N}{\partial p}p + \frac{\partial N}{\partial r}r + \frac{\partial N}{\partial \delta_r}\delta_r + \frac{\partial N}{\partial \delta_a}\delta_a \end{aligned} \tag{4.28}$$

In these equations, the variables δ_r and δ_a represent the perturbations from trim in the rudder and aileron control settings.

Note that the representations in Eqs. (4.27) and (4.28) are completely decoupled. That is, the perturbations in longitudinal forces and moments (ΔX, ΔZ, and ΔM) depend neither on the lateral/directional perturbations (v, p, and r) nor the lateral/directional control inputs (δ_r and δ_a); And the perturbations in lateral/directional forces and moments (ΔY, ΔL, and ΔN) depend neither on the longitudinal perturbations (u, w, $\dot{w}$, and q) nor the longitudinal control inputs (δ_e and δ_T). This is a good approximation for vehicles with left/right symmetry. This decoupling is *exact* for the dependence of the lateral/directional forces and moments on the longitudinal state variables, since a change in a longitudinal variable, say angle of attack, cannot produce a change in the side force, rolling moment, or yawing moment, for a perfectly symmetric vehicle. The decoupling is only *approximate* for the dependence of the longitudinal forces and moments on the lateral/directional state variables, since a change in a lateral/directional variable, say roll rate, produces no change in axial or vertical force or pitching moment only to within first order for a symmetric vehicle. Consider, for example, the change in lift force due to roll rate. The increased lift on the down-going wing is canceled by the decreased lift on the upgoing wing only to within the linear approximation.

The final form of the dimensional small-perturbation equations is developed by defining the stability derivatives corresponding to force perturbations by dividing them by the vehicle mass, and by defining the stability derivatives corresponding to moment perturbations by dividing them by the corresponding moments of inertia of the vehicle. Thus, we *define*

$$\begin{aligned}
X_u &\equiv \frac{1}{m}\frac{\partial X}{\partial u}, \qquad X_w \equiv \frac{1}{m}\frac{\partial X}{\partial w}, \qquad \ldots \qquad X_{\delta_T} \equiv \frac{1}{m}\frac{\partial X}{\partial \delta_T};\\
Y_v &\equiv \frac{1}{m}\frac{\partial Y}{\partial v}, \qquad Y_p \equiv \frac{1}{m}\frac{\partial Y}{\partial p}, \qquad \ldots \qquad Y_{\delta_r} \equiv \frac{1}{m}\frac{\partial Y}{\partial \delta_r};\\
Z_u &\equiv \frac{1}{m}\frac{\partial Z}{\partial u}, \qquad Z_w \equiv \frac{1}{m}\frac{\partial Z}{\partial w}, \qquad \ldots \qquad Z_{\delta_T} \equiv \frac{1}{m}\frac{\partial Z}{\partial \delta_T};
\end{aligned} \tag{4.29}$$

and

$$\begin{aligned}
L_v &\equiv \frac{1}{I_x}\frac{\partial L}{\partial v}, \qquad L_p \equiv \frac{1}{I_x}\frac{\partial L}{\partial p}, \qquad \ldots \qquad L_{\delta_a} \equiv \frac{1}{I_x}\frac{\partial L}{\partial \delta_a};\\
M_u &\equiv \frac{1}{I_y}\frac{\partial M}{\partial u}, \qquad M_w \equiv \frac{1}{I_y}\frac{\partial M}{\partial w}, \qquad \ldots \qquad M_{\delta_T} \equiv \frac{1}{I_y}\frac{\partial M}{\partial \delta_T};\\
N_v &\equiv \frac{1}{I_z}\frac{\partial N}{\partial v}, \qquad N_p \equiv \frac{1}{I_z}\frac{\partial N}{\partial p}, \qquad \ldots \qquad N_{\delta_a} \equiv \frac{1}{I_z}\frac{\partial N}{\partial \delta_a}.
\end{aligned} \tag{4.30}$$

It is important to emphasize that the quantities defined by these equations are not to be interpreted simply as (the usual mathematical notation for) partial derivatives but, rather, are the expected partial derivatives divided by the vehicle mass or appropriate moment of inertia.

When these definitions are substituted back into Eqs. (4.27) and (4.28), and these representations are then used in Eqs. (4.25) and (4.26), we arrive at the *small-disturbance equations for longitudinal motions:*

$$\begin{aligned}
\left[\frac{\mathrm{d}}{\mathrm{d}t} - X_u\right] u + g_0 \cos\Theta_0 \theta - X_w w &= X_{\delta_e}\delta_e + X_{\delta_T}\delta_T\\
-Z_u u + \left[(1 - Z_{\dot{w}})\frac{\mathrm{d}}{\mathrm{d}t} - Z_w\right] w - [u_0 + Z_q]\, q + g_0 \sin\Theta_0 \theta &= Z_{\delta_e}\delta_e + Z_{\delta_T}\delta_T\\
-M_u u - \left[M_{\dot{w}}\frac{\mathrm{d}}{\mathrm{d}t} + M_w\right] w + \left[\frac{\mathrm{d}}{\mathrm{d}t} - M_q\right] q &= M_{\delta_e}\delta_e + M_{\delta_T}\delta_T
\end{aligned} \tag{4.31}$$

and the *small-disturbance equations for lateral/directional motions:*

$$\begin{aligned}
&\left[\frac{\mathrm{d}}{\mathrm{d}t} - Y_v\right] v - Y_p p + [u_0 - Y_r]\, r - g_0 \cos\Theta_0 \phi = Y_{\delta_r}\delta_r \\
&-L_v v + \left[\frac{\mathrm{d}}{\mathrm{d}t} - L_p\right] p - \left[\frac{I_{xz}}{I_x}\frac{\mathrm{d}}{\mathrm{d}t} + L_r\right] r = L_{\delta_r}\delta_r + L_{\delta_a}\delta_a \\
&-N_v v - \left[\frac{I_{xz}}{I_z}\frac{\mathrm{d}}{\mathrm{d}t} + N_p\right] p + \left[\frac{\mathrm{d}}{\mathrm{d}t} - N_r\right] r = N_{\delta_r}\delta_r + N_{\delta_a}\delta_a
\end{aligned} \tag{4.32}$$

4.3.1 Longitudinal Stability Derivatives

In order to solve the equations describing longitudinal vehicle motions, we need to be able to evaluate all the coefficients appearing in Eqs. (4.31). This means we need to be able to provide estimates for the derivatives of X, Z, and M with respect to the relevant independent variables u, w, $\dot{w}$, and q. These stability derivatives usually are expressed in terms of dimensionless aerodynamic coefficient derivatives. For example, we can express the stability derivative X_u as

$$X_u \equiv \frac{1}{m}\frac{\partial X}{\partial u} = \frac{1}{m}\frac{\partial}{\partial u}\left[QS\mathbf{C}_X\right] = \frac{QS}{mu_0}\left[2\mathbf{C}_{X\,0} + \mathbf{C}_{X\,u}\right] \tag{4.33}$$

where

$$\mathbf{C}_{X\,u} \equiv \frac{\partial \mathbf{C}_X}{\partial(u/u_0)} \tag{4.34}$$

is the derivative of the dimensionless X-force coefficient with respect to the dimensionless velocity u/u_0. Note that the first term in the final expression of Eq. (4.33) arises because the dynamic pressure Q is, itself, a function of the flight velocity $u_0 + u$. Similar expressions can be developed for all the required derivatives.

Derivatives with respect to vertical velocity perturbations w are related to aerodynamic derivatives with respect to angle of attack α, since

$$\alpha = \tan^{-1}\left(\frac{w}{u}\right) \approx \frac{w}{u_0} \tag{4.35}$$

Then, for example

$$Z_w \equiv \frac{1}{m}\frac{\partial Z}{\partial w} = \frac{1}{m}\frac{\partial}{\partial(u_0\alpha)}\left[QS\mathbf{C}_Z\right] = \frac{QS}{mu_0}\mathbf{C}_{Z\,\alpha} \tag{4.36}$$

Derivatives with respect to pitch rate q are related to aerodynamic derivatives with respect to dimensionless pitch rate $\hat{q} \equiv \frac{\bar{c}q}{2u_0}$. Thus, for example

$$M_q \equiv \frac{1}{I_y}\frac{\partial M}{\partial q} = \frac{1}{I_y}\frac{\partial}{\partial\left(\frac{2u_0\hat{q}}{\bar{c}}\right)}\left[QS\bar{c}\mathbf{C}_m\right] = \frac{QS\bar{c}^2}{2I_y u_0}\mathbf{C}_{m\,q} \tag{4.37}$$

where

$$\mathbf{C}_{m\,q} \equiv \frac{\partial \mathbf{C}_m}{\partial \hat{q}} \tag{4.38}$$

is the derivative of the dimensionless pitching moment coefficient with respect to the dimensionless pitch rate $\hat{q}$. In a similar way, dimensionless derivatives with respect to rate of change of angle of attack $\dot{\alpha}$ are expressed in terms of the dimensionless rate of change $\hat{\dot{\alpha}} = \frac{\bar{c}\dot{\alpha}}{2u_0}$.

Variable	X	Z	M
u	$X_u = \frac{QS}{mu_0}\left[2\mathbf{C}_{X0} + \mathbf{C}_{Xu}\right]$	$Z_u = \frac{QS}{mu_0}\left[2\mathbf{C}_{Z0} + \mathbf{C}_{Zu}\right]$	$M_u = \frac{QS\bar{c}}{I_y u_0}\mathbf{C}_{mu}$
w	$X_w = \frac{QS}{mu_0}\mathbf{C}_{X\alpha}$	$Z_w = \frac{QS}{mu_0}\mathbf{C}_{Z\alpha}$	$M_w = \frac{QS\bar{c}}{I_y u_0}\mathbf{C}_{m\alpha}$
$\dot{w}$	$X_{\dot{w}} = 0$	$Z_{\dot{w}} = \frac{QS\bar{c}}{2mu_0^2}\mathbf{C}_{Z\dot{\alpha}}$	$M_{\dot{w}} = \frac{QS\bar{c}^2}{2I_y u_0^2}\mathbf{C}_{m\dot{\alpha}}$
q	$X_q = 0$	$Z_q = \frac{QS\bar{c}}{2mu_0}\mathbf{C}_{Zq}$	$M_q = \frac{QS\bar{c}^2}{2I_y u_0}\mathbf{C}_{mq}$

Table 4.1: Relation of dimensional stability derivatives for longitudinal motions to dimensionless derivatives of aerodynamic coefficients.

Expressions for all the dimensional stability derivatives appearing in Eqs. (4.31) in terms of the dimensionless aerodynamic coefficient derivatives are summarized in Table 4.1.

Aerodynamic Derivatives

In this section we relate the dimensionless derivatives of the preceding section to the usual aerodynamic derivatives, and provide simple formulas for estimating them. It is natural to express the axial and normal force coefficients in terms of the lift and drag coefficients, but we must take into account the fact that perturbations in angle of attack will rotate the lift and drag vectors with respect to the body axes. Here, consistent with Eq. (4.35), we define the angle of attack as the angle between the instantaneous vehicle velocity vector and the x-axis, and also assume that the propulsive thrust is aligned with the x-axis. Thus, as seen in Fig. 4.3, we have to within terms linear in angle of attack

$$\begin{aligned}\mathbf{C}_X &= \mathbf{C}_T - \mathbf{C}_D\cos\alpha + \mathbf{C}_L\sin\alpha \approx \mathbf{C}_T - \mathbf{C}_D + \mathbf{C}_L\alpha \\ \mathbf{C}_Z &= -\mathbf{C}_D\sin\alpha - \mathbf{C}_L\cos\alpha \approx -\mathbf{C}_D\alpha - \mathbf{C}_L\end{aligned} \tag{4.39}$$

Here the thrust coefficient

$$\mathbf{C}_T \equiv \frac{T}{QS} \tag{4.40}$$

where T is the net propulsive thrust, assumed to be aligned with the x-axis of the body-fixed system. Since all the dimensionless coefficients in Eqs. (4.39) are normalized by the same quantity QS, the representations of forces and force coefficients are equivalent.

Speed Derivatives

We first consider the derivatives with respect to vehicle speed u. The derivative

$$\mathbf{C}_{Xu} = \mathbf{C}_{Tu} - \mathbf{C}_{Du} \tag{4.41}$$

represents the *speed damping*, and

$$\mathbf{C}_{Du} = \mathbf{M}\frac{\partial \mathbf{C}_D}{\partial \mathbf{M}} \tag{4.42}$$

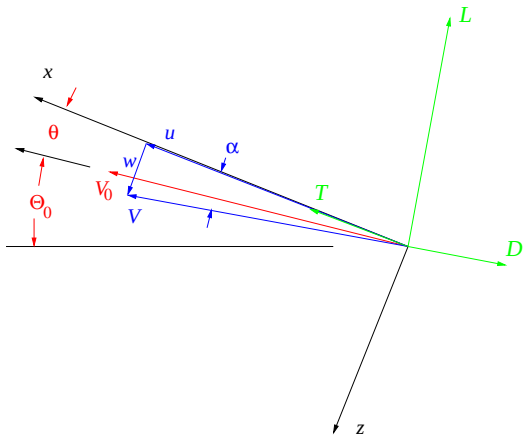

Figure 4.3: Orientation of body axes with respect to instantaneous and equilibrium vehicle velocity, illustrating relation between force components in body axes and lift, drag, and thrust forces. The angle of attack α denotes the angle between the x-axis and the instantaneous velocity vector V, while the perturbation in pitch angle θ denotes the angle between the x-axis and the equilibrium velocity vector V_0. Lift and drag act perpendicular to, and anti-parallel to, the instantaneous velocity, while thrust is assumed to act parallel to the x-axis.

represents the contribution of compressibility effects to this derivative.

The contribution of the derivative $\mathbf{C}_{T_u}$ must be estimated separately for the special cases of constant thrust (appropriate for jet-powered aircraft or for a power-off glide), or constant power (appropriate for piston-powered aircraft with constant-speed propellers). For the constant thrust case,

$$\mathbf{C}_{T_u} = \frac{\partial}{\partial(u/u_0)}\left(\frac{T}{QS}\right) = -2\mathbf{C}_{T0} \tag{4.43}$$

And for the constant power case,

$$\mathbf{C}_{T_u} = \frac{\partial}{\partial(u/u_0)}\left(\frac{P}{QSu}\right) = -3\mathbf{C}_{T0} \tag{4.44}$$

The equilibrium force equations shown in Eqs. (4.20) can be combined to express the equilibrium thrust coefficient as

$$\mathbf{C}_{T0} = \mathbf{C}_{D0} + \mathbf{C}_{L0}\tan\Theta_0 \tag{4.45}$$

which then gives

$$\mathbf{C}_{X_u} = \begin{cases} -2\mathbf{C}_{D0} - 2\mathbf{C}_{L0}\tan\Theta_0 - \mathbf{M}\mathbf{C}_{D\mathbf{M}} & \text{for constant thrust} \\ -3\mathbf{C}_{D0} - 3\mathbf{C}_{L0}\tan\Theta_0 - \mathbf{M}\mathbf{C}_{D\mathbf{M}} & \text{for constant power} \end{cases} \tag{4.46}$$

And, when these expressions are substituted into the equation for the dimensional stability derivative from the preceding section, we have

$$X_u = \begin{cases} -\frac{QS}{mu_0}\left[2\mathbf{C}_{D0} + \mathbf{M}\mathbf{C}_{D\mathbf{M}}\right] & \text{for constant thrust} \\ -\frac{QS}{mu_0}\left[3\mathbf{C}_{D0} + \mathbf{C}_{L0}\tan\Theta_0 + \mathbf{M}\mathbf{C}_{D\mathbf{M}}\right] & \text{for constant power} \end{cases} \tag{4.47}$$

The derivative of the normal force coefficient $\mathbf{C}_Z$ with respect to vehicle speed u is simply

$$\mathbf{C}_{Z_u} = -\mathbf{C}_{L_u} \tag{4.48}$$

since the drag coefficient contribution vanishes when evaluated at the initial trim condition, where $\alpha = 0$. The dependence of lift coefficient on speed arises due to compressibility and aeroelastic effects. We will neglect aeroelastic effects, but the effect of compressibility can be characterized as

$$\mathbf{C}_{Lu} = \mathbf{M}\frac{\partial \mathbf{C}_L}{\partial \mathbf{M}} \tag{4.49}$$

where $\mathbf{M}$ is the flight Mach number. The Prandtl-Glauert similarity law for subsonic flow gives

$$\mathbf{C}_L = \frac{\mathbf{C}_L|_{\mathbf{M}=0}}{\sqrt{1-\mathbf{M}^2}} \tag{4.50}$$

which can be used to show that

$$\frac{\partial \mathbf{C}_L}{\partial \mathbf{M}} = \frac{\mathbf{M}}{1-\mathbf{M}^2}\mathbf{C}_{L0} \tag{4.51}$$

whence

$$\mathbf{C}_{Zu} = -\frac{\mathbf{M}^2}{1-\mathbf{M}^2}\mathbf{C}_{L0} \tag{4.52}$$

Use of the corresponding form of the Prandtl-Glauert rule for supersonic flow results in exactly the same formula. We then have for the dimensional stability derivative

$$Z_u = -\frac{QS}{mu_0}\left[2\mathbf{C}_{L0} + \frac{\mathbf{M}^2}{1-\mathbf{M}^2}\mathbf{C}_{L0}\right] \tag{4.53}$$

Finally, the change in pitching moment coefficient $\mathbf{C}_m$ with speed u is generally due to effects of compressibility and aeroelastic deformation. The latter will again be neglected, so we have only the compressibility effect, which can be represented as

$$\mathbf{C}_{mu} = \mathbf{M}\frac{\partial \mathbf{C}_m}{\partial \mathbf{M}} \tag{4.54}$$

so we have

$$M_u = \frac{QS\bar{c}}{I_y u_0}\mathbf{M}\mathbf{C}_{m\mathbf{M}} \tag{4.55}$$

Angle-of-Attack Derivatives

As mentioned earlier, the derivatives with respect to vertical velocity w are expressed in terms of derivatives with respect to angle of attack α. Since from Eq. (4.39) we have

$$\mathbf{C}_X = \mathbf{C}_T - \mathbf{C}_D + \mathbf{C}_L\alpha \tag{4.56}$$

we have

$$\mathbf{C}_{X\alpha} = \mathbf{C}_{T\alpha} - \mathbf{C}_{D\alpha} + \mathbf{C}_{L\alpha}\alpha + \mathbf{C}_L = -\mathbf{C}_{D\alpha} + \mathbf{C}_{L0} \tag{4.57}$$

since we assume the propulsive thrust is independent of the angle of attack, i.e., $\mathbf{C}_{T\alpha} = 0$. Using the parabolic approximation for the drag polar

$$\mathbf{C}_D = \mathbf{C}_{Dp} + \frac{{\mathbf{C}_L}^2}{\pi e \mathbf{AR}} \tag{4.58}$$

we have

$$\mathbf{C}_{D\alpha} = \frac{2\mathbf{C}_L}{\pi e \mathbf{AR}}\mathbf{C}_{L\alpha} \tag{4.59}$$

and

$$X_w = \frac{QS}{mu_0}\left(\mathbf{C}_{L0} - \frac{2\mathbf{C}_{L0}}{\pi e \mathbf{AR}}\mathbf{C}_{L\alpha}\right) \tag{4.60}$$

Similarly, for the z-force coefficient Eq. (4.39) gives

$$\mathbf{C}_Z = -\mathbf{C}_D\alpha - \mathbf{C}_L \tag{4.61}$$

whence

$$\mathbf{C}_{Z\alpha} = -\mathbf{C}_{D0} - \mathbf{C}_{L\alpha} \tag{4.62}$$

so

$$Z_w = -\frac{QS}{mu_0}\left(\mathbf{C}_{D0} + \mathbf{C}_{L\alpha}\right) \tag{4.63}$$

Finally, the dimensional derivative of pitching moment with respect to vertical velocity w is given by

$$M_w = \frac{QS\bar{c}}{I_y u_0}\mathbf{C}_{m\alpha} \tag{4.64}$$

Pitch-rate Derivatives

The pitch rate derivatives have already been discussed in our review of static longitudinal stability. As seen there, the principal contribution to pitch damping $\mathbf{C}_{mq}$ is from the horizontal tail and is given by

$$\mathbf{C}_{mq} = -2\eta\frac{\ell_t}{\bar{c}}V_H a_t \tag{4.65}$$

Also,

$$\mathbf{C}_{Lq} = 2\eta V_H a_t \tag{4.66}$$

so

$$\mathbf{C}_{Zq} = -\mathbf{C}_{Lq} = -2\eta V_H a_t \tag{4.67}$$

The derivative $\mathbf{C}_{Xq}$ is usually assumed to be negligibly small. In practice, the value given above for $\mathbf{C}_{mq}$ is often multiplied by a factor of 1.1 to account for contributions of other components, particularly the wing.

Angle-of-attack Rate Derivatives

The derivatives with respect to *rate of change* of angle of attack $\dot{\alpha}$ arise primarily from the time lag associated with wing downwash affecting the horizontal tail. This affects the lift force on the horizontal tail and the corresponding pitching moment; the effect on vehicle drag usually is neglected.

The wing downwash is associated with the vorticity trailing behind the wing and, since vorticity is convected with the local fluid velocity, the time lag for vorticity to convect from the wing to the tail is approximately

$$\Delta t = \frac{\ell_t}{u_0}$$

The instantaneous angle of attack seen by the horizontal tail is therefore

$$\alpha_t = \alpha + i_t - \varepsilon = \alpha + i_t - \left[\varepsilon_0 + \frac{\mathrm{d}\varepsilon}{\mathrm{d}\alpha}\left(\alpha - \dot{\alpha}\Delta t\right)\right] \tag{4.68}$$

so

$$\frac{\mathrm{d}\alpha_t}{\mathrm{d}\dot{\alpha}} = \frac{\mathrm{d}\varepsilon}{\mathrm{d}\alpha}\Delta t = \frac{\ell_t}{u_0}\frac{\mathrm{d}\varepsilon}{\mathrm{d}\alpha} \tag{4.69}$$

The rate of change of tail lift with $\dot{\alpha}$ is then seen to be

$$\frac{\mathrm{d}L_t}{\mathrm{d}\dot{\alpha}} = Q_t S_t a_t \frac{\ell_t}{u_0}\frac{\mathrm{d}\varepsilon}{\mathrm{d}\alpha} = \eta Q S_t a_t \frac{\ell_t}{u_0}\frac{\mathrm{d}\varepsilon}{\mathrm{d}\alpha} \tag{4.70}$$

so the change in normal force coefficient with respect to dimensionless $\dot{\alpha}$ is

$$\mathbf{C}_{Z\dot{\alpha}} \equiv \frac{\partial \mathbf{C}_Z}{\partial \frac{\bar{c}\dot{\alpha}}{2u_0}} = -2\eta V_H a_t \frac{\mathrm{d}\varepsilon}{\mathrm{d}\alpha} \tag{4.71}$$

The corresponding change in pitching moment is

$$\frac{\mathrm{d}M_{\mathrm{cg}}}{\mathrm{d}\dot{\alpha}} = -\ell_t \frac{\mathrm{d}L_t}{\mathrm{d}\dot{\alpha}} = -\eta Q S_t a_t \frac{\ell_t^2}{u_0}\frac{\mathrm{d}\varepsilon}{\mathrm{d}\alpha} \tag{4.72}$$

so the change in pitching moment coefficient with respect to dimensionless $\dot{\alpha}$ is

$$\mathbf{C}_{m\dot{\alpha}} \equiv \frac{\partial \mathbf{C}_m}{\partial \frac{\bar{c}\dot{\alpha}}{2u_0}} = -2\eta \frac{\ell_t}{\bar{c}} V_H a_t \frac{\mathrm{d}\varepsilon}{\mathrm{d}\alpha} = \frac{\ell_t}{\bar{c}}\mathbf{C}_{Z\dot{\alpha}} \tag{4.73}$$

4.3.2 Lateral/Directional Stability Derivatives

In order to solve the equations describing lateral/directional vehicle motions, we need to be able to evaluate all the coefficients appearing in Eqs. (4.32). This means we need to be able to provide estimates for the derivatives of Y, L, and N with respect to the relevant independent variables v, p, and r. As for the longitudinal case, these stability derivatives usually are expressed in terms of dimensionless aerodynamic coefficient derivatives.

Derivatives with respect to lateral velocity perturbations v are related to aerodynamic derivatives with respect to angle of sideslip β, since

$$\beta = \tan^{-1}\left(\frac{v}{V}\right) \approx \frac{v}{u_0} \tag{4.74}$$

For example, we can express the stability derivative Y_v as

$$Y_v \equiv \frac{1}{m}\frac{\partial Y}{\partial(u_0\beta)} = \frac{1}{mu_0}\frac{\partial}{\partial\beta}\left[QS\mathbf{C}_y\right] = \frac{QS}{mu_0}\mathbf{C}_{y_\beta} \tag{4.75}$$

where

$$\mathbf{C}_{y_\beta} \equiv \frac{\partial \mathbf{C}_y}{\partial\beta} \tag{4.76}$$

is the derivative of the dimensionless Y-force coefficient with respect to the sideslip angle $\beta = v/u_0$. Similar expressions can be developed for all the required derivatives.

Variable	Y	L	N
v	$Y_v = \frac{QS}{mu_0}\mathbf{C}_{y_\beta}$	$L_v = \frac{QSb}{I_x u_0}\mathbf{C}_{l\beta}$	$N_v = \frac{QSb}{I_z u_0}\mathbf{C}_{n\beta}$
p	$Y_p = \frac{QSb}{2mu_0}\mathbf{C}_{y_p}$	$L_p = \frac{QSb^2}{2I_x u_0}\mathbf{C}_{lp}$	$N_p = \frac{QSb^2}{2I_z u_0}\mathbf{C}_{np}$
r	$Y_r = \frac{QSb}{2mu_0}\mathbf{C}_{y_r}$	$L_r = \frac{QSb^2}{2I_x u_0}\mathbf{C}_{lr}$	$N_r = \frac{QSb^2}{2I_z u_0}\mathbf{C}_{nr}$

Table 4.2: Relation of dimensional stability derivatives for lateral/directional motions to dimensionless derivatives of aerodynamic coefficients.

Derivatives with respect to roll rate p and yaw rate r are related to aerodynamic derivatives with respect to the corresponding dimensionless rate, either $\hat{p} \equiv \frac{pb}{2u_0}$, or $\hat{r} \equiv \frac{rb}{2u_0}$. Thus, for example, the roll damping derivative

$$L_p \equiv \frac{1}{I_x}\frac{\partial L}{\partial p} = \frac{1}{I_x}\frac{\partial}{\partial\left(\frac{2u_0\hat{p}}{b}\right)}\left[QSb\mathbf{C}_l\right] = \frac{QSb^2}{2I_x u_0}\mathbf{C}_{lp} \tag{4.77}$$

where

$$\mathbf{C}_{lp} \equiv \frac{\partial \mathbf{C}_l}{\partial \hat{p}} \tag{4.78}$$

is the derivative of the dimensionless rolling moment coefficient with respect to the dimensionless roll rate $\hat{p}$.[4]

Expressions for all the dimensional stability derivatives appearing in Eqs. (4.32) in terms of the dimensionless aerodynamic coefficient derivatives are summarized in Table 4.2.

Sideslip Derivatives

Here we develop approximate expressions for the derivatives of side force and rolling and yawing moments due to sideslip. The side force derivative $\mathbf{C}_{y_\beta}$ is dominated by the contribution of the vertical tail. This side force, acting through a horizontal moment arm to the vehicle c.g. is the principal stabilizing factor for weathercock stability $\mathbf{C}_{n\beta}$; the fuselage contribution to weathercock is destabilizing (and is similar to its destabilizing contribution to pitch stiffness). The side force on the vertical tail, acting through a vertical moment arm to the vehicle c.g. also contributes to the dihedral effect $\mathbf{C}_{l\beta}$. Wing geometric dihedral and sweep, as well as wing fuselage interference also make important contributions to the dihedral effect. The balance of dihedral effect and weathercock stability plays an important role in the lateral/directional dynamics.

The side force due to sideslip is due primarily to the side force (or "lift") produced by the vertical tail, which can be expressed as

$$Y_v = -Q_v S_v \frac{\partial \mathbf{C}_{Lv}}{\partial \alpha_v}\alpha_v \tag{4.79}$$

[4]Note that the lateral and directional rates are nondimensionalized using the time scale $b/(2u_0)$ – i.e., the span dimension is used instead of the mean aerodynamic chord which appears in the corresponding quantities for longitudinal motions.

where the minus sign is required because we define the angle of attack as

$$\alpha_v = \beta + \sigma \tag{4.80}$$

where positive $\beta = \sin^{-1}(v/V)$ corresponds to positive v. The angle σ is the sidewash angle describing the distortion in angle of attack at the vertical tail due to interference effects from the wing and fuselage. The sidewash angle σ of the vertical tail is analogous to the downwash angle ε of the horizontal tail.[5]

The side force coefficient can then be expressed as

$$\mathbf{C}_y \equiv \frac{Y}{QS} = -\frac{Q_v}{Q}\frac{S_v}{S}\frac{\partial \mathbf{C}_{Lv}}{\partial \alpha_v}(\beta + \sigma) \tag{4.81}$$

whence

$$\mathbf{C}_{y\beta} \equiv \frac{\partial \mathbf{C}_y}{\partial \beta} = -\eta_v \frac{S_v}{S} a_v \left(1 + \frac{\mathrm{d}\sigma}{\mathrm{d}\beta}\right) \tag{4.82}$$

where

$$\eta_v = \frac{Q_v}{Q} \tag{4.83}$$

is the *vertical tail efficiency factor*.

The yawing moment due to side slip is called the *weathercock stability* derivative, and is caused by both, the vertical tail side force acting through the moment arm ℓ_v and the destabilizing yawing moment produced by the fuselage. This latter effect is analogous to the destabilizing contribution of the fuselage to the pitch stiffness $\mathbf{C}_{m_\alpha}$, and can be estimated from slender-body theory to be

$$\mathbf{C}_{n\beta}\big)_{fuse} = -2\frac{\mathcal{V}}{Sb} \tag{4.84}$$

where $\mathcal{V}$ is the volume of the equivalent fuselage – based on fuselage height (rather than width, as for the pitch stiffness). The yawing moment contribution due to the side force acting on the vertical tail is

$$N_v = -\ell_v Y_v$$

so the corresponding contribution of the vertical tail to the weathercock stability is

$$\mathbf{C}_{n\beta}\big)_V = \eta_v V_v a_v \left(1 + \frac{\mathrm{d}\sigma}{\mathrm{d}\beta}\right) \tag{4.85}$$

where

$$V_v = \frac{\ell_v S_v}{bS} \tag{4.86}$$

is the *tail volume ratio* for the vertical tail.

The sum of vertical tail and fuselage contributions to weathercock stability is then

$$\mathbf{C}_{n\beta} = \eta_v V_v a_v \left(1 + \frac{\mathrm{d}\sigma}{\mathrm{d}\beta}\right) - 2\frac{\mathcal{V}}{Sb} \tag{4.87}$$

[5]Note, however, that the sidewash angle is defined as having the opposite sign from the downwash angle. This is because the sidewash angle can easily *augment* the sideslip angle at the vertical tail, while the induced downwash at the horizontal tail always reduces the effective angle of attack.

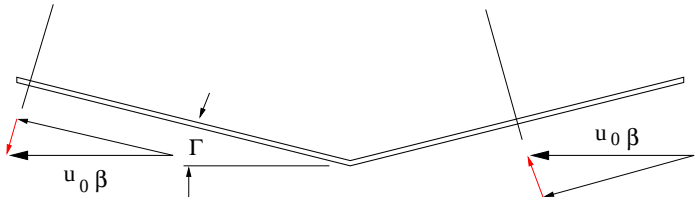

Figure 4.4: Effect of geometric dihedral angle Γ on angle of attack of the left and right wing panels. View is from behind the wing, i.e., looking along the positive x-axis.

Note that a positive value of $\mathbf{C}_{n_\beta}$ corresponds to stability, i.e., to the tendency for the vehicle to turn into the relative wind. The first term on the right hand side of Eq. (4.87), that due to the vertical tail, is stabilizing, while the second term, due to the fuselage, is destabilizing. In fact, providing adequate weathercock stability is the principal role of the vertical tail.

The final sideslip derivative describes the effect of sideslip on the rolling moment. The derivative $\mathbf{C}_{l_\beta}$ is called the *dihedral effect*, and is one of the most important parameters for lateral/directional stability and handling qualities. A stable dihedral effect causes the vehicle to roll away from the sideslip, preventing the vehicle from "falling off its lift vector." This requires a negative value of $\mathbf{C}_{l_\beta}$.

The dihedral effect has contributions from: (1) geometric dihedral; (2) wing sweep; (3) the vertical tail; and (4) wing-fuselage interaction. The contribution from geometric dihedral can be seen from the sketch in Fig. 4.4. There it is seen that the effect of sideslip is to increase the velocity normal to the plane of the right wing, and to decrease the velocity normal to the plane of the left wing, by the amount $u_0\beta\sin\Gamma$, where Γ is the geometric angle of dihedral. Thus, the effective angles of attack of the right and left wings are increased and decreased, respectively, by

$$\Delta\alpha = \frac{u_0\beta\sin\Gamma}{u_0} = \beta\sin\Gamma \tag{4.88}$$

Since the change in angle of attack on the right and left wings is of opposite sign, the corresponding change in lift on the two wings produces a rolling moment. The corresponding change in rolling moment coefficient is given by

$$\Delta\mathbf{C}_l = \frac{\Delta L}{QSb} = -\frac{1}{2}\left(a_w(\beta\sin\Gamma)\frac{\bar{y}}{b} + a_w(-\beta\sin\Gamma)\frac{-\bar{y}}{b}\right) = -a_w\sin\Gamma\frac{\bar{y}}{b}\beta \tag{4.89}$$

where $\bar{y}$ is the distance from the c.g. (symmetry plane) to the center of lift for each wing panel.

For an elliptic spanwise load distribution (see Eq. (4.142)), the centroid of lift on the right wing is located at

$$\bar{y} = \frac{4}{3\pi}\frac{b}{2} \tag{4.90}$$

so, combining this result with Eq. (4.89) we have for a wing with an elliptic spanwise loading

$$\mathbf{C}_{l_\beta} = -\frac{2}{3\pi}a_w\sin\Gamma \tag{4.91}$$

The contribution of wing sweep to dihedral effect arises from the change in effective dynamic pressure on the right and left wing panels due to sideslip, as is illustrated in the sketch in Fig. 4.5. According

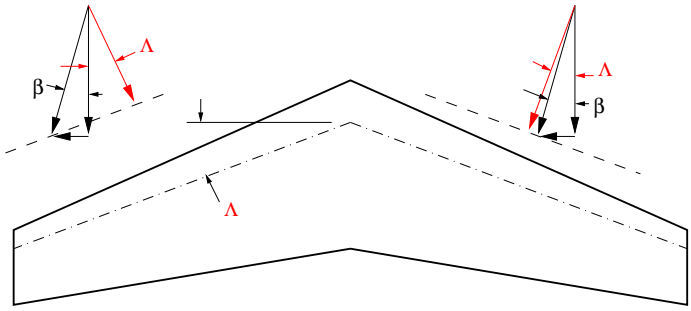

Figure 4.5: Effect of wing sweep dihedral effect. Sideslip increases the effective dynamic pressure on the right wing panel, and decreases it by the same amount on the left wing panel.

to simple sweep theory, it is only the components of velocity in the plane normal to the quarter-chord sweep line that contribute to the forces on the wing, so the lift on the each of the wing panels can be expressed as

$$\begin{aligned} (\text{Lift})_{\text{R}} &= \mathbf{C}_L \frac{S}{2} Q \cos^2\left(\Lambda_{c/4} - \beta\right) \\ (\text{Lift})_{\text{L}} &= \mathbf{C}_L \frac{S}{2} Q \cos^2\left(\Lambda_{c/4} + \beta\right) \end{aligned} \tag{4.92}$$

The net rolling moment coefficient resulting from this lift is then

$$\mathbf{C}_l = \frac{\mathbf{C}_L}{2} \frac{\bar{y}}{b} \left[\cos^2\left(\Lambda_{c/4} + \beta\right) - \cos^2\left(\Lambda_{c/4} - \beta\right)\right] \approx -\mathbf{C}_L \frac{\bar{y}}{b} \sin\left(2\Lambda_{c/4}\right) \beta \tag{4.93}$$

so the contribution of sweep to dihedral stability is

$$\mathbf{C}_{l\beta} = -\mathbf{C}_L \frac{\bar{y}}{b} \sin\left(2\Lambda_{c/4}\right) \tag{4.94}$$

Using Eq. (4.90), we have the expression specialized to the case of an elliptic spanwise loading:

$$\mathbf{C}_{l\beta} = -\frac{2}{3\pi} \mathbf{C}_L \sin\left(2\Lambda_{c/4}\right) \tag{4.95}$$

Note that the contribution of sweep to dihedral effect is proportional to wing lift coefficient (so it will be more significant at low speeds), and is stabilizing when the wing is swept back.

The contribution of the vertical tail to dihedral effect arises from the rolling moment generated by the side force on the tail. Thus, we have

$$\mathbf{C}_{l\beta} = \frac{z'_v}{b} \mathbf{C}_{y_\beta} \tag{4.96}$$

where z'_v is the distance of the vertical tail aerodynamic center above the vehicle center of mass. Using Eq. (4.82), this can be written

$$\mathbf{C}_{l\beta} = -\eta_v \left(\frac{z'_v S_v}{bS}\right) a_v \left(1 + \frac{\mathrm{d}\sigma}{\mathrm{d}\beta}\right) \tag{4.97}$$

At low angles of attack the contribution of the vertical tail to dihedral effect usually is stabilizing. But, at high angles of attack, z'_v can become negative, in which case the contribution is de-stabilizing.

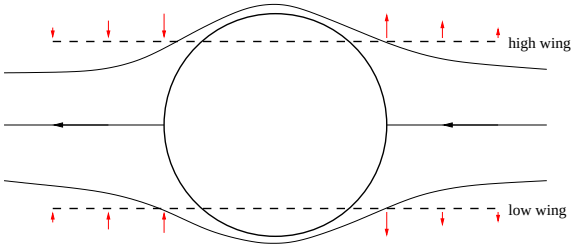

Figure 4.6: Effect of wing-fuselage interference on dihedral effect; figure corresponds to positive sideslip with vehicle viewed from behind. The presence of the fuselage alters the flow due to sideslip locally in the vicinity of the wing. Note that the resulting perturbations in angle of attack for a high-wing configuration are opposite in sign to those for a low-wing configuration, with this phenomenon contributing to stabilizing dihedral effect for the high-wing configuration.

(a) Boeing 747

(b) Lockheed C-5A

Figure 4.7: Illustration of effect of wing-fuselage interference on dihedral effect. The Boeing 747 and Lockheed C-5A have wings with nearly the same sweep angle, but the low-wing 747 requires significantly more geometric dihedral than the high-wing C-5A. Note: the (smaller) high-wing C-130 in the foreground of the photograph on the right requires less negative dihedral (anhedral) than the C-5A because it has an un-swept wing.

The contribution to dihedral effect from wing-fuselage interference will be described only qualitatively. The effect arises from the local changes in wing angle of attack due to the flow past the fuselage as sketched in Fig. 4.6. As indicated in the figure, for a low-wing configuration the presence of the fuselage has the effect of locally decreasing the angle of attack of the right wing in the vicinity of the fuselage, and increasing the corresponding angles of attack of the left wing, resulting in an unstable (positive) contribution to $\mathbf{C}_{l_\beta}$. For a high-wing configuration, the perturbations in angle of attack are reversed, so the interference effect results in a stable (negative) contribution to $\mathbf{C}_{l_\beta}$.

As a result of this wing-fuselage interaction, all other things being equal, a high-wing configuration needs less geometric dihedral than a low-wing one. This effect can be seen by comparing the geometric dihedral angle of a high-wing aircraft with a similar vehicle having a low-wing configuration. For example, the high-wing Lockheed C-5A actually has negative dihedral (or anhedral), while the low-wing Boeing 747 has about 5 degrees of dihedral; see Fig. 4.7.

Finally, it is interesting to consider the dihedral stability of the first powered airplane, the Wright

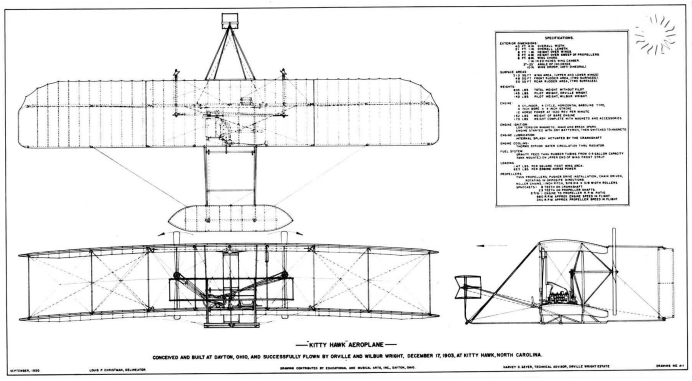

Figure 4.8: Three-view drawing of the Wright Flyer. Note the negative geometric dihedral which, in the absence of other significant contributions to dihedral effect, will almost certainly result in an unstable spiral mode.

Flyer; a three-view drawing is shown in Fig. 4.8. The Wright Flyer has virtually no fuselage (and, in any event, the biplane configuration of the wings is nearly symmetric with respect to all the bracing, etc.), so there is no wing-fuselage interference contribution to $\mathbf{C}_{l\beta}$. Also, the wing is unswept, so there is no sweep contribution. In fact, the wings have a slight *negative* dihedral, so the craft has a net unstable dihedral effect. The Wright brothers did not consider stability a necessary property for a flight vehicle; they started out as bicycle mechanics, and knew that almost anyone could learn to ride an unstable bicycle, so they spent much of their time in early experiments learning how to fly unstable aircraft. Recent re-enactments of Wright Flyer flights, in connection with the centennial celebrations in 2003 of the Wright brothers' first flight, have confirmed the difficulty in learning to fly a vehicle having an unstable dihedral effect!

Derivatives with Respect to Yaw Rate

Here we develop approximate expressions for the derivatives of side force and rolling and yawing moments due to yaw rate. The side force derivative $\mathbf{C}_{y_r}$ is dominated by the contribution of the vertical tail. This side force, acting through the vertical moment arm to the vehicle c.g. also contributes to the derivative $\mathbf{C}_{l_r}$, which couples rolling and yawing motions. Differential lift on the left and right wing panels also is a major contributor to this cross-coupling derivative. The side force on the vertical tail, acting through the horizontal moment arm to the vehicle c.g. is an important factor in yaw damping $\mathbf{C}_{n_r}$, as is the contribution due to differential drag on the left and right wing panels due to the yaw rate.

The stability derivative describing the side force due to yaw rate is

$$Y_r \equiv \frac{1}{m}\frac{\partial Y}{\partial r} = \frac{QSb}{2mu_0}\mathbf{C}_{y_r} \tag{4.98}$$

where

$$\mathbf{C}_{y_r} \equiv \frac{\partial \mathbf{C}_y}{\partial \hat{r}} \tag{4.99}$$

and $\hat{r} = rb/(2u_0)$ is the dimensionless yaw rate. The side force due to yaw rate arises primarily from the force on the vertical tail; thus the derivative $\mathbf{C}_{y_r}$ is analogous to the longitudinal derivative

$\mathbf{C}_{Zq}$. The change in angle of attack of the vertical tail due to yaw rate is

$$\Delta\alpha_v = \frac{r\ell_v}{u_0} = 2\frac{\ell_v}{b}\hat{r} \tag{4.100}$$

so the change in side force is

$$\Delta Y = 2Q_v S_v a_v \frac{\ell_v}{b}\hat{r} \tag{4.101}$$

and the corresponding value of the coefficient derivative is

$$\mathbf{C}_{y_r} = 2\eta_v V_v a_v \tag{4.102}$$

Both the wing and the vertical tail contribute to the rolling moment due to yaw rate. The vertical tail contribution is due to the side force acting through the moment arm z'_v, the distance the vertical tail aerodynamic center is above the vehicle center of mass. Thus,

$$\mathbf{C}_{lr})_V = \frac{z'_v}{b}\mathbf{C}_{y_r} = 2\eta_v \frac{z'_v}{b} V_v a_v \tag{4.103}$$

The contribution of the wing arises because, as a result of the yaw rate the effective velocity of the left wing is increased, and that of the right wing is decreased (for a positive yaw rate r). This effect increases the lift on the left wing, and decreases it on the right wing. The effect is proportional to the equilibrium lift coefficient and, for an elliptical spanwise loading simple strip theory gives (see Exercise 2)

$$(\mathbf{C}_{lr})_{\text{wing}} = \frac{\mathbf{C}_{L0}}{4} \tag{4.104}$$

The sum of the vertical tail and wing contributions gives the total

$$\mathbf{C}_{lr} = \frac{\mathbf{C}_{L0}}{4} + 2\eta_v \frac{z'_v}{b} V_v a_v \tag{4.105}$$

The yawing moment due to yaw rate is called the *yaw damping*, and also has contributions from both the vertical tail and the wing. The contribution of the vertical tail is due to the side force acting through the moment arm ℓ_v, and is analogous to that of the horizontal tail to pitch damping $\mathbf{C}_{mq}$. Thus, we have

$$\mathbf{C}_{nr})_V = -\frac{\ell_v}{b}\mathbf{C}_{y_r} = -2\eta_v \frac{\ell_v}{b} V_v a_v \tag{4.106}$$

The contribution of the wing to yaw damping is similar to its contribution to rolling moment, except now it is the variation of drag (rather than lift) along the span that generates the moment. Thus, if the sectional drag is also assumed to vary elliptically along the span, we find a contribution analogous to Eq. (4.104)

$$\mathbf{C}_{nr})_{\text{wing}} = -\frac{\mathbf{C}_{D0}}{4} \tag{4.107}$$

and the sum of vertical tail and wing contributions is

$$\mathbf{C}_{nr} = -\frac{\mathbf{C}_{D0}}{4} - 2\eta_v \frac{\ell_v}{b} V_v a_v \tag{4.108}$$

Derivatives with Respect to Roll Rate

Here we develop approximate expressions for the derivatives of side force and rolling and yawing moments due to roll rate. The side force derivative $\mathbf{C}_{y_p}$ is dominated by the contribution of the vertical tail. This side force, acting through the vertical moment arm to the vehicle c.g. also contributes to roll damping $\mathbf{C}_{l_p}$, as does differential lift on the left and right wing panels. The side force on the vertical tail, acting through the horizontal moment arm to the vehicle c.g. contributes to the cross coupling derivative $\mathbf{C}_{n_p}$, as does the differential drag on the left and right wing panels due to the roll rate. The wing drag contribution is complex because the downgoing wing sees an increase in profile drag, but a decrease in induced drag, so it is useful to consider the two components of drag separately.

The derivatives with respect to roll rate p include the side force

$$Y_p \equiv \frac{1}{m}\frac{\partial Y}{\partial p} = \frac{QSb}{2mu_0}\mathbf{C}_{y_p} \tag{4.109}$$

where

$$\mathbf{C}_{y_p} \equiv \frac{\partial \mathbf{C}_y}{\partial \hat{p}} \tag{4.110}$$

where $\hat{p} = pb/(2u_0)$ is the dimensionless roll rate, and the rolling moment

$$L_p \equiv \frac{1}{I_x}\frac{\partial L}{\partial p} = \frac{QSb^2}{2I_x u_0}\mathbf{C}_{l_p} \tag{4.111}$$

and yawing moment

$$N_p \equiv \frac{1}{I_z}\frac{\partial N}{\partial p} = \frac{QSb^2}{2I_z u_0}\mathbf{C}_{n_p} \tag{4.112}$$

The derivative of side force with respect to (dimensionless) roll rate $\hat{p}$ arises from the linear distribution of perturbation angle of attack along the span of the vertical tail

$$\Delta\alpha = \frac{pz'}{u_0} = \frac{z'}{b}\hat{p} \tag{4.113}$$

where, in this equation, z' is measured from the vehicle c.g. along the *negative* z-axis. The side force is then given by

$$\Delta Y = -\eta_v Q \int_0^{b_v} c_v \left(\frac{\partial \mathbf{c}_\ell}{\partial \alpha}\right)_v \Delta\alpha \, \mathrm{d}z' = -2\eta_v Q \left(\frac{b_v}{b}\right)^2 b\hat{p} \int_0^1 \left(\frac{\partial \ell}{\partial \alpha}\right)_v \eta' \, \mathrm{d}\eta' \tag{4.114}$$

If the spanwise lift curve slope distribution is approximated as elliptic,

$$\left(\frac{\partial \ell}{\partial \alpha}\right)_v = \ell_{0_\alpha}\sqrt{1-\eta'^2} \tag{4.115}$$

where

$$a_v = \frac{\partial \mathbf{C}_{Lv}}{\partial \alpha_v} = \frac{1}{S_v}\int_0^1 \ell_{0_\alpha}\sqrt{1-\eta'^2} b_v \, \mathrm{d}\eta' = \frac{\pi}{4}\frac{b_v}{S_v}\ell_{0_\alpha} \tag{4.116}$$

then the dimensionless side force derivative can be written

$$\mathbf{C}_{y_p} = \frac{\Delta Y}{QS\hat{p}} = -\frac{2\eta_v b}{S}\left(\frac{b_v}{b}\right)^2 \ell_{0_\alpha}\int_0^1 \eta'\sqrt{1-\eta'^2}\,\mathrm{d}\eta' = -\frac{2\eta_v b}{3S}\left(\frac{b_v}{b}\right)^2 \ell_{0_\alpha} \tag{4.117}$$

Equation (4.116) can then be used to express this in terms of the vertical tail lift-curve slope a_v as

$$\mathbf{C}_{y_p} = -\frac{8}{3\pi}\eta_v \left(\frac{b_v S_v}{bS}\right) a_v \tag{4.118}$$

In practice, this derivative usually is neglected, but it will be used in the estimation of the yawing moment due to roll rate later in this section.

The derivative of rolling moment with respect to (dimensionless) roll rate $\mathbf{C}_{l_p}$ is called *roll damping*, and is due almost entirely to the wing. The roll rate imposes a linear variation in angle of attack across the wing span given, approximately, by

$$\Delta\alpha = \frac{py}{u_0} = \frac{2y}{b}\hat{p} \tag{4.119}$$

This spanwise distribution in angle of attack produces a spanwise distribution of sectional lift coefficient equal to

$$\Delta\mathbf{c}_\ell = a_w \frac{2y}{b}\hat{p} \tag{4.120}$$

which produces a rolling moment equal to

$$\Delta L = -2Q\int_0^{b/2} c\Delta\mathbf{c}_\ell y \,\mathrm{d}y = -\frac{Qb^2 a_w}{2}\hat{p}\int_0^1 c\eta^2 \,\mathrm{d}\eta \tag{4.121}$$

or

$$\mathbf{C}_{l_p} = \frac{\Delta L}{QSb\hat{r}} = -\frac{b}{2S}a_w \int_0^1 c\eta^2 \,\mathrm{d}\eta \tag{4.122}$$

For an *untapered* wing,

$$\int_0^1 c\eta^2 \,\mathrm{d}\eta = \frac{S}{3b} \tag{4.123}$$

so

$$\mathbf{C}_{l_p} = -\frac{a_w}{6} \tag{4.124}$$

Note that, for a tapered wing, the roll damping will be somewhat less. In particular, for the elliptical spanwise loading

$$c\frac{\partial\mathbf{c}_\ell}{\partial\alpha} = \ell_{0_\alpha}\sqrt{1-\left(\frac{2y}{b}\right)^2} = \frac{4S}{\pi b}a_w\sqrt{1-\left(\frac{2y}{b}\right)^2} \tag{4.125}$$

it can be shown[6]that

$$\mathbf{C}_{l_p} = -\frac{a_w}{8} \tag{4.126}$$

Also, for angles of attack *past the stall*, the sign of the lift curve slope is negative, and the roll damping derivative becomes positive. Thus, any tendency for the vehicle to roll will be augmented, leading to autorotation, or spinning.

The yawing moment induced by roll rate has contributions from both the vertical tail and the wing. The vertical tail contribution comes from the side force induced by roll rate acting through the moment arm ℓ_v, the distance the vertical tail aerodynamic center is aft of the vehicle center of mass. Thus,

$$\mathbf{C}_{n_p}\big)_V = -\frac{\ell_v}{b}\mathbf{C}_{y_p} \tag{4.127}$$

[6]See Exercise 3.

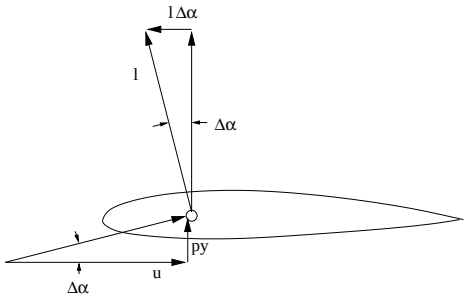

Figure 4.9: Induced drag contribution to yaw due to roll rate; the effect is illustrated for a typical section the right wing.

or, using Eq. (4.118), we have

$$\mathbf{C}_{np}\big)_V = \frac{8}{3\pi}\frac{b_v}{b}V_v a_v \tag{4.128}$$

Note that although the derivative $\mathbf{C}_{y_p}$ itself often is neglected, its contribution to $\mathbf{C}_{np}$ can be significant.

The contribution of the wing to $\mathbf{C}_{np}$ has two components: one due to the difference in profile drag on the left and right wing panels and one due to the yawing moment caused by the effective rotation of the lift vector on either wing panel in opposite directions – i.e., to changes in induced drag. The first component depends on the details of the wing sections and the equilibrium angle of attack. Due to the roll rate, the angle attack of the right wing is increased linearly along the span, and that of the left wing is decreased linearly along the span, as shown in Eq. (4.119). Associated with these changes in lift is an increase in profile drag on the right wing and a corresponding decrease in drag on the left wing, yielding a positive yawing moment.

The induced drag effect is associated with the rotation of the lift vector at each span station through the perturbation angle of attack induced by the roll rate, as illustrated for a typical section of the right wing in Fig. 4.9. As seen in the figure, there is a change in the sectional contribution to the induced drag given by

$$\Delta\mathbf{c}_d = -\mathbf{c}_\ell \Delta\alpha = -\mathbf{c}_\ell \frac{py}{u_0} = -\mathbf{c}_\ell \left(\frac{2y}{b}\right)\hat{p} \tag{4.129}$$

It can be shown that, for an elliptical span loading, simple strip theory integration of this effect across the span gives[7]

$$\big(\mathbf{C}_{np}\big)_{\text{induced}} = -\frac{\mathbf{C}_L}{8} \tag{4.130}$$

4.4 Control Derivatives

The control derivatives consist of the pitching moment due to elevator deflection

$$M_{\delta_e} \equiv \frac{1}{I_y}\frac{\partial M}{\partial \delta_e} = \frac{QS\bar{c}}{I_y}\mathbf{C}_{m\delta_e} \tag{4.131}$$

[7] See Exercise 4.

the rolling moment due to aileron deflection

$$L_{\delta_a} \equiv \frac{1}{I_x}\frac{\partial L}{\partial \delta_a} = \frac{QSb}{I_x}\mathbf{C}_{l\,\delta_a} \tag{4.132}$$

and the yawing moment due to rudder deflection

$$N_{\delta_r} \equiv \frac{1}{I_z}\frac{\partial N}{\partial \delta_r} = \frac{QSb}{I_z}\mathbf{C}_{n\,\delta_r} \tag{4.133}$$

There also can be significant cross-coupling of the rudder and aileron control moments. The yawing moment due to aileron deflection

$$N_{\delta_a} \equiv \frac{1}{I_z}\frac{\partial N}{\partial \delta_a} = \frac{QSb}{I_z}\mathbf{C}_{n\,\delta_a} \tag{4.134}$$

is called *adverse yaw*, since this derivative usually is negative, leading to a tendency to rotate the nose to the left when the vehicle rolls to the right. The rolling moment due to rudder deflection

$$L_{\delta_r} \equiv \frac{1}{I_x}\frac{\partial L}{\partial \delta_r} = \frac{QSb}{I_x}\mathbf{C}_{l\,\delta_r} \tag{4.135}$$

also tends to be unfavorable, as it tends to roll the vehicle to the left when trying to turn to the right.

These control derivatives are difficult to predict accurately using simple analyses, and wind-tunnel testing or computational fluid dynamics (CFD) analyses usually are required.

4.5 Properties of Elliptical Span Loadings

It is often useful to estimate lateral/directional stability derivatives and stability coefficients based on an elliptical spanwise load distribution. Since we usually write

$$\mathbf{C}_L = \frac{2}{S}\int_0^{b/2} c\mathbf{c}_\ell \,\mathrm{d}y \tag{4.136}$$

it is clear that it is the spanwise distribution of the local chord times the section lift coefficient that is most important. Thus, we introduce

$$\ell \equiv c\mathbf{c}_\ell \tag{4.137}$$

and for an elliptical span loading we have

$$\ell = \ell_0\sqrt{1-\left(\frac{2y}{b}\right)^2} \tag{4.138}$$

The constant ℓ_0 is related to the wing lift coefficient by

$$\mathbf{C}_L = \frac{2}{S}\int_0^{b/2} \ell_0\sqrt{1-\left(\frac{2y}{b}\right)^2}\,\mathrm{d}y = \frac{b\ell_0}{S}\int_0^1 \sqrt{1-\eta^2}\,\mathrm{d}\eta = \frac{\pi b\ell_0}{4S} \tag{4.139}$$

or

$$\ell_0 = \frac{4S}{\pi b}\mathbf{C}_L \tag{4.140}$$

The center of lift for a single wing panel having an elliptical span loading is then seen to be

$$\bar{y} = \frac{2}{S\mathbf{C}_L}\int_0^{b/2} yc\mathbf{c}_\ell \,\mathrm{d}y = \frac{b^2}{2S\mathbf{C}_L}\int_0^1 \eta\ell_0\sqrt{1-\eta^2}\,\mathrm{d}\eta = \frac{2b}{\pi}\int_0^1 \eta\sqrt{1-\eta^2}\,\mathrm{d}\eta = \frac{2b}{3\pi} \tag{4.141}$$

or

$$\frac{2\bar{y}}{b} = \frac{4}{3\pi} \tag{4.142}$$

That is, the center of lift of the wing panel is at approximately the 42 per cent semi-span station.

4.5.1 Useful Integrals

When estimating contributions of lifting surfaces having elliptic span loadings to various stability derivatives, integrals of the form

$$\int_0^1 \eta^n\sqrt{1-\eta^2}\,\mathrm{d}\eta \tag{4.143}$$

often need to be evaluated for various values of non-negative integer n. These integrals can be evaluated in closed form using trigonometric substitution. Thus, we have the following useful results:

$$\begin{aligned}\int_0^1 \sqrt{1-\eta^2}\,\mathrm{d}\eta &= \int_0^{\pi/2}\sqrt{1-\sin^2\xi}\cos\xi\,\mathrm{d}\xi \\ &= \int_0^{\pi/2}\cos^2\xi\,\mathrm{d}\xi = \int_0^{\pi/2}\frac{\cos 2\xi+1}{2}\,\mathrm{d}\xi = \frac{\pi}{4}\end{aligned} \tag{4.144}$$

$$\begin{aligned}\int_0^1 \eta\sqrt{1-\eta^2}\,\mathrm{d}\eta &= \int_0^{\pi/2}\sin\xi\sqrt{1-\sin^2\xi}\cos\xi\,\mathrm{d}\xi \\ &= \int_0^{\pi/2}\sin\xi\cos^2\xi\,\mathrm{d}\xi = \frac{1}{3}\end{aligned} \tag{4.145}$$

$$\begin{aligned}\int_0^1 \eta^2\sqrt{1-\eta^2}\,\mathrm{d}\eta &= \int_0^{\pi/2}\sin^2\xi\sqrt{1-\sin^2\xi}\cos\xi\,\mathrm{d}\xi \\ &= \int_0^{\pi/2}\sin^2\xi\cos^2\xi\,\mathrm{d}\xi = \int_0^{\pi/2}\left(\frac{\sin 2\xi}{2}\right)^2\mathrm{d}\xi = \int_0^{\pi/2}\frac{1-\cos 4\xi}{8}\,\mathrm{d}\xi = \frac{\pi}{16}\end{aligned} \tag{4.146}$$

4.6 Exercises

1. Show that for a straight, untapered wing (i.e., one having a rectangular planform) having a constant spanwise load distribution (i.e., constant section lift coefficient), simple strip theory gives the wing contribution to the rolling moment due to yaw rate as

$$(\mathbf{C}_{lr})_{\text{wing}} = \frac{\mathbf{C}_L}{3}$$

2. Show that for a wing having an elliptical spanwise load distribution, simple strip theory gives the wing contribution to the rolling moment due to yaw rate as

$$(\mathbf{C}_{lr})_{\text{wing}} = \frac{\mathbf{C}_L}{4}$$

Explain, in simple terms, why this value is smaller than that computed in Exercise 1.

3. Show that the contribution to roll damping of a wing having an elliptical span loading is

$$\mathbf{C}_{l_p} = -\frac{a_w}{8}$$

4. Show that for a wing having an elliptical spanwise load distribution, simple strip theory gives the induced drag contribution of the wing to the yawing moment due to roll rate as

$$\left(\mathbf{C}_{n_p}\right)_{\text{wing}} = -\frac{\mathbf{C}_L}{8}$$

Bibliography

[1] Bernard Etkin & Lloyd Duff Reid, **Dynamics of Flight, Stability and Control**, McGraw-Hill, Third Edition, 1996.

[2] Robert C. Nelson, **Aircraft Stability and Automatic Control**, McGraw-Hill, Second edition, 1998.

[3] Louis V. Schmidt, **Introduction to Aircraft Flight Dynamics**, AIAA Education Series, 1998.

Chapter 5

Dynamic Stability

These notes provide a brief background for the response of linear systems, with application to the equations of motion for a flight vehicle. The description is meant to provide the basic background in linear algebra for understanding modern tools for analyzing the response of linear systems, and provide examples of their application to flight vehicle dynamics. Examples for both longitudinal and lateral/directional motions are provided, and simple, lower-order approximations to the various modes are used to elucidate the roles of relevant aerodynamic properties of the vehicle.

5.1 Mathematical Background

5.1.1 An Introductory Example

The most interesting aircraft motions consist of oscillatory modes, the basic features of which can be understood by considering the simple system, sketched in Fig. 5.1, consisting of a spring, mass, and damper.

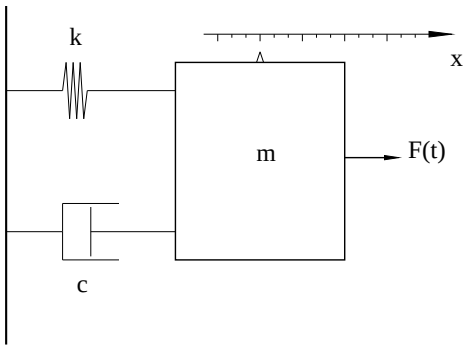

Figure 5.1: Schematic of spring-mass-damper system.

The dynamics of this system are described by the second-order ordinary differential equation

$$m\frac{\mathrm{d}^2x}{\mathrm{d}t^2} + c\frac{\mathrm{d}x}{\mathrm{d}t} + kx = F(t) \tag{5.1}$$

where m is the mass of the system, c is the damping parameter, and k is the spring constant of the restoring force. We generally are interested in both the *free response* of the system to an initial perturbation (with $F(t) = 0$), and the *forced response* to time-varying $F(t)$. The free response is relevant to the question of stability – i.e., the response to an infinitesimal perturbation from an equilibrium state of the system, while the forced response is relevant to control response.

The free response is the solution to the homogeneous equation, which can be written

$$\frac{\mathrm{d}^2x}{\mathrm{d}t^2} + \left(\frac{c}{m}\right)\frac{\mathrm{d}x}{\mathrm{d}t} + \left(\frac{k}{m}\right)x = 0 \tag{5.2}$$

Solutions of this equation are generally of the form

$$x = Ae^{\lambda t} \tag{5.3}$$

where A is a constant determined by the initial perturbation. Substitution of Eq. (5.3) into the differential equation yields the *characteristic equation*

$$\lambda^2 + \left(\frac{c}{m}\right)\lambda + \left(\frac{k}{m}\right) = 0 \tag{5.4}$$

which has roots

$$\lambda = -\frac{c}{2m} \pm \sqrt{\left(\frac{c}{2m}\right)^2 - \left(\frac{k}{m}\right)} \tag{5.5}$$

The nature of the response depends on whether the second term in the above expression is real or imaginary, and therefore depends on the relative magnitudes of the damping parameter c and the spring constant k. We can re-write the characteristic equation in terms of a variable defined by the ratio of the two terms in the square root

$$\frac{\left(\frac{c}{2m}\right)^2}{\left(\frac{k}{m}\right)} = \frac{c^2}{4mk} \equiv \zeta^2 \tag{5.6}$$

and a variable explicitly depending on the spring constant k, which we will choose (for reasons that will become obvious later) to be

$$\frac{k}{m} \equiv \omega_n^2 \tag{5.7}$$

In terms of these new variables, the original Eq. (5.2) can be written as

$$\frac{\mathrm{d}^2x}{\mathrm{d}t^2} + 2\zeta\omega_n\frac{\mathrm{d}x}{\mathrm{d}t} + \omega_n^2 x = 0 \tag{5.8}$$

The corresponding characteristic equation takes the form

$$\lambda^2 + 2\zeta\omega_n\lambda + \omega_n^2 = 0 \tag{5.9}$$

and its roots can now be written in the suggestive forms

$$\lambda = \begin{cases} -\zeta\omega_n \pm \omega_n\sqrt{\zeta^2 - 1} & \text{for } \zeta > 1 \\ -\zeta\omega_n & \text{for } \zeta = 1 \\ -\zeta\omega_n \pm i\omega_n\sqrt{1 - \zeta^2} & \text{for } \zeta < 1 \end{cases} \tag{5.10}$$

Overdamped System

For cases in which $\zeta > 1$, the characteristic equation has two (distinct) real roots, and the solution takes the form

$$x = a_1 e^{\lambda_1 t} + a_2 e^{\lambda_2 t} \tag{5.11}$$

where

$$\begin{aligned} \lambda_1 &= -\omega_n \left(\zeta + \sqrt{\zeta^2 - 1} \right) \\ \lambda_2 &= -\omega_n \left(\zeta - \sqrt{\zeta^2 - 1} \right) \end{aligned} \tag{5.12}$$

The constants a_1 and a_2 are determined from the initial conditions

$$\begin{aligned} x(0) &= a_1 + a_2 \\ \dot{x}(0) &= a_1 \lambda_1 + a_2 \lambda_2 \end{aligned} \tag{5.13}$$

or, in matrix form,

$$\begin{pmatrix} 1 & 1 \\ \lambda_1 & \lambda_2 \end{pmatrix} \begin{pmatrix} a_1 \\ a_2 \end{pmatrix} = \begin{pmatrix} x(0) \\ \dot{x}(0) \end{pmatrix} \tag{5.14}$$

Since the determinant of the coefficient matrix in these equations is equal to $\lambda_2 - \lambda_1$, the coefficient matrix is non-singular so long as the characteristic values λ_1 and λ_2 are distinct – which is guaranteed by Eqs. (5.12) when $\zeta > 1$. Thus, for the *overdamped* system ($\zeta > 1$), the solution is completely determined by the initial values of x and $\dot{x}$, and consists of a linear combination of two decaying exponentials.

The reciprocal of the *undamped natural frequency* ω_n forms a natural time scale for this problem, so if we introduce the dimensionless time

$$\hat{t} = \omega_n t \tag{5.15}$$

then Eq. (5.8) can be written

$$\frac{\mathrm{d}^2 x}{\mathrm{d}\hat{t}^2} + 2\zeta \frac{\mathrm{d}x}{\mathrm{d}\hat{t}} + x = 0 \tag{5.16}$$

which is seen to depend only on the damping ratio ζ. Figure 5.2 shows the response of overdamped systems for various values of the damping ratio as functions of the dimensionless time $\hat{t}$.

Critically Damped System

When the damping ratio $\zeta = 1$, the system is said to be *critically damped*, and there is only a single characteristic value

$$\lambda_1 = \lambda_2 = -\omega_n \tag{5.17}$$

Thus, only one of the two initial conditions can, in general, be satisfied by a solution of the form $e^{\lambda t}$. However, in this special case it is easily verified that $te^{\lambda t} = te^{-\omega_n t}$ is also a solution of Eq. (5.8), so the general form of the solution for the critically damped case can be written as

$$x = (a_1 + a_2 t)\, e^{-\omega_n t} \tag{5.18}$$

The constants a_1 and a_2 are again determined from the initial conditions

$$\begin{aligned} x(0) &= a_1 \\ \dot{x}(0) &= a_1 \lambda_1 + a_2 \end{aligned} \tag{5.19}$$

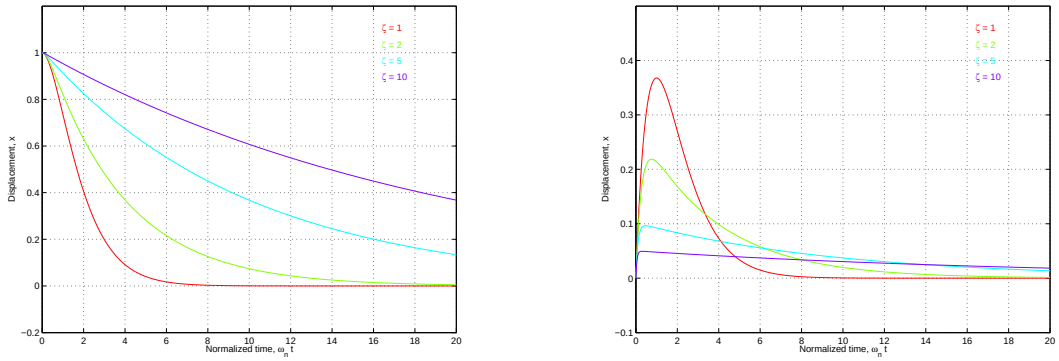

(a) $x(0) = 1.0$ (b) $\dot{x}(0) = 1.0$

Figure 5.2: Overdamped response of spring-mass-damper system. (a) Displacement perturbation: $x(0) = 1.0$; $\dot{x}(0) = 0$. (b) Velocity perturbation: $\dot{x}(0) = 1.0$; $x(0) = 0$.

or, in matrix form,

$$\begin{pmatrix} 1 & 0 \\ \lambda_1 & 1 \end{pmatrix} \begin{pmatrix} a_1 \\ a_2 \end{pmatrix} = \begin{pmatrix} x(0) \\ \dot{x}(0) \end{pmatrix} \tag{5.20}$$

Since the determinant of the coefficient matrix in these equations is always equal to unity, the coefficient matrix is non-singular. Thus, for the *critically damped* system ($\zeta = 1$), the solution is again completely determined by the initial values of x and $\dot{x}$, and consists of a linear combination of a decaying exponential and a term proportional to $te^{-\omega_n t}$. For any positive value of ω_n the exponential decays more rapidly than any positive power of t, so the solution again decays, *nearly* exponentially.

Figures 5.2 and 5.3 include the limiting case of critically damped response for Eq. (5.16).

Underdamped System

When the damping ratio $\zeta < 1$, the system is said to be *underdamped*, and the roots of the characteristic equation consist of the complex conjugate pair

$$\begin{aligned} \lambda_1 &= \omega_n \left(-\zeta + i\sqrt{1-\zeta^2} \right) \\ \lambda_2 &= \omega_n \left(-\zeta - i\sqrt{1-\zeta^2} \right) \end{aligned} \tag{5.21}$$

Thus, the general form of the solution can be written

$$x = e^{-\zeta\omega_n t} \left[a_1 \cos\left(\omega_n \sqrt{1-\zeta^2} t \right) + a_2 \sin\left(\omega_n \sqrt{1-\zeta^2} t \right) \right] \tag{5.22}$$

The constants a_1 and a_2 are again determined from the initial conditions

$$\begin{aligned} x(0) &= a_1 \\ \dot{x}(0) &= -\zeta\omega_n a_1 + \omega_n \sqrt{1-\zeta^2} a_2 \end{aligned} \tag{5.23}$$

or, in matrix form,

$$\begin{pmatrix} 1 & 0 \\ -\zeta\omega_n & \omega_n\sqrt{1-\zeta^2} \end{pmatrix} \begin{pmatrix} a_1 \\ a_2 \end{pmatrix} = \begin{pmatrix} x(0) \\ \dot{x}(0) \end{pmatrix} \tag{5.24}$$

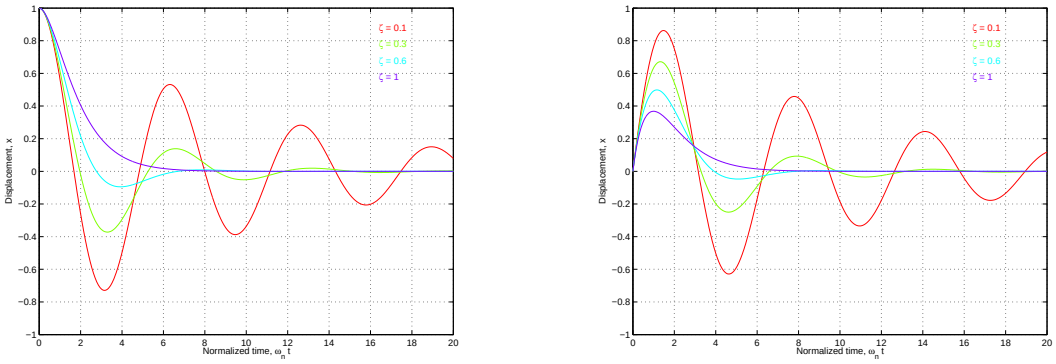

(a) $x(0) = 1.0$ (b) $\dot{x}(0) = 1.0$

Figure 5.3: Underdamped response of spring-mass-damper system. (a) Displacement perturbation: $x(0) = 1.0$; $\dot{x}(0) = 0$. (b) Velocity perturbation: $\dot{x}(0) = 1.0$; $x(0) = 0$.

Since the determinant of the coefficient matrix in these equations is equal to $\omega_n\sqrt{1-\zeta^2}$, the system is non-singular when $\zeta < 1$, and the solution is completely determined by the initial values of x and $\dot{x}$. Figure 5.3 shows the response of the underdamped system Eq. (5.16) for various values of the damping ratio, again as a function of the dimensionless time $\hat{t}$.

As is seen from Eq. (5.22), the solution consists of an exponentially decaying sinusoidal motion. This motion is characterized by its period and the rate at which the oscillations are damped. The period is given by

$$T = \frac{2\pi}{\omega_n\sqrt{1-\zeta^2}} \tag{5.25}$$

and the time to damp to $1/n$ times the initial amplitude is given by[1]

$$t_{1/n} = \frac{\ln n}{\omega_n \zeta} \tag{5.26}$$

For these oscillatory motions, the damping frequently is characterized by the *number of cycles* to damp to $1/n$ times the initial amplitude, which is given by

$$N_{1/n} = \frac{t_{1/n}}{T} = \frac{\ln n}{2\pi}\frac{\sqrt{1-\zeta^2}}{\zeta} \tag{5.27}$$

Note that this latter quantity is independent of the undamped natural frequency; i.e., it depends *only* on the damping ratio ζ.

5.1.2 Systems of First-order Equations

Although the equation describing the spring-mass-damper system of the previous section was solved in its original form, as a single second-order ordinary differential equation, it is useful for later

[1] The most commonly used values of n are 2 and 10, corresponding to the times to damp to 1/2 the initial amplitude and 1/10 the initial amplitude, respectively.

generalization to re-write it as a *system* of coupled first-order differential equations by defining

$$\begin{aligned} x_1 &= x \\ x_2 &= \frac{\mathrm{d}x}{\mathrm{d}t} \end{aligned} \tag{5.28}$$

Equation (5.8) can then be written as

$$\frac{\mathrm{d}}{\mathrm{d}t}\begin{pmatrix} x_1 \\ x_2 \end{pmatrix} = \begin{pmatrix} 0 & 1 \\ -\omega_n^2 & -2\zeta\omega_n \end{pmatrix}\begin{pmatrix} x_1 \\ x_2 \end{pmatrix} + \begin{pmatrix} 0 \\ \frac{1}{m} \end{pmatrix} F(t) \tag{5.29}$$

which has the general form

$$\dot{\mathbf{x}} = \mathbf{A}\mathbf{x} + \mathbf{B}\eta \tag{5.30}$$

where $\mathbf{x} = (x_1, x_2)^T$, the dot represents a time derivative, and $\eta(t) = F(t)$ will be identified as the control input.

The free response is then governed by the system of equations

$$\dot{\mathbf{x}} = \mathbf{A}\mathbf{x} \tag{5.31}$$

and substitution of the general form

$$\mathbf{x} = \mathbf{x}_i e^{\lambda_i t} \tag{5.32}$$

into Eqs. (5.31) requires

$$(\mathbf{A} - \lambda_i \mathbf{I})\,\mathbf{x}_i = 0 \tag{5.33}$$

Thus, the free response of the system in seen to be completely determined by the eigenstructure (i.e., the eigenvalues and eigenvectors) of the *plant matrix* $\mathbf{A}$. The vector $\mathbf{x}_i$ is seen to be the eigenvector associated with the eigenvalue λ_i of the matrix $\mathbf{A}$ and, when the eigenvalues are unique, the general solution can be expressed as a linear combination of the form

$$\mathbf{x} = \sum_{i=1}^{2} a_i \mathbf{x}_i e^{\lambda_i t} \tag{5.34}$$

where the constants a_i are determined by the initial conditions. The *modal matrix* $\mathbf{Q}$ of $\mathbf{A}$ is defined as the matrix whose columns are the eigenvectors of $\mathbf{A}$

$$\mathbf{Q} = \begin{pmatrix} \mathbf{x}_1 & \mathbf{x}_2 \end{pmatrix} \tag{5.35}$$

so the initial values of the vector $\mathbf{x}$ are given by

$$\mathbf{x}(0) = \sum_{i=1}^{2} a_i \mathbf{x}_i = \mathbf{Q}\mathbf{a} \tag{5.36}$$

where the elements of the vector

$$\mathbf{a} = \{a_1,\, a_2\}^T$$

correspond to the coefficients in the *modal expansion* of the solution in the form of Eq. (5.34). When the eigenvalues are complex, they must appear in complex conjugate pairs, and the corresponding eigenvectors also are complex conjugates, so the solution corresponding to a complex conjugate pair of eigenvalues again corresponds to an exponentially damped harmonic oscillation.

While the above analysis corresponds to the second-order system treated previously, the advantage of viewing is as a system of first-order equations is that, once we have shifted our viewpoint the analysis

carries through for a system of any order. In particular, the simplest complete linear analyses of either longitudinal or lateral/directional dynamics will lead to fourth-order systems – i.e., to systems of four coupled first-order differential equations. In practice, most of the required operations involving eigenvalues and eigenvectors can be accomplished easily using numerical software packages, such as MATLAB

5.2 Longitudinal Motions

In this section, we develop the small-disturbance equations for longitudinal motions in standard state-variable form. Recall that the linearized equations describing small longitudinal perturbations from a longitudinal equilibrium state can be written

$$\begin{aligned}
\left[\frac{\mathrm{d}}{\mathrm{d}t} - X_u\right] u + g_0 \cos\Theta_0 \theta - X_w w &= X_{\delta_e}\delta_e + X_{\delta_T}\delta_T \\
-Z_u u + \left[(1 - Z_{\dot{w}})\frac{\mathrm{d}}{\mathrm{d}t} - Z_w\right] w - [u_0 + Z_q]\, q + g_0 \sin\Theta_0 \theta &= Z_{\delta_e}\delta_e + Z_{\delta_T}\delta_T \\
-M_u u - \left[M_{\dot{w}}\frac{\mathrm{d}}{\mathrm{d}t} + M_w\right] w + \left[\frac{\mathrm{d}}{\mathrm{d}t} - M_q\right] q &= M_{\delta_e}\delta_e + M_{\delta_T}\delta_T
\end{aligned} \tag{5.37}$$

If we introduce the longitudinal state variable vector

$$\mathbf{x} = [u \quad w \quad q \quad \theta]^T \tag{5.38}$$

and the longitudinal control vector

$$\eta = [\delta_e \quad \delta_T]^T \tag{5.39}$$

these equations are equivalent to the system of first-order equations

$$\mathbf{I}_n \dot{\mathbf{x}} = \mathbf{A}_n \mathbf{x} + \mathbf{B}_n \eta \tag{5.40}$$

where $\dot{\mathbf{x}}$ represents the time derivative of the state vector $\mathbf{x}$, and the matrices appearing in this equation are

$$\begin{aligned}
\mathbf{A}_n &= \begin{pmatrix} X_u & X_w & 0 & -g_0\cos\Theta_0 \\ Z_u & Z_w & u_0 + Z_q & -g_0\sin\Theta_0 \\ M_u & M_w & M_q & 0 \\ 0 & 0 & 1 & 0 \end{pmatrix} \\
\mathbf{I}_n &= \begin{pmatrix} 1 & 0 & 0 & 0 \\ 0 & 1 - Z_{\dot{w}} & 0 & 0 \\ 0 & -M_{\dot{w}} & 1 & 0 \\ 0 & 0 & 0 & 1 \end{pmatrix}, \quad \mathbf{B}_n = \begin{pmatrix} X_{\delta_e} & X_{\delta_T} \\ Z_{\delta_e} & Z_{\delta_T} \\ M_{\delta_e} & M_{\delta_T} \\ 0 & 0 \end{pmatrix}
\end{aligned} \tag{5.41}$$

It is not difficult to show that the inverse of $\mathbf{I}_n$ is

$$\mathbf{I}_n^{-1} = \begin{pmatrix} 1 & 0 & 0 & 0 \\ 0 & \frac{1}{1 - Z_{\dot{w}}} & 0 & 0 \\ 0 & \frac{M_{\dot{w}}}{1 - Z_{\dot{w}}} & 1 & 0 \\ 0 & 0 & 0 & 1 \end{pmatrix} \tag{5.42}$$

so premultiplying Eq. (5.40) by $\mathbf{I}_n^{-1}$ gives the standard form

$$\dot{\mathbf{x}} = \mathbf{A}\mathbf{x} + \mathbf{B}\eta \tag{5.43}$$

where

$$\mathbf{A} = \begin{pmatrix} X_u & X_w & 0 & -g_0\cos\Theta_0 \\ \frac{Z_u}{1-Z_{\dot{w}}} & \frac{Z_w}{1-Z_{\dot{w}}} & \frac{u_0+Z_q}{1-Z_{\dot{w}}} & \frac{-g_0\sin\Theta_0}{1-Z_{\dot{w}}} \\ M_u + \frac{M_{\dot{w}}Z_u}{1-Z_{\dot{w}}} & M_w + \frac{M_{\dot{w}}Z_w}{1-Z_{\dot{w}}} & M_q + \frac{(u_0+Z_q)M_{\dot{w}}}{1-Z_{\dot{w}}} & \frac{-M_{\dot{w}}g_0\sin\Theta_0}{1-Z_{\dot{w}}} \\ 0 & 0 & 1 & 0 \end{pmatrix}$$
$$\mathbf{B} = \begin{pmatrix} X_{\delta_e} & X_{\delta_T} \\ \frac{Z_{\delta_e}}{1-Z_{\dot{w}}} & \frac{Z_{\delta_T}}{1-Z_{\dot{w}}} \\ M_{\delta_e} + \frac{M_{\dot{w}}Z_{\delta_e}}{1-Z_{\dot{w}}} & M_{\delta_T} + \frac{M_{\dot{w}}Z_{\delta_T}}{1-Z_{\dot{w}}} \\ 0 & 0 \end{pmatrix} \tag{5.44}$$

Note that

$$Z_{\dot{w}} = \frac{QS\bar{c}}{2mu_0^2}\mathbf{C}_{Z\,\dot{\alpha}} = -\frac{1}{2\mu}\mathbf{C}_{L\dot{\alpha}} \tag{5.45}$$

and

$$Z_q = \frac{QS\bar{c}}{2mu_0}\mathbf{C}_{Z\,q} = -\frac{u_0}{2\mu}\mathbf{C}_{Lq} \tag{5.46}$$

Since the aircraft mass parameter μ is typically large (on the order of 100), it is common to neglect $Z_{\dot{w}}$ with respect to unity and to neglect Z_q relative to u_0, in which case the matrices $\mathbf{A}$ and $\mathbf{B}$ can be approximated as

$$\mathbf{A} = \begin{pmatrix} X_u & X_w & 0 & -g_0\cos\Theta_0 \\ Z_u & Z_w & u_0 & -g_0\sin\Theta_0 \\ M_u + M_{\dot{w}}Z_u & M_w + M_{\dot{w}}Z_w & M_q + u_0M_{\dot{w}} & -M_{\dot{w}}g_0\sin\Theta_0 \\ 0 & 0 & 1 & 0 \end{pmatrix}$$
$$\mathbf{B} = \begin{pmatrix} X_{\delta_e} & X_{\delta_T} \\ Z_{\delta_e} & Z_{\delta_T} \\ M_{\delta_e} + M_{\dot{w}}Z_{\delta_e} & M_{\delta_T} + M_{\dot{w}}Z_{\delta_T} \\ 0 & 0 \end{pmatrix} \tag{5.47}$$

This is the approximate form of the linearized equations for longitudinal motions as they appear in many texts (see, e.g., Eqs. (4.53) and (4.54) in [3][2]).

The various dimensional stability derivatives appearing in Eqs. (5.44) and (5.47) are related to their dimensionless aerodynamic coefficient counterparts in Table 5.1; these data were also presented in Table 4.1 in the previous chapter.

5.2.1 Modes of Typical Aircraft

The natural response of most aircraft to longitudinal perturbations typically consists of two underdamped oscillatory modes having rather different time scales. One of the modes has a relatively short period and is usually quite heavily damped; this is called the *short period mode*. The other mode has a much longer period and is rather lightly damped; this is called the *phugoid mode*.

We illustrate this response using the stability derivatives for the Boeing 747 aircraft at its Mach 0.25 power approach configuration at standard sea-level conditions. The aircraft properties and flight

[2]The equations in [3] also assume level flight, or $\Theta_0 = 0$.

Variable	X	Z	M
u	$X_u = \frac{QS}{mu_0}\left[2\mathbf{C}_{X0} + \mathbf{C}_{Xu}\right]$	$Z_u = \frac{QS}{mu_0}\left[2\mathbf{C}_{Z0} + \mathbf{C}_{Zu}\right]$	$M_u = \frac{QS\bar{c}}{I_y u_0}\mathbf{C}_{mu}$
w	$X_w = \frac{QS}{mu_0}\mathbf{C}_{X\alpha}$	$Z_w = \frac{QS}{mu_0}\mathbf{C}_{Z\alpha}$	$M_w = \frac{QS\bar{c}}{I_y u_0}\mathbf{C}_{m\alpha}$
$\dot{w}$	$X_{\dot{w}} = 0$	$Z_{\dot{w}} = \frac{QS\bar{c}}{2mu_0^2}\mathbf{C}_{Z\dot{\alpha}}$	$M_{\dot{w}} = \frac{QS\bar{c}^2}{2I_y u_0^2}\mathbf{C}_{m\dot{\alpha}}$
q	$X_q = 0$	$Z_q = \frac{QS\bar{c}}{2mu_0}\mathbf{C}_{Zq}$	$M_q = \frac{QS\bar{c}^2}{2I_y u_0}\mathbf{C}_{mq}$

Table 5.1: Relation of dimensional stability derivatives for longitudinal motions to dimensionless derivatives of aerodynamic coefficients. The dimensionless coefficients on which these are based are described in Chapter 4.

condition are given by [2]

$$\begin{aligned} V &= 279.1 \text{ ft/sec}, \quad & \rho &= 0.002377 \text{ slug/ft}^3 \\ S &= 5,500. \text{ ft}^2, & \bar{c} &= 27.3 \text{ ft} \\ W &= 564,032. \text{ lb}, & I_y &= 32.3 \times 10^6 \text{ slug-ft}^2 \end{aligned} \tag{5.48}$$

and the relevant aerodynamic coefficients are

$$\begin{aligned} &\mathbf{C}_L = 1.108, \quad \mathbf{C}_D = 0.102, \quad \Theta_0 = 0 \\ &\mathbf{C}_{L\alpha} = 5.70, \quad \mathbf{C}_{L\dot{\alpha}} = 6.7, \quad \mathbf{C}_{Lq} = 5.4, \quad \mathbf{C}_{LM} = 0 \\ &\mathbf{C}_{D\alpha} = 0.66, \end{aligned} \tag{5.49}$$

$$\mathbf{C}_{m\alpha} = -1.26, \quad \mathbf{C}_{m\dot{\alpha}} = -3.2, \quad \mathbf{C}_{mq} = -20.8, \quad \mathbf{C}_{mM} = 0 \tag{5.50}$$

These values correspond to the following dimensional stability derivatives

$$\begin{aligned} X_u &= -0.0212, \quad & X_w &= 0.0466 \\ Z_u &= -0.2306, \quad & Z_w &= -0.6038, \quad & Z_{\dot{w}} &= -0.0341, \quad & Z_q &= -7.674 \\ M_u &= 0.0, & M_w &= -0.0019, \quad & M_{\dot{w}} &= -0.0002, \quad & M_q &= -0.4381 \end{aligned} \tag{5.51}$$

and the plant matrix is

$$\mathbf{A} = \begin{pmatrix} -0.0212 & 0.0466 & 0.000 & -32.174 \\ -0.2229 & -0.5839 & 262.472 & 0.0 \\ 0.0001 & -0.0018 & -0.5015 & 0.0 \\ 0.0 & 0.0 & 1.0 & 0.0 \end{pmatrix} \tag{5.52}$$

The characteristic equation is given by

$$|\mathbf{A} - \lambda\mathbf{I}| = \lambda^4 + 1.1066\lambda^3 + 0.7994\lambda^2 + 0.0225\lambda + 0.0139 = 0 \tag{5.53}$$

and its roots are

$$\begin{aligned} \lambda_{\text{sp}} &= -0.5515 \pm \imath\ 0.6880 \\ \lambda_{\text{ph}} &= -0.00178 \pm \imath\ 0.1339 \end{aligned} \tag{5.54}$$

where, as suggested by the subscripts, the first pair of roots corresponds to the short period mode, and the second pair corresponds to the phugoid mode. The damping ratios of the two modes are thus given by

$$\begin{aligned}\zeta_{\text{sp}} &= \sqrt{\frac{1}{1+\left(\frac{\eta}{\xi}\right)^2_{\text{sp}}}} = \sqrt{\frac{1}{1+\left(\frac{0.6880}{0.5515}\right)^2}} = 0.6255 \\ \zeta_{\text{ph}} &= \sqrt{\frac{1}{1+\left(\frac{\eta}{\xi}\right)^2_{\text{ph}}}} = \sqrt{\frac{1}{1+\left(\frac{0.1339}{0.00178}\right)^2}} = 0.0133\end{aligned} \tag{5.55}$$

where ξ and η are the real and imaginary parts of the respective roots, and the undamped natural frequencies of the two modes are

$$\begin{aligned}\omega_{n_{\text{sp}}} &= \frac{-\xi_{\text{sp}}}{\zeta_{\text{sp}}} = \frac{0.5515}{0.6255} = 0.882 \text{ sec}^{-1} \\ \omega_{n_{\text{ph}}} &= \frac{-\xi_{\text{ph}}}{\zeta_{\text{ph}}} = \frac{0.00178}{0.0133} = 0.134 \text{ sec}^{-1}\end{aligned} \tag{5.56}$$

The periods of the two modes are given by

$$T_{\text{sp}} = \frac{2\pi}{\omega_{n_{\text{sp}}}\sqrt{1-\zeta^2_{\text{sp}}}} = 9.13 \text{ sec} \tag{5.57}$$

and

$$T_{\text{ph}} = \frac{2\pi}{\omega_{n_{\text{ph}}}\sqrt{1-\zeta^2_{\text{ph}}}} = 46.9 \text{ sec} \tag{5.58}$$

respectively, and the numbers of cycles to damp to half amplitude of the respective modes are given by

$$N_{1/2_{\text{sp}}} = \frac{\ln 2}{2\pi}\frac{\sqrt{1-\zeta^2_{\text{sp}}}}{\zeta_{\text{sp}}} = \frac{\ln 2}{2\pi}\frac{\sqrt{1-(0.6255)^2}}{0.6255} = 0.1376 \tag{5.59}$$

and

$$N_{1/2_{\text{ph}}} = \frac{\ln 2}{2\pi}\frac{\sqrt{1-\zeta^2_{\text{ph}}}}{\zeta_{\text{ph}}} = \frac{\ln 2}{2\pi}\frac{\sqrt{1-(0.0133)^2}}{0.0133} = 8.29 \tag{5.60}$$

Figure 5.4 illustrates the short period and phugoid responses for the Boeing 747 under these conditions. These show the time histories of the state variables following an initial perturbation that is chosen to excite *only* the (a) short period mode or the (b) phugoid mode, respectively.

It should be noted that the dimensionless velocity perturbations u/u_0 and $\alpha = w/u_0$ are plotted in these figures, in order to allow comparisons with the other state variables. The plant matrix can be modified to reflect this choice of state variables as follows. The elements of the first two columns of the original plant matrix should be multiplied by u_0, then the entire plant matrix should be premultiplied by the diagonal matrix having elements $\text{diag}(1/u_0, 1/u_0, 1, 1)$. The combination of these two steps is equivalent to dividing the elements in the upper right two-by-two block of the plant matrix $\mathbf{A}$ by u_0, and multiplying the elements in the lower left two-by-two block by u_0. The

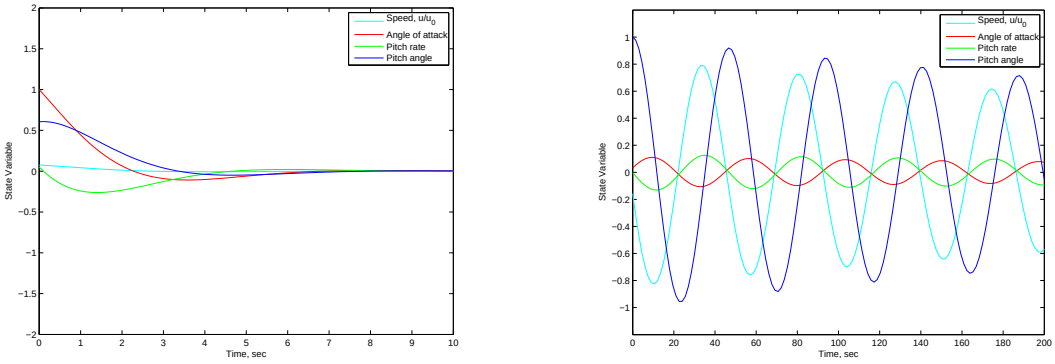

(a) Short period (b) Phugoid

Figure 5.4: Response of Boeing 747 aircraft to longitudinal perturbations. (a) Short period response; (b) Phugoid response.

resulting scaled plant matrix is then given by

$$\mathbf{A} = \begin{pmatrix} -0.0212 & 0.0466 & 0.000 & -0.1153 \\ -0.2229 & -0.5839 & 0.9404 & 0.0 \\ 0.0150 & -0.5031 & -0.5015 & 0.0 \\ 0.0 & 0.0 & 1.0 & 0.0 \end{pmatrix} \tag{5.61}$$

Note that, after this re-scaling, the magnitudes of the elements in the upper-right and lower-left two by two blocks of the plant matrix are more nearly the same order as the other terms (than they were in the original form).

It is seen in the figures that the short period mode is, indeed, rather heavily damped, while the phugoid mode is very lightly damped. In spite of the light damping of the phugoid, it generally does not cause problems for the pilot because its time scale is long enough that minor control inputs can compensate for the excitation of this mode by disturbances.

The relative magnitudes and phases of the perturbations in state variables for the two modes can be seen from the *phasor diagrams* for the various modes. These are plots in the complex plane of the components of the mode eigenvector corresponding to each of the state variables. The phasor plots for the short period and phugoid modes for this example are shown in Fig. 5.5. It is seen that the airspeed variation in the short period mode is, indeed, negligibly small, and the pitch angle θ lags the pitch rate q by substantially more than 90 degrees (due to the relatively large damping). The phugoid is seen to consist primarily of perturbations in airspeed and pitch angle. Although it is difficult to see on the scale of Fig. 5.5 (b), the pitch angle θ lags the pitch rate q by almost exactly 90 degrees for the phugoid (since the motion is so lightly damped it is nearly harmonic).

An arbitrary initial perturbation will generally excite both the short period and phugoid modes. This is illustrated in Fig. 5.6, which plots the time histories of the state variables following an initial perturbation in angle of attack. Figure 5.6 (a) shows the early stages of the response (on a time scale appropriate for the short period mode), while Fig. 5.6 (b) shows the response on a time scale appropriate for describing the phugoid mode.

The pitch- and angle-of-attack-damping are important for damping the short period mode, while its frequency is determined primarily by the pitch stiffness. The period of the phugoid mode is

nearly independent of vehicle parameters, and is very nearly inversely proportional to airspeed. The damping ratio for the phugoid is approximately proportional to the ratio $\mathbf{C}_D/\mathbf{C}_L$, which is small for efficient aircraft. These properties can be seen from the approximate analyses of the two modes presented in the following two sections.

5.2.2 Approximation to Short Period Mode

The short period mode typically occurs so quickly that it proceeds at essentially constant vehicle speed. A useful approximation for the mode can thus be developed by setting $u = 0$ and solving

$$\begin{aligned} (1 - Z_{\dot{w}})\,\dot{w} &= Z_w w + (u_0 + Z_q)\,q \\ -M_{\dot{w}}\dot{w} + \dot{q} &= M_w w + M_q q \end{aligned} \tag{5.62}$$

which can be written in state-space form as

$$\frac{\mathrm{d}}{\mathrm{d}t}\begin{pmatrix} w \\ q \end{pmatrix} = \begin{pmatrix} \frac{Z_w}{1-Z_{\dot{w}}} & \frac{u_0+Z_q}{1-Z_{\dot{w}}} \\ M_w + \frac{M_{\dot{w}}Z_w}{1-Z_{\dot{w}}} & M_q + M_{\dot{w}}\frac{u_0+Z_q}{1-Z_{\dot{w}}} \end{pmatrix}\begin{pmatrix} w \\ q \end{pmatrix} \tag{5.63}$$

Since

$$\frac{Z_q}{u_0} = \frac{QS\bar{c}}{2mu_0^2}\mathbf{C}_{Z\,q} = -\frac{\eta V_H a_t}{\mu} \tag{5.64}$$

where μ, the aircraft relative mass parameter, is usually large (on the order of one hundred), it is consistent with the level of our approximation to neglect Z_q relative to u_0. Also, we note that

$$Z_{\dot{w}} = \frac{QS\bar{c}}{2mu_0^2}\mathbf{C}_{Z\,\dot{\alpha}} = -\frac{\eta V_H a_t}{\mu}\frac{\mathrm{d}\epsilon}{\mathrm{d}\alpha} \tag{5.65}$$

is generally also very small. Thus, Eqs. (5.63) can be further approximated as

$$\frac{\mathrm{d}}{\mathrm{d}t}\begin{pmatrix} w \\ q \end{pmatrix} = \begin{pmatrix} Z_w & u_0 \\ M_w + M_{\dot{w}}Z_w & M_q + M_{\dot{w}}u_0 \end{pmatrix}\begin{pmatrix} w \\ q \end{pmatrix} \tag{5.66}$$

The characteristic equation for the simplified plant matrix of Eq. (5.66) is

$$\lambda^2 - (Z_w + M_q + u_0 M_{\dot{w}})\,\lambda + Z_w M_q - u_0 M_w = 0 \tag{5.67}$$

(a) Short period (b) Phugoid

Figure 5.5: Phasor diagrams for longitudinal modes of the Boeing 747 aircraft in powered approach at $\mathbf{M} = 0.25$. Perturbation in normalized speed u/u_0 is too small to be seen in short period mode.

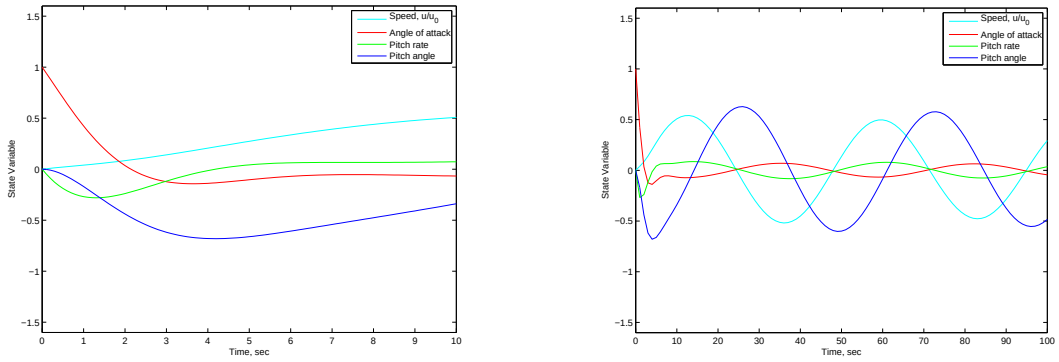

(a) Short period (b) Phugoid

Figure 5.6: Response of Boeing 747 aircraft to unit perturbation in angle of attack. (a) Time scale chosen to emphasize short period response; (b) Time scale chosen to emphasize phugoid response.

or, if the derivatives with respect to w are expressed as derivatives with respect to α,

$$\lambda^2 - \left(M_q + M_{\dot{\alpha}} + \frac{Z_\alpha}{u_0} \right) \lambda - M_\alpha + \frac{Z_\alpha M_q}{u_0} = 0 \tag{5.68}$$

The undamped natural frequency and damping ratio for this motion are thus

$$\begin{aligned} \omega_n &= \sqrt{-M_\alpha + \frac{Z_\alpha M_q}{u_0}} \\ \zeta &= -\frac{M_q + M_{\dot{\alpha}} + \frac{Z_\alpha}{u_0}}{2\omega_n} \end{aligned} \tag{5.69}$$

Thus, it is seen that the undamped natural frequency of the mode is determined primarily by the pitch stiffness M_α, and the damping ratio is determined largely by the pitch- and angle-of-attack-damping.

For the example considered in the preceding sections of the Boeing 747 in powered approach we find

$$\begin{aligned} \omega_n &= \sqrt{0.54 + \frac{(-168.5)(-.4381)}{279.1}} \text{ sec}^{-1} = 0.897 \text{ sec}^{-1} \\ \zeta &= -\frac{-.4381 - .056 + \frac{(-168.5)}{279.1}}{2(0.897)} = 0.612 \end{aligned} \tag{5.70}$$

When these numbers are compared to $\omega_n = 0.882$ sec^{-1} and $\zeta = 0.6255$ from the more complete analysis (of the full fourth-order system), we see that the approximate analysis over predicts the undamped natural frequency by only about 1 per cent, and under predicts the damping ratio by less than 2 per cent. As will be seen in the next subsection when we consider approximating the phugoid mode, it generally is easier to approximate the large roots than the small ones, especially when the latter are lightly damped.

5.2.3 Approximation to Phugoid Mode

Since the phugoid mode typically proceeds at nearly constant angle of attack, and the motion is so slow that the pitch rate q is very small, we can approximate the behavior of the mode by writing only the X- and Z-force equations

$$\begin{aligned} \dot{u} &= X_u u + X_w w - g_0 \cos\Theta_0 \theta \\ (1 - Z_{\dot{w}})\,\dot{w} &= Z_u u + Z_w w + (u_0 + Z_q)\,q - g_0 \sin\Theta_0 \theta \end{aligned} \tag{5.71}$$

which, upon setting $w = \dot{w} = 0$, can be written in the form

$$\frac{\mathrm{d}}{\mathrm{d}t}\begin{pmatrix} u \\ \theta \end{pmatrix} = \begin{pmatrix} X_u & -g_0 \cos\Theta_0 \\ -\frac{Z_u}{u_0 + Z_q} & \frac{g_0 \sin\Theta_0}{u_0 + Z_q} \end{pmatrix} \begin{pmatrix} u \\ \theta \end{pmatrix} \tag{5.72}$$

Since, as has been seen in Eq. (5.64), Z_q is typically very small relative to the speed u_0, it is consistent with our neglect of $\dot{q}$ and w also to neglect Z_q relative to u_0. Also, we will consider only the case of level flight for the initial equilibrium, so $\Theta_0 = 0$, and Eq. (5.72) becomes

$$\frac{\mathrm{d}}{\mathrm{d}t}\begin{pmatrix} u \\ \theta \end{pmatrix} = \begin{pmatrix} X_u & -g_0 \\ -\frac{Z_u}{u_0} & 0 \end{pmatrix} \begin{pmatrix} u \\ \theta \end{pmatrix} \tag{5.73}$$

The characteristic equation for the simplified plant matrix of Eq. (5.73) is

$$\lambda^2 - X_u \lambda - \frac{g_0}{u_0} Z_u = 0 \tag{5.74}$$

The undamped natural frequency and damping ratio for this motion are thus

$$\begin{aligned} \omega_n &= \sqrt{-\frac{g_0}{u_0} Z_u} \\ \zeta &= \frac{-X_u}{2\omega_n} \end{aligned} \tag{5.75}$$

It is useful to express these results in terms of dimensionless aerodynamic coefficients. Recall that

$$Z_u = -\frac{QS}{mu_0}\left[2\mathbf{C}_{L0} + \mathbf{M}\mathbf{C}_{L\mathbf{M}}\right] \tag{5.76}$$

and, for the case of a constant-thrust propulsive system,

$$X_u = -\frac{QS}{mu_0}\left[2\mathbf{C}_{D0} + \mathbf{M}\mathbf{C}_{D\mathbf{M}}\right] \tag{5.77}$$

so, if we further neglect compressibility effects, we have

$$\begin{aligned} \omega_n &= \sqrt{2}\frac{g_0}{u_0} \\ \zeta &= \frac{1}{\sqrt{2}}\frac{\mathbf{C}_{D0}}{\mathbf{C}_{L0}} \end{aligned} \tag{5.78}$$

Thus, according to this approximation, the undamped natural frequency of the phugoid is a function only of the flight velocity, and the damping ratio is proportional to the drag-to-lift ratio. Since the

latter quantity is small for an efficient flight vehicle, this explains why the phugoid typically is very lightly damped.

For the example of the Boeing 747 in powered approach we find

$$\begin{aligned} \omega_n &= \sqrt{2}\frac{32.174 \text{ ft/sec}^2}{279.1 \text{ ft/sec}} = 0.163 \text{ sec}^{-1} \\ \zeta &= \frac{1}{\sqrt{2}}\frac{0.102}{1.108} = 0.0651 \end{aligned} \tag{5.79}$$

When these numbers are compared to $\omega_n = 0.134$ sec^{-1} and $\zeta = 0.0133$ from the more complete analysis (of the full fourth-order system), we see that the approximate analysis over predicts the undamped natural frequency by about 20 per cent, and over predicts the damping ratio by a factor of almost 5. Nevertheless, this simplified analysis gives insight into the important parameters governing the mode.

5.2.4 Summary of Longitudinal Modes

We have seen that the response of a typical aircraft to longitudinal perturbations consists of two oscillatory modes:

1. A *short period* mode that usually is heavily damped, whose period is determined largely by the vehicle pitch stiffness $\mathbf{C}_{m_\alpha}$, and which is damped primarily by pitch- and angle-of-attack-damping, $\mathbf{C}_{m_q}$ and $\mathbf{C}_{m_{\dot{\alpha}}}$, respectively; and
2. A lightly damped, low frequency, *phugoid* mode whose period is nearly independent of vehicle parameters and inversely proportional to the flight velocity, and for which the damping ratio is proportional approximately to the ratio $\mathbf{C}_D/\mathbf{C}_L$, which is small for efficient vehicles.

We here illustrate the variation in response for a typical vehicle as a function of the vehicle static margin – which determines the pitch stiffness. The behavior of the roots of the characteristic equation of the complete fourth-order plant matrix is shown in Fig. 5.7 as a function of the pitch stiffness for our Boeing 747 example. The plot shows the locations of the roots as the static margin is reduced from an initial value of 0.22. As the c.g. is moved aft, both the phugoid and short period roots move toward the real axis. The short period mode becomes critically damped at a static margin of approximately 0.0158, and the phugoid becomes critically damped at a value of approximately 0.0021. One of the phugoid roots then moves toward the right-hand plane, and becomes neutrally stable at a static margin of 0.0. The other phugoid root moves to the left and, at a static margin of approximately -.0145, joins one of the short-period roots to create another oscillatory mode, which is called the *third oscillatory mode*.

5.3 Lateral/Directional Motions

In this section, we develop the small-disturbance equations for lateral/directional motions in standard state-variable form. Recall that the linearized equations describing small lateral/directional

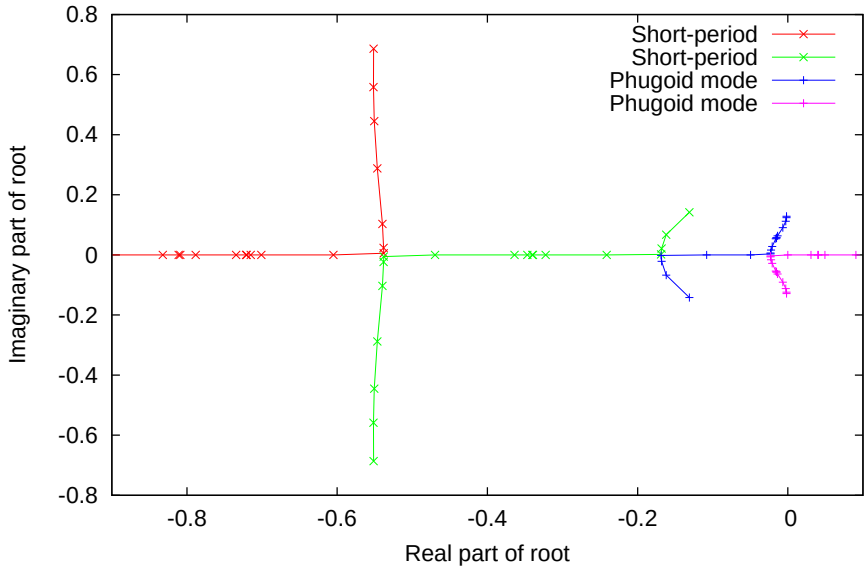

Figure 5.7: Locus of roots of longitudinal plant matrix for Boeing 747 in level flight at $\mathbf{M} = 0.25$ as standard seal level conditions as functions of c.g. location for values of static margin ranging from 0.22 to -.05. As the static margin is reduced, the roots of both oscillatory modes coalesce on the real axis; one of the phugoid roots moves to the right and becomes unstable, while the other moves to the left and joins with one of the short period roots to form a third oscillatory mode.

perturbations from a longitudinal equilibrium state can be written

$$\begin{aligned}
\left[\frac{\mathrm{d}}{\mathrm{d}t} - Y_v\right] v - Y_p p + [u_0 - Y_r]\, r - g_0 \cos\Theta_0 \phi &= Y_{\delta_r}\delta_r \\
-L_v v + \left[\frac{\mathrm{d}}{\mathrm{d}t} - L_p\right] p - \left[\frac{I_{xz}}{I_x}\frac{\mathrm{d}}{\mathrm{d}t} + L_r\right] r &= L_{\delta_r}\delta_r + L_{\delta_a}\delta_a \\
-N_v v - \left[\frac{I_{xz}}{I_z}\frac{\mathrm{d}}{\mathrm{d}t} + N_p\right] p + \left[\frac{\mathrm{d}}{\mathrm{d}t} - N_r\right] r &= N_{\delta_r}\delta_r + N_{\delta_a}\delta_a
\end{aligned} \tag{5.80}$$

If we introduce the lateral/directional state variable vector

$$\mathbf{x} = [v \quad p \quad \phi \quad r]^T \tag{5.81}$$

and the lateral/directional control vector

$$\eta = [\delta_r \quad \delta_a]^T \tag{5.82}$$

these equations are equivalent to the system of first-order equations

$$\mathbf{I}_n \dot{\mathbf{x}} = \mathbf{A}_n \mathbf{x} + \mathbf{B}_n \eta \tag{5.83}$$

where $\dot{\mathbf{x}}$ represents the time derivative of the state vector $\mathbf{x}$, and the matrices appearing in this equation are

$$\begin{aligned}\mathbf{A}_n &= \begin{pmatrix} Y_v & Y_p & g_0\cos\Theta_0 & Y_r - u_0 \\ L_v & L_p & 0 & L_r \\ 0 & 1 & 0 & 0 \\ N_v & N_p & 0 & N_r \end{pmatrix} \\ \mathbf{I}_n &= \begin{pmatrix} 1 & 0 & 0 & 0 \\ 0 & 1 & 0 & -i_x \\ 0 & 0 & 1 & 0 \\ 0 & -i_z & 0 & 1 \end{pmatrix}, \quad \mathbf{B}_n = \begin{pmatrix} Y_{\delta_r} & 0 \\ L_{\delta_r} & L_{\delta_a} \\ 0 & 0 \\ N_{\delta_r} & N_{\delta_a} \end{pmatrix}\end{aligned} \tag{5.84}$$

where

$$i_x \equiv \frac{I_{xz}}{I_x}, \quad i_z \equiv \frac{I_{xz}}{I_z} \tag{5.85}$$

It is not difficult to show that the inverse of $\mathbf{I}_n$ is

$$\mathbf{I}_n^{-1} = \begin{pmatrix} 1 & 0 & 0 & 0 \\ 0 & \frac{1}{1-i_x i_z} & 0 & \frac{i_x}{1-i_x i_z} \\ 0 & 0 & 1 & 0 \\ 0 & \frac{i_z}{1-i_x i_z} & 0 & \frac{1}{1-i_x i_z} \end{pmatrix} \tag{5.86}$$

so premultiplying Eq. (5.83) by $\mathbf{I}_n^{-1}$ gives the standard form

$$\dot{\mathbf{x}} = \mathbf{A}\mathbf{x} + \mathbf{B}\eta$$

where

$$\begin{aligned}\mathbf{A} &= \begin{pmatrix} Y_v & Y_p & g_0\cos\Theta_0 & Y_r - u_0 \\ \frac{L_v + i_x N_v}{1-i_x i_z} & \frac{L_p + i_x N_p}{1-i_x i_z} & 0 & \frac{L_r + i_x N_r}{1-i_x i_z} \\ 0 & 1 & 0 & 0 \\ \frac{N_v + i_z L_v}{1-i_x i_z} & \frac{N_p + i_z L_p}{1-i_x i_z} & 0 & \frac{N_r + i_z L_r}{1-i_x i_z} \end{pmatrix} \\ \mathbf{B} &= \begin{pmatrix} Y_{\delta_r} & 0 \\ \frac{L_{\delta_r} + i_x N_{\delta_r}}{1-i_x i_z} & \frac{L_{\delta_a} + i_x N_{\delta_a}}{1-i_x i_z} \\ 0 & 0 \\ \frac{N_{\delta_r} + i_z L_{\delta_r}}{1-i_x i_z} & \frac{N_{\delta_a} + i_z L_{\delta_a}}{1-i_x i_z} \end{pmatrix}\end{aligned} \tag{5.87}$$

For most flight vehicles and situations, the ratios i_x and i_z are quite small. Neglecting these quantities with respect to unity allows us to write the $\mathbf{A}$ and $\mathbf{B}$ matrices for lateral directional motions as

$$\begin{aligned}\mathbf{A} &= \begin{pmatrix} Y_v & Y_p & g_0\cos\Theta_0 & Y_r - u_0 \\ L_v & L_p & 0 & L_r \\ 0 & 1 & 0 & 0 \\ N_v & N_p & 0 & N_r \end{pmatrix} \\ \mathbf{B} &= \begin{pmatrix} Y_{\delta_r} & 0 \\ L_{\delta_r} & L_{\delta_a} \\ 0 & 0 \\ N_{\delta_r} & N_{\delta_a} \end{pmatrix}\end{aligned} \tag{5.88}$$

This is the approximate form of the linearized equations for lateral/directional motions as they appear in many texts (see, e.g., Eqs. (5.33) in [3]).

Variable	Y	L	N
v	$Y_v = \frac{QS}{mu_0}\mathbf{C}_{y_\beta}$	$L_v = \frac{QSb}{I_x u_0}\mathbf{C}_{l_\beta}$	$N_v = \frac{QSb}{I_z u_0}\mathbf{C}_{n_\beta}$
p	$Y_p = \frac{QSb}{2mu_0}\mathbf{C}_{y_p}$	$L_p = \frac{QSb^2}{2I_x u_0}\mathbf{C}_{l_p}$	$N_p = \frac{QSb^2}{2I_z u_0}\mathbf{C}_{n_p}$
r	$Y_r = \frac{QSb}{2mu_0}\mathbf{C}_{y_r}$	$L_r = \frac{QSb^2}{2I_x u_0}\mathbf{C}_{l_r}$	$N_r = \frac{QSb^2}{2I_z u_0}\mathbf{C}_{n_r}$

Table 5.2: Relation of dimensional stability derivatives for lateral/directional motions to dimensionless derivatives of aerodynamic coefficients.

The various dimensional stability derivatives appearing in Eqs. (5.87) and (5.88) are related to their dimensionless aerodynamic coefficient counterparts in Table 5.2; these data were also presented in Table 4.2 in the previous chapter.

5.3.1 Modes of Typical Aircraft

The natural response of most aircraft to lateral/directional perturbations typically consists of one damped oscillatory mode and two exponential modes, one of which is usually very heavily damped. The oscillatory mode has a relatively short period and can be relatively lightly damped, especially for swept-wing aircraft; this is called the *Dutch Roll mode*, as the response consists of a combined rolling, sideslipping, yawing motion reminiscent of a (Dutch) speed-skater. One of the exponential modes is very heavily damped, and represents the response of the aircraft primarily in roll; it is called the *rolling mode*. The second exponential mode, called the *spiral mode*, can be either stable or unstable, but usually has a long enough time constant that it presents no difficulty for piloted vehicles, even when it is unstable.[3]

We illustrate this response again using the stability derivatives for the Boeing 747 aircraft at its Mach 0.25 powered approach configuration at standard sea-level conditions. This is the same vehicle and trim condition used to illustrate typical longitudinal behavior, and the basic aircraft properties and flight condition are given in Eq. (5.48). In addition, for the lateral/directional response we need the following vehicle parameters

$$\begin{aligned} &W = 564,032.\ \text{lbf}, \qquad b = 195.7\ \text{ft} \\ &I_x = 14.3\times10^6\ \text{slug ft}^2, \quad I_z = 45.3\times10^6\ \text{slug ft}^2, \quad I_{xz} = -2.23\times10^6\ \text{slug ft}^2 \end{aligned} \tag{5.89}$$

and the aerodynamic derivatives

$$\begin{aligned} &\mathbf{C}_{y_\beta} = -.96 \quad \mathbf{C}_{y_p} = 0.0 \quad \mathbf{C}_{y_r} = 0.0 \\ &\mathbf{C}_{l_\beta} = -.221 \quad \mathbf{C}_{l_p} = -.45 \quad \mathbf{C}_{l_r} = 0.101 \\ &\mathbf{C}_{n_\beta} = 0.15 \quad \mathbf{C}_{n_p} = -.121 \quad \mathbf{C}_{n_r} = -.30 \end{aligned} \tag{5.90}$$

[3]This is true at least when flying under visual flight rules and a horizontal reference is clearly visible. Under instrument flight rules pilots must learn to trust the artificial horizon indicator to avoid entering an unstable spiral.

These values correspond to the following dimensional stability derivatives

$$\begin{array}{lll} Y_v = -0.0999, & Y_p = 0.0, & Y_r = 0.0 \\ L_v = -0.0055, & L_p = -1.0994, & L_r = 0.2468 \\ N_v = 0.0012, & N_p = -.0933, & N_r = -.2314 \end{array} \tag{5.91}$$

and the dimensionless product of inertia factors are

$$i_x = -.1559, \qquad i_z = -.0492 \tag{5.92}$$

Using these values, the plant matrix is found to be

$$\mathbf{A} = \begin{pmatrix} -0.0999 & 0.0000 & 32.174 & -279.10 \\ -0.0057 & -1.0932 & 0.0 & 0.2850 \\ 0.0 & 1.0 & 0.0 & 0.0 \\ 0.0015 & -.0395 & 0.0 & -.2454 \end{pmatrix} \tag{5.93}$$

The characteristic equation is given by

$$|\mathbf{A} - \lambda \mathbf{I}| = \lambda^4 + 1.4385\lambda^3 + 0.8222\lambda^2 + 0.7232\lambda + 0.0319 = 0 \tag{5.94}$$

and its roots are

$$\begin{aligned} \lambda_{\text{DR}} &= -.08066 \pm \imath\ 0.7433 \\ \lambda_{\text{roll}} &= -1.2308 \\ \lambda_{\text{spiral}} &= -.04641 \end{aligned} \tag{5.95}$$

where, as suggested by the subscripts, the first pair of roots corresponds to the Dutch Roll mode, and the real roots corresponds to the rolling and spiral modes, respectively.

The damping ratio of the Dutch Roll mode is thus given by

$$\zeta_{\text{DR}} = \sqrt{\frac{1}{1 + \left(\frac{\eta}{\xi}\right)^2_{\text{DR}}}} = \sqrt{\frac{1}{1 + \left(\frac{0.7433}{0.08066}\right)^2}} = 0.1079 \tag{5.96}$$

and the undamped natural frequency of the mode is

$$\omega_{n_{\text{DR}}} = \frac{-\xi_{\text{DR}}}{\zeta_{\text{DR}}} = \frac{0.08066}{0.1079} = 0.7477 \text{ sec}^{-1} \tag{5.97}$$

The period of the Dutch Roll mode is then given by

$$T_{\text{DR}} = \frac{2\pi}{\omega_n \sqrt{1 - \zeta^2}} = \frac{2\pi}{0.7477\sqrt{1 - 0.1079^2}} = 8.45 \text{ sec} \tag{5.98}$$

and the number of cycles to damp to half amplitude is

$$N_{1/2_{\text{DR}}} = \frac{\ln 2}{2\pi} \frac{\sqrt{1 - \zeta^2}}{\zeta} = \frac{\ln 2}{2\pi} \frac{\sqrt{1 - 0.1079^2}}{0.1079} = 1.016 \tag{5.99}$$

Thus, the period of the Dutch Roll mode is seen to be on the same order as that of the longitudinal short period mode, but is much more lightly damped.

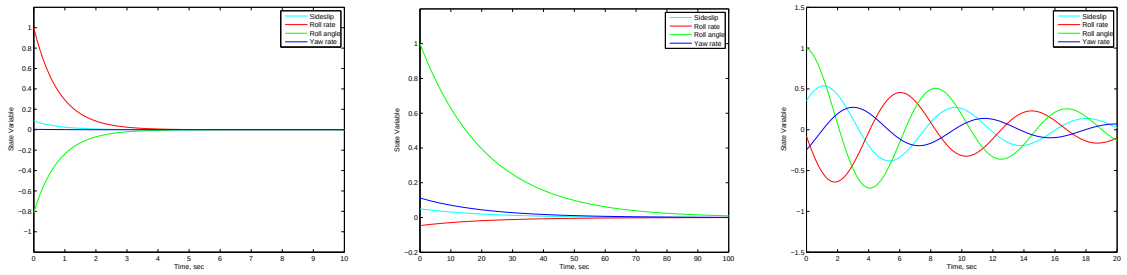

(a) Rolling mode (b) Spiral mode (c) Dutch Roll

Figure 5.8: Response of Boeing 747 aircraft to unit perturbation in eigenvectors corresponding to the three lateral/directional modes of the vehicle. (a) Rolling mode; (b) Spiral mode; and (c) Dutch Roll mode.

The times to damp to half amplitude for the rolling and spiral modes are seen to be

$$t_{1/2_{\text{roll}}} = \frac{\ln 2}{-\xi_{\text{roll}}} = \frac{\ln 2}{1.2308} = 0.563 \text{ sec} \tag{5.100}$$

and

$$t_{1/2_{\text{spiral}}} = \frac{\ln 2}{-\xi_{\text{spiral}}} = \frac{\ln 2}{0.04641} = 14.93 \text{ sec} \tag{5.101}$$

respectively.

The responses characteristic of these three modes are illustrated in Fig. 5.8. The figure shows the time histories of the state variables following initial perturbations that are designed to excite only a single mode. For each of the three subfigures the initial perturbation has unit amplitude for the largest component and is parallel to the corresponding eigenvector in the state space.

Here the first state variable is again plotted in dimensionless form as $\beta = v/u_0$. The plant matrix can be modified to reflect this change in state variable as follows. The first column of the original plant matrix is first multiplied by u_0, then the entire plant matrix is pre-multiplied by the diagonal matrix having elements $\text{diag}(1/u_0, 1, 1, 1)$. This is equivalent to dividing all but the first element in the first row by u_0, and multiplying all but the first element in the first column by u_0. The first element in the first column remains unchanged. With this re-scaling the plant matrix becomes

$$\mathbf{A} = \begin{pmatrix} -0.0999 & 0.0000 & 0.1153 & -1.0000 \\ -1.6038 & -1.0932 & 0.0 & 0.2850 \\ 0.0 & 1.0 & 0.0 & 0.0 \\ 0.4089 & -.0395 & 0.0 & -.2454 \end{pmatrix} \tag{5.102}$$

Note that, after this re-scaling, the magnitudes of the elements in the first row and first column of the plant matrix are more nearly the same order as the other terms (than they were in the original form).

It is seen that the rolling mode consists of almost pure rolling motion (with a very small amount of sideslip). The spiral mode consists of mostly coordinated roll and yaw. And for the the Dutch Roll mode, all the state variables participate, so the motion is characterized by coordinated rolling, sideslipping, and yawing motions.

An arbitrary initial perturbation will generally excite all three modes. This is illustrated in Fig. 5.9 which plots the time histories of the state variables following an initial perturbation in roll rate. The

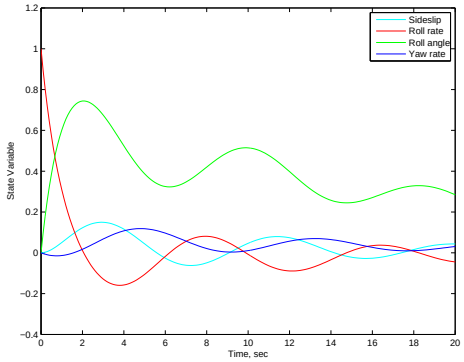

Figure 5.9: Response of Boeing 747 aircraft to unit perturbation in roll rate. Powered approach at $\mathbf{M} = 0.25$ under standard sea-level conditions.

roll rate is seen to be quickly damped, leaving a slowly decaying spiral mode (appearing primarily in the roll angle anad yaw rate), with the lightly-damped, oscillatory Dutch Roll mode superimposed.

The phasor plots for the rolling and spiral modes are relatively uninteresting, since these correspond to real roots. The eigenvector amplitudes, however, show that the rolling mode is dominated by perturbations in bank angle ϕ and roll rate p, with a very small amount of sideslip and negligible yaw rate. The spiral mode is dominated by changes in bank angle. Since the motion is so slow, the roll rate is quite small, and the yaw rate is almost 2.5 times the roll rate, so we would expect significant changes in heading, as well as bank angle. The phasor diagram for the Dutch Roll mode is shown in Fig. 5.10. Note that all four state variables participate with significant amplitudes in the Dutch Roll, and that the bank angle ϕ lags the roll rate p by almost exactly 90 degrees, as the motion is very lightly damped. Active control, usually to supply additional yaw damping, is often required on swept-wing transports to bring the damping of this mode to within acceptable limits.

5.3.2 Approximation to Rolling Mode

It has been seen that the rolling mode typically corresponds to almost pure roll. Thus, it is reasonable to neglect all equations except the rolling moment equation, and all perturbations except p. We

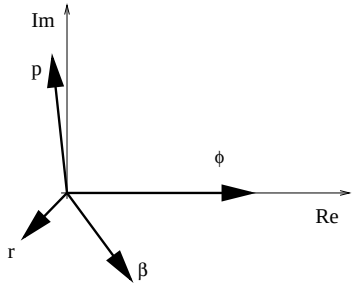

Figure 5.10: Phasor diagram for Dutch Roll mode of the Boeing 747 aircraft in powered approach at $\mathbf{M} = 0.25$.

thus approximate the rolling mode by the single first-order equation

$$\dot{p} = \frac{L_p + i_x N_p}{1 - i_x i_z} p \tag{5.103}$$

for which the characteristic value is

$$\lambda = \frac{L_p + i_x N_p}{1 - i_x i_z} \tag{5.104}$$

Since the product of inertia coefficients i_x and i_z usually are small, the rolling mode is seen to be dominated by roll damping L_p, which is almost always large and negative.

For our example of the Boeing 747 in powered approach at $\mathbf{M} = 0.25$, using the values from Eqs. (5.91) and (5.92), the approximate formula gives

$$\lambda = \frac{-1.0994 + (-.1559)(-.0933)}{1 - (-.1559)(-.0492)} \text{ sec}^{-1} = -1.093 \text{ sec}^{-1} \tag{5.105}$$

which is a bit more than 10 per cent less than the value of -1.2308 from the analysis for the full fourth-order system.

5.3.3 Approximation to Spiral Mode

The spiral mode consists of a slow rolling/yawing motion for which the sideslip is relatively small. The roll rate is quite small compared to the yaw rate, so a reasonable approximation is to set

$$\frac{\mathrm{d}p}{\mathrm{d}t} = 0 = \frac{L_v + i_x N_v}{1 - i_x i_z} v + \frac{L_r + i_x N_r}{1 - i_x i_z} r \tag{5.106}$$

whence

$$v \approx -\frac{L_r + i_x N_r}{L_v + i_x N_v} r \tag{5.107}$$

Since i_x and i_z are generally very small, this can be approximated as

$$v \approx -\frac{L_r}{L_v} r \tag{5.108}$$

The yaw equation

$$\frac{\mathrm{d}r}{\mathrm{d}t} = \frac{N_v + i_z L_v}{1 - i_x i_z} v + \frac{N_r + i_z L_r}{1 - i_x i_z} r \tag{5.109}$$

upon substitution of Eq. (5.108) and neglect of the product of inertia terms can then be written

$$\frac{\mathrm{d}r}{\mathrm{d}t} = \left(N_r - \frac{L_r N_v}{L_v} \right) r \tag{5.110}$$

so the root of the characteristic equation for the spiral mode is

$$\lambda = N_r - \frac{L_r N_v}{L_v} \tag{5.111}$$

Thus, it is seen that, according to this approximation, the spiral mode is stabilized by yaw damping N_r. Also, since stable dihedral effect corresponds to negative L_v and weathercock stability N_v and

roll due to yaw rate L_r are always positive, the second term in Eq. (5.111) is destabilizing; thus increasing weathercock destabilizes the spiral mode while increasing dihedral effect stabilizes it.[4]

For our example of the Boeing 747 in powered approach at $\mathbf{M} = 0.25$, using the values from Eqs. (5.91) and (5.92), the approximate formula gives

$$\lambda = -.2314 - \frac{0.2468}{-.0055}(0.0012) = -.178 \tag{5.112}$$

which is almost four times the value of -.0464 from the analysis of the full fourth-order system. This is consistent with the usual difficulty in approximating small roots, but Eq. (5.111) still gives useful qualitative information about the effects of weathercock and dihedral stability on the spiral mode.

5.3.4 Approximation to Dutch Roll Mode

The Dutch Roll mode is particularly difficult to approximate because it usually involves significant perturbations in all four state variables. The most useful approximations require neglecting either the roll component or simplifying the sideslip component by assuming the vehicle c.g. travels in a straight line. This latter approximation means that $\psi = -\beta$, or

$$r = -\frac{\dot{v}}{u_0} \tag{5.113}$$

The roll and yaw moment equations (neglecting the product of inertia terms i_x and i_z) can then be written as

$$\frac{\mathrm{d}}{\mathrm{d}t}\begin{pmatrix} p \\ r \end{pmatrix} = \begin{pmatrix} L_v & L_p & L_r \\ N_v & N_p & N_r \end{pmatrix}\begin{pmatrix} v \\ p \\ r \end{pmatrix} \tag{5.114}$$

Introduction of Eq. (5.113) completes this equation system in the form

$$\frac{\mathrm{d}}{\mathrm{d}t}\begin{pmatrix} v \\ p \\ r \end{pmatrix} = \begin{pmatrix} 0 & 0 & -u_0 \\ L_v & L_p & L_r \\ N_v & N_p & N_r \end{pmatrix}\begin{pmatrix} v \\ p \\ r \end{pmatrix} \tag{5.115}$$

The characteristic equation for this system is

$$\lambda^3 - (L_p + N_r)\,\lambda^2 + (L_p N_r + u_0 N_v - L_r N_p)\,\lambda + u_0\,(L_v N_p - L_p N_v) = 0 \tag{5.116}$$

This is still a cubic equation, however, for which there is no general closed-form solution. A useful approach to cubic equations that have a lightly damped oscillatory mode is Bairstow's approximation, which proceeds as follows. If the general cubic

$$\lambda^3 + a_2\lambda^2 + a_1\lambda + a_0 = 0 \tag{5.117}$$

has a lightly damped oscillatory mode, its undamped natural frequency can be approximated as

$$a_2\lambda^2 + a_0 \approx 0 \quad \text{or} \quad \lambda^2 \approx -\frac{a_0}{a_2} \tag{5.118}$$

[4] Even if the spiral mode is unstable, its time constant usually is long enough that the pilot has no trouble countering it. Unpiloted aircraft, however, must have a stable spiral mode, which accounts for the excessive dihedral usually found on free-flight model aircraft.

This can then be used to write the first term of Eq. (5.117) as

$$-\frac{a_0}{a_2}\lambda + a_2\lambda^2 + a_1\lambda + a_0 = 0 \tag{5.119}$$

giving

$$a_2\lambda^2 + \left(a_1 - \frac{a_0}{a_2}\right)\lambda + a_0 = 0 \tag{5.120}$$

This quadratic equation can be solved in closed form (or at least the terms contributing to the undamped natural frequency and the damping ratio can be identified directly).

Applying Bairstow's approximation to Eq. (5.116) yields

$$\lambda^2 - \left[\frac{L_pN_r + u_0N_v - L_rN_p}{L_p + N_r} + \frac{u_0\left(L_vN_p - L_pN_v\right)}{\left(L_p + N_r\right)^2}\right]\lambda + \frac{u_0\left(L_pN_v - L_vN_p\right)}{L_p + N_r} = 0 \tag{5.121}$$

Thus, the undamped natural frequency is given by

$$\omega_n^2 = \frac{u_0\left(L_pN_v - L_vN_p\right)}{L_p + N_r} \tag{5.122}$$

Since N_p is usually negative, both terms in the numerator have the same sign for stable dihedral. Thus, increasing either weathercock stability N_v or dihedral effect L_v increases the natural frequency of the motion.

The damping ratio is seen to be proportional to

$$2\zeta\omega_n = \frac{-L_pN_r - u_0N_v + L_rN_p}{L_p + N_r} + \frac{u_0\left(-L_vN_p + L_pN_v\right)}{\left(L_p + N_r\right)^2} \tag{5.123}$$

For most aircraft, the ratio N_r/L_p is small, and expanding Eq. (5.123) in powers of this parameter and keeping only leading order terms gives

$$2\zeta\omega_n \approx -N_r\left(1 + \frac{u_0}{L_p^2}N_v\right) + \frac{N_p}{L_p}\left(L_r - \frac{u_0}{L_p}L_v\right) \tag{5.124}$$

Yaw damping is thus seen to contribute to positive ζ and be stabilizing, and weathercock stability N_v augments this effect. Since both N_p and L_p usually are negative, however, the dihedral effect L_v is seen to destabilize the Dutch Roll mode.[5]

For our example of the Boeing 747 in powered approach at $\mathbf{M} = 0.25$, using the values from Eqs. (5.91) and (5.92), the approximate formulas give

$$\omega_n = \left[\frac{(279.1)\left[(-1.0994)(0.0012) - (-.0055)(-.0933)\right]}{-1.0994 - .2314}\ \text{sec}^{-2}\right]^{1/2} = 0.620\ \text{sec}^{-1} \tag{5.125}$$

and

$$\begin{aligned}\zeta &= -\frac{\frac{(-1.0994)(-.2314)-(.2468)(-.0933)+(279.1)(0.0012)}{-1.0994-.2314} + (279.1)\frac{(-.0055)(-.0933)-(-1.0994)(0.0012)}{(-1.0994-.2314)^2}}{2(0.620)} \\ &= 0.138\end{aligned} \tag{5.126}$$

[5]Recall that there are two contributions from the wing to the yaw-due-to-roll derivative N_p; profile drag contributes to positive N_p, while induced drag contributes to negative N_p. At low values of lift coefficient (i.e., high speeds) the profile drag contribution can dominate, in which case N_p becomes positive. In this case, increased dihedral effect can improve damping of the Dutch Roll mode. Consistent with this observation is the fact that Dutch Roll tends to be a more serious problem at low speeds.

The approximation for the undamped natural frequency is only about 15 per cent less than the exact value of 0.748, but the exact damping ratio of 0.1079 is over predicted by almost 30 per cent. Nevertheless, the approximate Eq. (5.124) gives useful qualitative information about the effect of dihedral and weathercock on the damping of the mode.

5.3.5 Summary of Lateral/Directional Modes

We have seen that the response of a typical aircraft to lateral/directional perturbations consists of two exponential modes and one oscillatory mode:

1. A *rolling* mode that usually is heavily damped, whose time to damp to half amplitude is determined largely by the roll damping L_p;
2. A *spiral* mode that usually is only lightly damped, or may even be unstable. Dihedral effect is an important stabilizing influence, while weathercock stability is destabilizing, for this mode; and
3. A lightly damped oscillatory, intermediate frequency *Dutch Roll* mode, which consists of a coordinated yawing, rolling, sideslipping motion. For this mode, dihedral effect is generally destabilizing, while weathercock stability is stabilizing.

Thus, the effects of weathercock and dihedral stability are reversed for the spiral and Dutch Roll modes, and compromise is required. We here present root locus plots illustrating this behavior for the full fourth-order system, corresponding to our example Boeing 747 vehicle in powered approach at standard sea level conditions at $\mathbf{M} = 0.25$. Figure 5.11 shows the locus of the roots of the plant matrix as the dihedral effect $\mathbf{C}_{l\beta}$ is increased from -.041 to -.561. As the dihedral effect is increased (i.e., made more negative) the spiral and rolling mode roots move to the left, while the complex pair corresponding to the Dutch Roll mode moves to the right. Consistent with our approximate analysis, increasing the dihedral effect is seen to increase the natural frequency of the Dutch Roll mode.

Figure 5.12 shows the locus of the roots of the plant matrix as the weathercock stability coefficient $\mathbf{C}_{n\beta}$ is increased from -.07 to 0.69. As the weathercock stability is increased (i.e., made more positive) the spiral and rolling mode roots move to the right, while the complex conjugate pair of roots corresponding to the Dutch Roll mode moves to the left. Again, consistent with our approximate analysis, increasing the weathercock stability increases the natural frequency of the Dutch Roll mode.

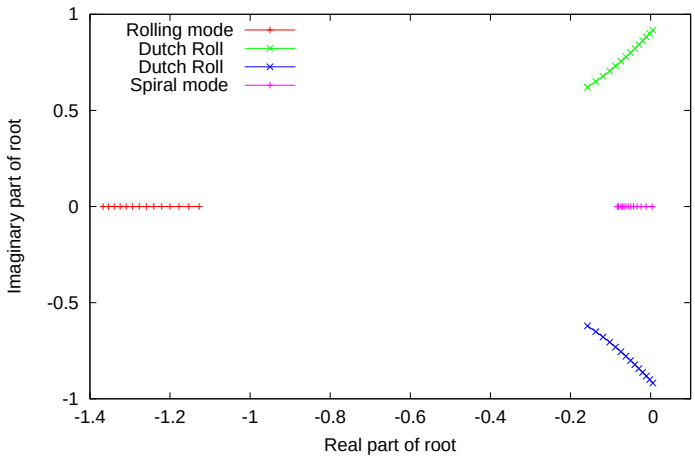

Figure 5.11: Locus of roots of plant matrix for Boeing 747 aircraft in powered approach at $\mathbf{M} = 0.25$ under standard sea-level conditions. Dihedral effect is varied from -.041 to -.561 in steps of -.04, while all other stability derivatives are held fixed at their nominal values. Rolling and spiral modes become increasingly stable as dihedral effect is increased; spiral mode becomes stable at approximately $\mathbf{C}_{l_\beta} = -.051$. Dutch Roll mode becomes less stable as dihedral effect is increased and becomes unstable at approximately $\mathbf{C}_{l_\beta} = -.532$.

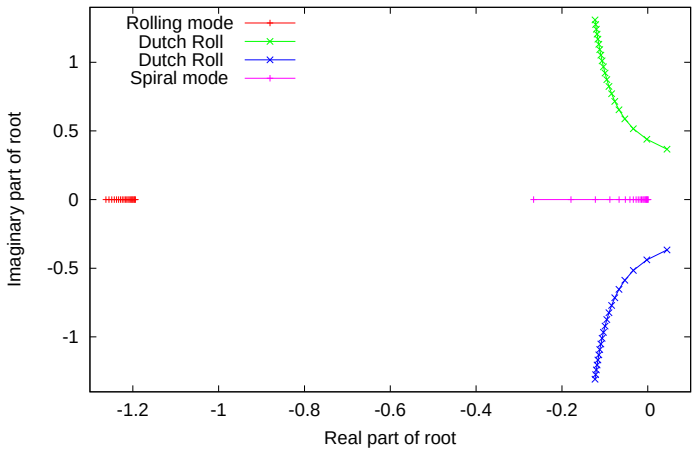

Figure 5.12: Locus of roots of plant matrix for Boeing 747 aircraft in powered approach at $\mathbf{M} = 0.25$ under standard sea-level conditions. Weathercock stability is varied from -.07 to 0.69 in steps of 0.04, while all other stability derivatives are held fixed at their nominal values. Rolling and spiral modes become less stable as weathercock stability is increased; spiral mode becomes unstable at approximately $\mathbf{C}_{n_\beta} = 0.6567$. Dutch roll mode becomes increasingly stable as weathercock stability is increased, but is unstable for less than about $\mathbf{C}_{n_\beta} = -.032$.

5.4 Stability Characteristics of the Boeing 747

5.4.1 Longitudinal Stability Characteristics

In this section we summarize the longitudinal mass distribution and aerodynamic stability characteristics of a large, jet transport aircraft, the Boeing 747, at selected flight conditions. Data are summarized from the report by Heffley et al. [2]. Values for aerodynamic coefficients were scaled directly from plots of these variables, except for the derivatives $\mathbf{C}_{L_q}$ and $\mathbf{C}_{L_{\dot{\alpha}}}$ for which no data are provided. These values were computed from the values of the corresponding dimensional stability derivatives Z_q and $Z_{\dot{w}}$, which are provided in tabular form, with the sign of $Z_{\dot{w}}$ changed to correct a seemingly obvious error.

Condition numbers correspond to those in the report; Conditions 5-10 are for a clean aircraft, Condition 2 corresponds to a powered approach with gear up and 20° flaps. Angles of attack are with respect to the fuselage reference line.

Condition	2	5	7	9	10
h (ft)	SL	20,000	20,000	40,000	40,000
$\mathbf{M}_\infty$	0.25	0.500	0.800	0.800	0.900
α (degrees)	5.70	6.80	0.0	4.60	2.40
W (lbf)	564,032.	636,636.	636,636.	636,636.	636,636.
I_y (slug-ft^2)	32.3×10^6	33.1×10^6	33.1×10^6	33.1×10^6	33.1×10^6
$\mathbf{C}_L$	1.11	0.680	0.266	0.660	0.521
$\mathbf{C}_D$	0.102	0.0393	0.0174	0.0415	0.0415
$\mathbf{C}_{L_\alpha}$	5.70	4.67	4.24	4.92	5.57
$\mathbf{C}_{D\alpha}$	0.66	0.366	0.084	0.425	0.527
$\mathbf{C}_{m_\alpha}$	-1.26	-1.146	-.629	-1.033	-1.613
$\mathbf{C}_{L_{\dot{\alpha}}}$	6.7	6.53	5.99	5.91	5.53
$\mathbf{C}_{m_{\dot{\alpha}}}$	-3.2	-3.35	-5.40	-6.41	-8.82
$\mathbf{C}_{L_q}$	5.40	5.13	5.01	6.00	6.94
$\mathbf{C}_{m_q}$	-20.8	-20.7	-20.5	-24.0	-25.1
$\mathbf{C}_{L_\mathbf{M}}$	0.0	-.0875	0.105	0.205	-.278
$\mathbf{C}_{D_\mathbf{M}}$	0.0	0.0	0.008	0.0275	0.242
$\mathbf{C}_{m_\mathbf{M}}$	0.0	0.121	-.116	0.166	-.114
$\mathbf{C}_{L_{\delta_e}}$	0.338	0.356	0.270	0.367	0.300
$\mathbf{C}_{m_{\delta_e}}$	-1.34	-1.43	-1.06	-1.45	-1.20

Table 5.3: Longitudinal mass properties and aerodynamic stability derivatives for the Boeing 747 at selected flight conditions.

5.4.2 Lateral/Directional Stability Characteristics

In this section we summarize the lateral/directional mass distribution and aerodynamic stability characteristics of a large, jet transport aircraft, the Boeing 747, at selected flight conditions. Data are summarized from the report by Heffley et al. [2]. Values for aerodynamic coefficients were scaled directly from plots of these variables.

Condition numbers correspond to those in the report; Conditions 5-10 are for a clean aircraft, Condition 2 corresponds to a powered approach with gear up and 20° flaps. Moments and products of inertia are with respect to stability axes for the given flight condition. Angles of attack are with respect to the fuselage reference line.

Condition	2	5	7	9	10
h (ft)	SL	20,000	20,000	40,000	40,000
$\mathbf{M}_\infty$	0.25	0.500	0.800	0.800	0.900
α (degrees)	5.70	6.80	0.0	4.60	2.40
W (lbf)	564,032.	636,636.	636,636.	636,636.	636,636.
I_x (slug-ft^2)	14.3×10^6	18.4×10^6	18.2×10^6	18.2×10^6	18.2×10^6
I_z (slug-ft^2)	45.3×10^6	49.5×10^6	49.7×10^6	49.7×10^6	49.7×10^6
I_{xz} (slug-ft^2)	-2.23×10^6	-2.76×10^6	0.97×10^6	-1.56×10^6	$-.35 \times 10^6$
$\mathbf{C}_{y_\beta}$	-.96	-.90	-.81	-.88	-.92
$\mathbf{C}_{l_\beta}$	-.221	-.193	-.164	-.277	-.095
$\mathbf{C}_{n_\beta}$	0.150	0.147	0.179	0.195	0.207
$\mathbf{C}_{l_p}$	-.45	-.323	-.315	-.334	-.296
$\mathbf{C}_{n_p}$	-.121	-.0687	0.0028	-.0415	0.0230
$\mathbf{C}_{l_r}$	0.101	0.212	0.0979	0.300	0.193
$\mathbf{C}_{n_r}$	-.30	-.278	-.265	-.327	-.333
$\mathbf{C}_{l_{\delta_a}}$	0.0461	0.0129	0.0120	0.0137	0.0139
$\mathbf{C}_{n_{\delta_a}}$	0.0064	0.0015	0.0008	0.0002	-.0027
$\mathbf{C}_{y_{\delta_r}}$	0.175	0.1448	0.0841	0.1157	0.0620
$\mathbf{C}_{l_{\delta_r}}$	0.007	0.0039	0.0090	0.0070	0.0052
$\mathbf{C}_{n_{\delta_r}}$	-.109	-.1081	-.0988	-.1256	-.0914

Table 5.4: Lateral/Directional mass properties and aerodynamic stability derivatives for the Boeing 747 at selected flight conditions.

Bibliography

[1] Bernard Etkin & Lloyd Duff Reid, **Dynamics of Flight, Stability and Control**, McGraw-Hill, Third Edition, 1996.

[2] R. K. Heffley & W. F. Jewell, **Aircraft Handling Qualities Data**, NASA CR-2144, December 1972.

[3] Robert C. Nelson, **Aircraft Stability and Automatic Control**, McGraw-Hill, Second edition, 1998.

[4] Louis V. Schmidt, **Introduction to Aircraft Flight Dynamics**, AIAA Education Series, 1998.

Chapter 6

Control of Aircraft Motions

These notes provide a brief background in modern control theory and its application to the equations of motion for a flight vehicle. The description is meant to provide the basic background in linear algebra for understanding how modern tools for the analysis of linear systems work, and provide examples of their application to flight vehicle dynamics and control. The treatment includes a brief introduction to optimal control.

6.1 Control Response

6.1.1 Laplace Transforms and State Transition

So far, we have investigated only the response of a system to a perturbation, which corresponds to the *homogeneous* solution to the system of ordinary differential equations describing the system. In order to study the response of the system to *control input*, it is convenient to use Laplace transforms; see Section 6.7 for a brief review of Laplace transforms.

The Laplace transform of the function $y(t)$, assumed identically zero for $t < 0$, is

$$\mathcal{L}(y(t)) = Y(s) = \int_0^\infty y(t)e^{-st}\,\mathrm{d}t \tag{6.1}$$

and this operation can be applied to each component of a state vector to give the Laplace transform of the state vector

$$\mathcal{L}(\mathbf{x}(t)) = \begin{pmatrix} \mathcal{L}(x_1(t)) \\ \mathcal{L}(x_2(t)) \\ \cdots \\ \mathcal{L}(x_n(t)) \end{pmatrix} = \begin{pmatrix} X_1(s)) \\ X_2(s)) \\ \cdots \\ X_n(s)) \end{pmatrix} = \mathbf{X}(s) \tag{6.2}$$

Applying this operation to the terms of the (linear) state space equation (see Eq. (6.233) in Section 6.7 for the Laplace transform of the derivative of a function)

$$\dot{\mathbf{x}} = \mathbf{A}\mathbf{x} + \mathbf{B}\eta \tag{6.3}$$

gives

$$-\mathbf{x}(0) + s\mathbf{X}(s) = \mathbf{A}\mathbf{X}(s) + \mathbf{B}\eta(s)$$

or

$$[s\mathbf{I} - \mathbf{A}]\,\mathbf{X}(s) = \mathbf{x}(0) + \mathbf{B}\eta(s) \tag{6.4}$$

Assuming that the inverse $[s\mathbf{I} - \mathbf{B}]^{-1}$ exists, this can be written as

$$\mathbf{X}(s) = [s\mathbf{I} - \mathbf{A}]^{-1}\,[\mathbf{x}(0) + \mathbf{B}\eta(s)] \tag{6.5}$$

The matrix $[s\mathbf{I} - \mathbf{B}]^{-1}$ is called the *resolvent*, and its inverse Laplace transform is called the *transition matrix*

$$\mathbf{\Phi}(t) = \mathcal{L}^{-1}\left\{(s\mathbf{I} - \mathbf{A})^{-1}\right\} \tag{6.6}$$

Taking the inverse Laplace transform of Eq. (6.5) gives

$$\mathcal{L}^{-1}\left(\mathbf{X}(s)\right) = \mathbf{x}(t) = \mathcal{L}^{-1}\left([s\mathbf{I} - \mathbf{A}]^{-1}\right)\mathbf{x}(0) + \mathcal{L}^{-1}\left([s\mathbf{I} - \mathbf{A}]^{-1}\,\mathbf{B}\eta(s)\right) \tag{6.7}$$

The convolution theorem (see Eq. (6.251)) can be used to write the inverse Laplace transform of the product appearing in the second term on the right hand side of this equation as

$$\mathcal{L}^{-1}\left([s\mathbf{I} - \mathbf{A}]^{-1}\,\mathbf{B}\eta(s)\right) = \mathcal{L}^{-1}\left(\mathcal{L}(\mathbf{\Phi})\mathbf{B}\eta(s)\right) = \int_0^t \mathbf{\Phi}(t-\tau)B\eta(\tau)\,\mathrm{d}\tau \tag{6.8}$$

whence Eq. (6.7) can be written

$$\mathbf{x}(t) = \mathbf{\Phi}(t)\mathbf{x}(0) + \int_0^t \mathbf{\Phi}(t-\tau)\mathbf{B}\eta(\tau)\,\mathrm{d}\tau \tag{6.9}$$

Thus, it is seen that the matrix $\mathbf{\Phi}$ "transitions" the state vector from its initial state $\mathbf{x}(0)$ to its state at a later time t, including the effects of control input through the convolution integral in the second term on the right-hand side.

6.1.2 The Matrix Exponential

A useful expression for the transition matrix for the case of *linear, time-invariant systems* – i.e., those systems that can be described by systems of differential equations of the form of Eqs. (6.3) in which the matrices $\mathbf{A}$ and $\mathbf{B}$ are constants, independent of time – can be written in terms of the so-called *matrix exponential*.

As motivation, recall that for the case of a single (scalar) equation

$$\dot{x} = ax \tag{6.10}$$

the Laplace transform gives

$$-x(0) + sX(s) = aX(s)$$

or

$$X(s) = \frac{1}{s-a}x(0) \tag{6.11}$$

and we can write

$$x(t) = \mathcal{L}^{-1}\left(\frac{1}{s-a}\right)x(0) \tag{6.12}$$

Now, recall that (see Eq. (6.239) in the Section 6.7)

$$\mathcal{L}^{-1}\left(\frac{1}{s-a}\right) = e^{at} \tag{6.13}$$

so the solution to Eq. (6.10) is

$$x(t) = e^{at}x(0) \tag{6.14}$$

This is, of course, no surprise; we have simply determined the solution to the almost trivial Eq. (6.10) using the very powerful tool of Laplace transforms. But Eq. (6.14) shows us that, for the case of a single equation the transition matrix is simply

$$\mathbf{\Phi}(t) = e^{at}$$

Now, we can also write

$$\frac{1}{s-a} = \frac{1}{s(1-a/s)} = \frac{1}{s} + \frac{a}{s^2} + \frac{a^2}{s^3} + \frac{a^3}{s^4} + \cdots \tag{6.15}$$

and, since

$$\mathcal{L}(t^n) = \frac{n!}{s^{n+1}} \quad \text{or} \quad \mathcal{L}^{-1}\left(\frac{n!}{s^{n+1}}\right) = t^n \tag{6.16}$$

the series of Eq. (6.15) can be inverted, term by term, to give

$$\mathcal{L}^{-1}\left(\frac{1}{s-a}\right) = 1 + at + \frac{(at)^2}{2!} + \frac{(at)^3}{3!} + \frac{(at)^4}{4!} + \cdots \tag{6.17}$$

Now, it may seem that we've just taken the long way around to illustrate the usual power series representation of e^{at}. But our goal was to suggest that the *matrix analog* of Eq. (6.13) is

$$\mathcal{L}^{-1}\left([s\mathbf{I} - \mathbf{A}]^{-1}\right) = e^{\mathbf{A}t} \tag{6.18}$$

where the *matrix exponential* is understood to be defined as

$$e^{\mathbf{A}t} \equiv \mathbf{I} + \mathbf{A}t + \frac{(\mathbf{A}t)^2}{2!} + \frac{(\mathbf{A}t)^3}{3!} + \frac{(\mathbf{A}t)^4}{4!} + \cdots \tag{6.19}$$

To verify this conjecture, we note that the matrix analog of Eq. (6.15) is

$$[s\mathbf{I} - \mathbf{A}]^{-1} = \frac{\mathbf{I}}{s} + \frac{\mathbf{A}}{s^2} + \frac{\mathbf{A}^2}{s^3} + \frac{\mathbf{A}^3}{s^4} + \cdots \tag{6.20}$$

The validity of this equation can be verified by premultiplying by $s\mathbf{I} - \mathbf{A}$ to give

$$\mathbf{I} = \mathbf{I} - \frac{\mathbf{A}}{s} + \left(\frac{\mathbf{A}}{s} - \frac{\mathbf{A}^2}{s^2}\right) + \left(\frac{\mathbf{A}^2}{s^2} - \frac{\mathbf{A}^3}{s^3}\right) + \cdots$$

Successive terms on the right hand side cancel to give the identity $\mathbf{I} = \mathbf{I}$, so long as the series converges, which will be assumed here.

Now, taking the inverse Laplace transform of Eq. (6.20) gives

$$\mathcal{L}^{-1}\left([s\mathbf{I} - \mathbf{A}]^{-1}\right) = \mathbf{I} + \mathbf{A}t + \frac{(\mathbf{A}t)^2}{2!} + \frac{(\mathbf{A}t)^3}{3!} + \cdots = e^{\mathbf{A}t} \tag{6.21}$$

Thus, we have shown that the state transition matrix for the general linear time-invariant system can be expressed as

$$\mathbf{\Phi}(t) = e^{\mathbf{A}t} \tag{6.22}$$

where the definition of the matrix exponential appearing here is taken to be Eq. (6.19). The numerical computation of the matrix exponential is not always a trivial task, especially if the matrix is large and ill-conditioned; but most software packages, such as MATLAB have standard routines that work well for most cases of interest.

Using Eq. (6.22), we can express the solution of the state space system as

$$\mathbf{x}(t) = e^{\mathbf{A}t}\mathbf{x}(0) + \int_0^t e^{\mathbf{A}(t-\tau)}\mathbf{B}\eta(\tau)\,\mathrm{d}\tau$$

or

$$\mathbf{x}(t) = e^{\mathbf{A}t}\left[\mathbf{x}(0) + \int_0^t e^{-\mathbf{A}\tau}\mathbf{B}\eta(\tau)\,\mathrm{d}\tau\right] \tag{6.23}$$

Some useful properties of the state transition matrix, which can be seen from its definition in terms of the matrix exponential are:

1. The transition matrix evaluated at $t = 0$ is the identity matrix; i.e.,

$$\mathbf{\Phi}(0) = \mathbf{I} \tag{6.24}$$

2. The transition matrix for the sum of two time intervals is the product of the individual transition matrices in either order; i.e.,

$$\mathbf{\Phi}(t_1 + t_2) = \mathbf{\Phi}(t_1)\mathbf{\Phi}(t_2) = \mathbf{\Phi}(t_2)\mathbf{\Phi}(t_1) \tag{6.25}$$

   This is equivalent to

$$e^{\mathbf{A}(t_1+t_2)} = e^{\mathbf{A}t_1}e^{\mathbf{A}t_2} = e^{\mathbf{A}t_2}e^{\mathbf{A}t_1} \tag{6.26}$$

   which can be verified directly by substitution into Eq. (6.19).

3. The relation

$$e^{-\mathbf{A}t} = \left[e^{\mathbf{A}t}\right]^{-1} \tag{6.27}$$

   can be verified by setting $t_2 = -t_1$ in Property 2, then using Property 1.

4. The commutativity property

$$\mathbf{A}e^{\mathbf{A}t} = e^{\mathbf{A}t}\mathbf{A} \tag{6.28}$$

   can be verified directly by pre- and post-multiplying Eq. (6.19) by the matrix $\mathbf{A}$.

5. The differentiation property

$$\frac{\mathrm{d}}{\mathrm{d}t}\left(e^{\mathbf{A}t}\right) = \mathbf{A}e^{\mathbf{A}t} \tag{6.29}$$

   can be verified by differentiating Eq. (6.19) term by term.

6.2 System Time Response

The state vector solution for the *homogeneous* response of the system

$$\begin{aligned} \dot{\mathbf{x}} &= \mathbf{A}\mathbf{x} + \mathbf{B}\eta \\ \mathbf{y} &= \mathbf{C}\mathbf{x} + \mathbf{D}\eta \end{aligned} \tag{6.30}$$

has been seen to be

$$\mathbf{x}(t) = e^{\mathbf{A}t}\mathbf{x}(0) \tag{6.31}$$

and hence

$$\mathbf{y}(t) = \mathbf{C}e^{\mathbf{A}t}\mathbf{x}(0) \tag{6.32}$$

We now consider the system response to several typical control inputs.

6.2.1 Impulse Response

For an impulsive input, we define

$$\eta(\tau) = \eta_0\delta(\tau) \tag{6.33}$$

where $\eta_0 = [\delta_{1_0} \quad \delta_{2_0} \quad \dots \quad \delta_{p_0}]^T$ is a constant vector that determines the relative weights of the various control inputs and $\delta(t)$ is the *Dirac delta function*. Recall that the Dirac delta (or *impulse*) function has the properties

$$\begin{aligned} \delta(t-\tau) &= 0 \quad \text{for} \quad t \neq \tau \\ \int_{-\infty}^{\infty} \delta(t-\tau)\,\mathrm{d}t &= 1 \end{aligned} \tag{6.34}$$

These properties can be used to see that

$$\int_0^t e^{-\mathbf{A}\tau}\mathbf{B}\eta_0\delta(\tau)\,\mathrm{d}\tau = \mathbf{B}\eta_0 \tag{6.35}$$

so the system response to the impulsive input of Eq. (6.33) is seen to be

$$\begin{aligned} \mathbf{x}(t) &= e^{\mathbf{A}t}\mathbf{B}\eta_0 \\ \mathbf{y}(t) &= \mathbf{C}e^{\mathbf{A}t}\mathbf{B}\eta_0 \end{aligned} \tag{6.36}$$

Note that since the vector $\mathbf{B}\eta_0$ can be interpreted as a specified initial perturbation $\mathbf{x}(0)$, we see that the system response to an impulsive input at $t = 0$ is equivalent to the homogeneous solution for the specified $\mathbf{x}(0) = \mathbf{B}\eta_0$.

6.2.2 Doublet Response

A doublet is the derivative of the delta function, so the system response to a doublet control input is simply the derivative of the analogous impulsive response. Thus, if

$$\eta(\tau) = \eta_0\frac{\mathrm{d}\delta(\tau)}{\mathrm{d}\tau} \tag{6.37}$$

where $\eta_0 = [\delta_{1_0} \quad \delta_{2_0} \quad \dots \quad \delta_{p_0}]^T$ is a constant vector that determines the relative weights of the various control inputs and $\delta(t)$ is the *Dirac delta function*, the system response will be the derivative of the impulsive response given by Eq. (6.36), i.e.,

$$\begin{aligned} \mathbf{x}(t) &= e^{\mathbf{A}t}\mathbf{A}\mathbf{B}\eta_0 \\ \mathbf{y}(t) &= \mathbf{C}e^{\mathbf{A}t}\mathbf{A}\mathbf{B}\eta_0 \end{aligned} \tag{6.38}$$

As for the impulsive response, here the vector $\mathbf{AB}\eta_0$ can be interpreted as a specified initial perturbation $\mathbf{x}(0)$, so we see that the system response to a doublet input at $t = 0$ is equivalent to the homogeneous solution for the specified initial perturbation $\mathbf{x}(0) = \mathbf{AB}\eta_0$.

6.2.3 Step Response

For a step input, we define

$$\eta(\tau) = \eta_0 H(\tau) \tag{6.39}$$

where the *Heaviside step function* is defined as

$$H(\tau) = \begin{cases} 0, & \text{for } \tau < 0 \\ 1, & \text{for } \tau \geq 0 \end{cases} \tag{6.40}$$

These properties can be used to see that

$$\int_0^t e^{-\mathbf{A}\tau}\mathbf{B}\eta_0 H(\tau)\,\mathrm{d}\tau = \int_0^t e^{-\mathbf{A}\tau}\mathbf{B}\eta_0\,\mathrm{d}\tau = \left(\int_0^t e^{-\mathbf{A}\tau}\,\mathrm{d}\tau\right)\mathbf{B}\eta_0 \tag{6.41}$$

We can evaluate the integral in this expression by integrating the definition of the matrix exponential term by term to give

$$\begin{aligned} \int_0^t e^{-\mathbf{A}\tau}\,\mathrm{d}\tau &= \int_0^t \left(\mathbf{I} - \mathbf{A}\tau + \frac{(\mathbf{A}\tau)^2}{2!} - \frac{(\mathbf{A}\tau)^3}{3!}\cdots\right)\mathrm{d}\tau \\ &= \mathbf{I}t - \frac{\mathbf{A}t^2}{2!} + \frac{\mathbf{A}^2t^3}{3!} - \frac{\mathbf{A}^3t^4}{4!} + \cdots \\ &= \left(\mathbf{A}t - \frac{(\mathbf{A}t)^2}{2!} + \frac{(\mathbf{A}t)^3}{3!} - \frac{(\mathbf{A}t)^4}{4!} + \cdots\right)\mathbf{A}^{-1} \\ &= \left(\mathbf{I} - e^{-\mathbf{A}t}\right)\mathbf{A}^{-1} \end{aligned} \tag{6.42}$$

so the system response to a step input becomes

$$\begin{aligned} \mathbf{x}(t) &= \left[e^{\mathbf{A}t} - \mathbf{I}\right]\mathbf{A}^{-1}\mathbf{B}\eta_0 \\ \mathbf{y}(t) &= \mathbf{C}\left[e^{\mathbf{A}t} - \mathbf{I}\right]\mathbf{A}^{-1}\mathbf{B}\eta_0 + \mathbf{D}\eta_0 \end{aligned} \tag{6.43}$$

For a stable system,[1]

$$\lim_{t\to\infty} e^{\mathbf{A}t} = 0 \tag{6.44}$$

so Eq. (6.43) gives

$$\lim_{t\to\infty} \mathbf{x}(t) = -\mathbf{A}^{-1}\mathbf{B}\eta_0 \tag{6.45}$$

as the steady state limit for the step response.

[1] The easiest way to see the validity of Eq. (6.44) is to realize that the response to an initial perturbation is shown by Eq. (6.23) to be equal to this matrix exponential times the initial perturbation. For a stable system, this must vanish in the limit as $t \to \infty$ for any initial perturbation.

6.2.4 Example of Response to Control Input

We here include two examples of aircraft response to control input. We examine the longitudinal response to both, impulsive and step, elevator input for the Boeing 747 in powered approach at $\mathbf{M} = 0.25$ and standard sea level conditions. This is the same equilibrium flight condition studied in the earlier chapter on unforced response. The aircraft properties and flight condition are given by

$$\begin{aligned} V &= 279.1 \text{ ft/sec}, \quad & \rho &= 0.002377 \text{ slug/ft}^3 \\ S &= 5,500. \text{ ft}^2, & \bar{c} &= 27.3 \text{ ft} \\ W &= 564,032. \text{ lb}, & I_y &= 32.3 \times 10^6 \text{ slug-ft}^2 \end{aligned} \tag{6.46}$$

and the relevant aerodynamic coefficients are

$$\begin{aligned} &\mathbf{C}_L = 1.108, \quad \mathbf{C}_D = 0.102, \quad \Theta_0 = 0 \\ &\mathbf{C}_{L\alpha} = 5.70, \quad \mathbf{C}_{L\dot{\alpha}} = 6.7, \quad \mathbf{C}_{Lq} = 5.4, \quad \mathbf{C}_{LM} = 0 \quad \mathbf{C}_{L\delta_e} = 0.338 \\ &\mathbf{C}_{D\alpha} = 0.66, \\ &\mathbf{C}_{m\alpha} = -1.26, \quad \mathbf{C}_{m\dot{\alpha}} = -3.2, \quad \mathbf{C}_{mq} = -20.8, \quad \mathbf{C}_{mM} = 0 \quad \mathbf{C}_{m\delta_e} = -1.34 \end{aligned} \tag{6.47}$$

These values correspond to the following dimensional stability derivatives

$$\begin{aligned} &X_u = -0.0212, \quad X_w = 0.0466 \\ &Z_u = -0.2306, \quad Z_w = -0.6038, \quad Z_{\dot{w}} = -0.0341, \quad Z_q = -7.674 \quad Z_{\delta_e} = -9.8175 \\ &M_u = 0.0, \quad M_w = -0.0019, \quad M_{\dot{w}} = -0.0002, \quad M_q = -0.4381 \quad M_{\delta_e} = -.5769 \end{aligned} \tag{6.48}$$

and the plant and control matrices are

$$\mathbf{A} = \begin{pmatrix} -0.0212 & 0.0466 & 0.0000 & -.1153 \\ -0.2229 & -0.5839 & 0.9404 & 0.0000 \\ 0.0150 & -0.5031 & -0.5015 & 0.0000 \\ 0.0 & 0.0 & 1.0 & 0.0 \end{pmatrix} \quad \text{and} \quad \mathbf{B} = \begin{pmatrix} 0.0000 \\ -.0340 \\ -.5746 \\ 0.0000 \end{pmatrix} \tag{6.49}$$

when the state vector is chosen to be[2]

$$\mathbf{x} = \begin{pmatrix} u/u_0 & \alpha & q & \theta \end{pmatrix}^T \tag{6.50}$$

The response to an impulsive input is shown in Fig. 6.1. Both short period and phugoid modes are excited, and the phugoid is very lightly damped and persists for a long time. Ultimately, however, original equilibrium state will be restored, since impulsive input is equivalent to unforced response with a particular initial perturbation, as shown if Eq.(6.36).

The response to a one-degree step input is shown in Fig. 6.2. Both short period and phugoid modes are again excited, the short-period less than for the impulsive input as the step input has less high-frequency content. Since the phugoid is very lightly damped it again persists for a long time.

In this case, the system ultimately settles into a new equilibrium state, that given by Eq. (6.45) which, for this case, is found to be

$$\lim_{t\to\infty} \mathbf{x}(t) = -\mathbf{A}^{-1}\mathbf{B}\eta_0 = [0.0459 \quad -.0186 \quad 0.0 \quad -.0160]^T \tag{6.51}$$

[2]Note that this is the form introduced in Chapter 5 in which the velocities have been normalized by the equilibrium flight speed.

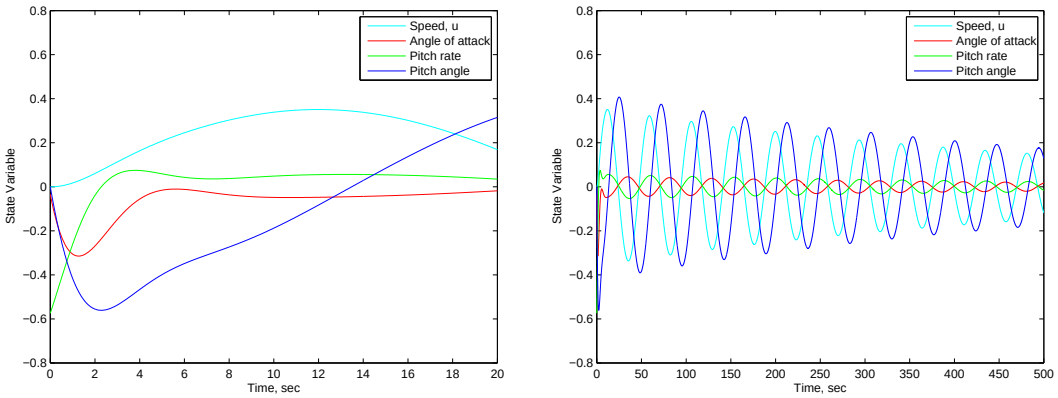

Figure 6.1: Response of Boeing 747 in powered approach at $\mathbf{M} = 0.25$ and standard sea level conditions to impulsive elevator input. Left plot is scaled to illustrate short-period response, and right plot is scaled to illustrate phugoid.

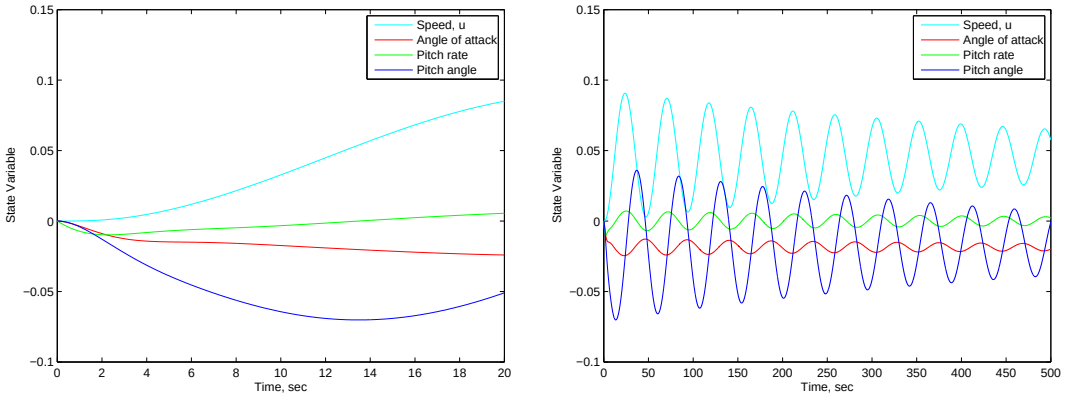

Figure 6.2: Response of Boeing 747 in powered approach at $\mathbf{M} = 0.25$ and standard sea level conditions to one-degree step elevator input. Left plot is scaled to illustrate short-period response, and right plot is scaled to illustrate phugoid.

for the one-degree value of η_0. The new equilibrium state corresponds to an increase in flight speed at a reduced angle of attack. Since the resulting lift coefficient is reduced, the pitch angle becomes negative – i.e., the aircraft has begun to descend.

The approximations of the preceding analysis are completely consistent with those made in our earlier study of *static* longitudinal control, where we found the control sensitivity to be

$$\left.\frac{\mathrm{d}\delta_e}{\mathrm{d}\mathbf{C}_L}\right)_{\text{trim}} = \frac{\mathbf{C}_{m\alpha}}{\Delta} \tag{6.52}$$

where

$$\Delta = -\mathbf{C}_{L\alpha}\mathbf{C}_{m\delta_e} + \mathbf{C}_{m\alpha}\mathbf{C}_{L\delta_e} \tag{6.53}$$

Thus, from the static analysis we estimate for a step input of one degree in elevator

$$\Delta\mathbf{C}_L = \frac{\delta_e}{\mathbf{C}_{m\alpha}/\Delta} = \frac{\pi/180}{(-1.26)/(7.212)} = -.100 \tag{6.54}$$

The asymptotic steady state of the dynamic analysis gives exactly the same result

$$\Delta\mathbf{C}_L = \mathbf{C}_{L\alpha}\alpha + \mathbf{C}_{L\delta_e} = 5.70(-.0186) + 0.338(\pi/180) = -.100 \tag{6.55}$$

This result illustrates the consistency of the static and dynamic analyses. Note, however, that if the dynamic analysis included compressibility or aeroelastic effects, the results would not have agreed exactly, as these effects were not taken into account in the static control analysis.

6.3 System Frequency Response

The *frequency response* of a system corresponds to its response to harmonic control input of the form

$$\begin{aligned}\eta(t) &= \eta_0 e^{\imath\omega t} H(t) \\ &= \eta_0 \left(\cos\omega t + \imath \sin\omega t\right) H(t)\end{aligned} \tag{6.56}$$

where $H(t)$ is the Heaviside step function, see Eq. (6.40). This input corresponds to a sinusoidal oscillation of the control at frequency ω, and the system response consists of a start-up transient which ultimately evolves into an asymptotically steady-state harmonic response. Plots of the amplitude of the steady-state harmonic response as a function of the input frequency ω are known as *Bode plots*, and are useful for identifying resonant frequencies of the system.

Frequency response is an important element of classical control theory, and is the principal reason that Laplace transforms are such an important tool for control system designers. We will, however, constrain ourselves (at least for now) to dealing with response in the time domain, and not consider frequency response further.

6.4 Controllability and Observability

Two important properties of a system are its controllability and its observability. *Controllability* relates to the ability of the control input to influence all modes of the system. For a system having

a single scalar control variable $\eta(t)$ the system is described by

$$\dot{\mathbf{x}} = \mathbf{A}\mathbf{x} + \mathbf{B}\eta(t) \tag{6.57}$$

The system response is related to the eigenvalues of the matrix $\mathbf{A}$, and these are invariant under a transformation of coordinates. The state vector can be transformed to *modal coordinates* by

$$\mathbf{v}(t) = \mathbf{P}^{-1}\mathbf{x}(t) \tag{6.58}$$

where $\mathbf{P}$ is the *modal matrix* of $\mathbf{A}$. That is, the *similarity transformation*

$$\mathbf{P}^{-1}\mathbf{A}\mathbf{P} = \mathbf{\Lambda} \tag{6.59}$$

transforms $\mathbf{A}$ to the *diagonal* matrix $\mathbf{\Lambda}$. If such a transformation exists,[3] then the state equations can be written as

$$\mathbf{P}\dot{\mathbf{v}} = \mathbf{A}\mathbf{P}\mathbf{v} + \mathbf{B}\eta(t) \tag{6.60}$$

or, after pre-multiplying by $\mathbf{P}^{-1}$,

$$\dot{\mathbf{v}} = \mathbf{\Lambda}\mathbf{v} + \mathbf{P}^{-1}\mathbf{B}\eta(t) \tag{6.61}$$

Since $\mathbf{\Lambda}$ is a diagonal matrix, this transformation has completely *decoupled* the equations; i.e., Eqs. (6.61) are equivalent to

$$\dot{v}_j = \lambda_j v_j + f_j\eta(t) \tag{6.62}$$

where f_j are the elements of the vector $\mathbf{P}^{-1}\mathbf{B}$. Thus, the evolution of each mode is independent of all the others, and the j-th mode is affected by the control so long as $f_j \neq 0$. In other words, all the modes are controllable so long as no element of $\mathbf{P}^{-1}\mathbf{B}$ is zero.

This same transformation process can be applied to the case when η is a vector – i.e., when there are multiple control inputs. In this case, all modes are controllable so long as at least one element in each *row* of the matrix $\mathbf{P}^{-1}\mathbf{B}$ is non-zero.

6.4.1 Controllability

For cases in which the plant matrix is not diagonalizable a more general procedure must be followed to determine whether the system is controllable. In these cases, we introduce the more specific definition of controllability:

> **Definition:** A system is said to be controllable if it is possible by means of an unconstrained controller to transfer the physical system between any two arbitrarily specified states in a finite time.

The requirement for controllability is well understood for linear, time-invariant systems. For such systems we can write

$$\dot{\mathbf{x}} = \mathbf{A}\mathbf{x} + \mathbf{B}\eta(t) \tag{6.63}$$

where we assume, for simplicity of presentation, that $\eta(t)$ represents a single control variable. Thus, if the state vector $\mathbf{x}$ has n elements, $\mathbf{A}$ is an $n \times n$ matrix and $\mathbf{B}$ is an $n \times 1$ column vector.

[3] A diagonalizing transformation will exist if the matrix $\mathbf{A}$ has a complete set of linearly independent eigenvectors; in this case the modal matrix $\mathbf{P}$ will be non-singular and its inverse will exist. A sufficient condition for the matrix $\mathbf{A}$ to have a complete set of linearly independent eigenvectors is that its eigenvalues be real and distinct, but this condition is not necessary.

The system of Eqs. (6.63) has the response

$$\dot{\mathbf{x}}(t) = e^{\mathbf{A}t}\left[\mathbf{x}(0) + \int_0^t e^{-\mathbf{A}t}\mathbf{B}\eta(\tau)\,\mathrm{d}\tau\right] \tag{6.64}$$

Since the states are arbitrary, we can choose the final state $\mathbf{x}(t) = 0$ with no loss of generality, in which case Eqs. (6.64) become

$$\mathbf{x}(0) = -\int_0^t e^{-\mathbf{A}t}\mathbf{B}\eta(\tau)\,\mathrm{d}\tau \tag{6.65}$$

Thus, the question of controllability reduces to whether a control law $\eta(\tau)$ exists that satisfies Eqs. (6.65) for every possible initial state $\mathbf{x}(0)$.

Recall that the Cayley-Hamilton theorem tells us that, if the characteristic equation of the plant matrix is

$$\lambda^n + a_{n-1}\lambda^{n-1} + a_{n-2}\lambda^{n-2} + \cdots + a_1\lambda + a_0 = 0 \tag{6.66}$$

then we also have

$$\mathbf{A}^n + a_{n-1}\mathbf{A}^{n-1} + a_{n-2}\mathbf{A}^{n-2} + \cdots + a_1\mathbf{A} + a_0\mathbf{I} = 0 \tag{6.67}$$

This equation can be used to represent any polynomial in the matrix $\mathbf{A}$ as a polynomial of order $n-1$. In particular, it can be used to represent the matrix exponential as the *finite* sum

$$\begin{aligned} e^{-\mathbf{A}\tau} &= \mathbf{I} - \mathbf{A}\tau + \frac{\mathbf{A}^2\tau^2}{2!} - \frac{\mathbf{A}^3\tau^3}{3!} + \cdots \\ &= \sum_{k=0}^{n-1} f_k(\tau)\mathbf{A}^k \end{aligned} \tag{6.68}$$

The actual process of determining the coefficient functions $f_k(\tau)$ might be very difficult and tedious, but for our purposes here we don't need to determine these coefficient functions explicitly, we only need to believe that such a representation is always possible.

Using Eq. (6.68) allows us to write the controllability requirement as

$$\mathbf{x}(0) = -\int_0^t \sum_{k=0}^{n-1} f_k(\tau)\mathbf{A}^k\mathbf{B}\eta(\tau)\,\mathrm{d}\tau \tag{6.69}$$

or

$$\mathbf{x}(0) = -\sum_{k=0}^{n-1} \mathbf{A}^k\mathbf{B}\int_0^t f_k(\tau)\eta(\tau)\,\mathrm{d}\tau \tag{6.70}$$

Now, for any $f_k(\tau)$ and $\eta(\tau)$ we can write

$$\int_0^t f_k(\tau)\eta(\tau)\,\mathrm{d}\tau = g_k \quad \text{for } k = 0, 1, 2, \ldots, n-1 \tag{6.71}$$

so Eqs.(6.70) can be written as

$$\begin{aligned}\mathbf{x}(0) &= -\sum_{k=0}^{n-1}\mathbf{A}^k\mathbf{B}g_k \\ &= -\mathbf{B}g_0 - \mathbf{A}\mathbf{B}g_1 - \mathbf{A}^2\mathbf{B}g_2 - \cdots - \mathbf{A}^{n-1}\mathbf{B}g_{n-1} \\ &= -\begin{bmatrix}\mathbf{B} & \mathbf{A}\mathbf{B} & \mathbf{A}^2\mathbf{B} & \cdots & \mathbf{A}^{n-1}\mathbf{B}\end{bmatrix}\begin{pmatrix} g_0 \\ g_1 \\ g_2 \\ . \\ . \\ . \\ g_{n-1}\end{pmatrix}\end{aligned} \tag{6.72}$$

This is a system of equations for the vector $\mathbf{g} = [g_0 \quad g_1 \quad g_2 \quad \ldots \quad g_{n-1}]^T$ of the form

$$\mathbf{V}\mathbf{g} = -\mathbf{x}(0) \tag{6.73}$$

which will have a solution for any arbitrarily chosen $\mathbf{x}(0)$ if the *controllability matrix*

$$\mathbf{V} = \begin{bmatrix}\mathbf{B} & \mathbf{A}\mathbf{B} & \mathbf{A}^2\mathbf{B} & \cdots & \mathbf{A}^{n-1}\mathbf{B}\end{bmatrix} \tag{6.74}$$

has full rank n.

Our analysis here has assumed there is only a single (scalar) control variable, but the analysis follows through with no essential change in the case when the control variable $\eta(\tau)$ is a p-element vector. In this case $\mathbf{g}$ will be an $n \cdot p \times 1$ vector, and the corresponding controllability matrix will have the same form as in Eq. (6.74), but since each element there has the same shape as $\mathbf{B}$ – an $n \times p$ matrix – the controllability matrix will have n rows and $n \cdot p$ columns. The controllability criterion still requires that the rank of this matrix be n.

Generally, elevator control alone is sufficient to control all longitudinal modes, and *either* rudder or aileron control is sufficient to control all lateral/directional modes.

It should be noted that controllability alone says nothing about the *quality* of the control, since arbitrarily large control input was assumed to be available. So, it is still important to look at specific control responses and/or sensitivities to determine if sufficient control action is available to achieve desired motions without saturating the controls.

Example

We consider the example of the system

$$\dot{\mathbf{x}} = \mathbf{A}\mathbf{x} + \mathbf{B}\eta(t) \tag{6.75}$$

where

$$\mathbf{A} = \begin{pmatrix} 0 & 1 \\ -2 & -3\end{pmatrix}, \quad \text{and} \quad \mathbf{B} = \begin{pmatrix} 0 \\ 1\end{pmatrix} \tag{6.76}$$

The characteristic equation of the plant matrix is

$$\det(\mathbf{A} - \lambda\mathbf{I}) = \lambda^2 + 3\lambda + 2 = 0 \tag{6.77}$$

whose roots are $\lambda = -1, -2$.

The eigenvectors of $\mathbf{A}$ are thus determined from

$$(\mathbf{A} - \lambda_1 \mathbf{I})\,\mathbf{u}_1 = 0$$

which gives

$$u_{1_1} + u_{1_2} = 0$$

whence

$$\mathbf{u}_1 = [1 \quad -1]^T$$

Similarly,

$$(\mathbf{A} - \lambda_2 \mathbf{I})\,\mathbf{u}_2 = 0$$

gives

$$2u_{2_1} + u_{2_2} = 0$$

whence

$$\mathbf{u}_2 = [1 \quad -2]^T$$

The modal matrix of $\mathbf{A}$ and its inverse are then

$$\mathbf{P} = \begin{pmatrix} 1 & 1 \\ -1 & -2 \end{pmatrix} \quad \text{and} \qquad \mathbf{P}^{-1} = \begin{pmatrix} 2 & 1 \\ -1 & -1 \end{pmatrix} \tag{6.78}$$

The characteristic variables are thus

$$\mathbf{v} = \mathbf{P}^{-1}\mathbf{x} = \begin{pmatrix} 2 & 1 \\ -1 & -1 \end{pmatrix} \begin{pmatrix} x_1 \\ x_2 \end{pmatrix} = \begin{pmatrix} 2x_1 + x_2 \\ -x_1 - x_2 \end{pmatrix} \tag{6.79}$$

and

$$\mathbf{P}\mathbf{A}\mathbf{P}^{-1} = \begin{pmatrix} \lambda_1 & 0 \\ 0 & \lambda_2 \end{pmatrix} = \begin{pmatrix} -1 & 0 \\ 0 & -2 \end{pmatrix} \tag{6.80}$$

and

$$\mathbf{P}^{-1}\mathbf{B} = \begin{pmatrix} 2 & 1 \\ -1 & -1 \end{pmatrix} = \begin{pmatrix} 0 \\ 1 \end{pmatrix} = \begin{pmatrix} 1 \\ -1 \end{pmatrix} \tag{6.81}$$

The canonical form of the equations describing the system can thus be written

$$\dot{\mathbf{v}} = \begin{pmatrix} -1 & 0 \\ 0 & -2 \end{pmatrix} \mathbf{v} + \begin{pmatrix} 1 \\ -1 \end{pmatrix} \eta(t) \tag{6.82}$$

Both modes are thus seen to be controllable.

Alternatively, since

$$\mathbf{A}\mathbf{B} = \begin{pmatrix} 0 & 1 \\ -2 & -3 \end{pmatrix} \begin{pmatrix} 0 \\ 1 \end{pmatrix} = \begin{pmatrix} 1 \\ -3 \end{pmatrix} \tag{6.83}$$

the controllability matrix is

$$\mathbf{V} = [\mathbf{B} \quad \mathbf{A}\mathbf{B}] = \begin{pmatrix} 0 & 1 \\ 1 & -3 \end{pmatrix} \tag{6.84}$$

The determinant of the controllability matrix $\det(\mathbf{V}) = -1$, is non-zero, so its rank must be 2, and the system is again seen to be controllable.

Note that if the control matrix is changed to

$$\mathbf{B} = \begin{pmatrix} -1 \\ 1 \end{pmatrix} \tag{6.85}$$

then

$$\mathbf{P}^{-1}\mathbf{B} = \begin{pmatrix} 2 & 1 \\ -1 & -1 \end{pmatrix} = \begin{pmatrix} -1 \\ 1 \end{pmatrix} = \begin{pmatrix} -1 \\ 0 \end{pmatrix} \tag{6.86}$$

and the second mode is seen to be uncontrollable. Equivalently, since we now have

$$\mathbf{AB} = \begin{pmatrix} 0 & 1 \\ -2 & -3 \end{pmatrix} \begin{pmatrix} -1 \\ 1 \end{pmatrix} = \begin{pmatrix} 1 \\ -1 \end{pmatrix} \tag{6.87}$$

the controllability matrix becomes

$$\mathbf{V} = [\mathbf{B} \quad \mathbf{AB}] = \begin{pmatrix} -1 & 1 \\ 1 & -1 \end{pmatrix} \tag{6.88}$$

The determinant of the controllability matrix $\det(\mathbf{V}) = 0$, is now zero, so its rank must be less than 2, and the modified system is again seen to be uncontrollable.

6.4.2 Observability

The mathematical *dual* of controllability is *observability*, which is defined according to:

> **Definition:** A system is observable at time t_0 if the output history $\mathbf{y}(t)$ in the time interval $[t_0, t_f]$ is sufficient to determine $\mathbf{x}(t_0)$.

It can be shown, by a process analogous to that of the preceding section, that, for linear, time-invariant systems, observability is guaranteed when the rank of the *observability matrix*

$$\mathbf{U} = \begin{bmatrix} \mathbf{C} \\ \mathbf{CA} \\ \mathbf{CA}^2 \\ \cdot \\ \cdot \\ \cdot \\ \mathbf{CA}^{n-1} \end{bmatrix} \tag{6.89}$$

is equal to n. Note that if the output vector $\mathbf{y}$ has q elements, the observability matrix will have $q \cdot n$ rows and n columns.

6.4.3 Controllability, Observability, and MATLAB

Once the plant matrix $\mathbf{A}$, the control matrix $\mathbf{B}$, and the output matrix $\mathbf{C}$ have been defined, the MATLAB function

$$\mathbf{V} = ctrb(\mathbf{A},\mathbf{B})$$

determines the controllability matrix $\mathbf{V}$, and the MATLAB function

$$\mathbf{U} = obsv(\mathbf{A},\mathbf{C})$$

determines the observability matrix $\mathbf{U}$. The rank of either of these matrices can then be determined using the MATLAB function *rank*.

6.5 State Feedback Design

A feedback control system can be designed within the state-variable framework to provide a specific eigenvalue structure for the closed-loop plant matrix. Consider the system

$$\begin{aligned} \dot{\mathbf{x}} &= \mathbf{A}\mathbf{x} + \mathbf{B}\eta \\ \mathbf{y} &= \mathbf{C}\mathbf{x} \end{aligned} \tag{6.90}$$

It can be shown that, if the system is controllable it is possible to define a linear control law to achieve any desired closed-loop eigenvalue structure. For a single-input system, a linear control law is given by

$$\eta = -\mathbf{k}^T\mathbf{x} + \eta' \tag{6.91}$$

where η' is the control input in the absence of feedback, and $\mathbf{k}$ is a vector of feedback gains. The block diagram of this system is illustrated in Fig. 6.3.

Introducing the control law into the state equation system gives

$$\begin{aligned} \dot{\mathbf{x}} &= \mathbf{A}\mathbf{x} + \mathbf{B}\left[\eta' - \mathbf{k}^T\mathbf{x}\right] \\ &= \left[\mathbf{A} - \mathbf{B}\mathbf{k}^T\right]\mathbf{x} + \mathbf{B}\eta' \\ &= \mathbf{A}^*\mathbf{x} + \mathbf{B}\eta' \end{aligned} \tag{6.92}$$

where the plant matrix describing the behavior of the closed-loop system

$$\mathbf{A}^* = \mathbf{A} - \mathbf{B}\mathbf{k}^T \tag{6.93}$$

is called the *augmented matrix* for the system.

For cases in which the plant matrix $\mathbf{A}$ of the system has undesirable eigenvalues, the augmented matrix $\mathbf{A}^*$ can be made to have more desirable eigenvalues by proper choice of the elements of the feedback gain vector $\mathbf{k}$. Note that the effect of state-variable feedback can be interpreted as modifying the plant matrix of the system; i.e., the effect of the feedback can be interpreted as effectively changing the properties of the system – the aerodynamic stability derivatives – to achieve more desirable response characteristics.

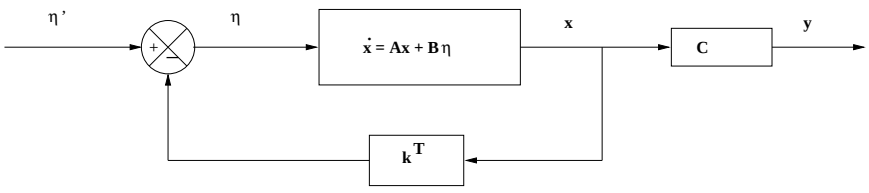

Figure 6.3: Block diagram for system with state-variable feedback.

Example: State Feedback Design

Given the system

$$\begin{aligned} \dot{\mathbf{x}} &= \mathbf{A}\mathbf{x} + \mathbf{B}\eta \\ \mathbf{y} &= \mathbf{C}\mathbf{x} \end{aligned} \tag{6.94}$$

with

$$\mathbf{A} = \begin{pmatrix} -3 & 8 \\ 0 & 0 \end{pmatrix}, \quad \mathbf{B} = \begin{pmatrix} 0 \\ 4 \end{pmatrix}, \quad \mathbf{C} = \begin{pmatrix} 1 & 0 \end{pmatrix} \tag{6.95}$$

we wish to use state-variable feedback to provide closed-loop response having

$$\omega_n = 25 \text{ sec}^{-1} \quad \text{and} \quad \zeta = 0.707 \tag{6.96}$$

Note that the characteristic equation of the original plant matrix is

$$\det(\mathbf{A} - \lambda\mathbf{I}) = (-3 - \lambda)(-\lambda) = \lambda^2 + 3\lambda = \lambda(\lambda + 3) = 0 \tag{6.97}$$

so the original system has one neutrally stable eigenvalue.

First, the controllability of the system is verified. For this system the controllability matrix is

$$\mathbf{V} = [\mathbf{B} \quad \mathbf{AB}] = \begin{pmatrix} 0 & 32 \\ 4 & 0 \end{pmatrix} \tag{6.98}$$

so, $\det(\mathbf{V}) = -128$, whence $\mathbf{V}$ has full rank so the system is controllable. The general form of the augmented matrix is

$$\mathbf{A}^* = \mathbf{A} - \mathbf{B}\mathbf{k}^T = \begin{pmatrix} -3 & 8 \\ 0 & 0 \end{pmatrix} - \begin{pmatrix} 0 \\ 4 \end{pmatrix} \begin{pmatrix} k_1 & k_2 \end{pmatrix} = \begin{pmatrix} -3 & 8 \\ -4k_1 & -4k_2 \end{pmatrix} \tag{6.99}$$

The characteristic equation of the augmented matrix $\mathbf{A}^*$ is then

$$\det(\mathbf{A}^* - \lambda\mathbf{I}) = (-3 - \lambda)(-4k_2 - \lambda) + 32k_1 = \lambda^2 + (3 + 4k_2)\lambda + 32k_1 + 12k_2 = 0 \tag{6.100}$$

Since the desired system response corresponds to the characteristic equation

$$\begin{aligned} \lambda^2 + 2\zeta\omega_n\lambda + \omega_n^2 &= 0 \\ \lambda^2 + 2(0.707)(25)\lambda + (25)^2 = 0 &= \lambda^2 + 35.35\lambda + 625 \end{aligned} \tag{6.101}$$

a comparison of Eqs. (6.100) and (6.101) shows that we must choose the elements of the gain vector such that

$$\begin{aligned} 3 + 4k_2 &= 35.35 \\ 32k_1 + 12k_2 &= 625 \end{aligned}$$

or

$$\begin{aligned} k_2 &= \frac{35.35 - 3}{4} = 8.09 \\ k_1 &= \frac{625 - 12(8.09)}{32} = 16.5 \end{aligned} \tag{6.102}$$

The response of the original system and the closed-loop response are compared in Fig. 6.4 for two different initial perturbations. Figure 6.4(a) illustrates the response when the neutrally stable mode is not excited. Figure 6.4(b) illustrates the response when the neutrally stable mode is excited; in this case the original system never returns to the original equilibrium state. But, in both cases the closed-loop system returns quickly, with minimal overshoot, to the original equilibrium state. Note, however, that significant excitation of x_2 is required in the latter case, even for the first initial condition.

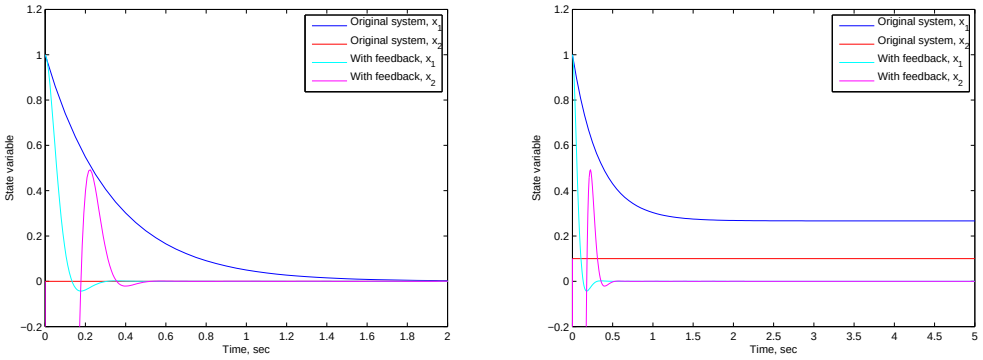

(a) $\mathbf{x}(0) = [1.0 \quad 0.0]$ (b) $\mathbf{x}(0) = [1.0 \quad 0.1]$

Figure 6.4: Response of linear, second-order system, showing effect of state variable feedback. Original system has $\lambda_1 = -3.0$, $\lambda_2 = 0.0$. Modified system has $\omega_n = 25$ sec^{-1} and $\zeta = 0.707$. (a) $\mathbf{x}(0) = [1.0 \quad 0.0]^T$; (b) $\mathbf{x}(0) = [1.0 \quad 0.1]^T$.

6.5.1 Single Input State Variable Control

When the control variable is a single scalar, the feedback gains are uniquely determined by the locations of the roots of the characteristic equation of the augmented matrix. In this case, the algorithm of Bass & Gura (see, e.g., [3]) can be used to determine the elements of the gain vector.

We describe the procedure for the system described by

$$\dot{\mathbf{x}} = \mathbf{A}\mathbf{x} + \mathbf{B}\eta \tag{6.103}$$

with the control law

$$\eta = -\mathbf{k}^T\mathbf{x} + \eta' \tag{6.104}$$

It is desirable to have the plant matrix in the (first) *companion form*,

$$\mathbf{A} = \begin{pmatrix} -a_1 & -a_2 & -a_3 & \cdots & -a_{n-1} & -a_n \\ 1 & 0 & 0 & \cdots & 0 & 0 \\ 0 & 1 & 0 & \cdots & 0 & 0 \\ 0 & 0 & 1 & \cdots & 0 & 0 \\ & & & \cdots & & \\ 0 & 0 & 0 & \cdots & 1 & 0 \end{pmatrix} \tag{6.105}$$

where it is clear from direct calculation of the determinant of $\mathbf{A} - \lambda\mathbf{I}$ that the elements a_i are the coefficients of the characteristic equation

$$\lambda^n + a_1\lambda^{n-1} + a_2\lambda^{n-2} + \cdots + a_{n-1}\lambda + a_n = 0 \tag{6.106}$$

of the plant matrix $\mathbf{A}$. Note that the homogeneous equations corresponding to the plant matrix of

Eq. (6.105) are of the form

$$\begin{aligned}
\dot{x}_1 &= -a_1x_1 - a_2x_2 - a_3x_3 - \cdots - a_{n-1}x_{n-1} - a_nx_n \\
\dot{x}_2 &= \quad x_1 \\
\dot{x}_3 &= \qquad x_2 \\
\dot{x}_4 &= \qquad\quad x_3 \\
&\qquad\qquad \cdots \\
\dot{x}_n &= \qquad\qquad\qquad x_{n-1}
\end{aligned} \tag{6.107}$$

so the system is equivalent to the single higher-order equation

$$\frac{\mathrm{d}^n y}{\mathrm{d}t^n} + a_1\frac{\mathrm{d}^{n-1} y}{\mathrm{d}t^{n-1}} + a_2\frac{\mathrm{d}^{n-2} y}{\mathrm{d}t^{n-2}} + \cdots + a_{n-1}\frac{\mathrm{d}y}{\mathrm{d}t} + a_n y = f(t) \tag{6.108}$$

where $y = x_n$. Thus, when the equations are in companion form, the control matrix takes the special form

$$\mathbf{B} = \begin{bmatrix} 1 & 0 & 0 & \cdots & 0 \end{bmatrix}^T \tag{6.109}$$

Now, as we have seen, when the control law of Eq. (6.104) is substituted into the Eqs. (6.103), the equations take the form

$$\dot{\mathbf{x}} = \mathbf{A}^*\mathbf{x} + \mathbf{B}\eta' \tag{6.110}$$

where

$$\mathbf{A}^* = \mathbf{A} - \mathbf{B}\mathbf{k}^T \tag{6.111}$$

is the augmented matrix. Because of the special form of the control matrix when the equations are in companion form, the augmented matrix takes the form

$$\mathbf{A}^* = \begin{pmatrix} -a_1 - k_1 & -a_2 - k_2 & -a_3 - k_3 & \cdots & -a_{n-1} - k_{n-1} & -a_n - k_n \\ 1 & 0 & 0 & \cdots & 0 & 0 \\ 0 & 1 & 0 & \cdots & 0 & 0 \\ 0 & 0 & 1 & \cdots & 0 & 0 \\ & & & \cdots & & \\ 0 & 0 & 0 & \cdots & 0 & 0 \\ 0 & 0 & 0 & \cdots & 1 & 0 \end{pmatrix} \tag{6.112}$$

The characteristic equation of the augmented matrix can thus be computed directly as

$$\lambda^n + (a_1 + k_1)\,\lambda^{n-1} + (a_2 + k_2)\,\lambda^{n-2} + \cdots (a_{n-1} + k_{n-1})\,\lambda + (a_n + k_n) = 0 \tag{6.113}$$

Now, once the *desired* eigenvalues $\bar{\lambda}_i$ have been established, the characteristic equation of the *desired* augmented matrix can also be computed directly from

$$\begin{aligned}
\left(\lambda - \bar{\lambda}_1\right)\left(\lambda - \bar{\lambda}_2\right)\left(\lambda - \bar{\lambda}_3\right)\cdots\left(\lambda - \bar{\lambda}_n\right) &= 0 \\
\lambda^n + \bar{a}_1\lambda^{n-1} + \bar{a}_2\lambda^{n-2} + \bar{a}_3\lambda^{n-3} + \cdots + \bar{a}_{n-1}\lambda + \bar{a}_n &= 0
\end{aligned} \tag{6.114}$$

and the desired gains are determined by equating the coefficients in Eqs. (6.113) and (6.114):

$$a_i + k_i = \bar{a}_i\,, \text{ for } i = 1, 2, \ldots, n$$

or

$$k_i = \bar{a}_i - a_i\,, \text{ for } i = 1, 2, \ldots, n \tag{6.115}$$

Transformation to Companion Form

In order to use the results of the preceding section for a general system, we need to be able to transform an arbitrary plant matrix $\mathbf{A}$ to its (first) companion form

$$\bar{\mathbf{A}} = \begin{pmatrix} -a_1 & -a_2 & -a_3 & \cdots & -a_{n-1} & -a_n \\ 1 & 0 & 0 & \cdots & 0 & 0 \\ 0 & 1 & 0 & \cdots & 0 & 0 \\ 0 & 0 & 1 & \cdots & 0 & 0 \\ & & & \cdots & & \\ 0 & 0 & 0 & \cdots & 1 & 0 \end{pmatrix} \tag{6.116}$$

That is, it is necessary to find the matrix $\mathbf{T}$ such that

$$\bar{\mathbf{A}} = \mathbf{T}\mathbf{A}\mathbf{T}^{-1} \tag{6.117}$$

where $\bar{\mathbf{A}}$ has the desired form illustrated in Eq. (6.116). It is convenient to represent the needed matrix as the product of two simpler matrices

$$\mathbf{T} = \mathbf{R}\mathbf{S} \tag{6.118}$$

so that

$$\bar{\mathbf{A}} = \mathbf{R}\mathbf{S}\mathbf{A}\mathbf{S}^{-1}\mathbf{R}^{-1} \tag{6.119}$$

where the intermediate transformation

$$\tilde{\mathbf{A}} = \mathbf{S}\mathbf{A}\mathbf{S}^{-1} \tag{6.120}$$

takes the matrix to the (second) *companion form*

$$\tilde{\mathbf{A}} = \begin{pmatrix} 0 & 0 & 0 & \cdots & 0 & -a_n \\ 0 & 1 & 0 & \cdots & 0 & -a_{n-1} \\ 0 & 0 & 1 & \cdots & 0 & -a_{n-2} \\ 0 & 0 & 0 & \cdots & 0 & -a_{n-3} \\ & & & \cdots & & \\ 0 & 0 & 0 & \cdots & 1 & -a_1 \end{pmatrix} \tag{6.121}$$

We first show that the intermediate transformation

$$\tilde{\mathbf{A}} = \mathbf{S}\mathbf{A}\mathbf{S}^{-1} \tag{6.122}$$

is achieved when $\mathbf{S}$ is chosen to be the inverse of the controllability matrix $\mathbf{V}$, defined in Eq. (6.74). Thus, we must show that

$$\mathbf{S}^{-1}\tilde{\mathbf{A}} = \mathbf{A}\mathbf{S}^{-1} \tag{6.123}$$

or

$$\mathbf{V}\tilde{\mathbf{A}} = \mathbf{A}\mathbf{V} \tag{6.124}$$

For a single-input system, the controllability matrix takes the form

$$\mathbf{V} = \begin{bmatrix} \mathbf{b} & \mathbf{A}\mathbf{b} & \mathbf{A}^2\mathbf{b} & \cdots & \mathbf{A}^{n-1}\mathbf{b} \end{bmatrix} \tag{6.125}$$

where $\mathbf{b}$ is an n-vector and, for $\tilde{\mathbf{A}}$ in the (second) *companion form*, we have

$$\begin{aligned}\mathbf{V}\tilde{\mathbf{A}} &= \begin{bmatrix}\mathbf{b} & \mathbf{A}\mathbf{b} & \mathbf{A}^2\mathbf{b} & \cdots & \mathbf{A}^{n-1}\mathbf{b}\end{bmatrix}\begin{pmatrix}0 & 0 & 0 & \cdots & 0 & -a_n\\ 1 & 0 & 0 & \cdots & 0 & -a_{n-1}\\ 0 & 1 & 0 & \cdots & 0 & -a_{n-2}\\ 0 & 0 & 1 & \cdots & 0 & -a_{n-3}\\ & & & \cdots & & \\ 0 & 0 & 0 & \cdots & 0 & -a_2\\ 0 & 0 & 0 & \cdots & 1 & -a_1\end{pmatrix}\\ &= \begin{bmatrix}\mathbf{A}\mathbf{b} & \mathbf{A}^2\mathbf{b} & \mathbf{A}^3\mathbf{b} & \cdots & -a_n\mathbf{b} - a_{n-1}\mathbf{A}\mathbf{b}\cdots - a_1\mathbf{A}^{n-1}\mathbf{b}\end{bmatrix}\end{aligned} \tag{6.126}$$

The Cayley-Hamilton Theorem can be used to express the final column in the above matrix as

$$\left(-a_n\mathbf{I} - a_{n-1}\mathbf{A} - a_{n-2}\mathbf{A}^2 - \cdots - a_1\mathbf{A}^{n-1}\right)\mathbf{b} = \mathbf{A}^n\mathbf{b} \tag{6.127}$$

Thus,

$$\mathbf{V}\tilde{\mathbf{A}} = \mathbf{A}\begin{bmatrix}\mathbf{b} & \mathbf{A}\mathbf{b} & \mathbf{A}^2\mathbf{b} & \cdots & \mathbf{A}^{n-1}\mathbf{b}\end{bmatrix} = \mathbf{A}\mathbf{V} \tag{6.128}$$

as was to be shown.

For the final transformation, we require

$$\bar{\mathbf{A}} = \mathbf{R}\tilde{\mathbf{A}}\mathbf{R}^{-1} \tag{6.129}$$

to have the desired form, or

$$\mathbf{R}^{-1}\bar{\mathbf{A}} = \tilde{\mathbf{A}}\mathbf{R}^{-1} \tag{6.130}$$

The required matrix $\mathbf{R}^{-1}$ has the form

$$\mathbf{R}^{-1} = \begin{pmatrix}1 & a_1 & a_2 & a_3 & \cdots & a_{n-2} & a_{n-1}\\ 0 & 1 & a_1 & a_2 & \cdots & a_{n-3} & a_{n-2}\\ 0 & 0 & 1 & a_1 & \cdots & a_{n-4} & a_{n-3}\\ 0 & 0 & 0 & 1 & \cdots & a_{n-5} & a_{n-4}\\ & & & & \cdots & & \\ 0 & 0 & 0 & 0 & \cdots & 0 & 1\end{pmatrix} = \mathbf{W} \tag{6.131}$$

which can be verified by noting that

$$\begin{aligned}\mathbf{R}^{-1}\bar{\mathbf{A}} &= \begin{pmatrix}1 & a_1 & a_2 & a_3 & \cdots & a_{n-2} & a_{n-1}\\ 0 & 1 & a_1 & a_2 & \cdots & a_{n-3} & a_{n-2}\\ 0 & 0 & 1 & a_1 & \cdots & a_{n-4} & a_{n-3}\\ 0 & 0 & 0 & 1 & \cdots & a_{n-5} & a_{n-4}\\ & & & & \cdots & & \\ 0 & 0 & 0 & 0 & \cdots & 0 & 1\end{pmatrix}\begin{pmatrix}-a_1 & -a_2 & -a_3 & \cdots & -a_{n-1} & -a_n\\ 1 & 0 & 0 & \cdots & 0 & 0\\ 0 & 1 & 0 & \cdots & 0 & 0\\ 0 & 0 & 1 & \cdots & 0 & 0\\ & & & \cdots & & \\ 0 & 0 & 0 & \cdots & 1 & 0\end{pmatrix}\\ &= \begin{pmatrix}0 & 0 & 0 & \cdots & 0 & -a_n\\ 1 & a_1 & a_2 & \cdots & a_{n-2} & 0\\ 0 & 1 & a_1 & \cdots & a_{n-3} & 0\\ 0 & 0 & 1 & \cdots & a_{n-4} & 0\\ & & & \cdots & & \\ 0 & 0 & 0 & \cdots & a_1 & 0\\ 0 & 0 & 0 & \cdots & 1 & 0\end{pmatrix}\end{aligned} \tag{6.132}$$

while

$$\begin{aligned}\tilde{\mathbf{A}}\mathbf{R}^{-1} &= \begin{pmatrix} 0 & 0 & 0 & \cdots & 0 & -a_n \\ 1 & 0 & 0 & \cdots & 0 & -a_{n-1} \\ 0 & 1 & 0 & \cdots & 0 & -a_{n-2} \\ 0 & 0 & 1 & \cdots & 0 & -a_{n-3} \\ & & & \cdots & & \\ 0 & 0 & 0 & \cdots & 0 & -a_2 \\ 0 & 0 & 0 & \cdots & 1 & -a_1 \end{pmatrix} \begin{pmatrix} 1 & a_1 & a_2 & a_3 & \cdots & a_{n-2} & a_{n-1} \\ 0 & 1 & a_1 & a_2 & \cdots & a_{n-3} & a_{n-2} \\ 0 & 0 & 1 & a_1 & \cdots & a_{n-4} & a_{n-3} \\ 0 & 0 & 0 & 1 & \cdots & a_{n-5} & a_{n-4} \\ & & & & \cdots & & \\ 0 & 0 & 0 & 0 & \cdots & 0 & 1 \end{pmatrix} \\ &= \begin{pmatrix} 0 & 0 & 0 & \cdots & 0 & -a_n \\ 1 & a_1 & a_2 & \cdots & a_{n-2} & 0 \\ 0 & 1 & a_1 & \cdots & a_{n-3} & 0 \\ 0 & 0 & 1 & \cdots & a_{n-4} & 0 \\ & & & \cdots & & \\ 0 & 0 & 0 & \cdots & a_1 & 0 \\ 0 & 0 & 0 & \cdots & 1 & 0 \end{pmatrix} = \mathbf{R}^{-1}\bar{\mathbf{A}}\end{aligned} \tag{6.133}$$

as was to be shown.

Now, we have seen for the system in companion form

$$\dot{\mathbf{z}} = \bar{\mathbf{A}}\mathbf{z} + \bar{\mathbf{B}}\eta \tag{6.134}$$

subject to the control law

$$\eta = -\bar{\mathbf{k}}^T\mathbf{z} + \eta' \tag{6.135}$$

the roots of the augmented matrix are driven to those of the characteristic equation

$$\lambda^n + \bar{a}_1\lambda^{n-1} + \bar{a}_2\lambda^{n-2} + \cdots + \bar{a}_{n-1}\lambda + \bar{a}_0 = 0 \tag{6.136}$$

by the gain vector having elements

$$\bar{k}_i = \bar{a}_i - a_i \tag{6.137}$$

where a_i are the coefficients of the characteristic equation of the original (open-loop) plant matrix.

The system of Eqs.(6.134) in companion form can be related back to the original system by introducing the transformation

$$\mathbf{z} = \mathbf{T}\mathbf{x} \tag{6.138}$$

to give

$$\mathbf{T}\dot{\mathbf{x}} = \mathbf{T}\mathbf{A}\mathbf{T}^{-1}\mathbf{T}\mathbf{x} + \bar{\mathbf{B}}\eta \tag{6.139}$$

or

$$\dot{\mathbf{x}} = \mathbf{A}\mathbf{x} + \mathbf{T}^{-1}\bar{\mathbf{B}}\eta \tag{6.140}$$

The control law then transforms as

$$\eta = -\mathbf{k}^T\mathbf{x} = -\mathbf{k}^T\mathbf{T}^{-1}\mathbf{z} = -\bar{\mathbf{k}}^T\mathbf{z} \tag{6.141}$$

whence

$$\mathbf{k}^T\mathbf{T}^{-1} = \bar{\mathbf{k}}^T \tag{6.142}$$

or

$$\mathbf{k} = \mathbf{T}^T\bar{\mathbf{k}} \tag{6.143}$$

Finally, since

$$\mathbf{T} = \mathbf{RS} = \mathbf{W}^{-1}\mathbf{V}^{-1} = (\mathbf{VW})^{-1} \tag{6.144}$$

we can write

$$\mathbf{k} = \left[(\mathbf{VW})^{-1}\right]^T \bar{\mathbf{k}} \tag{6.145}$$

where the matrices $\mathbf{V}$ and $\mathbf{W}$ are defined in Eqs. (6.125) and (6.131), respectively. Equation (6.145), known as the Bass-Gura formula, gives the gain matrix for the original state space (in which the plant matrix is $\mathbf{A}$), in terms of the coefficients of the desired characteristic equation, given by Eq. (6.137).

Example of Single-Variable Feedback Control

We here present an example of single-variable feedback control used to stabilize the Dutch Roll mode of the Boeing 747 aircraft in powered approach at sea level. We saw in an earlier chapter that the Dutch Roll mode for this flight condition was very lightly damped, so we will use state-variable feedback to increase the damping ratio of this mode to $\zeta = 0.30$, while keeping the undamped natural frequency of the mode, and the times to damp to half amplitude of the rolling and spiral modes, unchanged.

For the Boeing 747 powered approach condition (at $\mathbf{M} = 0.25$, standard sea-level conditions), the relevant vehicle parameters are

$$\begin{aligned} &W = 564,032 \text{ lbf} \qquad b = 195.7 \text{ ft} \qquad u_0 = 279.1 \text{ ft/sec} \\ &I_x = 14.3 \times 10^6 \text{ slug ft}^2, \quad I_z = 45.3 \times 10^6 \text{ slug ft}^2, \quad I_{xz} = -2.23 \times 10^6 \text{ slug ft}^2 \end{aligned} \tag{6.146}$$

and the relevant aerodynamic derivatives are

$$\begin{array}{lllll} \mathbf{C}_{y_\beta} = -.96 & \mathbf{C}_{y_p} = 0.0 & \mathbf{C}_{y_r} = 0.0 & \mathbf{C}_{y_{\delta_r}} = 0.175 & \mathbf{C}_{y_{\delta_a}} = 0 \\ \mathbf{C}_{l_\beta} = -.221 & \mathbf{C}_{l_p} = -.45 & \mathbf{C}_{l_r} = 0.101 & \mathbf{C}_{l_{\delta_r}} = 0.007 & \mathbf{C}_{l_{\delta_a}} = 0.0461 \\ \mathbf{C}_{n_\beta} = 0.15 & \mathbf{C}_{n_p} = -.121 & \mathbf{C}_{n_r} = -.30 & \mathbf{C}_{n_{\delta_r}} = -.109 & \mathbf{C}_{n_{\delta_a}} = 0.0064 \end{array} \tag{6.147}$$

These values correspond to the following dimensional stability derivatives

$$\begin{array}{lllll} Y_v = -0.0999, & Y_p = 0.0, & Y_r = 0.0 & Y_{\delta_r} = 5.083 & Y_{\delta_a} = 0.0 \\ L_v = -0.0055, & L_p = -1.0994, & L_r = 0.2468 & L_{\delta_r} = 0.0488 & L_{\delta_a} = 0.3212 \\ N_v = 0.0012, & N_p = -.0933, & N_r = -.2314 & N_{\delta_r} = -.2398 & N_{\delta_a} = 0.0141 \end{array} \tag{6.148}$$

and the dimensionless product of inertia factors

$$i_x = -.156, \qquad i_z = -.0492 \tag{6.149}$$

Using these values, the plant matrix is found to be

$$\mathbf{A} = \begin{pmatrix} -0.0999 & 0.0000 & 0.1153 & -1.0000 \\ -1.6038 & -1.0932 & 0.0 & 0.2850 \\ 0.0 & 1.0 & 0.0 & 0.0 \\ 0.4089 & -.0395 & 0.0 & -.2454 \end{pmatrix} \tag{6.150}$$

when the state vector is defined as[4]

$$\mathbf{x} = \begin{pmatrix} \beta & p & \phi & r \end{pmatrix}^T \tag{6.151}$$

[4]Note that this is the form introduced in Chapter 5 in which the sideslip velocity has been normalized by the equilibrium flight speed.

(i.e., is based on sideslip *angle* rather than sideslip *velocity*).

The roots of the characteristic equation are found to be the same as those in Chapter 5 of the class notes:

$$\begin{aligned} \lambda_{\text{DR}} &= -.08066 \pm \imath\ 0.7433 \\ \lambda_{\text{roll}} &= -1.2308 \\ \lambda_{\text{spiral}} &= -.04641 \end{aligned} \tag{6.152}$$

The undamped natural frequency and damping ratio of the Dutch Roll mode are thus

$$\omega_{n_{\text{DR}}} = 0.7477 \text{ sec}^{-1} \quad \text{and} \quad \zeta_{\text{DR}} = 0.1079 \tag{6.153}$$

The times to damp to half amplitude for the rolling and spiral modes are seen to be

$$t_{1/2_{\text{roll}}} = 0.56 \text{ sec} \quad \text{and} \quad t_{1/2_{\text{spiral}}} = 14.93 \text{ sec} \tag{6.154}$$

respectively.

We now determine the gains required, using *rudder control only*, to increase the damping ratio of the Dutch Roll mode to $\zeta = 0.30$, while keeping the other modal properties fixed.

The original plant matrix is the same as that in Eq. (6.150), and its characteristic equation is given by

$$\lambda^4 + 1.4385\lambda^3 + 0.8222\lambda^2 + 0.7232\lambda + 0.0319 = 0 \tag{6.155}$$

The characteristic equation of the desired system is

$$\begin{aligned} (\lambda - \lambda_{\text{roll}})(\lambda - \lambda_{\text{spiral}})(\lambda^2 + 2\zeta\omega_n\lambda + \omega_n^2)_{\text{DR}} &= 0 \\ (\lambda + 1.2308)(\lambda + 0.04641)(\lambda^2 + 2\zeta\omega_n\lambda + \omega_n^2) &= 0 \\ (\lambda^2 + 1.2772\lambda + 0.05712)(\lambda^2 + 2(0.30)(0.7477)\lambda + (0.7477)^2) &= 0 \\ (\lambda^2 + 1.2772\lambda + 0.05712)(\lambda^2 + 0.4486\lambda + 0.5591) &= 0 \\ \lambda^4 + 1.7258\lambda^3 + 1.1891\lambda^2 + 0.7396\lambda + 0.0319 &= 0 \end{aligned} \tag{6.156}$$

and by construction the roots will be the same as for the original system, except the damping ratio for the Dutch Roll mode will be increased to

$$\zeta = 0.30$$

Comparing the coefficients in the characteristic Eqs. (6.155) and (6.156), the gain vector in the *companion form* space is seen to be

$$\begin{aligned} \bar{\mathbf{k}} &= [1.7258 \quad 1.1891 \quad 0.7396 \quad 0.0319]^T - [1.4385 \quad 0.8222 \quad 0.7232 \quad 0.0319]^T \\ &= [0.2873 \quad 0.3669 \quad 0.0164 \quad 0.0000]^T \end{aligned} \tag{6.157}$$

The control matrix, assuming rudder-only control, is

$$\mathbf{B} = [0.0182 \quad 0.0868 \quad 0.0 \quad -.2440]^T \tag{6.158}$$

and the gain vector in the original state vector space required to achieve the desired augmented matrix is

$$\mathbf{k} = \left[(\mathbf{VW})^{-1}\right]^T \bar{\mathbf{k}} = [0.1383 \quad 0.0943 \quad 0.1250 \quad -1.1333]^T \tag{6.159}$$

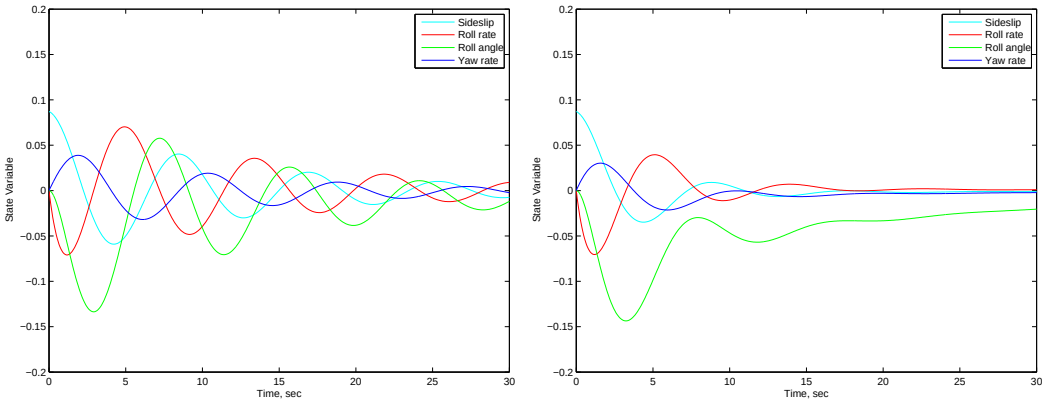

(a) (b)

Figure 6.5: Boeing 747 aircraft in powered approach at standard sea level conditions and $\mathbf{M} = 0.25$; response to 5 degree (0.08727 radian) perturbation in sideslip. (a) Original open-loop response; (b) Closed loop response with Dutch Roll damping ratio changed to $\zeta = 0.30$ using rudder state-variable feedback.

where

$$\mathbf{V} = [\mathbf{B} \quad \mathbf{AB} \quad \mathbf{A}^2\mathbf{B} \quad \mathbf{A}^3\mathbf{B}] \tag{6.160}$$

is the controllability matrix and

$$\mathbf{W} = \begin{pmatrix} 1 & a_1 & a_2 & a_3 \\ 0 & 1 & a_1 & a_2 \\ 0 & 0 & 1 & a_1 \\ 0 & 0 & 0 & 1 \end{pmatrix} \tag{6.161}$$

where the element a_i is the coefficient of λ^{4-i} in the characteristic equation of the original system.

The augmented plant matrix for the closed-loop system is

$$\mathbf{A}^* = \begin{pmatrix} -0.1024 & -.0017 & 0.1130 & -.9794 \\ -1.6158 & -1.1014 & -.0109 & 0.3834 \\ 0.0 & 1.0 & 0.0 & 0.0 \\ 0.4427 & -.0165 & 0.0305 & -.5220 \end{pmatrix} \tag{6.162}$$

Comparing the augmented plant matrix of Eq. (6.162) with that for the original (open-loop) system in Eq. (6.150), we see that by far the largest change is in the $a_{4,4}$ element, indicating that the effective value of *yaw damping* has more than doubled. We saw from our approximate analysis that yaw damping had a stabilizing effect on both, the spiral and Dutch Roll modes.

The response of the closed-loop system to a 5 degree perturbation in sideslip angle is compared to that of the original open-loop system in Fig. 6.5. The Dutch Roll response of the closed-loop system is seen, as expected, to be much more heavily damped than that of the original system.

We next determine the gains required, using *aileron control only*, to increase the damping ratio of the Dutch Roll mode to $\zeta = 0.30$, while keeping the other modal parameters unchanged. The original plant matrix, its characteristic equation, and the characteristic equation of the desired system are

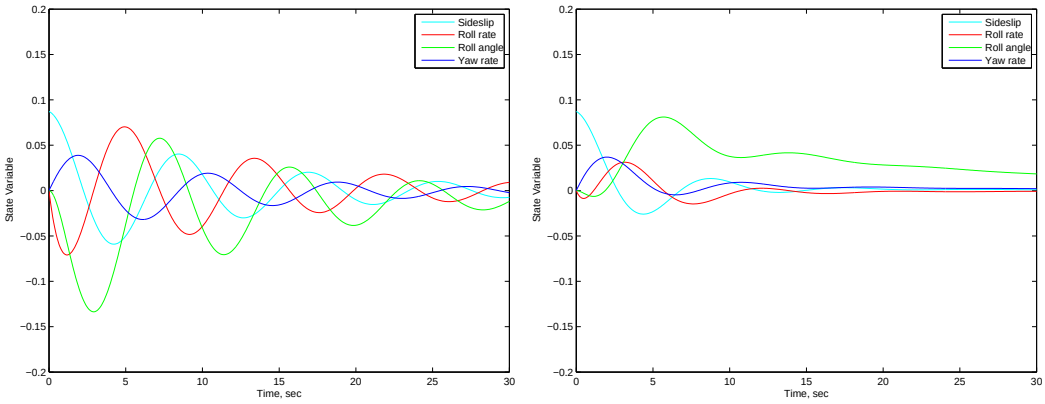

Figure 6.6: Boeing 747 aircraft in powered approach at standard sea level conditions and $\mathbf{M} = 0.25$; response to 5 degree (0.08727 radian) perturbation in sideslip. (a) Original open-loop response; (b) Closed loop response with Dutch Roll damping ratio changed to $\zeta = 0.30$ using aileron state-variable feedback.

all the same as in the previous exercise, so the gain matrix for the *companion form* system is also unchanged. The control matrix, however, is now that for aileron-only control, and is given by

$$\mathbf{B} = [0.0000 \quad 0.3215 \quad 0.0000 \quad -.0017]^T \tag{6.163}$$

The gain vector in the original state vector space required to achieve the desired augmented matrix is then

$$\mathbf{k} = \left[(\mathbf{VW})^{-1}\right]^T \bar{\mathbf{k}} = [-3.5417 \quad 0.8715 \quad 0.6746 \quad -4.0504]^T \tag{6.164}$$

The response of the closed-loop system to a 5 degree perturbation in sideslip angle is compared with that of the original system in Fig. 6.6. As for the case of rudder-only control, the closed-loop response is seen to be much more heavily damped than that of the open-loop system.

The augmented plant matrix for the closed-loop system in this case is

$$\mathbf{A}^* = \begin{pmatrix} -0.0999 & 0.0000 & 0.1153 & -1.0000 \\ -0.4651 & -1.3734 & -.2169 & 1.5873 \\ 0.0 & 1.0 & 0.0 & 0.0 \\ 0.4027 & -.0380 & .0012 & -.2525 \end{pmatrix} \tag{6.165}$$

Comparing this plant matrix with that for the original (open-loop) system in Eq. (6.150), we see that by far the largest changes are in the $a_{2,1}$ and $a_{2,4}$ elements. The effective dihedral effect has been reduced to less than 30% of its original value, while the effective *roll-due-to-yaw rate* has been increased by more than a factor of five. Thus, it seems that the control algorithm has stabilized the Dutch Roll mode by reducing the effective dihedral effect; then, in order to not increase the spiral mode stability it has effectively increased the (positive) roll-due-to-yaw rate derivative.

6.5.2 Multiple Input-Output Systems

For multiple input-output systems having p controls, the feedback control law has the form

$$\eta = -\mathbf{K}\mathbf{x} + \eta' \tag{6.166}$$

where $\mathbf{K}$ is the $p \times n$ *gain matrix*. Thus, there are now $p \times n$ gains to be specified, but there are still only n eigenvalues to be specified.

This additional flexibility can be used to configure the control system in a more optimal way if the control engineer understands the system well enough to make intelligent choices for how to allocate the gains. But, even for the single-input system, it is not always clear what is the best placement for the eigenvalues of the augmented matrix. Clearly, more stability is desirable for the less stable modes, but too much stability can result in a system that requires great effort from the pilot to achieve required maneuvers. Equations (6.137) and (6.145) indicate that more control effort will be required as the roots of the augmented matrix are moved further and further to the left of those of the original plant matrix. Also, it is generally important that the closed-loop frequency response not be increased too much to avoid exciting modes that have not been modeled, such as those arising from structural deformation due to aeroelasticity.

6.6 Optimal Control

As has been seen in the previous sections, use of the Bass-Gura procedure often is difficult, or results in sub-optimal performance for a variety of reasons. These include:

1. The best choice of desired placement for the eigenvalues of the augmented matrix is not always obvious;
2. Particular eigenvalue placement may require more control input than it available; this can result in saturation of the control action, which introduces non-linearity and can even result in instability;
3. For multiple input-output systems, we need to develop strategies for deciding on how to allocate the gains among the $n \times p$ elements, since we have only n eigenvalues to place;
4. The process may not be controllable; i.e., if the rank of the controllability matrix $\mathbf{V}$ is less than n, the method fails since Eq. (6.145) requires determination of the inverse of $\mathbf{V}$.

All these points argue for a control design strategy that, in some sense, optimizes the gain matrix for stabilizing a given system. This is the goal of what has come to be called *optimal control*.

6.6.1 Formulation of Linear, Quadratic, Optimal Control

The *optimal control* of the linear system

$$\dot{\mathbf{x}} = \mathbf{A}\mathbf{x} + \mathbf{B}\eta(t) \tag{6.167}$$

is defined as the control vector $\eta(t)$ that drives the state from a specified initial state $\mathbf{x}(t)$ to a desired final state $\mathbf{x}_d(t_f)$ such that a specified performance index

$$J = \int_t^{t_f} g(\mathbf{x}(\tau), \eta(\tau), \tau)\, \mathrm{d}\tau \tag{6.168}$$

is minimized. For *quadratic* optimal control, the performance index is specified in the form

$$g = \mathbf{x}^T \mathbf{Q} \mathbf{x} + \eta^T \mathbf{R} \eta \tag{6.169}$$

where $\mathbf{Q}$ and $\mathbf{R}$ are symmetric, positive-definite matrices, and the performance index becomes

$$J = \int_t^{t_f} \left(\mathbf{x}^T \mathbf{Q} \mathbf{x} + \eta^T \mathbf{R} \eta \right)\, \mathrm{d}\tau \tag{6.170}$$

If the control law is assumed to be linear, i.e., of the form

$$\eta = -\mathbf{K}\mathbf{x} + \eta' \tag{6.171}$$

then the determination of the gain matrix $\mathbf{K}$ that minimizes J is called the linear quadratic regulator (LQR) problem. For this control law the closed-loop response of the system to a perturbation is given by

$$\dot{\mathbf{x}} = [\mathbf{A} - \mathbf{B}\mathbf{K}]\, \mathbf{x} = \mathbf{A}^* \mathbf{x} \tag{6.172}$$

where

$$\mathbf{A}^* = \mathbf{A} - \mathbf{B}\mathbf{K} \tag{6.173}$$

is the *augmented* plant matrix.

We usually are interested in cases for which the matrices $\mathbf{A}$, $\mathbf{B}$, and $\mathbf{K}$ are independent of time, but the development here is easier if we allow the augmented matrix $\mathbf{A}^*$ to vary with time. In this case, we cannot express the solution to Eq. (6.172) in terms of a matrix exponential, but we can still express it in terms of the general state transition matrix $\mathbf{\Phi}^*$ as

$$\mathbf{x}(\tau) = \mathbf{\Phi}^*(\tau, t)\mathbf{x}(t) \tag{6.174}$$

Equation (6.174) simply implies that the state of the system at any time τ depends linearly on the state at any other time t. When the control law of Eq. (6.171) is substituted into the performance index of Eq. (6.170) and Eq. (6.174) is used to express the evolution of the state variable, the quantity to be minimized becomes

$$\begin{aligned} J &= \int_t^{t_f} \mathbf{x}^T(\tau) \left[\mathbf{Q} + \mathbf{K}^T \mathbf{R} \mathbf{K} \right] \mathbf{x}(\tau)\, \mathrm{d}\tau \\ &= \int_t^{t_f} \mathbf{x}^T(t) \mathbf{\Phi}^{*T}(\tau, t) \left[\mathbf{Q} + \mathbf{K}^T \mathbf{R} \mathbf{K} \right] \mathbf{\Phi}^*(\tau, t) \mathbf{x}(t)\, \mathrm{d}\tau \\ &= \mathbf{x}^T(t) \left(\int_t^{t_f} \mathbf{\Phi}^{*T}(\tau, t) \left[\mathbf{Q} + \mathbf{K}^T \mathbf{R} \mathbf{K} \right] \mathbf{\Phi}^*(\tau, t)\, \mathrm{d}\tau \right) \mathbf{x}(t) \end{aligned} \tag{6.175}$$

or

$$J = \mathbf{x}^T(t) \mathbf{S} \mathbf{x}(t) \tag{6.176}$$

where

$$\mathbf{S}(t, t_f) = \int_t^{t_f} \mathbf{\Phi}^{*T}(\tau, t) \left[\mathbf{Q} + \mathbf{K}^T \mathbf{R} \mathbf{K} \right] \mathbf{\Phi}^*(\tau, t)\, \mathrm{d}\tau \tag{6.177}$$

Note that, by its construction, the matrix $\mathbf{S}$ is symmetric, since the weighting matrices $\mathbf{Q}$ and $\mathbf{R}$ are both symmetric.

The simple appearance of Eq. (6.176) belies the complexity of determining $\mathbf{S}$ from Eq. (6.177). In fact, if we had to use the latter equation to determine the matrix $\mathbf{S}$, we would face an almost hopeless task. Our expression of the solution in terms of the general state transition matrix seems to have resulted in a simple expression for the integral we wish to minimize, but it is almost impossible to develop a useful expression for the state transition matrix, itself, in general. Instead, in order to find the gain matrix $\mathbf{K}$ that minimizes J, it is convenient to find a differential equation that the matrix $\mathbf{S}$ satisfies. To this end, we note that since

$$J = \int_t^{t_f} \mathbf{x}^T(\tau)\mathbf{L}\mathbf{x}(\tau)\,\mathrm{d}t \tag{6.178}$$

where

$$L = \mathbf{Q} + \mathbf{K}^T\mathbf{R}\mathbf{K} \tag{6.179}$$

we can write

$$\frac{\mathrm{d}J}{\mathrm{d}t} = -\,\mathbf{x}^T(\tau)\mathbf{L}\mathbf{x}(\tau)\big|_{\tau=t} = -\mathbf{x}^T(t)\mathbf{L}\mathbf{x}(t) \tag{6.180}$$

But, from differentiating Eq. (6.176), we have

$$\frac{\mathrm{d}J}{\mathrm{d}t} = \dot{\mathbf{x}}^T(t)\mathbf{S}(t,t_f)\mathbf{x}(t) + \mathbf{x}^T(t)\dot{\mathbf{S}}(t,t_f)\mathbf{x}(t) + \mathbf{x}^T(t)\mathbf{S}(t,t_f)\dot{\mathbf{x}}(t) \tag{6.181}$$

and, substituting the closed-loop differential equation, Eq. (6.172), for $\dot{\mathbf{x}}$ gives

$$\frac{\mathrm{d}J}{\mathrm{d}t} = \mathbf{x}^T(t)\left[\mathbf{A}^{*T}\mathbf{S}(t,t_f) + \dot{\mathbf{S}}(t,t_f) + \mathbf{S}(t,t_f)\mathbf{A}^*(t)\right]\mathbf{x}(t) \tag{6.182}$$

Thus, we have two expressions for the derivative $\mathrm{d}J/\,\mathrm{d}t$: Eqs. (6.180) and (6.182). Both are quadratic forms in the initial state $\mathbf{x}(t)$, which must be *arbitrary*. The only way that two quadratic forms in $\mathbf{x}$ can be equal for any choice of $\mathbf{x}$ is if the underlying matrices are equal; thus, we must have

$$-\mathbf{L} = \mathbf{A}^{*T}\mathbf{S} + \dot{\mathbf{S}} + \mathbf{S}\mathbf{A}^*$$

or

$$-\dot{\mathbf{S}} = \mathbf{S}\mathbf{A}^* + \mathbf{A}^{*T}\mathbf{S} + \mathbf{L} \tag{6.183}$$

Equation (6.183) is a first-order differential equation for the matrix $\mathbf{S}$, so it requires a single initial condition to completely specify its solution. We can use Eq. (6.177), evaluated at $t = t_f$ to give the required condition

$$\mathbf{S}(t_f, t_f) = 0 \tag{6.184}$$

Once a gain matrix $\mathbf{K}$ has been chosen to close the loop, the corresponding performance of the system is given by Eq. (6.176), where $\mathbf{S}(t,t_f)$ is the solution of Eq. (6.183), which can be written in terms of the original plant and gain matrices as

$$-\dot{\mathbf{S}} = \mathbf{S}\left(\mathbf{A} - \mathbf{B}\mathbf{K}\right) + \left(\mathbf{A}^T - \mathbf{K}^T\mathbf{B}^T\right)\mathbf{S} + \mathbf{Q} + \mathbf{K}^T\mathbf{R}\mathbf{K} \tag{6.185}$$

Our task, then, is to find the gain matrix $\mathbf{K}$ that makes the solution to Eq. (6.185) as small as possible – in the sense that the quadratic forms (Eq. (6.176)) associated with the matrix $\mathbf{S}$ are minimized. That is, we want to find the matrix $\hat{\mathbf{S}}$ for which

$$\hat{J} = \mathbf{x}^T\hat{\mathbf{S}}\mathbf{x} < \mathbf{x}^T\mathbf{S}\mathbf{x} \tag{6.186}$$

for any arbitrary initial state $\mathbf{x}(t)$ and every matrix $\mathbf{S} \neq \hat{\mathbf{S}}$.

We will proceed by assuming that such an optimum exists, and use the calculus of variations to find it. The minimizing matrix $\hat{\mathbf{S}}$ must, of course, satisfy Eq. (6.185)

$$-\dot{\hat{\mathbf{S}}} = \hat{\mathbf{S}}\left(\mathbf{A} - \mathbf{B}\hat{\mathbf{K}}\right) + \left(\mathbf{A}^T - \hat{\mathbf{K}}^T\mathbf{B}^T\right)\hat{\mathbf{S}} + \mathbf{Q} + \hat{\mathbf{K}}^T\mathbf{R}\hat{\mathbf{K}} \tag{6.187}$$

and any *non*-optimum gain matrix, and its corresponding matrix $\mathbf{S}$, can be expressed as

$$\begin{aligned} \mathbf{S} &= \hat{\mathbf{S}} + \mathbf{N} \\ \mathbf{K} &= \hat{\mathbf{K}} + \mathbf{Z} \end{aligned} \tag{6.188}$$

Substituting this form into Eq. (6.185) and subtracting Eq. (6.187) gives

$$-\dot{\mathbf{N}} = \mathbf{N}\mathbf{A}^* + \mathbf{A}^{*^T}\mathbf{N} + \left(\hat{\mathbf{K}}^T\mathbf{R} - \hat{\mathbf{S}}\mathbf{B}\right)\mathbf{Z} + \mathbf{Z}^T\left(\mathbf{R}\hat{\mathbf{K}} - \mathbf{B}^T\hat{\mathbf{S}}\right) + \mathbf{Z}^T\mathbf{R}\mathbf{Z} \tag{6.189}$$

where

$$\mathbf{A}^* = \mathbf{A} - \mathbf{B}\mathbf{K} = \mathbf{A} - \mathbf{B}\left(\hat{\mathbf{K}} + \mathbf{Z}\right) \tag{6.190}$$

Note that Eq. (6.189) has exactly the same form as Eq. (6.183) with

$$\mathbf{L} = \left(\hat{\mathbf{K}}^T\mathbf{R} - \hat{\mathbf{S}}\mathbf{B}\right)\mathbf{Z} + \mathbf{Z}^T\left(\mathbf{R}\hat{\mathbf{K}} - \mathbf{B}^T\hat{\mathbf{S}}\right) + \mathbf{Z}^T\mathbf{R}\mathbf{Z} \tag{6.191}$$

so its solution must be of the form of Eq. (6.177)

$$\mathbf{N}(t, t_f) = \int_t^{t_f} \mathbf{\Phi}^{*^T}(\tau, t)\mathbf{L}\mathbf{\Phi}^*(\tau, t)\,\mathrm{d}\tau \tag{6.192}$$

Now, if $\hat{J}$ is a minimum, then we must have

$$\mathbf{x}^T\hat{\mathbf{S}}\mathbf{x} \leq \mathbf{x}^T\left(\hat{\mathbf{S}} + \mathbf{N}\right)\mathbf{x} = \mathbf{x}^T\hat{\mathbf{S}}\mathbf{x} + \mathbf{x}^T\mathbf{N}\mathbf{x} \tag{6.193}$$

and this equation requires that the quadratic form $\mathbf{x}^T\mathbf{N}\mathbf{x}$ be positive definite (or, at least, positive semi-definite). But, if $\mathbf{Z}$ is sufficiently small, the linear terms in $\mathbf{Z}$ (and $\mathbf{Z}^T$) in Eq. (6.191) will dominate the quadratic terms in $\mathbf{Z}^T\mathbf{R}\mathbf{Z}$, and we could easily find values of $\mathbf{Z}$ that would make $\mathbf{L}$, and hence $\mathbf{N}$, negative definite. Thus, *the linear terms in Eq. (6.191) must be absent altogether*. That is, for the gain matrix $\hat{\mathbf{K}}$ to be optimum, we must have

$$\hat{\mathbf{K}}^T\mathbf{R} - \hat{\mathbf{S}}\mathbf{B} = 0 = \mathbf{R}\hat{\mathbf{K}} - \mathbf{B}^T\hat{\mathbf{S}} \tag{6.194}$$

or, assuming that the weighting matrix $\mathbf{R}$ is not singular,

$$\hat{\mathbf{K}} = \mathbf{R}^{-1}\mathbf{B}^T\hat{\mathbf{S}} \tag{6.195}$$

Equation (6.195) gives the optimum gain matrix $\hat{\mathbf{K}}$, once the matrix $\hat{\mathbf{S}}$ has been determined. When this equation is substituted back into Eq. (6.187) we have

$$-\dot{\hat{\mathbf{S}}} = \hat{\mathbf{S}}\mathbf{A} + \mathbf{A}^T\hat{\mathbf{S}} - \hat{\mathbf{S}}\mathbf{B}\mathbf{R}^{-1}\mathbf{B}^T\hat{\mathbf{S}} + \mathbf{Q} \tag{6.196}$$

This equation, one of the most famous in modern control theory, is called the *matrix Riccati equation*, consistent with the mathematical nomenclature that identifies an equation with a quadratic nonlinearity as a Riccati equation. The solution to this equation gives the matrix $\hat{\mathbf{S}}$ which, when substituted into Eq. (6.195), gives the optimum gain matrix $\hat{\mathbf{K}}$.

Because of the quadratic nonlinearity in the Riccati equation, it is necessary, except in a few very special cases, to solve it numerically. Since the matrix $\hat{\mathbf{S}}$ is symmetric, Eq. (6.196) represents $n(n+1)/2$ coupled, first-order equations. Since the "initial" condition is

$$\hat{\mathbf{S}}(t_f, t_f) = 0 \tag{6.197}$$

the equation must be integrated *backward* in time, since we are interested in $\hat{\mathbf{S}}(t, t_f)$ for $t < t_f$.

When the control interval $[t, t_f]$ is finite, the gain matrix $\mathbf{K}$ will generally be time-dependent, even when the matrices $\mathbf{A}$, $\mathbf{B}$, $\mathbf{Q}$, and $\mathbf{R}$ are all constant. But, suppose the control interval is *infinite*, so that we want to find the gain matrix $\hat{\mathbf{K}}$ that minimizes the performance index

$$J_\infty = \int_t^\infty \left(\mathbf{x}^T\mathbf{Q}\mathbf{x} + \eta^T\mathbf{R}\eta\right)\, \mathrm{d}\tau \tag{6.198}$$

In this case, integration of Eq. (6.196) backward in time will either grow without limit or converge to a *constant* matrix $\bar{\mathbf{S}}$. If it converges to a limit, the derivative $\dot{\hat{\mathbf{S}}}$ must tend to zero, and $\bar{\mathbf{S}}$ must satisfy the *algebraic* equation

$$0 = \bar{\mathbf{S}}\mathbf{A} + \mathbf{A}^T\bar{\mathbf{S}} - \bar{\mathbf{S}}\mathbf{B}\mathbf{R}^{-1}\mathbf{B}^T\bar{\mathbf{S}} + \mathbf{Q} \tag{6.199}$$

and the optimum gain in the steady state is given by

$$\bar{\mathbf{K}} = \mathbf{R}^{-1}\mathbf{B}^T\bar{\mathbf{S}} \tag{6.200}$$

The single *quadratic* matrix Eq. (6.199) represents $n(n+1)/2$ coupled scalar, quadratic equations, so we expect there will be $n(n+1)$ different (symmetric) solutions. The nature of these solutions is, as one might expect, connected with issues of controllability and observability – and a treatment of these issues is beyond the scope of our treatment here. But, for most design applications, it is enough to know that

1. If the system is asymptotically stable; or

2. If the system defined by ($\mathbf{A}$, $\mathbf{B}$) is *controllable*, and the system defined by ($\mathbf{A}$, $\mathbf{C}$), where the weighting matrix $\mathbf{Q} = \mathbf{C}^T\mathbf{C}$, is observable,

then the algebraic Riccati equation has an unique positive definite solution $\bar{\mathbf{S}}$ that minimizes J_∞ when the control law

$$\eta = -\bar{\mathbf{K}}\mathbf{x} = -\mathbf{R}^{-1}\mathbf{B}^T\bar{\mathbf{S}}\mathbf{x} \tag{6.201}$$

is used.[5]

[5]It should be understood that there are still $n(n+1)$ symmetric solutions; the assertion here is that, of these multiple solutions, one, and only one, is *positive definite*.

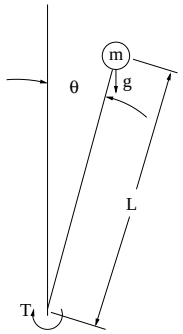

Figure 6.7: Inverted pendulum affected by gravity g and control torque T.

6.6.2 Example of Linear, Quadratic, Optimal Control

We consider here the application of linear, quadratic optimal control to an example that is simple enough that we can carry our the analysis in closed form, illustrating the concepts of the preceding section. We consider using optimal control to stabilize an inverted pendulum. The equation of motion for an inverted pendulum near its (unstable) equilibrium point, as illustrated in Fig. 6.7 is

$$mL^2\ddot{\theta} = mgL\sin\theta + T = mgL\theta + T \tag{6.202}$$

where m is the mass of the pendulum, L is the pendulum length, g is the acceleration of gravity, and T is the externally-applied (control) torque; the second form of the right-hand side assumes the angle θ is small.

If we introduce the angular velocity $\omega = \dot{\theta}$ as a second state variable, Eq. (6.202) can be written in the standard state variable form

$$\frac{\mathrm{d}}{\mathrm{d}t}\begin{pmatrix}\theta\\ \omega\end{pmatrix} = \begin{pmatrix}0 & 1\\ \gamma & 0\end{pmatrix}\begin{pmatrix}\theta\\ \omega\end{pmatrix} + \begin{pmatrix}0\\ 1\end{pmatrix}\tau \tag{6.203}$$

where $\gamma = g/L$ and $\tau = T/(mL^2)$ are reduced gravity and input torque variables.

Now, we seek the control law that minimizes the performance index

$$J_\infty = \int_t^\infty \left(\theta^2 + \frac{\tau^2}{c^2}\right)\mathrm{d}t' \tag{6.204}$$

where c is a parameter that determines the relative weighting of control input and angular deviation in the penalty function. It is clear that this performance index corresponds to

$$\mathbf{Q} = \begin{pmatrix}1 & 0\\ 0 & 0\end{pmatrix} \quad \text{and} \quad \mathbf{R} = \frac{1}{c^2} \tag{6.205}$$

If we define the elements of the matrix $\bar{\mathbf{S}}$ to be

$$\bar{\mathbf{S}} = \begin{pmatrix}s_1 & s_2\\ s_2 & s_3\end{pmatrix} \tag{6.206}$$

then the optimum gain matrix is

$$\bar{\mathbf{K}} = \mathbf{R}^{-1}\mathbf{B}^T\bar{\mathbf{S}} = c^2\begin{bmatrix}0 & 1\end{bmatrix}\begin{pmatrix}s_1 & s_2\\ s_2 & s_3\end{pmatrix} = \begin{bmatrix}c^2 s_2 & c^2 s_3\end{bmatrix} \tag{6.207}$$

which is seen to be independent of the element s_1.

The terms needed for the algebraic Riccati equation

$$0 = \bar{\mathbf{S}}\mathbf{A} + \mathbf{A}^T\bar{\mathbf{S}} - \bar{\mathbf{S}}\mathbf{B}\mathbf{R}^{-1}\mathbf{B}^T\bar{\mathbf{S}} + \mathbf{Q} \tag{6.208}$$

are

$$\bar{\mathbf{S}}\mathbf{A} = \begin{pmatrix} s_1 & s_2 \\ s_2 & s_3 \end{pmatrix}\begin{pmatrix} 0 & 1 \\ \gamma & 0 \end{pmatrix} = \begin{pmatrix} s_2\gamma & s_1 \\ s_3\gamma & s_2 \end{pmatrix} \tag{6.209}$$

$$\mathbf{A}^T\bar{\mathbf{S}} = \begin{pmatrix} 0 & \gamma \\ 1 & 0 \end{pmatrix}\begin{pmatrix} s_1 & s_2 \\ s_2 & s_3 \end{pmatrix} = \begin{pmatrix} s_2\gamma & s_3\gamma \\ s_1 & s_2 \end{pmatrix} \tag{6.210}$$

and

$$\bar{\mathbf{S}}\mathbf{B}\mathbf{R}^{-1}\mathbf{B}^T\bar{\mathbf{S}} = \begin{pmatrix} s_1 & s_2 \\ s_2 & s_3 \end{pmatrix}\begin{pmatrix} 0 \\ 1 \end{pmatrix} c^2 \begin{bmatrix} 0 & 1 \end{bmatrix}\begin{pmatrix} s_1 & s_2 \\ s_2 & s_3 \end{pmatrix} = c^2\begin{pmatrix} s_2^2 & s_2s_3 \\ s_2s_3 & s_3^2 \end{pmatrix} \tag{6.211}$$

Thus, the Riccati equation is

$$0 = \begin{pmatrix} s_2\gamma & s_1 \\ s_3\gamma & s_2 \end{pmatrix} + \begin{pmatrix} s_2\gamma & s_3\gamma \\ s_1 & s_2 \end{pmatrix} - c^2\begin{pmatrix} s_2^2 & s_2s_3 \\ s_2s_3 & s_3^2 \end{pmatrix} + \begin{pmatrix} 1 & 0 \\ 0 & 0 \end{pmatrix} \tag{6.212}$$

which is equivalent to the three scalar equations

$$\begin{aligned} 0 &= 2s_2\gamma - c^2s_2^2 + 1 \\ 0 &= s_1 + s_3\gamma - c^2s_2s_3 \\ 0 &= 2s_2 - c^2s_3^2 \end{aligned} \tag{6.213}$$

These equations are simple enough that we can solve them in closed form. The first of Eqs. (6.213) gives

$$s_2 = \frac{\gamma \pm \sqrt{\gamma^2 + c^2}}{c^2} \tag{6.214}$$

and the third of Eqs. (6.213) gives

$$s_3 = \pm\frac{1}{c}\sqrt{2s_2} \tag{6.215}$$

Since the elements of $\bar{\mathbf{S}}$ must be real, s_2 must be positive (or s_3 would be complex). Thus, we must choose the positive root in Eq. (6.203). Further, the second of Eqs. (6.213) gives

$$s_1 = c^2s_2s_3 - \gamma s_3 = s_3\sqrt{\gamma^2 + c^2} \tag{6.216}$$

Thus, elements s_1 and s_3 have the same sign which, for $\bar{\mathbf{S}}$ to be positive definite, must be positive. Thus,

$$\begin{aligned} s_2 &= \frac{\gamma + \sqrt{\gamma^2 + c^2}}{c^2} \\ s_3 &= \frac{1}{c}\sqrt{2s_2} = \frac{\sqrt{2}}{c^2}\left[\gamma + \sqrt{\gamma^2 + c^2}\right]^{1/2} \end{aligned} \tag{6.217}$$

represents the unique solution for the corresponding elements for which $\bar{\mathbf{S}}$ is positive definite.

Thus, the gain matrix is seen to be

$$\mathbf{K} = \begin{bmatrix} c^2s_2 & c^2s_3 \end{bmatrix} = \left[\gamma + \sqrt{\gamma^2 + c^2} \quad \sqrt{2}\left[\gamma + \sqrt{\gamma^2 + c^2}\right]^{1/2}\right] \tag{6.218}$$

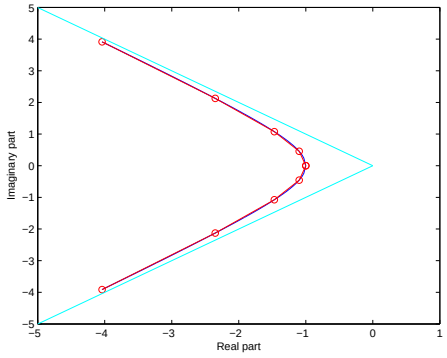

Figure 6.8: Locus of roots of characteristic equation of augmented plant matrix for inverted pendulum. Axes are scaled to give roots in units of γ. Open symbols represent roots at values of $c/\gamma = 0, 1, 10, 100, 1000$, with real root corresponding to $c/\gamma = 0$. Cyan lines represent asymptotes of root positions in the limit of large c/γ.

The augmented matrix is then given by

$$\mathbf{A}^* = \mathbf{A} - \mathbf{B}\bar{\mathbf{K}} = \begin{pmatrix} 0 & 1 \\ -\sqrt{\gamma^2 + c^2} & -\sqrt{2}\left[\gamma + \sqrt{\gamma^2 + c^2}\right]^{1/2} \end{pmatrix} \tag{6.219}$$

and its characteristic equation is

$$\lambda^2 + \sqrt{2}\left[\gamma + \sqrt{\gamma^2 + c^2}\right]^{1/2}\lambda + \sqrt{\gamma^2 + c^2} = 0 \tag{6.220}$$

which has roots

$$\lambda = \frac{\sqrt{2}}{2}\left[-\sqrt{\gamma + \bar{\gamma}} \pm \imath\sqrt{\bar{\gamma} - \gamma}\right] \tag{6.221}$$

where we have introduced

$$\bar{\gamma} = \sqrt{\gamma^2 + c^2} \tag{6.222}$$

The locus of these roots is plotted in Fig. 6.8 as the weighting factor c is varied over the range $0 < c < 10^3$.

Note that as c/γ becomes large, $\bar{\gamma}$ becomes large relative to γ, so

$$\lim_{c/\gamma \to \infty} \lambda = -\sqrt{\frac{\bar{\gamma}}{\sqrt{2}}}\,(1 \pm \imath) \tag{6.223}$$

Thus, as c becomes large, the damping ratio of the system approaches a constant value of

$$\zeta = \frac{1}{\sqrt{2}}$$

while the undamped natural frequency increases as

$$\omega_n = \sqrt{\bar{\gamma}} \approx \sqrt{c}$$

Large values of c correspond to a performance index in which the weighting of the control term is small compared to that of the deviations in state variables – i.e., to a situation in which we are

willing to spend additional energy in control to maintain very small perturbations of the state from its equilibrium position.

On the other hand, as c becomes small, the weighting of the control term in the performance index becomes large compared to that of the state variables. This is consistent with the fact that the gains in Eq. (6.218)

$$K_1 = \gamma + \sqrt{\gamma^2 + c^2}$$
$$K_2 = \sqrt{2}\left[\gamma + \sqrt{\gamma^2 + c^2}\right]^{1/2}$$

decrease monotonically with c. In the limit $c = 0$, however, the gains remain finite, with

$$\lim_{c\to 0} K_1 = 2\gamma$$
$$\lim_{c\to 0} K_2 = 2\sqrt{\gamma}$$

since *some* control is necessary to stabilize this, otherwise unstable, system.

6.6.3 Linear, Quadratic, Optimal Control as a Stability Augmentation System

We here present an example of the application of linear, quadratic optimal control to stabilize the motion of the Boeing 747 aircraft in powered approach at $\mathbf{M} = 0.25$ at standard sea level conditions. This is the same aircraft and flight condition for which we used the Bass-Gura procedure to design a feedback control system to stabilize the lateral/directional modes in Section. 6.5.1. In that earlier section, we determined the gains for specific placement of the eigenvalues of the associated augmented matrix using only one control, either rudder or ailerons, at a time.

Here, we apply linear, quadratic, optimal control to minimize the steady state performance index

$$J_\infty = \int_t^\infty \left(\mathbf{x}^T\mathbf{Q}\mathbf{x} + \frac{1}{c^2}\eta^T\mathbf{R}\eta\right)\,\mathrm{d}\tau \tag{6.224}$$

where, as in the previous simple example, c is a parameter that determines the relative weights given to control action and perturbations in the state variable in the penalty function. For lateral/directional motions at this flight condition, the plant matrix is given by Eq. (6.150), while the control matrix is the union of the two vectors given in Eqs. (6.158) and (6.163)

$$\mathbf{B} = \begin{pmatrix} 0.0182 & 0.0868 & 0.0000 & -.2440 \\ 0.0000 & 0.3215 & 0.0000 & -.0017 \end{pmatrix}^T \tag{6.225}$$

where the control vector is

$$\eta = [\delta_r \quad \delta_a]^T \tag{6.226}$$

The weighting matrices in the performance index are taken to be simply

$$\mathbf{Q} = \mathbf{I} \quad \text{and} \quad \mathbf{R} = \mathbf{I} \tag{6.227}$$

where $\mathbf{Q}$ is a 4×4 matrix and $\mathbf{R}$ is a 2×2 matrix.

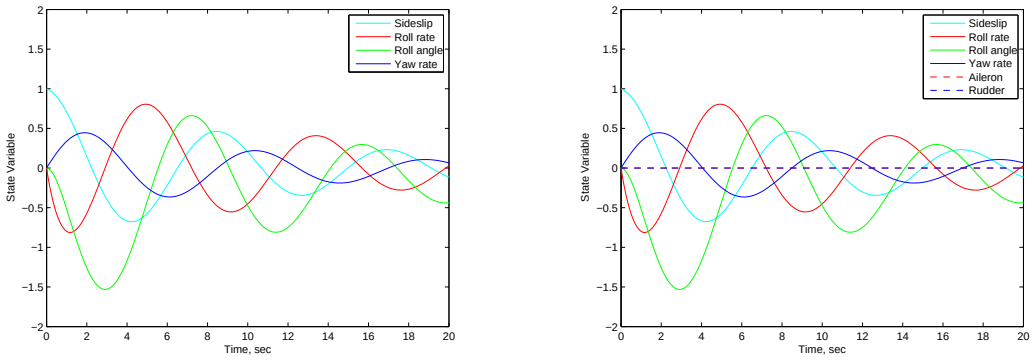

(a) No feedback (b) $c = 0.001$

Figure 6.9: Boeing 747 aircraft in powered approach at standard sea level conditions and $\mathbf{M} = 0.25$; response to unit perturbation in sideslip. (a) Original open-loop response; (b) Optimal closed loop response with performance parameter $c = 0.001$.

The MATLAB function

$$[S,\ L,\ G] = care(A,B,Q,R,T,E);$$

is used to solve the generalized matrix Riccati equation

$$\mathbf{E}^T\mathbf{S}\mathbf{A} + \mathbf{A}^T\mathbf{S}\mathbf{E} - \left(\mathbf{E}^T\mathbf{S}\mathbf{B} + \mathbf{T}\right)\mathbf{R}^{-1}\left(\mathbf{B}^T\mathbf{S}\mathbf{E} + \mathbf{T}^T\right) + \mathbf{Q} = 0 \tag{6.228}$$

which, with the additional input matrices are defined as

$$T = zeros(size(B));$$

and

$$E = eye(size(A));$$

reduces to Eq. (6.199). In addition to the solution matrix S, the MATLAB function *care* also returns the gain matrix

$$\mathbf{G} = \mathbf{R}^{-1}\left(\mathbf{B}^T\mathbf{S}\mathbf{E} + \mathbf{T}^T\right) \tag{6.229}$$

and the vector

$$L = eig(A - BG,\ E)$$

containing the eigenvalues of the augmented matrix.

For small values of the parameter c, the control action is weighted heavily in the performance index. Figure 6.9 compares the open-loop response to a unit perturbation in sideslip to the closed-loop system response for a value of $c = 0.001$. This value penalizes control input so heavily that the open-loop and closed-loop responses are virtually identical. This is a quite different result from that for the simple example of Section 6.6.2, and results from the fact that this system is *stable*, so the natural (un-forced) return of the system to equilibrium is optimal when control action is heavily penalized.

Figure 6.10 shows the closed-loop system response for values of $c = 0.5, 1.0,$ and 2.0, respectively. Also plotted in these figures are the time histories of control response required to stabilize the motions, calculated as

$$\eta = -\mathbf{K}\mathbf{x} \tag{6.230}$$

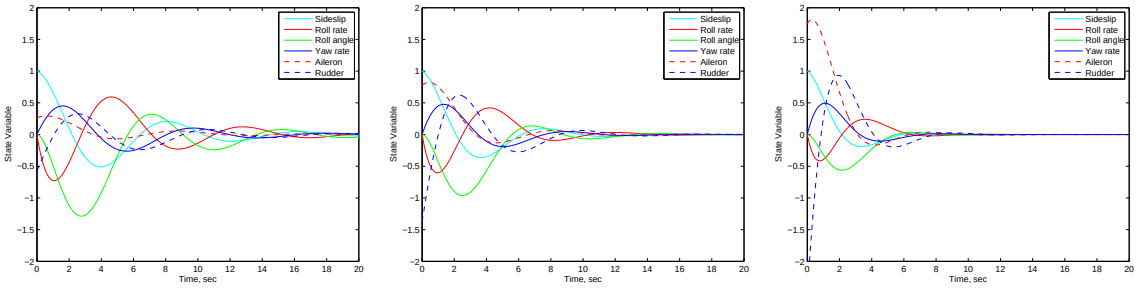

(a) $c = 0.50$ (b) $c = 1.0$ (c) $c = 2.0$

Figure 6.10: Boeing 747 aircraft in powered approach at standard sea level conditions and $\mathbf{M} = 0.25$; response to unit perturbation in sideslip illustrating effect of varying weighting parameter c. Optimal closed-loop responses with (a) $c = 0.50$; (b) $c = 1.0$; and (c) $c = 2.0$. Control deflections required to stabilize the motions are also shown.

This control response is calculated in MATLAB simply by defining the matrices $\mathbf{C}$ and $\mathbf{D}$ defining the output response as

$$C = \text{-}G;$$

and

$$D = zeros(2);$$

and then adding the output variables

$$\mathbf{y} = \mathbf{C}\mathbf{x} + \mathbf{D}\eta \tag{6.231}$$

to the plots. It is seen in the plots that, as c is increased the motion becomes more heavily damped, but at the cost of significantly greater control input.

The role of the parameter c can be seen more clearly if we examine the behavior of the individual terms in the performance index J_∞. Figure 6.11 plots the quadratic forms $\mathbf{x}^T\mathbf{Q}\mathbf{x}$ and $\eta^T\mathbf{R}\eta$ as functions of time for the three values of c illustrated in Fig. 6.10. For greater clarity in the figure, *minus* the control term is plotted. Thus, for each value of c the optimal control strategy selects the gains that minimize the net area between the two curves. Three trends resulting from increasing c are evident in the figure: (1) the value of J_∞ – i.e., the area between the two curves – decreases; (2) the return of the system to its equilibrium state is more rapid and heavily damped; (3) most of the improvement happens for modest increases in the value of c, with continued increases requiring ever larger control inputs for relatively little further improvement in response.

Finally, we illustrate the behavior of the roots of the augmented equation as the parameter c is increased. Figure 6.12 shows the locations of the roots in the complex plane for selected values of c. Note that, in this range of values, all roots move to the left as c is increased until the Dutch Roll mode becomes critically damped at a value of approximately $c = 9.973$, as indicated by the joining of the roots on the real axis. With further increase in c, one of the Dutch Roll roots moves to the right. The value of c required to achieve critical damping of the Dutch Roll mode generally corresponds to much larger values of c than would ever be used in a practical system.

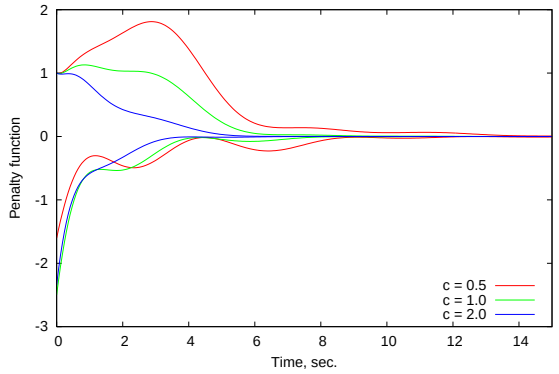

Figure 6.11: Penalty functions in performance index for optimal control solution; Boeing 747 aircraft in powered approach at standard sea level conditions and $\mathbf{M} = 0.25$. Upper curves are $\mathbf{x}^T\mathbf{Q}\mathbf{x}$, and lower curves are $-\eta^T\mathbf{R}\eta$, as functions of time for response to unit perturbation in sideslip angle β, so the area between the curves is equal to the performance index J_∞.

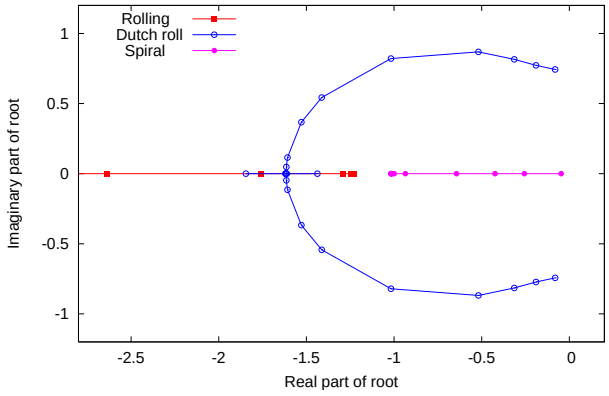

Figure 6.12: Boeing 747 aircraft in powered approach at standard sea level conditions and $\mathbf{M} = 0.25$; locus of roots of characteristic equation of augmented matrix as control weighting parameter c is increased. Symbols represent root locations for $c = 0.001, 0.5, 1.0, 2.0, 5.0, 8.0, 9.0, 9.7, 9.76, 9.7727, 9.7728, 10.0$; as c is increased, all roots move to the left (except for one of the Dutch Roll roots after that mode becomes critically damped between $9.7227 < c < 9.7228$).

Bibliography

[1] Arthur Bryson & Yu-Chi Ho, **Applied Optimal Control: Optimization, Estimation, and Control**, Hemisphere, 1975.

[2] Bernard Etkin & Lloyd Duff Reid, **Dynamics of Flight, Stability and Control**, McGraw-Hill, Third Edition, 1996.

[3] Bernard Friedland, **Control System Design: An Introduction to State-Space Methods**, McGraw-Hill, 1986.

[4] Frances B. Hildebrand, **Advanced Calculus for Applications**, Prentice-Hall, 1962.

[5] Robert C. Nelson, **Aircraft Stability and Automatic Control**, McGraw-Hill, Second edition, 1998.

[6] Louis V. Schmidt, **Introduction to Aircraft Flight Dynamics**, AIAA Education Series, 1998.

6.7 Review of Laplace Transforms

The Laplace transform of the function $f(t)$, assumed identically zero for $t < 0$, is defined as

$$\mathcal{L}\left[f(t)\right] = F(s) = \int_0^\infty f(t)e^{-st}\,\mathrm{d}t \tag{6.232}$$

The Laplace transform $F(s)$ of the function $f(t)$ can be shown to exist, for sufficiently large s, when [4]:

1. The function $f(t)$ is continuous or piecewise continuous in every finite interval $t_1 \leq t \leq T$, where $t_1 > 0$;
2. The function $t^n|f(t)|$ is bounded near $t = 0$ for some number $n < 1$; and
3. The function $e^{-s_0 t}|f(t)|$ is bounded for large values of t, for some number s_0.

All the functions we normally deal with in stability and control problems satisfy these conditions.

6.7.1 Laplace Transforms of Selected Functions

We here review the Laplace transforms of several important functions.

Laplace Transform of a Derivative

If $F(s)$ is the Laplace transform of the function $f(t)$, then the Laplace transform of the derivative $\mathrm{d}f/\mathrm{d}t$ can be determined as

$$\begin{aligned}\mathcal{L}\left[\frac{\mathrm{d}f}{\mathrm{d}t}\right] = \int_0^\infty \frac{\mathrm{d}f}{\mathrm{d}t}e^{-st}\,\mathrm{d}t = fe^{-st}\big|_0^\infty + \int_0^\infty fse^{-st}\,\mathrm{d}t = -f(0) + s\int_0^\infty fe^{-st}\,\mathrm{d}t \\ = -f(0) + sF(s)\end{aligned} \tag{6.233}$$

Heaviside Step Function

The Heaviside step function is defined as

$$H(t-\tau) = \begin{cases} 0, & \text{for } t < \tau \\ 1, & \text{for } t \geq \tau \end{cases} \tag{6.234}$$

The Laplace transform of $H(t)$ is thus

$$H(s) = \int_0^\infty e^{-st}H(t)\,\mathrm{d}t = \int_0^\infty e^{-st}\,\mathrm{d}t = -\left.\frac{e^{st}}{s}\right|_0^\infty = \frac{1}{s} \tag{6.235}$$

Dirac Delta Function

The Dirac delta function is defined by the properties

$$\begin{aligned}\delta(t-\tau) = 0 \quad \text{for} \quad t \neq \tau \\ \int_{-\infty}^\infty \delta(t-\tau)\,\mathrm{d}t = 1\end{aligned} \tag{6.236}$$

The Laplace transform of $\delta(t)$ is thus

$$\delta(s) = \int_0^\infty e^{-st}\delta(t)\,\mathrm{d}t = e^0 = 1 \tag{6.237}$$

The function $f(t) = t$

The Laplace transform of $f(t) = t$ is

$$F(s) = \int_0^\infty te^{-st}\,\mathrm{d}t = -\left.\frac{te^{-st}}{s}\right|_0^\infty + \int_0^\infty \frac{e^{-st}}{s}\,\mathrm{d}t = -\left.\frac{e^{-st}}{s^2}\right|_0^\infty = \frac{1}{s^2} \tag{6.238}$$

The function $f(t) = e^{-at}$

The Laplace transform of $f(t) = e^{-at}$ is

$$F(s) = \int_0^\infty e^{-at}e^{-st}\,\mathrm{d}t = \int_0^\infty e^{-(a+s)t}\,\mathrm{d}t = -\frac{e^{-(a+s)t}}{a+s}\bigg|_0^\infty = \frac{1}{s+a} \tag{6.239}$$

The Trigonometric Functions, $\cos\omega t$ and $\sin\omega t$

The Laplace transform of $f(t) = \cos\omega t$ is determined as follows. Since

$$\begin{aligned}\int_0^\infty \cos\omega t e^{-st}\,\mathrm{d}t &= -\frac{\cos\omega t e^{-st}}{s}\bigg|_0^\infty - \omega\int_0^\infty \sin\omega t\frac{e^{-st}}{s}\,\mathrm{d}t \\ &= \frac{1}{s} - \frac{\omega}{s}\int_0^\infty \sin\omega t e^{-st}\,\mathrm{d}t = \frac{1}{s} + \frac{\omega}{s}\left[\frac{\sin\omega t e^{-st}}{s} - \omega\int_0^\infty \cos\omega t\frac{te^{-st}}{s}\,\mathrm{d}t\right] \\ &= \frac{1}{s} - \frac{\omega^2}{s^2}\int_0^\infty \cos\omega t e^{-st}\,\mathrm{d}t\end{aligned} \tag{6.240}$$

we have

$$\left(1 + \frac{\omega^2}{s^2}\right)\int_0^\infty \cos\omega t e^{-st}\,\mathrm{d}t = \frac{1}{s} \tag{6.241}$$

whence

$$F(s) = \int_0^\infty \cos\omega t e^{-st}\,\mathrm{d}t = \frac{1}{s\left(1+\frac{\omega^2}{s^2}\right)} = \frac{s}{s^2+\omega^2} \tag{6.242}$$

Similarly, to determine the Laplace transform of $f(t) = \sin\omega t$, since

$$\begin{aligned}\int_0^\infty \sin\omega t e^{-st}\,\mathrm{d}t &= -\frac{\sin\omega t e^{-st}}{s}\bigg|_0^\infty + \frac{\omega}{s}\int_0^\infty \cos\omega t e^{-st}\,\mathrm{d}t \\ &= \frac{\omega}{s}\int_0^\infty \cos\omega t e^{-st}\,\mathrm{d}t = \frac{\omega}{s}\left[\frac{1}{s} - \frac{\omega}{s}\int_0^\infty \sin\omega t e^{-st}\,\mathrm{d}t\right]\end{aligned} \tag{6.243}$$

we have

$$\left(1 + \frac{\omega^2}{s^2}\right)\int_0^\infty \sin\omega t e^{-st}\,\mathrm{d}t = \frac{\omega}{s^2} \tag{6.244}$$

whence

$$F(s) = \int_0^\infty \sin\omega t e^{-st}\,\mathrm{d}t = \frac{\omega}{s^2\left(1+\frac{\omega^2}{s^2}\right)} = \frac{\omega}{s^2+\omega^2} \tag{6.245}$$

The Attenuation Rule

Exponentially damped harmonic functions appear often in linear system dynamics, so the following *attenuation rule* is useful.

If $F(s)$ is the Laplace transform of $f(t)$, then the Laplace transform of $e^{-at}f(t)$ is

$$\begin{aligned}\mathcal{L}\left[e^{-at}f(t)\right] = \int_0^\infty e^{-at}f(t)e^{-st}\,\mathrm{d}t &= \int_0^\infty e^{-(s+a)t}f(t)\,\mathrm{d}t \\ &= \int_0^\infty e^{-s't}f(t)\,\mathrm{d}t = F(s') = F(s+a)\end{aligned} \tag{6.246}$$

Thus, since Eq. (6.242) gives

$$\mathcal{L}\left[\cos\omega t\right] = \frac{s}{s^2+\omega^2} \tag{6.247}$$

we have

$$\mathcal{L}\left[e^{-at}\cos\omega t\right] = \frac{s+a}{(s+a)^2+\omega^2} \tag{6.248}$$

Also, since Eq. (6.245) gives

$$\mathcal{L}\left[\sin\omega t\right] = \frac{\omega}{s^2+\omega^2} \tag{6.249}$$

we have

$$\mathcal{L}\left[e^{-at}\sin\omega t\right] = \frac{\omega}{(s+a)^2+\omega^2} \tag{6.250}$$

The Convolution Integral

The convolution integral

$$\mathcal{L}^{-1}\left[F(s)G(s)\right] = \int_0^t f(t-\tau)g(\tau)\,\mathrm{d}\tau \tag{6.251}$$

where $F(s)$ and $G(s)$ are the Laplace transforms of $f(t)$ and $g(t)$, respectively, can be verified formally as follows.

From the definition of the Laplace transform,

$$\begin{aligned}F(s)G(s) &= \int_0^\infty e^{-sv}f(v)\,\mathrm{d}v \int_0^\infty e^{-su}g(u)\,\mathrm{d}u \\ &= \int_0^\infty \int_0^\infty e^{-s(v+u)}f(v)g(u)\,\mathrm{d}v\,\mathrm{d}u \\ &= \int_0^\infty g(u)\left(\int_0^\infty e^{-s(v+u)}f(v)\,\mathrm{d}v\right)\mathrm{d}u\end{aligned} \tag{6.252}$$

Then, with the change of variable

$$v+u=t \tag{6.253}$$

we have

$$\int_0^\infty e^{-s(v+u)}f(v)\,\mathrm{d}v = \int_u^\infty e^{-st}f(t-u)\,\mathrm{d}t \tag{6.254}$$

so

$$\begin{aligned} F(s)G(s) &= \int_0^\infty \left(\int_u^\infty e^{-st} f(t-u) g(u)\, \mathrm{d}t \right) \mathrm{d}u \\ &= \int_0^\infty \left(\int_0^t e^{-st} f(t-u) g(u)\, \mathrm{d}u \right) \mathrm{d}t \\ &= \int_0^\infty e^{-st} \left(\int_0^t f(t-u) g(u)\, \mathrm{d}u \right) \mathrm{d}t = \mathcal{L}\left[\int_0^t f(t-u) g(u)\, \mathrm{d}u \right] \end{aligned} \tag{6.255}$$

which was to be proved. The interchange of order of integration in this last step can be shown to be legitimate, by appropriate limiting procedures, when the Laplace transforms of $f(t)$ and $g(t)$ exist.